

**INVESTIGATION OF CORROSION OF CARBON STEEL UNDER
INSULATION**

A THESIS SUBMITTED BY

JOHN BASSEY EDET

FOR THE AWARD OF DEGREE OF MASTER OF PHILOSOPHY

IN

CHEMICAL AND PROCESS ENGINEERING

UNIVERSITY OF STRATHCLYDE

MARCH 2023

DECLARATION OF AUTHENTICITY AND AUTHOR'S RIGHTS

This thesis is an original work carried out by the author. It has not been previously submitted to any institution which led to the award of a degree.

The copyright of this thesis belongs to the author under the terms of the United Kingdom Copyright Acts as specified by University of Strathclyde Regulation 3.50. Any information derived from this thesis must be adequately acknowledged.

Signed: John Edet

Date: 24th March 2023

ABSTRACT

Corrosion of metals under insulation is a serious concern for industries due to the fact that the insulation hides the metal from view which increases the likelihood of sudden failure. Carbon steel is one of the metal alloys frequently used in industries due to economic and technical reasons. However, it is quite susceptible to corrosion under insulation (CUI). The factors affecting corrosion of carbon steel under mineral wool insulation such as temperature, effectiveness of inhibitor, quantity and distribution of electrolyte in the insulation have not been extensively studied in the literature. In fact, studies on corrosion of metals under insulation are quite sparse compared to immersion (uninsulated) conditions.

Therefore, the objectives of this study were to assess the effect of temperature (60 °C to 130 °C) on corrosion of carbon steel under insulation, effectiveness of a new commercial inhibitor (VpCI 619) in mitigating CUI of carbon steel, quantity and distribution of electrolyte (1wt. % NaCl) in mineral wool insulation as well as investigation of the drying times of the insulation using galvanic current and electrochemical impedance measurements. In addition, the prediction of CUI rate using Artificial Neural Network (ANN) was carried out with the aim of assessing the accuracy of prediction of different network parameters such as number of hidden layers, number of input parameters and choice of activation function.

Prior to CUI studies, the water absorption capacity of mineral wool insulation was determined using standard procedures (ASTM C1511). This was carried out to assess the time it will take for the insulation to be saturated with water, the variability of repeated measurements as well as the total water content in the insulation. The CUI studies were carried out using a test rig that was based on ASTM G189-07 standard. The corrosion rates were estimated using weight loss technique and the effects of temperature, vapour phase inhibitor consisting primarily of sodium molybdate, quantity of electrolyte in insulation were investigated. The drying out profile of the insulation was assessed using galvanic current and electrochemical impedance measurements. Furthermore, the prediction of CUI rate was carried out using Artificial Neural Network and the effect of single and double hidden layers, sigmoid and hyperbolic tangent

activation functions, as well as number of input parameters on accuracy of prediction of CUI rate were assessed.

The results of the water absorption studies indicated continuous absorption of water even after immersion for 22 days. The water absorption capacity was greater for thermally treated insulation compared to untreated insulation samples due to thermal degradation of the oily additives and polymeric binders. The effect of temperature on CUI indicated an increase in corrosion rate from 60 °C to 80 °C. Further increase in temperature up to 130 °C resulted in a decrease in corrosion rate. The existence of a maximum point in the curve was attributed to the competing effects of two factors which include increased diffusivity of oxygen which dominates at low temperature and decreasing solubility of oxygen and insulation dry-out which dominates at temperatures exceeding 80 °C.

The new commercial inhibitor was observed to mitigate the corrosion rate at the temperatures investigated in this study. The inhibition efficiency indicated an average of 89% when a dosage of 5.2 g/m² of the inhibitor was used. The effectiveness was also observed to be dosage dependent with lower doses having less inhibition efficiency. The drying times of the insulation assessed using galvanic current and impedance methods were observed to decrease as temperature increased. The galvanic current was observed to decrease to zero while the impedance increased to high values as the insulation dries out. However, the drying times obtained from galvanic current method showed a higher variability compared to impedance method.

The result of prediction of CUI rate using Artificial Neural Network indicated an increase in accuracy as the number of input parameters increased. Surprisingly, the accuracy of the predicted output from the four input parameters (temperature, dosage of inhibitor, quantity of electrolyte in insulation and sample position) was higher than the accuracy of the most influential parameters (temperature and dosage of inhibitor). This suggests that incorporation of more input parameters having some relationship with the output is more important in achieving a higher accuracy compared to using the most influential parameters only.

In conclusion, this study indicated that mineral wool insulation absorbs water for a long period without saturation which increases the risk of CUI. Also, CUI rate increased with temperature up to 80 °C but decreased on further increase up to 130 °C. The new commercial inhibitor was effective in mitigating CUI at the temperatures investigated. Also, more test solution was observed at the lower part of the insulation compared to the upper part when installed on the CUI test rig which increases the risk of severe corrosion at the lower section of the insulation. The prediction of CUI rate using ANN indicated that inclusion of more input parameters could improve prediction accuracy. Moreover, the choice of activation functions also has effect on the accuracy of the predicted output.

ACKNOWLEDGEMENTS

I wish to express my profound gratitude to the Almighty God for His grace, mercy, and good health. Also, I am grateful to my supervisors Dr Todd Green and Professor Roy for the technical advice and guidance that they provided to me throughout the period of this program. I wish to thank my parents Mr Bassey Edet Etuk and Late Mrs Mercy Etuk for their unrelenting effort in supporting me financially.

Special thanks go to my elder brother Dr Emmanuel Edet and the wife (Mrs Juliet) who have been encouraging and supporting me financially. I wish to also thank my siblings, Theresa and the husband (Pastor Dominion Inyang), Mr Paul and the wife (Mrs Ruth), Mr/Mrs Joseph Edet, and my junior sister Miss Ruth Etuk for their prayers and moral support. I can't forget the support of my Fiancee, Miss Oluwayemisi Oyedun who always encouraged me to wake up, study, and rest when I am tired.

I also wish to thank the members of Electrochemistry and Corrosion group Thomas, Eleni, Shaon, Christine, Pamela, Grace, and Dr Edward Brightman for the positive feedback they have been giving me during research group presentation. In addition, special thanks go to the technicians for accommodating me in the Thomas Graham's lab and providing a conducive atmosphere for me to carry out my research. Also, I wish to thank the University of Strathclyde for giving me the opportunity as well as the sponsorship to carry out this research.

Worthy of appreciation are my senior colleagues which includes Paul, Precious, Maclean and Odira. I will like to thank Mr Billy who has been a significant source of encouragement during difficult times. I will not forget the moments I shared with him during meet ups in Kelvingrove park and coffee shops. Also, I am grateful to all the Esteem group of Glasgow who have been monitoring my health for the past three years to ensure that I am consistent and focused as well as Pastor Segun Akingkugbe, Pastor Prosper, Mr Damilola, the worship warship team, Salt and Light, and all members of Redeemed Christian Church of God, City of God parish, Glasgow, for their prayers and continual support throughout the period of my studies.

TABLE OF CONTENTS

CHAPTER 1 : INTRODUCTION.....	1
1.1) Definition of corrosion	2
1.2) Types of corrosion damage	3
1.3) Background of Corrosion under insulation	4
1.4) Factors affecting the occurrence of CUI.....	7
1.5) Typical incidence of CUI in different chemical plants	8
1.6) Strategies to mitigate corrosion of metals under insulation.....	10
1.6.1) Corrosion under insulation management program.....	11
1.7) Problem Statement and Justification	14
1.8) Motivations for the research.....	14
1.9) Objectives of the study.....	15
1.10) Organisation of Thesis	15
CHAPTER 2 : FUNDAMENTALS	21
2.1) Mechanism of corrosion of metals	22
2.2) Mechanism of Corrosion under Insulation (CUI)	27
2.2.1) Mechanism of corrosion of carbon steel in sodium chloride solution	30
2.3) Theory of galvanic corrosion.....	31
2.4) Fundamental concepts on insulation dry out using galvanic current measurement.....	32
2.4.1) Theory of Electrochemical impedance technique in measuring insulation dry out.....	36
2.5) Theory of predictions using Artificial Neural Network.....	41
2.5.1) Components and Classification of Artificial Neural Network	43
2.6) The role of activation functions in artificial neural network	44
2.6.1) Types of Activation functions	45
2.6.1.1) Sigmoid activation function.....	46
2.6.1.2) Hyperbolic tangent activation function.....	47

2.7) Mechanism of prediction	48
2.8) Limitations of Artificial Neural Network.....	50
2.9) Summary	51
CHAPTER 3 : REVIEW OF RELATED LITERATURE	58
3.1 Available literature on determination of water absorption capacity of mineral wool insulation	60
3.2 Test rigs for studying the rate of CUI in the laboratory	67
3.2.1 The ASTM CUI test rig.....	67
3.2.2 Limitations of the ASTM test rig.....	69
3.3 The rain chamber	70
3.4 Other modifications of ASTM test rig.....	71
3.5 Challenges and precautions associated with CUI test rigs.....	74
3.6 Determination of CUI rate and effect of some influencing factors	75
3.7 Effectiveness of inhibitors in mitigating corrosion under insulation.....	80
3.8 Prediction of CUI rate using Artificial Neural Network (ANN)	83
3.9 Summary.....	87
CHAPTER 4 : EXPERIMENTAL AND PREDICTIVE MODELLING OF CUI	95
4.1 Determination of water absorption capacity of mineral wool insulation	97
4.2 Design of corrosion under insulation test rigs	102
4.2.1 Test rig used in this research for corrosion studies	103
4.3 Distribution of test solution between the top and bottom sections of the insulation.....	111
4.4 Distribution of test solution between the ends and centre of the insulation	112
4.5 Monitoring temperature variations across the six carbon steel rings.....	113
4.6 Quantifying the corrosion rate between the top and bottom parts of carbon steel rings.....	114
4.7 Effectiveness of a new commercial inhibitor (VpCI 619) on corrosion rate	115
4.7.1 Effect of dosage of inhibitor on CUI of carbon steel.....	117

4.8	Monitoring of drying out times of mineral wool insulation using galvanic current and impedance measurements.....	117
4.9	Predictive Modelling of Corrosion of Carbon Steel under Insulation using Artificial Neural Network.....	120
CHAPTER 5 : RESULTS AND DISCUSSION.....		126
5.1)	Water absorption capacity of mineral wool insulation	128
5.1.1)	Comparison of water absorption data with available reports in the literature.....	132
5.2)	Effect of temperature on corrosion rate of carbon steel under insulation	135
5.2.1)	Averaging results of corrosion rate with temperature	136
5.2.2)	Inter-ring average of CUI data	136
5.2.3)	Intra-ring average of CUI data	141
5.3)	Overall trend of CUI rate with temperature	143
5.3.1)	Mechanism of CUI of carbon steel.....	144
5.4)	Comparison of laboratory CUI results with field data	146
5.4.1)	Comparison of laboratory CUI data with field data reported in the ASTM standard.....	146
5.4.2)	Comparison of laboratory CUI results with field data reported in the API 581 standard.....	148
5.4.3)	Comparison of Laboratory CUI data with other field data reported in the literature.....	150
5.5)	Risk Based Assessment of CUI	152
5.6)	Effectiveness of corrosion inhibitor (VpCI 619) at different temperatures	154
5.6.1)	Effectiveness of the inhibitor at different operating temperatures	155
5.6.2)	Effect of varying dosage of inhibitor.....	158
5.6.3)	Mechanism of Inhibition.....	162
5.7)	Conclusion.....	163
CHAPTER 6 : RESULTS AND DISCUSSION.....		169

6.1) Insulation dry out at different temperatures.....	171
6.1.1 Insulation dry-out between the top and bottom parts and effect on CUI rate	172
6.1.2 Insulation dry out between the ends and middle sections	175
6.2 Drying out profile of insulation using galvanic current measurements.....	178
6.2.1 Drying out profile of mineral wool insulation using Electrochemical impedance measurements	185
6.3 Comparison of drying times of galvanic and impedance measurements ..	190
6.4 Conclusions.....	193
CHAPTER 7 : RESULTS AND DISCUSSION.....	196
7.1 Relationship between the input parameters with CUI rate	199
7.1.1 Principal Component Analysis (PCA) Results of CUI Data.....	200
7.1.2 Percentage contribution of input parameters using ANN	204
7.1.3 Mapping of input parameters	207
7.1.4 Relationship of input parameters with CUI rate	209
7.2 Accuracy of ANN in predicting CUI rate of carbon steel.....	211
7.2.1 Comparison of prediction accuracy between Logistic sigmoid and hyperbolic tangent activation functions	212
7.2.2 Effect of network architecture on prediction accuracy of CUI rate	214
7.3 Precision of predicted CUI rate using ANN	219
7.4 Conclusions.....	221
CHAPTER 8: CONCLUSIONS AND FUTURE WORK.....	226
8.1 Conclusions.....	227
8.2 Future works	229

LIST OF FIGURES

Figure 1.1 : Conversion of ore to pure metals and susceptibility to corrosion	2
Figure 1.2: Types of corrosion damage [4].....	3
Figure 1.3: Image of a corroded metal under insulation [8].	4
Figure 1.4: Estimated annual cost of corrosion in affected industries [17]-----	6
Figure 1.5: Overview of the variables in a CUI process.....	7
Figure 1.6: Number of leakages due to CUI in oil and gas industry in Norway [18]....	9
Figure 1.7: Corrosion under insulation management program [27].	12
Figure 1.8: Framework for assessing the possibility of CUI failure [27].	13
Figure 2.1: Fundamental requirements for corrosion of metals to occur	23
Figure 2.2: Electrochemical reactions showing the corrosion of iron [2].....	24
Figure 2.3: Schematic representation of uniform and localized corrosion.	26
Figure 2.4: Pourbaix diagram for an iron-water system, $\alpha_{Fe^{2+}} = 10^{-6}M$ [11].	26
Figure 2.5: The process of condensation within an insulated system-----	29
Figure 2.6: (a) Components of an insulated system [22] (b) Top view of an insulated system showing ingress of water, oxygen, and chlorides.....	29
Figure 2.7: Schematic representation of corrosion under insulation in the presence of oxygen at neutral pH.	30
Figure 2.8: Galvanic corrosion of aluminium/copper couple.....	31
Figure 2.9: Schematic representation showing preferential corrosion of Al in an Al/Cu galvanic couple.	33
Figure 2.10: Equivalent circuit of the Cu-Al electrode system	33
Figure 2.11: Equivalent circuit of a metal-solution interface [34]	36
Figure 2.12: Equivalent circuit of the two-ring system used in this study	37
Figure 2.13: Representation of imaginary impedance, real impedance, and the absolute value of the impedance [37].....	38
Figure 2.14: Typical Bode plot for an electrochemical surface [34]	39
Figure 2.15: Schematic representation of the phase shift between current and potential operating at the same frequency.	40
Figure 2.16: Comparison of artificial neural network with biological neural network [41]	42
Figure 2.17: Components of ANN	44
Figure 2.18: Classification of artificial neural network [47].....	44

Figure 2.19: Representation of a sigmoid function and its derivative	46
Figure 2.20: Representation of hyperbolic tangent function and its derivative	48
Figure 2.21: Mechanism of prediction using ANN-----	51
Figure 3.1: Thermal decomposition products of phenolic resin of mineral wool insulation [25]-----	64
Figure 3.2: : Water absorption of mineral wool samples with different hydrophobic additives using EN13472:2012 standard: samples 1-5 represent mineral oil-based additive, 6 and 7 represent silicone oil-based additive while sample 8 represent inorganic resin [28].	63
Figure 3.3 : Effect of thermal treatment on the absorption of water by mineral wool insulation using ASTM C1511 standard [29].	65
Figure 3.4 : The absorption capacity of mineral wool insulation in different media using EN ISO 12571:2013-12 standard [32].	66
Figure 3.5 : The water absorption of mineral wool board and pipe [33].	67
Figure 3.6 : Schematic representation of ASTM test rig [34].	68
Figure 3.7 : A rain chamber for simulating CUI [35]	71
Figure 3.8: A modified CUI test rig by researchers at Curtin University [36].	72
Figure 3.9: A CUI test rack for field studies [32].	73
Figure 3.10 A modified CUI test rig by Essien and Neville [41]-----	76
Figure 3.11: A plot showing the difference between an isothermal and a cyclic condition	76
Figure 3.12: The corrosion rate of carbon steel under mineral wool insulation for isothermal and cyclic conditions [42].	78
Figure 3.13: CUI rate under isothermal and cyclic conditions [37]	79
Figure 3.14: The effectiveness of a commercial volatile inhibitor in mitigating corrosion under mineral wool insulation wetted with artificial sea water at 80 °C for 14 days [43].	81
Figure 3.15: A comparison of the corrosion rate of carbon steel for the top and bottom rings under mineral wool insulation [36].	82
Figure 3.16: A comparison of the actual and predicted CUI rates using ANN [16]. ..	84
Figure 3.17: A plot showing the prediction accuracy for atmospheric corrosion of carbon steel using ANN [57].	85
Figure 3.18: An ANN architecture showing the input variables [58].	86

Figure 4.1 : Experimental set up for the determination of water absorption capacity of mineral wool.	100
Figure 4.2 : Pictures of mineral wool insulation (a) with aluminium foil removed (b) with aluminium foil intact	100
Figure 4.3: Experimental set up of BS EN 13472:2012 [8]-----	103
Figure 4.4: Experimental set up for BS EN 1609:2013 standard [9]-----	104
Figure 4.5 : A CUI test rig as designed by ASTM G189 [10]	103
Figure 4.6 : Pictures of CUI test rig used in this study (a) without insulation installed (b) with insulation and end caps installed.....	108
Figure 4.7 : A schematic representation of the CUI test rig used in this study.	108
Figure 4.8 : Picture showing the complete set up of the CUI test rig.....	109
Figure 4.9 : Picture of the test rig showing the arrangement of rings and spacers.	109
Figure 4.10 : Temperature program for each cycle used for CUI study.....	109
Figure 4.11 : Flow chart showing the steps involved in the determination of corrosion rate of carbon steel under insulation by weight loss.....	110
Figure 4.12: Determination of the variation of test solution between top and bottom parts of insulation (a) Full insulation showing the axis to be sectioned (b) Insulation sectioned into top and bottom parts (c) Insulation installed around rings (d) Complete set up including use of end caps to hold the insulation together.	111
Figure 4.13 : Determination of the variation in test solution between ends and centre of insulation (a) Full insulation showing the axis to be sectioned (b) An insulation sectioned into three pieces (c) A test rig without the insulation in place (d) A test rig with the three pieces of insulation installed.	112
Figure 4.14 : A schematic diagram showing the application of Lacomit lacquer to the carbon steel rings (a) Application of the lacquer to top part of the ring samples (b) Application of the lacquer to the bottom part of the rings.	114
Figure 4.15 : Top view images of test rig showing (a) lacomit lacquer applied to the bottom part of the rings (b) Lacomit lacquer applied to the top part of the carbon steel ring samples.....	115
Figure 4.16 : CUI test rig showing connections for insulation dry out using galvanic current and electrochemical impedance measurements.	118
Figure 4.17 : Schematic representation of the connections for measurements of insulation dry out using galvanic current and electrochemical impedance measurements.	118

Figure 4.18 : A flow chart showing the steps involved in the modelling process. ...	122
Figure 5.1 : The water absorption profiles (a) Triplicate measurements without preheating the insulation (b) The average absorption of untreated samples (c) Triplicate measurements for insulation treated at 250 °C for 3 h (d) Average of treated samples.....	129
Figure 5.2 : Results showing the long term water absorption test of mineral wool insulation	130
Figure 5.3 : Results showing the water absorption capacity of mineral wool insulation with and without heat treatment at 250 °C for 3h.	131
Figure 5.4: Results showing the long term water absorption of MW insulation obtained in this study and results reported in the literature [4]. All studies were conducted according to ASTM C1511 standard.-----	134
Figure 5.5: Comparison of water uptake of mineral wool board and cylindrical mineral wool used on pipe as reported by Williams and Evans [5] with the results obtained from this study.-----	136
Figure 5.6: (a) Arrangement of the six carbon steel rings (b) Inter-ring average of the corrosion rate across the six rings at all the temperatures investigated. Error bars represent the standard deviation of four replicate measurements.-----	139
Figure 5.7: Average CUI rate of carbon steel under mineral wool insulation at 80 oC [11]-----	139
Figure 5.8: Average CUI rate of carbon steel under mineral wool insulation at 80 oC [12].-----	139
Figure 5.9: Corrosion of mild steel under mineral wool insulation [13].	140
Figure 5.10: (a) Arrangement of the six carbon steel rings (b) Inter-ring average of the corrosion rate across the six rings at all the temperatures investigated. Error bars represent the standard deviation of four replicate measurements.....	137
Figure 5.11 : Temperature variation across the six ring samples.	144
Figure 5.12 : Global average corrosion rates of all the four replicates for the six metal rings (Error bars represent the standard deviation of all the replicates for the six metal rings).....	145
Figure 5.13 : Mechanism of corrosion of insulated carbon steel at different temperatures	146
Figure 5.14 : Comparison of CUI data from this study with the field data showing the effect of temperature on corrosion of metals as reported in ASTM G189 standard.	137

Figure 5.15 : Effect of temperature on corrosion of iron in water [18].....	139
Figure 5.16 : Comparison of the laboratory CUI data from this study with the field CUI data reported in API 581 standard [8].....	139
Figure 5.17: Relationship between the CUI of carbon steel and the operating temperature [8, 20]..	140
Figure 5.18: Corrosion rate as a function of temperature and condition of insulation	142
Figure 5.19: Variation of corrosion depth of carbon steel pipe under calcium silicate insulation with temperature [24].	143
Figure 5.20: Probability of failure of material barrier as a function of temperature [25]	144
Figure 5.21: Plot of mean corrosion rate of insulated carbon steel and inhibition efficiency of VpCI 619 as a function of temperature.....	147
Figure 5.22: Images of carbon steel rings showing the degree of corrosion at 80 °C (a, b) and 95 oC (c, d). Inhibitor was only used in b and d, no inhibitor was applied in a and c.	148
Figure 5.23: Effect of inhibitor dosage of CUI rate	149
Figure 5.24: The mechanism of inhibition of corrosion of insulated carbon steel. ...	149
Figure 6.1 : Quantity of test solution lost between the top and bottom parts of MW insulation at different temperatures.	172
Figure 6.2: Distribution of test solution at the top and bottom parts of the insulation at 80 °C (A) initial weight of insulation (B) Weight after experiment (C) Quantity of test solution lost.	173
Figure 6.3: Comparison of top (section 1) and bottom (section 2) CUI data of Pojtanabuntoeng et al. [1] with the average CUI rate obtained in this study which was carried out at 80 °C. Error bars represent the standard deviation of three replicates.	173
Figure 6.4: Results showing the corrosion rate at the top and bottom parts of carbon steel pipe (UNS G10220) under mineral wool insulation. (A) Pojtanabuntoeng et al. [8] (B) Hou <i>et al.</i> [7].	175
Figure 6.5: Quantity of test solution lost in the inlet (I), middle (II) and outlet (III) regions of mineral wool insulation.	175
Figure 6.6 : Temperature variation across the six rings.....	176

Figure 6.7: A plot of the corrosion rate as a function of the sample position at the different temperatures investigated.	177
Figure 6.8: Estimation of initial (t_0), mid (t_1) and late drying stages (t_2)-----	181
Figure 6.9: A plot of galvanic current density (A/cm ²) against drying time (seconds) at different temperatures (primary axis) and temperature ramp against time (secondary axis). The vertically dotted lines of each colour correspond to the colour of each trial, which represents the estimated time where drying of the insulation is initiated.-----	183
Figure 6.10: Average drying times estimated from the galvanic current density-time profile at different temperatures-----	184
Figure 6.11: Galvanic current density-time profile for the top, bottom and lateral sections of the insulation at 100 °C.-----	186
Figure 6.12: Average drying time estimated from the galvanic current density-time profile in Figure 6.7.-----	186
Figure 6.13: Impedance-time plot showing an estimation of the different drying times-----	188
Figure 6.14: Impedance-time plot and phase versus time plot at different temperatures (T).-----	189
Figure 6.15: Plot showing the drying stages at different temperatures-----	190
Figure 6.16: An impedance-time plot for mineral wool insulation wetted with 0.5 M NaCl and water at 40 °C at a frequency of 100 kHz [10].-----	191
Figure 6.17: An electrochemical impedance plot showing the drying times of wet mineral wool insulation installed on carbon steel rings at a frequency of 10 kHz (a) without drain holes (b) with drain holes [11]-----	191
Figure 6.18: Solution resistance values showing the drying of mineral wool insulation-----	192
Figure 6.19: A comparison of the drying times of the galvanic current (G.C.) and impedance measurements (E. I.).-----	193
Figure 6.20: A comparison of the change in drying times of both galvanic current and impedance methods with the change in corrosion rate at 70 °C, 80 °C and 110 °C-----	194
Figure 7.1 : (a) An Orthogonal component plot of CUI data (b) A Scree plot showing the decreasing order of significant data in each component	203

Figure 7.2 : Significance plot of the input parameters (a) Data sets including inhibitor (b) data without inhibitor	205
Figure 7.3 : Feedforward ANN architecture with a single hidden layer with j nodes used in this study (b=bias, w= synaptic weight, n=nodes).....	207
Figure 7.4 : Relationship between the input parameters and the hidden layer for hyperbolic tangent activation function (a) with inhibitor (b) without inhibitor (TS=amount of test solution in insulation, SP= sample position, CR=corrosion rate).	210
Figure 7.5 : The relationship of the input parameters at the input layer for a logistic sigmoid activation function (a) with inhibitor (b) without inhibitor (TS=amount of test solution in insulation, SP= sample position, CR=corrosion rate).	211
Figure 7.6: A comparison of the predicted and experimentally determined CUI rates estimated using Logistic sigmoid activation function (a) 4 input parameters (DI, T, TS and SP), (b) 3 input parameters (DI, T, TS), (c) 2 input parameters (DI and T).	213
Figure 7.7 : A comparison of the predicted and experimentally determined CUI rates estimated using hyperbolic tangent activation function (a) 4 input parameters (DI, T, TS and SP), (b) 3 input parameters (DI, T, TS), (c) 2 input parameters (DI and T)	213
Figure 7.8 : Network architecture used in this study (a) single hidden layer and (b) double hidden layers	214
Figure 7.9 : Comparison of the prediction accuracy of (a) A single hidden layer and (b) A double hidden layer for logistic sigmoid activation function	215
Figure 7.10 : Comparison of the prediction accuracy of (a) A single hidden layer (b) A double hidden layer for hyperbolic tangent function.	216
Figure 7.11 : Predicted weight loss (mg) versus actual weight loss (mg) of atmospheric corrosion of carbon steel using 12 neurons in a single hidden layer [19].	217
Figure 7.12 : Predicted weight loss (mg) versus target weight loss (mg) of mild steel in marine environment [20]......	217
Figure 7.13 : Predicted and actual corrosion rates of carbon steel (mm/yr) using ANN [22].	218
Figure 7.14 : Repeatability of the CUI rate prediction using logistic sigmoid activation function with one hidden layer.....	219
Figure 7.15 : Repeatability of the CUI rate prediction using hyperbolic tangent activation function with one hidden layer.....	220

LIST OF TABLES

Table 1.1: Failure due to corrosion under insulation and impacts	10
Table 2.1: Galvanic series of metals and alloys in seawater [30]	34
Table 3.1 : Comparison of the four standards used in determining the water absorption characteristics of thermal insulation materials.	63
Table 3.2 : Suggested times for isothermal and cyclic conditions [30]	76
Table 3.3: Comparison of predicted and experimental corrosion rates [54]	86
Table 4.1 : Properties of mineral wool insulation ('RockLap' from Rockwool) as described in the product data sheet [4].	98
Table 4.2 : Chemical composition of mineral wool insulation as described in the product data sheet [5].....	98
Table 4.3 : Chemical composition of the carbon steel pipe used in this study [21].	107
Table 4.4 : Chemical composition of Lacomit lacquer and remover [22].	115
Table 4.5 : Properties of VpCI 619 inhibitor as reported in the safety data sheet [23]	117
Table 5.1 : Available laboratory data showing corrosion rate of carbon steel under mineral wool insulation at a fixed temperature	140
Table 5.2 : Global average and standard deviations of corrosion rate with increasing temperature.....	143
Table 5.3 : Comparing the average corrosion rates in the presence and absence of the inhibitor as well as inhibition efficiencies.	156
Table 5.4 : Average corrosion rate (mm/yr) of carbon steel with different dosage of inhibitor.....	159
Table 5.5: Cost analysis of inhibitor for a given area of insulation.....	160
Table 5.6 : Performance of inhibitors for CUI	161
Table 6.1 : Drying times (minutes) of insulation at different temperatures.....	182
Table 7.1 : PCA table showing the correlation coefficients between each component and the variables studied	201
Table 7.2 : Importance of the input variables	205
Table 7.3 : Summary of studied parameters and the corresponding coefficient of determination	220

LIST OF SYMBOLS AND MEANING

Symbols	Meaning
e^-	electron
i_{corr}	corrosion current density (A/cm^2)
Σ	Summation
f	function
h	hidden layer
w_i	weight of input parameter
x_i	ith input parameter
b	bias
y_a	Actual output
y_o	Predicted output
<	less than
>	greater than
Δ	change
T	Time (Mins)
A_r	Area (cm^2)
ρ	Density (g/cm^3)
I	Current (A)
V	Voltage (V)
Z	Total impedance (Ω)
Z'	Real part of the impedance (Ω)
Z''	Imaginary part of the impedance (Ω)

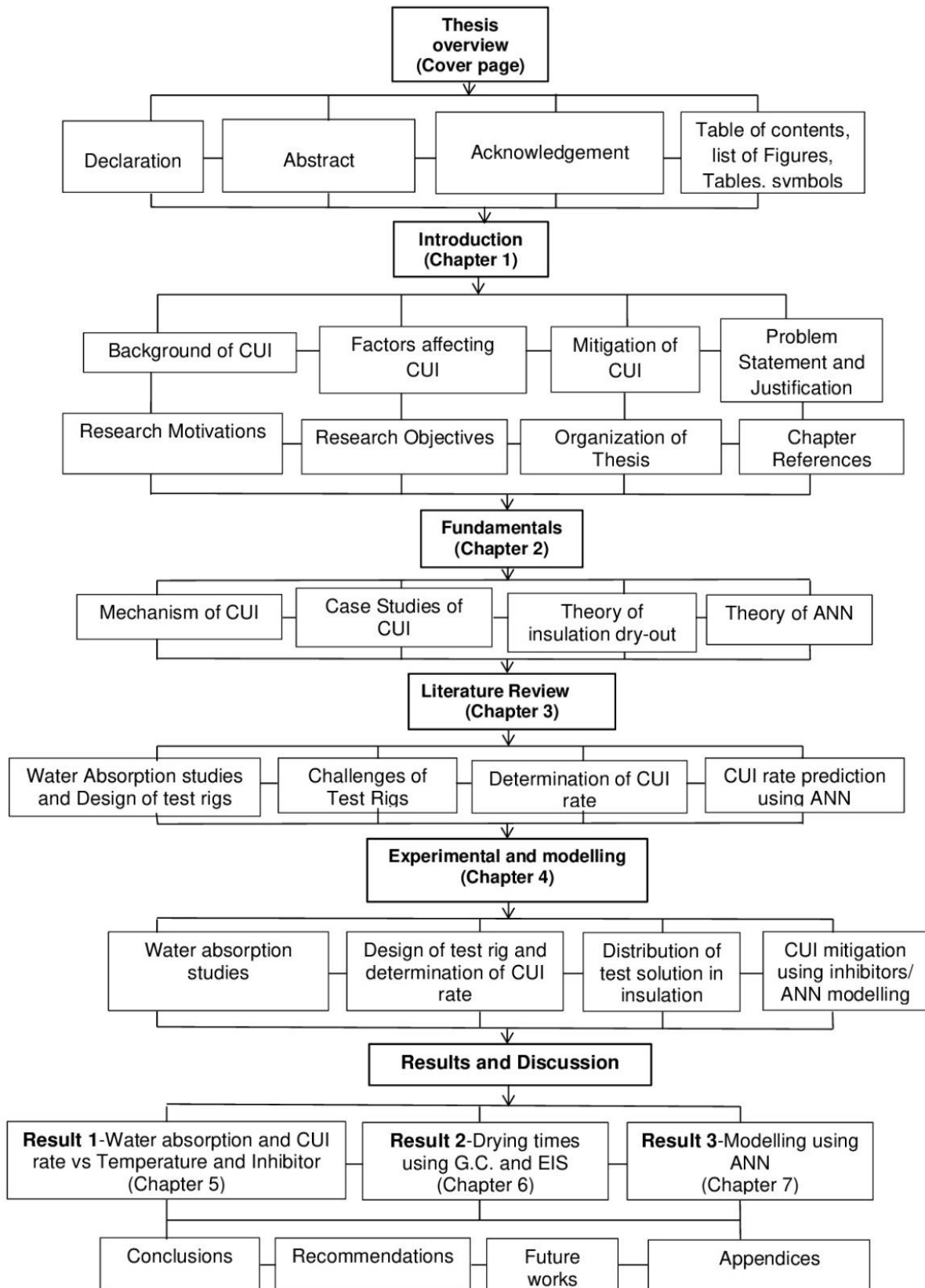
R_s	Solution resistance (Ω)
R_p	Polarization resistance (Ω)
R_{ext}	External resistance (Ω)
I_g	Galvanic current (A)
ω	Angular frequency (rad/s)
θ	Phase angle ($^\circ$)
I_R	Resistive current (A)
I_C	Capacitive current (A)
C_{dl}	Double layer capacitance (F)
R_T	Total resistance (Ω)
A	Anode
C	Cathode
α	Activity (M)

LIST OF ABBREVIATIONS

Abbreviation	Meaning
CUI	Corrosion under insulation
CR	Corrosion rate
ANN	Artificial neural network
G.C.	Galvanic current
E.I.	Electrochemical impedance
M.S.E.	Mean square error
S.D.	Standard deviation
PCA	Principal component analysis
VpCI	Vapour phase corrosion inhibitor
ASTM	Association of Standard Test and Materials
BS EN:	British standard adopted by European nations
PTFE	Poly tetrafluoroethylene
DI	Deionized water
IPA	Isopropyl alcohol
API	American Petroleum Institute
MSDS	Material Safety Data Sheet
PDS	Product data sheet
NR	Not reported
ppm	parts per million
SP	Sample Position
TS	Test Solution

IBM	International Business Machine
Sg(x)	Sigmoid function
Tanh(x)	Hyperbolic tangent function
Id(x)	Identity function
PoF	Probability of failure
Li(x _i)	Linear combination of x variables
DT	Drying time

THESIS LAYOUT



CHAPTER 1 : INTRODUCTION

CHAPTER ONE

INTRODUCTION

1.1) Definition of corrosion

Corrosion is the deterioration of a material as a result of its chemical or electrochemical reaction with the environment [1]. The corrosion of metals is a hybrid process involving chemical reactions and electron transfer occurring between the metal and its environment [2]. Although corrosion is possible with different materials, this study will particularly focus on corrosion of metals or alloys. For corrosion to occur, there must be an anode where metal oxidation takes place, a cathode where reduction of species occurs, an electrolytic path for transport of ions and electronic pathway for transport of electrons [3]. Naturally, most metals exist as oxides and lots of energy is required to convert it to the metallic state. Although most metals are more useful when processed, however, they have a natural tendency to return to its original state (lower energy state) in the presence of favourable conditions which is the reason why metals corrode as shown in Figure 1.1.

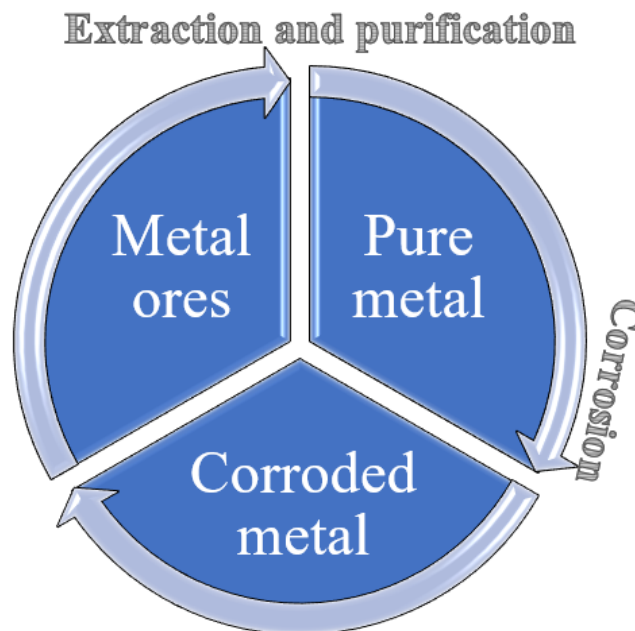


Figure 1.1 : Conversion of ore to pure metals and susceptibility to corrosion

1.2) Types of corrosion damage

Corrosion can occur in different forms as shown in Figure 1.2. This could be uniform corrosion which takes place when the attack on the metal occurs throughout the entire surface. In this case, the anodes and cathodes are not fixed but are changing at any given time resulting in deterioration across the entire metallic surface. On the other hand, it is also possible to have localised corrosion such as pitting where degradation is restricted to a certain location. This is often characterised by fixed anodic and cathodic points [4]. In addition, corrosion accompanied by mechanical stress will result in stress corrosion cracking, while metals with different electrode potentials would result in galvanic corrosion if they were in direct contact with each other. In this case, the less noble metal will preferentially corrode. Intergranular corrosion occurs when the attack on the metal occurs at the grain boundaries while crevice corrosion occurs due to differences in oxygen availability [3]. Selective leaching occurs when one of the components of the alloy dissolves under certain conditions, while erosion corrosion arises from a combination of electrochemical reaction and mechanical wear which may be caused by solids or a flowing liquid [4].

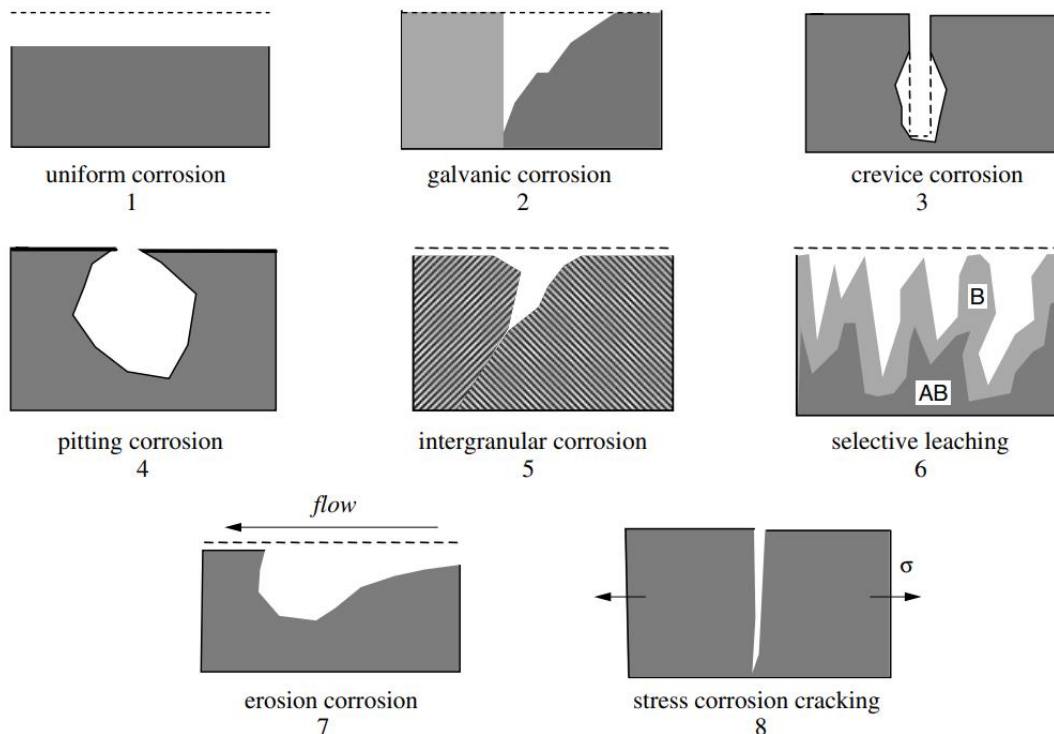


Figure 1.2: Types of corrosion damage [4]

1.3) Background of corrosion under insulation

Corrosion under insulation (CUI) is a special case of corrosion which takes place beneath the insulation due to the ingress of water and contaminants such as chlorides [5]. An insulated metal system comprises of an outer jacketing, the insulation material, and a metal substrate which may be coated or uncoated. The term 'corrosion under insulation' is usually used to refer to degradation occurring at the external surface of metals as shown in Figure 1.3. The metal is hidden underneath the insulation making it difficult to access unless the insulation is removed for visual inspection which is quite time consuming and expensive. The fact that the insulation covers the underlying metal and hides it from view implies that degradation may proceed unnoticed, potentially leading to severe consequences [6]. The challenging aspect is that CUI is a continuous issue rather than a one-off problem [7].

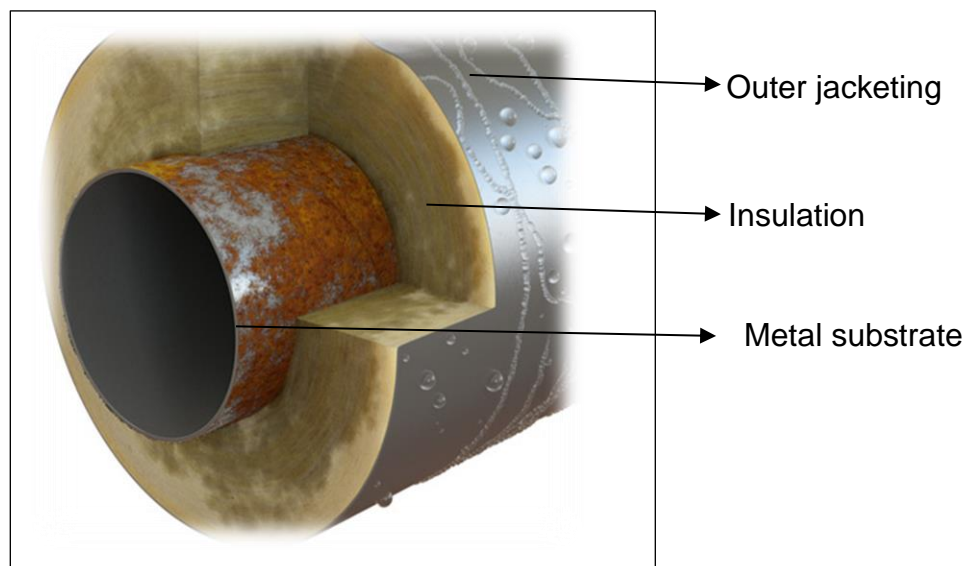


Figure 1.3: Image of a corroded metal under insulation [8].

The corrosion of insulated metals is influenced by a combination of factors such as temperature, quality of insulation, quantity and distribution of electrolyte in the insulation, chemical composition of the insulation among others. The root cause of CUI is the penetration of water through the insulation to the surface of the metal [5]. This can take place externally where the insulation has not been properly installed or where there is a breach giving opportunity for water to enter the insulation. In this case, sources of water ingress could be rain, snow, dew, and other forms of precipitation. In

addition, there could be condensation occurring internally due to temperature difference at the insulation-metal interface which might occur when air is cooling down at a temperature below the dew point [9]. In a three-tier configuration, the dew point is the temperature at which the first change from the gaseous phase to the liquid phase is observed, this is crucial to the formation of water film or droplets on the surface of the metal [10]. The entrapment of moisture beneath the insulation culminates in the corrosion of the metal especially if there was no form of additional protection.

Corrosion under insulation is a challenging problem for the oil and gas industry as well as other chemical industries [11]. The risks associated with CUI can range from leakages to explosions which does not only affect normal operations but also puts the lives of personnel at risk. It has been reported that there is a yearly increase in the number of accidents due to loss of containment in different countries which mounts lots of pressure on chemical companies in the bid to mitigate these occurrences [12]. Moreover, failure analyses of these occurrences in industry have revealed that most of the severe incidences were traced to CUI [13, 14].

Furthermore, removal of insulation for visual inspection is not economically feasible as well as being time consuming and requiring lots of effort and risks of exposing the substrate to moisture if not properly reinsulated. Moreover, corrosion under insulation has been reported to have significant economic implications for industries. For example, a leakage from a 4" pipe in a petrochemical plant in USA which culminated in fire was traced to corrosion under insulation, which cost the company \$50 million [15]. In addition, a study conducted by Exxon Mobil in 2003 has revealed that 40-60 % of leakages in the oil and gas industry were attributed to CUI [16]. An estimate of the corrosion cost in different industries as reported by the American Society of Civil Engineers (ASCE 2013) is shown in Figure 1.4.

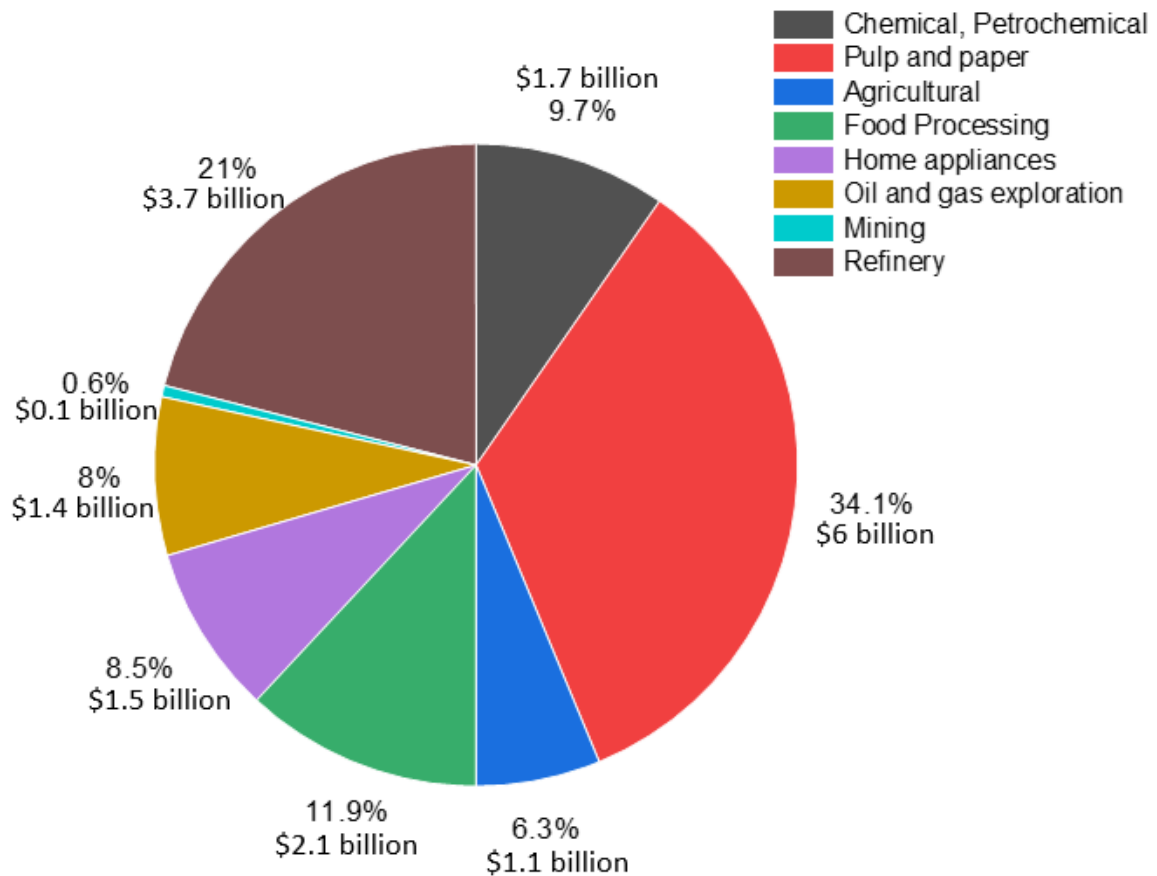


Figure 1.4: Estimated annual cost of corrosion in affected industries [17]

These undesirable occurrences associated with insulated metals which has enormous consequences begs the question why insulation should be used on metals in the first instance. Insulation is needed in industry to control process conditions such as temperature or conserve energy, it can also be used to protect personnel from direct contact with metal surfaces [16]. The need for insulation in industry based on these reasons should be balanced by adequate inspection and maintenance plans to ensure that the structural integrity of insulated metals is maintained to avoid failure due to corrosion. The potential problems associated with CUI should be factored in during planning and regular reviews. Besides, adequate risk assessment regarding asset integrity should be frequently carried out to ensure that degradation is identified early and attended to before it escalates. Although there are various inspection methods for CUI which may not require removal of insulation, there are still lots of challenges associated with these techniques which are reported by Amer *et al.* [18]. Therefore, there is need to quantify the rate of corrosion under insulation which would give an

overview of the extent of damage needed to make informed decision about the potential risks.

1.4) Factors affecting the occurrence of CUI

The major factors influencing the occurrence of CUI include water, contaminants such as chlorides, temperature, and quality of insulation. Water can enter the insulation due to poor installation or damage to the insulation. During installation, difficult areas such as bends, welds, joints, and junctions are the challenging areas that usually serve as entry points of water into the insulation system. This is because these areas are quite complex and require expertise to ensure that they are installed correctly. Water from different forms of precipitation may enter the insulation and migrate to the metal surface where they are trapped and prolonged contact with the metal surface might result in CUI. Moreover, the presence of chlorides in the water could also aggravate CUI. Chloride can also be leached from the insulation when water penetrates it, especially if the metal is operating under cyclic conditions.

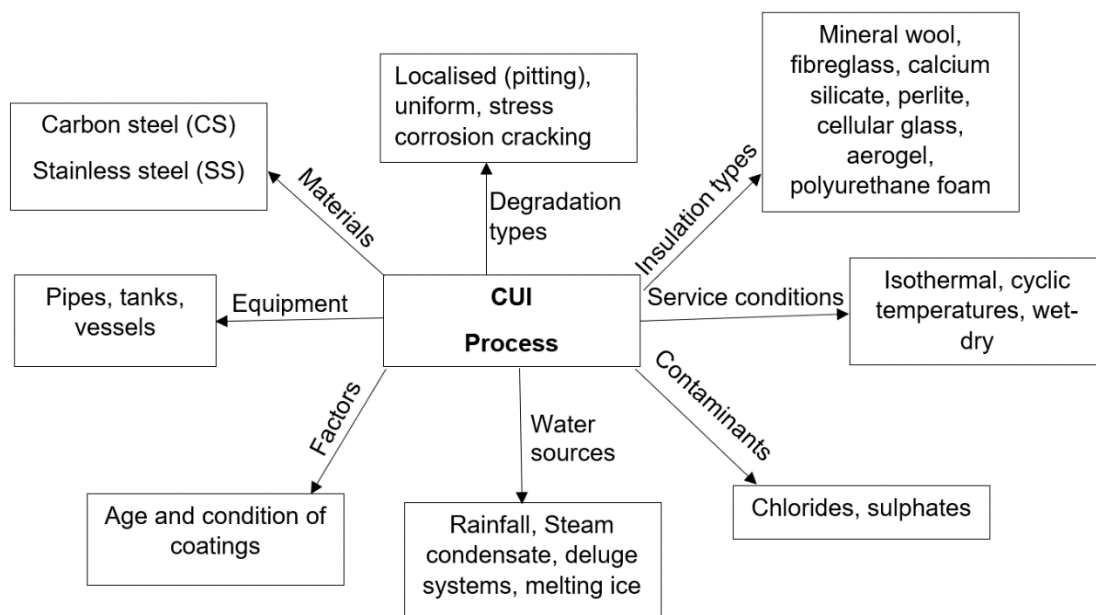


Figure 1.5: Overview of the variables in a CUI process

In addition, the operating temperature of pipe could also lead to the occurrence of CUI. De Vogelaere [9] has identified two different temperatures that could initiate CUI. This include: service temperatures operating between 0 °C and 100 °C where water is expected to exist as a liquid and cyclic temperature involving a switch between two

extreme temperatures [9]. In transporting gas from one site to another in an insulated pipe, temperature has been identified as a critical factor to be considered when assessing the possibility of CUI [19]. In fact, the temperature range where aggressive CUI should be expected on carbon steel and stainless steel include 50 °C to 175 °C [19]. Also, the quality of the insulation can also influence the occurrence of CUI. It is expected that insulation materials used in chemical industries should be hydrophobic. Different insulation materials have different water absorption and retention capacities. Therefore, it is important that these qualities be assessed when considering the choice of insulation materials.

1.5) Typical incidence of CUI in different chemical plants

In this section, typical examples of corrosion under insulation are discussed. The adverse impacts of CUI to chemical industries are two-fold, this include economic concerns involving production loss, and safety concerns where the environment and human life are at risk [16]. Incidences of CUI have been reported in different chemical industries which includes leakage of ammonia in 2004 at Yara's chemical facility, which was caused by corrosion of an insulated elbow joint resulting in a significant loss of chemicals [16] as presented in Table 1.1. Statistics provided by Exxon Mobil in 2003 indicated that 40-60 % of failures in oil and gas industry is due to CUI [15, 13]. This resonates with the recent DNV report that 50% of the leakages in chemical industry in Norway is caused by CUI as shown in Figure 1.6.

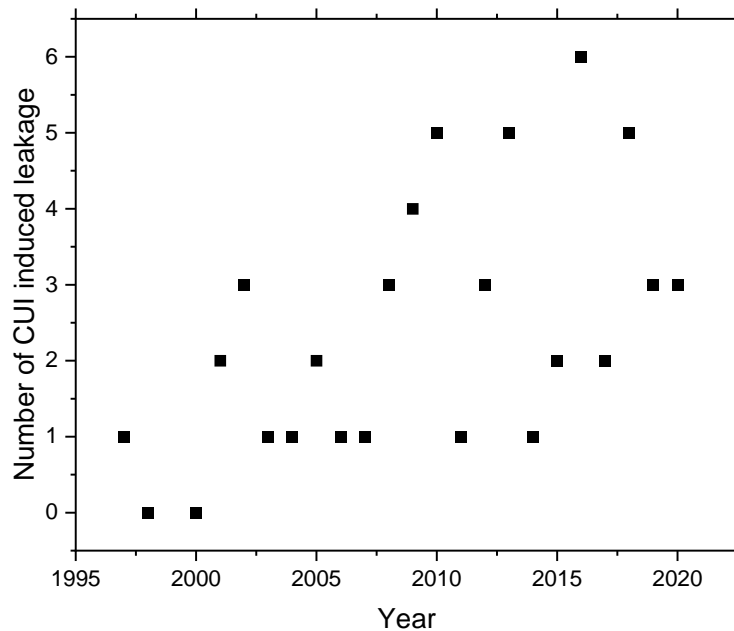


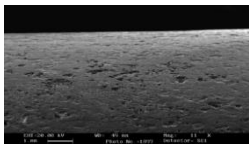



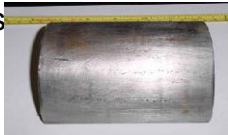
Figure 1.6: Number of leakages due to CUI in oil and gas industry in Norway [18]

Figure 1.6 shows the frequency of CUI induced leakages in the oil and gas industry in Norway as reported by Amer *et al.* [18]. The report indicates repeated fluctuations in the number of CUI induced leakages in chemical industries every year from 2001 till 2020. The fact that CUI induced leakage is observed every year for ten years implies that CUI is a serious issue which needs to be frequently observed to avoid undesirable occurrences.

Other CUI related incidences as well as the cause of failure as reported in different literatures are summarized and presented in Table 1.1. The main cause of failure presented in these reports include ingress of water and chloride ions into the insulation, which resulted in continuous wall loss of the metal till leakage occurs. The consequences include gas fires as well as leakages which poses environmental and health concerns. For instance, in 2006, a leak was reported in an aging petrochemical plant, which was attributed to CUI, this culminated in a fire that burnt half the processing unit, incurring a cost of about USD 50 million including an irreversible damage to the environment [5]. This suggests that CUI comes with enormous consequences and adequate understanding of the causes of CUI including factors that

aggravate it could help in developing preventive measures to avoid unexpected failures. A summary of the failure occurrences due to CUI is summarized in Table 1.1.

Table 1.1: Failure due to corrosion under insulation and impacts

Examples of failure in process facilities	Reasons for failure	Impacts	References
Hydrogen pipeline insulated with glass wool. 	The presence of chloride ions under the foil of the glass wool insulation.	Leakages were observed in service.	[19]
A pipeline under Insulation. 	Water was observed to enter the insulation due to poor installation.	There was a fire outbreak.	[20]
A transport pipe under Insulation. 	The quality of the insulation was poor.	Leakages were observed in service.	[16]
A pipeline conveying ammonia 	The insulation was damaged	Gas fire	[16]
Stainless steel cracks after being removed from mineral wool insulation. 	Chloride ions was observed to leach from the insulation.	Contents leaked out.	[21]
Corrosion along the bending region of insulated carbon steel.	Penetration of water due to poor installation.	Increased wall thinning.	[22]

1.6) Strategies to mitigate corrosion of metals under insulation

The accumulation of water underneath the insulation is the main cause of CUI in industry. These are influenced by the type of insulation, the design of the equipment, maintenance, and inspection schedule, as well as presence of any first line of defence such as paints or coatings [23]. Corrosion under insulation has been managed using

methods that is aimed at mitigating its effect. Such methods include the use of inhibitors [24], cathodic protection [25], and the use of coatings [26] to avoid direct contact of water with the surface of the metals. This is because it seems there is no one-off solution that could completely eradicate the problem of CUI. At best, proactive measures of reducing the likelihood of water penetration are usually employed for new installations or adequate management strategy are used for existing structures. The requirements of some of these measures of mitigating CUI has been discussed extensively in the literature [20]. Among these methods of mitigating CUI, the focus of discussion will be on the use of inhibitors. This is because that is the most studied method which may be quite cost effective depending on the type of inhibitor.

Corrosion inhibitors are chemical substances that retard the rate of the reactions leading to corrosion. The reactions culminating in corrosion involve anodic dissolution of the metal giving out electrons which migrate to the cathode areas and are consumed in the reduction of oxygen to water if the medium is a neutral solution. The inhibitor that mitigates the anodic reaction is regarded as anodic inhibitors or passivators which forms a film of oxide on the surface of the metal preventing further dissolution of the base metal [21]. Example of anodic inhibitors include molybdates, chromates, nitrates etc. Cathodic inhibitors inhibit the reactions at the cathode by forming a protective coating for example sodium pyrophosphate [21]. Some inhibitors may have potential to inhibit both anodic and cathodic reactions, these are called mixed inhibitors. The inhibitors may be applied to the insulation or the metal, which forms a film at the insulation-metal interface preventing direct contact of water with the metal. The method of application should ensure uniform distribution of the inhibitor at the metal surface to ensure effective protection [22].

1.6.1) Corrosion under insulation management program

CUI management programs include activities carried out to assess the possibility of CUI and ways to tackle it. This is usually aimed at reducing the risks of failure to an accepted level which could be beneficial to industry as it guarantees safety, reliability, and cost reduction [27]. CUI management process involves risk assessment, mitigation, update, and systematic experience transfer [28]. Risk assessment involves inspecting the insulated metal or assessing the corrosion rate, while risk mitigation

involves approach to reduce the likelihood of failure which includes the use of inhibitors, coatings, cathodic protection amongst others. Risk update involves a review of all risks that have been identified and places it in order of priority as well as tracks the mitigation progress, while experience transfer is a systematic way of reducing the likelihood of failure by experts after assessing all the possible options [28]. There are two broad perspectives to explore when discussing CUI management process. First, the possibilities that CUI could exist under the present conditions and the likelihood that it might soon result in failure. A typical procedure to determine the existence of CUI and the likelihood of failure due to CUI are shown in Figure 1.7 and Figure 1.8.

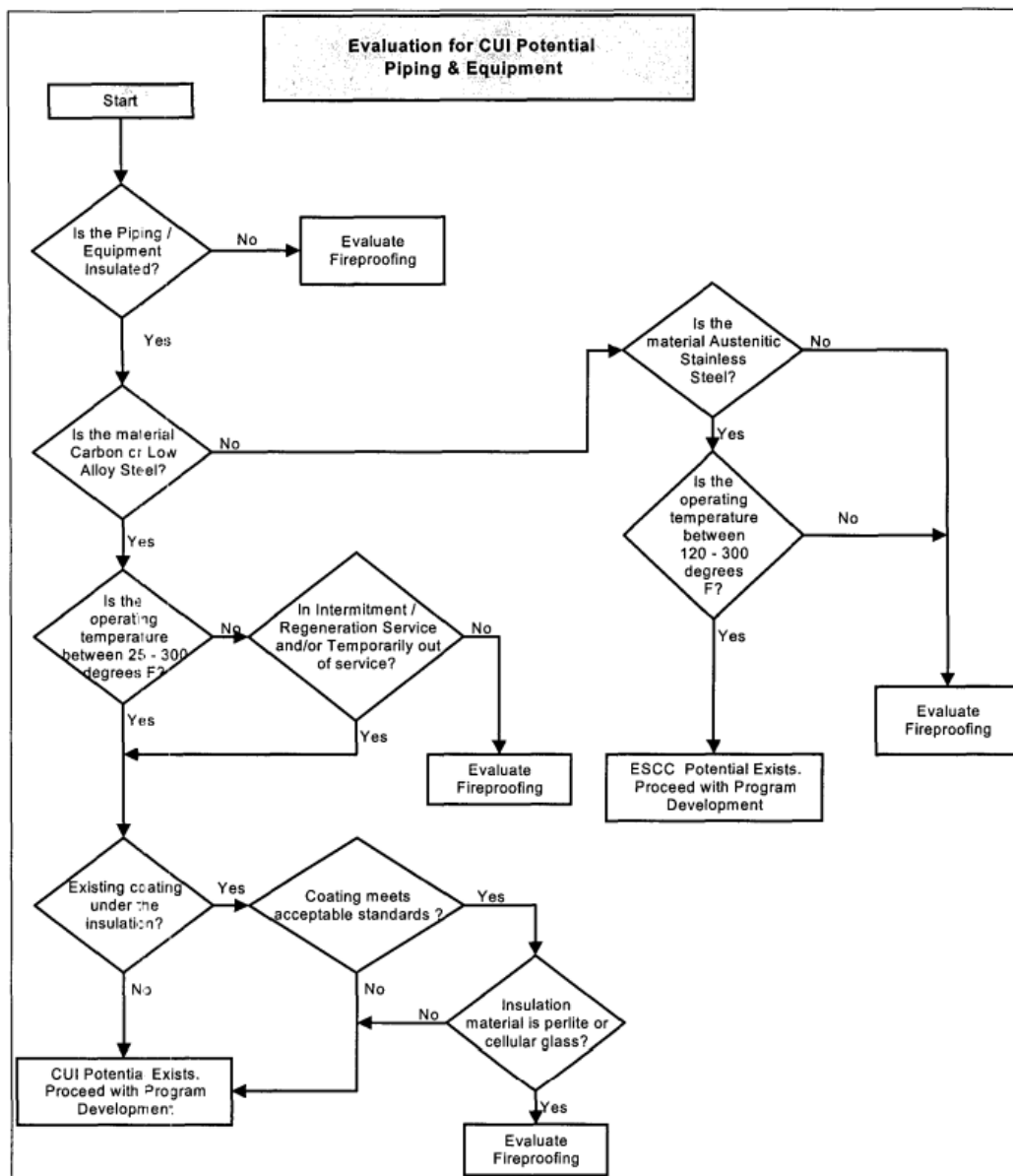


Figure 1.7: Corrosion under insulation management program [27].

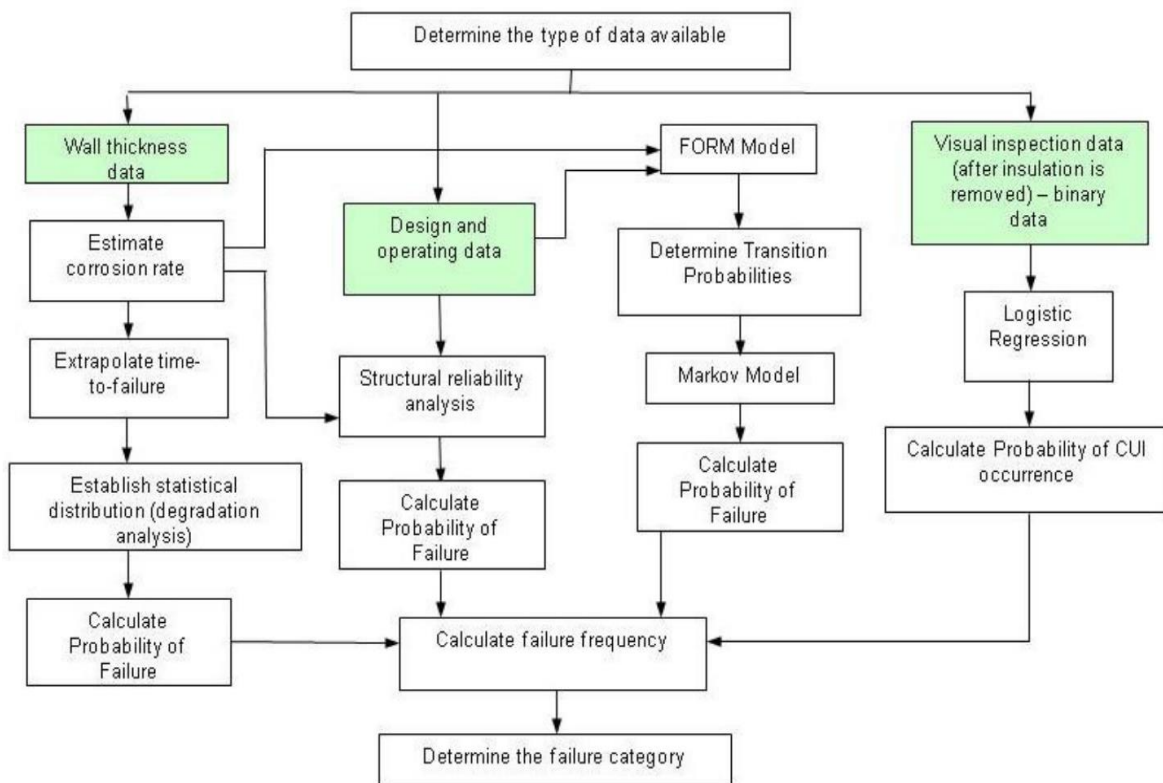


Figure 1.8: Framework for assessing the possibility of CUI failure [29].

In Figure 1.7, the possibility of CUI depends on the type of metal, operating conditions, and the presence of any additional protection such as coatings or inhibitors. Carbon steel or low alloy steel without any additional protection and operating between the temperature range of $-4\text{ }^{\circ}\text{C}$ and $60\text{ }^{\circ}\text{C}$ are likely to be susceptible to CUI [27]. On the other hand, assessing the likelihood of failure due to corrosion under insulation depend on the type of data available. The probability of failure can be calculated from quantitative CUI data using degradation analysis models and time to failure can be extrapolated from the results [29]. In addition, the likelihood of CUI failure can also be estimated from qualitative data obtained from visual inspections which can be used to ascertain the severity of corrosion and identify measures to mitigate its effects.

1.7) Problem statement and justification

Corrosion under insulation is a serious issue for the oil and gas industry as well as other chemical industries. CUI is hidden under the insulation which implies that degradation can proceed unnoticed till failure becomes imminent. A number of factors such as quality of insulation, temperature of the metallic substrate (skin temperature), presence of chemical contaminants such as chlorides can have significant impact on CUI. The fact that the fluid flowing through insulated pipes are usually at targeted temperatures implies that there is need to investigate the effects of different temperatures on CUI. In addition, the water absorption capacity of insulation also determines the severity of CUI. Therefore, there is need to investigate measures of mitigating the effects of CUI as well as assessing the possibilities of predicting the occurrence of CUI using mathematical models which serves as a proactive step towards mitigating the adverse effects of CUI.

1.8) Motivations for the research

The severity of corrosion under insulation in terms of the risks it imposes on humans and the environment is one of the key motivations for this research. Moreover, there has been dearth of information regarding key factors that causes CUI. For instance, there has been scarcity of laboratory data showing the trend of temperature with CUI rate. The available data in the literature on effect of temperature on CUI rate were either reported at two temperature points for wet/dry cycle [6, 16], or at most 3 temperature points when testing for the effectiveness of protective coatings [25] which cannot be used to form a trend. Most of the temperature trends on CUI found in the literature were measured in the field [16]. However, field data cannot be relied upon because temperature is difficult to control under field condition. In addition, study of CUI mitigation using inhibitors is quite scarce. Most of the inhibitors reported in the literature are mostly organic inhibitors used in uninsulated conditions [21].

Moreover, the time of wetness of the insulation is likely to have significant effect on the corrosion process; therefore, there is need to assess the drying times of the insulation using electrochemical techniques. In addition, the ability to predict corrosion rates obtained in the laboratory using mathematical models employed in artificial

neural network could be quite useful in estimating the corrosion rates of metals in the field based on the prevailing conditions. This could serve as a proactive measure of preventing undesirable occurrences due to CUI. Therefore, the precision and accuracy of different network architectures of artificial neural network such as number of hidden layers, choice of activation function and number of input parameters in predicting corrosion under insulation were carried out. These parameters could serve as a useful starting point to consider when building a neural network to solve a CUI problem in the industry.

1.9) Objectives of the study

The main objectives of this study include the following:

- ❖ To determine the water absorption capacity of mineral wool insulation which will provide information on the time it takes to be saturated with water.
- ❖ To determine the effects of temperature ranging from 60 °C to 130 °C on CUI, which includes the range where aggressive CUI has been reported.
- ❖ To assess the water distribution in mineral wool insulation as well as the drying out times using galvanic current and electrochemical impedance measurements.
- ❖ To investigate the effectiveness of a new commercial inhibitor (VpCI 619) in mitigating corrosion of carbon steel under insulation.
- ❖ To assess the accuracy and precision of Artificial Neural Network in predicting corrosion of carbon steel under mineral wool insulation.

1.10) Organisation of thesis

This thesis is structured to provide an overview of the research and the results that were obtained. The thesis has 8 chapters, details of each chapter is summarised as follows:

Chapter 1 introduces the background information of corrosion under insulation, factors affecting CUI as well as measures to mitigate the effects of CUI. In addition, the chapter also highlights the problems posed by CUI and the need to undertake the research.

Chapter 2 discusses the fundamental concepts of corrosion of iron and its mechanisms. Also, the theory of insulation dry-out using galvanic current and impedance measurements as well as theory of CUI prediction using artificial neural network are also covered.

Chapter 3 reviews the available literature on corrosion of carbon steel under mineral wool insulation. This covers water absorption studies, effects of temperature and inhibitors on CUI, as well as prediction accuracy of CUI using Artificial neural network.

Chapter 4 provides details of the experiments including water absorption capacity of mineral wool insulation, the design of the test rig used in this study, effects of temperature, distribution of electrolyte in insulation, drying out, as well as inhibitors on CUI rate. Also, the steps in carrying out CUI rate predictions using ANN are also discussed.

Chapter 5 presents the results of water absorption capacity of mineral wool insulation including the effects of temperature, dosage of inhibitor on CUI. Also, the available field data on the effect of temperature on CUI are discussed.

Chapter 6 presents the results of the water distribution in mineral wool insulation, quantification of the CUI rate between the top and bottom parts of carbon steel rings as well as the drying times of the insulation using galvanic current and electrochemical impedance measurements.

Chapter 7 discusses the results of CUI rate predictions using Artificial Neural Network including the effect of number of hidden layers, choice of activation function, number of input parameters and repeatability of predictions.

Chapter 8 provides a general conclusion of the research and future works that could further expand the research.

In addition, some appendices are attached at the end of the thesis, including the results that were omitted from the body of the thesis which included replicate measurements of the results and some calculations that were carried out.

Chapter References

1. Revie, W. R. and Uhlig, H. H. (2008). Corrosion and Corrosion Control. 4th edition, John Wiley & Sons Inc., Hoboken, New Jersey, USA.
2. Tait, W. S. (2018). Electrochemical corrosion basics. Handbook of environmental degradation. 3rd edition, Applied Science publishers, USA., pp. 97-115.
3. Kelly, R. G., Scully, J. R., Shoesmith, D. W. and Buccheit, R. G. (2003). Electrochemical techniques in corrosion science and engineering. Marcel Dekker Inc., New York, pp. 2-436.
4. Landolt, D. (2007). Corrosion and surface chemistry of metals. 1st edition, EPFL press, Lausanne, Switzerland, p. 286.
5. Cao, Q., Pojtanabuntoeng, T., Esmaily, M., Thomas, S., Brameld, M., Amer, A., Birbilis, N. A. (2022). Review of corrosion under insulation: A critical issue in the oil and gas industry. *Metals*,12:561.
6. Caines, S., Khan, F., Shirokoff, J. and Qiu, W. (2015). Experimental design to study corrosion under insulation in harsh marine environments. *Journal of Loss Prevention in the Process Industries*, 33:39-51.
7. Morey, A. (2018). Corrosion under insulation revisited: Aren't we about to finish that project? *Process Safety Progress*, 37(4):502-505.
8. Armacell (2018). Best in test: ArmaFlex insulation materials reduce the risk of corrosion under insulation (CUI). <https://local.armacell.com/en/armacell-switzerland/about-us/news/press-releases/detail/view/best-in-test-armaflex-insulation-materials-reduce-the-risk-of-corrosion-under-insulation-cui/>, date accessed 23rd January 2023.
9. De Vogelaere, F. (2009). Corrosion under Insulation. *Process progress safety*, 28:30-35.

10. Huijbregts, W. M. M. and Leferink, R. (2004). Latest advances in the understanding of dew point acid corrosion: Corrosion and stress corrosion cracking in combustion gas condensates. *Anticorrosion Methods and Materials*, 51:173-188.
11. Scanlan, R., Valbuena, R. and Harrison, I. (2008). A refinery approach to address corrosion under insulation and external corrosion. NACE publications, paper number 08558.
12. Funahashi, M. (2014). Solution to CUI with three layered control and warning systems. NACE publications, paper number 4079.
13. Geary, W. (2013). Analysis of corrosion under insulation failure in a carbon steel refinery hydrocarbon line. *Case Studies in Engineering Failure Analysis*, 1:249-256.
14. Marquez, A., Singh, J. and Maharaj, C. (2021). Corrosion under insulation examination to prevent failures in equipment at a petrochemical plant. *Journal of Failure Analysis and Prevention*, 21:723-732.
15. Javaherdashti, R. (2014). Corrosion under Insulation (CUI): A review of essential knowledge and practice. *Journal of Material Science and Engineering*, 2(1):1-8.
16. Caines, S., Khan, F., Shirokoff, J. and Qiu, W. (2015). Experimental design to study corrosion under insulation in harsh marine environments. *Journal of Loss Prevention in the Process Industries*, 33:39-51.
17. The American Society of Civil Engineers (2013). Infrastructure Report Card. <https://energyskeptic.com/2016/corrosion-eats-552-billion-infrastructure-per-year-6-pct-of-gdp-billion-cost-per-year-6-of-gdp/>, date accessed 1st October 2023.
18. Amer, A., AlShehri, A., Cunningham, V., Taie, I. (2018). Inspection challenges for detecting corrosion under insulation (CUI) in the oil and gas industry. NACE publications, paper number 12400.

19. Cao, Q., Pojtanabuntoeng, T., Esmaily, M., Thomas, S., Brameld, M., Amer, A., Birbilis, N. A. (2022). Review of corrosion under insulation: A critical issue in the oil and gas industry. *Metals*,12:561.
20. Dunn, P. J., and Norsworthy, R. (2003). Control of corrosion under insulation. *ASHRAE Journal*, 45(3):32-40.
21. Nam, N. D., Hien, P. V., Hoai, N. T. and Thu, T. H. (2018). A study on the mixed corrosion inhibitor with a dominant cathodic inhibitor for mild steel in aqueous chloride solution. *Journal of the Taiwan Institute of Chemical Engineers*, 91:556-569.
22. Lian, Z., Yuan, L., Wei, W., Zhou, Q. and Jiang, J. (2015), "Controlled release and synergistic effects of polyvinyl alcohol (PVA) on phosphate corrosion inhibitor at the interface of thermal insulation and carbon steel", *Anti-Corrosion Methods and Materials*, 62 (2):109-115.
23. Amer, A., AlShehri, A., Cunningham, V. and Taie, I. (2018). Inspection challenges for detecting corrosion under insulation (CUI) in the oil and gas industry. NACE publications, paper number 12400.
24. Bavarian, B., Samimi, B., Ikder, Y. and Reiner, L. (2015). Protection effectiveness of vapour corrosion inhibitor for corrosion under insulation. NACE publications, paper number 5448.
25. Cao, Q., Brameld, M., Birbilis, N. and Thomas, S. (2019). On the mitigation of corrosion under insulation (CUI) of mild steel using local cathodic protection. *NACE International*, 75(12):1541-1551.
26. Fitzgerald, B., Lazar, P., Kay, R. M., and Winnik, S. (2003). Strategies to prevent corrosion under insulation in petrochemical industry piping. NACE publications, paper number 03029.
27. Sanders, J. D. (2002). Effectively using risk-based inspection results to implement a corrosion under insulation program. ASME Engineering Technology Conference on Energy, paper number 29125.

28. Wiggen, F. (2020). Risk based management of corrosion under insulation. *Inspectioneering Journal*, 26(3):2-8.
29. Mokhtar, A. A., Ismail, M. C., Zainordin, A. B., Shahid, S. (2014). A framework for estimating piping reliability subject to corrosion under insulation. *Matec web of conferences*, 13:1-5.

CHAPTER 2 : FUNDAMENTALS

CHAPTER 2

FUNDAMENTALS

This chapter covers the basic concepts of general corrosion of metals and corrosion under insulation which will provide background information that would enhance understanding of the results in this study. The fundamental concepts covered in this chapter include: the mechanism of general corrosion, the types of corrosion (concentration cell corrosion and differential aeration corrosion), as well as the electrochemical reactions driving corrosion processes. In addition, the fundamental concepts of corrosion under insulation, which is focused on explaining the mechanism of CUI are explained. The purpose is to provide the background information required in understanding the causes of CUI as well as its potential impact.

In addition, the fundamental concepts of galvanic current and electrochemical impedance spectroscopy with regards to the measurement of insulation dry out times will be discussed. This will provide the basis for understanding the results of insulation dry out obtained from the galvanic current and electrochemical impedance measurements. Also, the theory of artificial neural network and the mechanism of CUI rate predictions are also covered. This will explain the hidden calculations performed by the software to arrive at the predicted output. Moreover, ANN, like other predictive models have certain limitations; some of these limitations which determines its boundaries in predictive modelling are also discussed.

2.1) Mechanism of corrosion of metals

The corrosion of metals involves an electron loss and the subsequent transfer to an acceptor leading to the deterioration of the metal in the presence of certain conditions such as water, acid, oxygen, chlorides among others [1, 2]. The four fundamental criteria for corrosion of metals to occur include the presence of an anode, a cathode, an ionic circuit, and an electrical circuit [3] as shown in Figure 2.1.

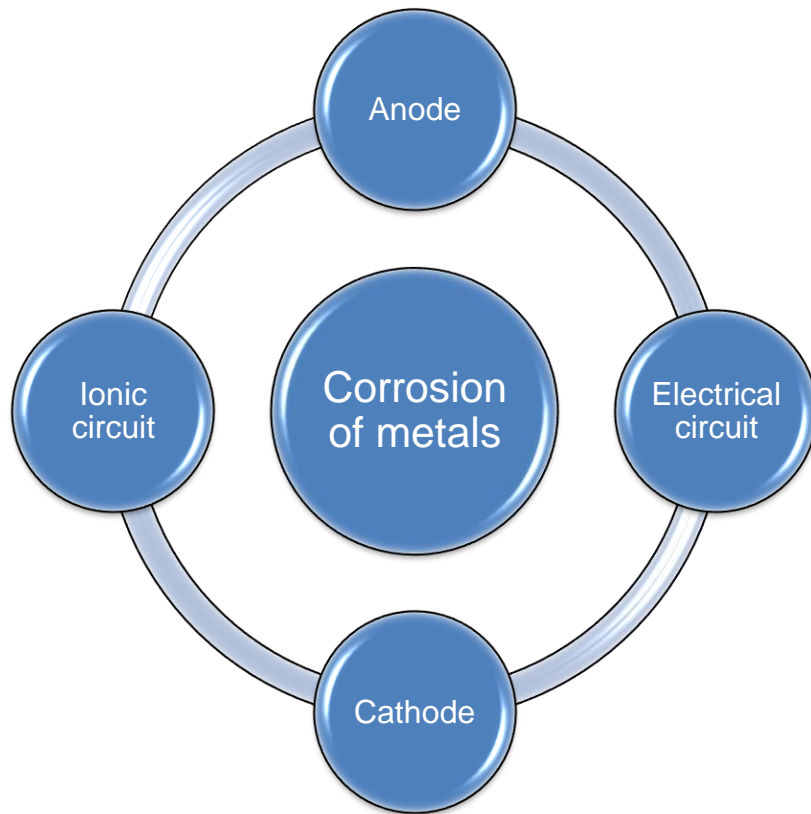
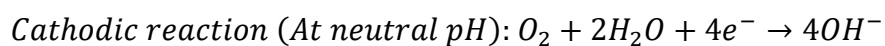
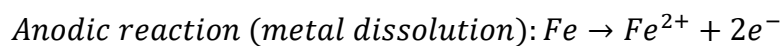
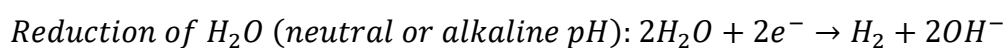
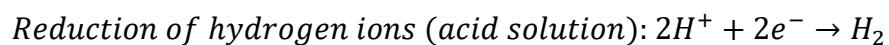


Figure 2.1: Fundamental requirements for corrosion of metals to occur

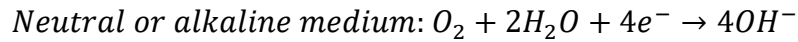
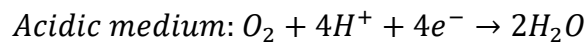
The active sites on the surface of the metal where degradation takes place include the anode and cathode. At the anode, the metal loses electrons and goes into solution as ions, while the electron is accepted by another specie at the cathode, which may be oxygen, or an acid [2]. The anodic reaction involves a single reaction where the metal is oxidized to its ions, while the cathodic reaction involves different possible reactions depending on the chemistry of the medium where the corrosion takes place as shown in the chemical reactions below [3]:



Cathodic reactions may also include the following reactions:



Reduction of dissolved oxygen can take place in an acidic, neutral, or alkaline medium.



Complete corrosion reactions involve the coupling of these electrochemical half-cell reactions to yield metal oxides. For Iron and carbon steel, the initial product consists of ferrous hydroxide which can be further oxidized to give ferric hydroxide. Dehydration of ferric hydroxide results in the formation of rust as shown in Figure 2.2.

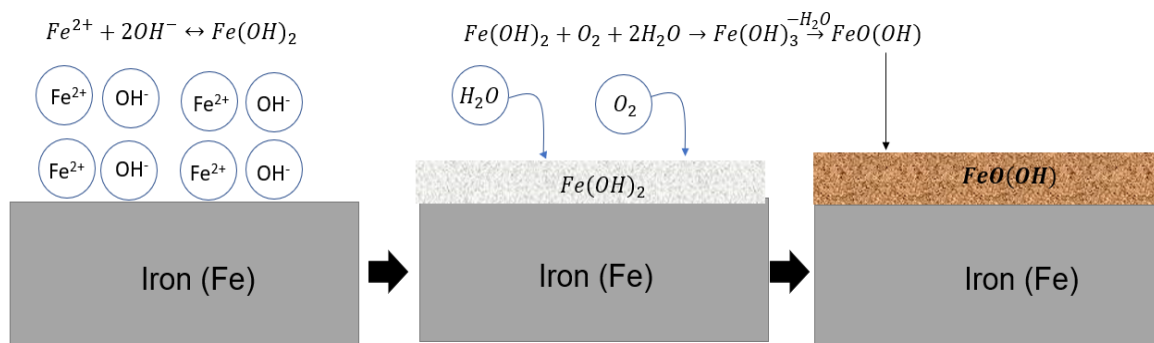


Figure 2.2: Electrochemical reactions showing the corrosion of iron [2].

The distribution of the active sites (anode and cathode) on the surface of the metal depends on certain conditions. For instance, oxygen rich areas of the metal will likely serve as the cathode, while oxygen deficient areas will likely serve as the anode [4]. In addition, the corrosion of metals can either be uniform or localized [5]. This is determined by some factors such as surface properties and conditions under which corrosion occur. In uniform corrosion, the anode and cathode are not restricted to any region of the metal but are constantly changing resulting in deterioration across the metal surface. However, localized corrosion tends to have fixed anodic and cathodic sites where degradation occurs and are restricted to only these areas [6].

2.1.1) Uniform and Localized corrosion

In uniform aqueous corrosion, the dissolution of the metal resulting in material loss occurs across the metal surface. On the other hand, localized corrosion results when discrete regions of the metal surface are selectively attacked by the corrosive medium, culminating in accelerated corrosion rates at specific sites relative to the bulk surface [7]. A metal surface consists of different anodic and cathodic sites. These active sites may be permanently fixed to certain regions of the metal surface, or they may be flipping temporarily across the entire surface depending on certain conditions.

Localized corrosion arises from a metal surface that has a fixed or permanent anodic and cathodic sites, while uniform corrosion is due to continuous flipping of these active sites as shown in Figure 2.3. Areas of the metal surface with high concentration of oxygen is likely to serve as the cathode, while areas with low availability of oxygen will likely serve as the anode. For localized corrosion, the distribution of the active sites can be fixed such that degradation of the metal (corrosion) only occur at these regions only. For example, defects in the surface of the metal can create anodic sites, or less noble metal in a combination of two different metals could become the anode. A typical example of localized corrosion is the formation of pits in chloride-laden region [8]. In addition, the formation of partially protective films could also serve as conduits for initiation of localized corrosion [9].

Carbon steel is generally known to undergo uniform corrosion and it is widely used in different structural applications. However, there are a number of environmental factors that can determine whether localized corrosion of carbon steels would predominate rather than a slow uniform corrosion. Such factors include temperature, concentration of chlorides and pH. Brossia and Cragolino [10] have reported that there is a critical pH which serves as the boundary between uniform and localized corrosion, which may be attributed to the dependence of the formation and stability of passive film on pH. The susceptibility of metals to corrosion at different pH could be evaluated using Pourbaix diagrams. A typical Pourbaix diagram for assessing the susceptibility of iron to corrosion at different pH is shown in Figure 2.4.

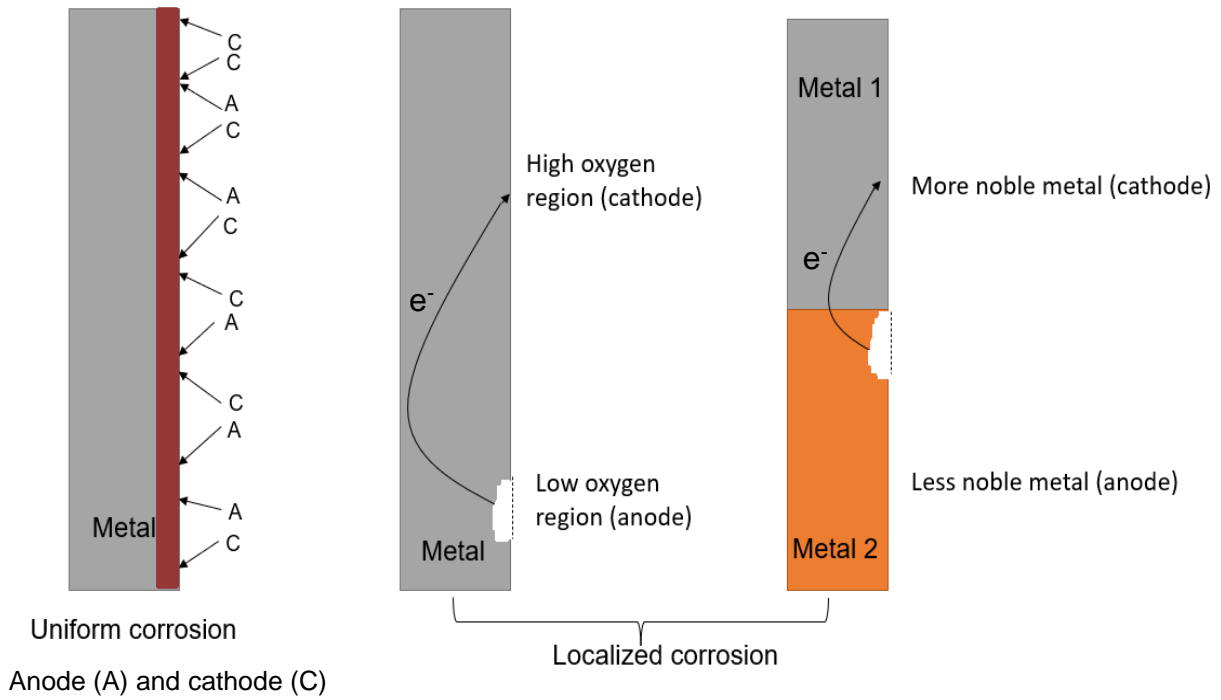


Figure 2.3: Schematic representation of uniform and localized corrosion.

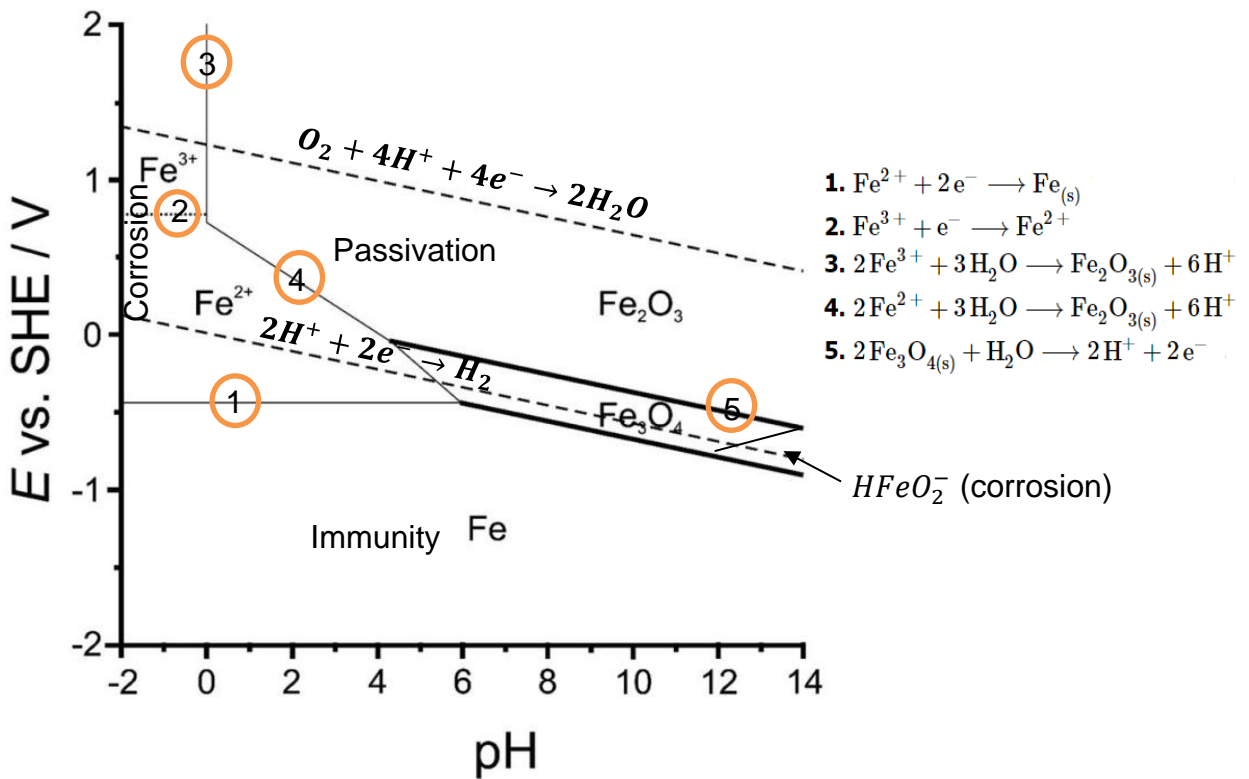


Figure 2.4: Pourbaix diagram for an iron-water system, $\alpha_{\text{Fe}^{2+}} = 10^{-6}M$ [11].

In Figure 2.4, the lines in bold face indicate the boundary between two solid species, the thin lines represent the boundary between a solid and an aqueous species and the dotted lines indicate the boundary between two aqueous species. The lines marked 1 and 2 are horizontal lines which indicates pure redox reactions which are independent of pH. Line 3 is a vertical line representing an acid-base type of reaction which is independent of the potential. Lines 4 and 5 represent a combination of redox and acid base reactions which are pH dependent [12].

Three distinct regions have been identified which includes, immune region indicating region of unreacted metal, corrosion region representing region where stable ionic species are formed and passive region indicating the formation of an oxide layer which hinders further corrosion [11]. Therefore, corrosion is not expected to occur within the immune and passive regions. Although Pourbaix diagrams are quite useful in describing corrosion behaviour of metals, it does not provide information on the kinetics of corrosion. Moreover, it only applies to pure metals and does not account for the corrosion behaviour of alloys which are frequently used in engineering structures. In addition, Pourbaix diagrams does not consider the effect of anions such as chlorides which can penetrate passive films and induce localized corrosion.

2.2) Mechanism of Corrosion under Insulation (CUI)

Corrosion of metals under insulation is an external degradation of metals due to the ingress of water and contaminants such as chlorides [13]. This can take place in both hot and cold service equipment. The occurrence of CUI depends on certain factors such as the frequency of operation, the conditions under which the metal is being operated, as well as the type of metal [14]. The areas where CUI are most likely to occur are the lower regions where moisture tends to accumulate, irregular insulation surface, openings of jacketing etc [15]. In addition, metal pipes with small bore have been reported to be more susceptible to CUI due to the small thickness and surface area [16]. The history of CUI started in the early 1970's, during which thermal insulations was not quite necessary until process temperatures reached about 150 °C [17]. This necessitated the use of thermal insulations to protect personnel from hot metal surface and control process conditions. Within a short period of time, the need for high quality insulation materials arose when about 50 % of the degraded assets

were observed to be caused by corrosion under insulation [17]. Since then, the search for solution has continued and gone through several phases.

When metals are exposed to air, moisture present in the air will likely condense on the surface, if the equipment was not properly insulated; this condensate will find its way to the surface of the metal substrate and will initiate corrosion as shown in Figure 2.5. The aim of corrosion engineers regarding this problem has been to try as much as possible to prevent such condensation in chemical plants [18]. One of such strategy is the use of vapour barriers on the external surface of pipes which should prevent moisture from the external environment from penetrating the insulated metal surface. However, despite these efforts, it has been observed in the field that some tiny holes in the jacketing or sealed joints not properly fixed serves as conduits by which water enters the insulation and penetrates the metal surface. This could significantly depreciate the thermal performance of the insulation leading to corrosion under insulation.

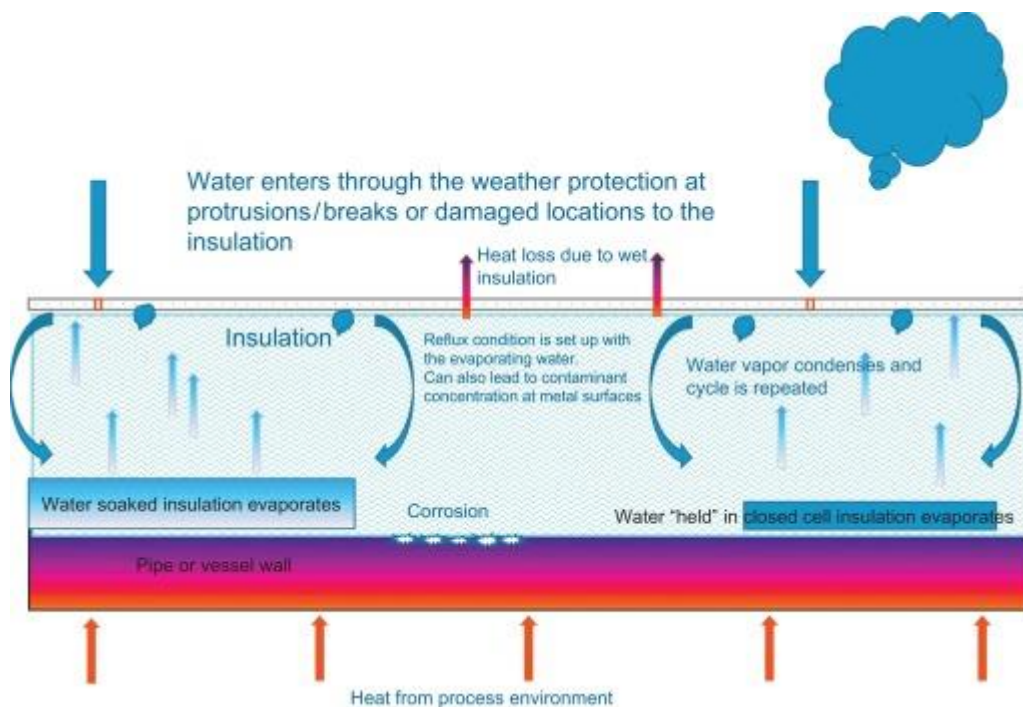


Figure 2.5: The process of condensation within an insulated system [19]

Some corrosion experts in industry do assume that CUI is more significant in old metal facilities compared to new ones; however, it has been advised that such assumptions

could have severe consequences as CUI is aggravated by the operating conditions and should be treated as a serious issue irrespective of the age of the metal [20]. Early maintenance and inspection schedule could help to identify vulnerable areas and appropriate action can be taken prior to failure [21]. In order to have a better understanding of CUI, the components of a typical metal insulated system is hereby described.

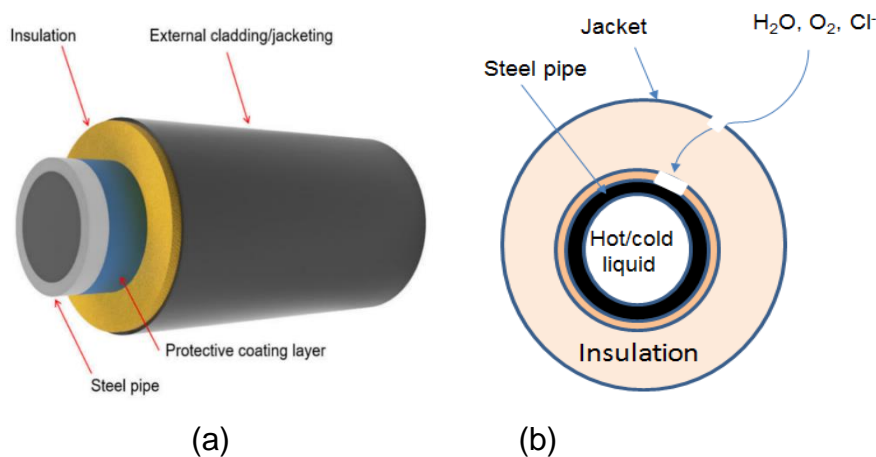


Figure 2.6: (a) Components of an insulated system [22] (b) Top view of an insulated system showing the ingress of water, oxygen, and chlorides.

An insulated metal system comprises of the metal (with or without coating) as the inner layer, this is followed by the insulation that contacts the metal surface. The outer part consists of the jacketing that prevents the intrusion of water into the insulation. A schematic representation of this composition is shown in Figure 2.6. Water from rain, dew, snow, and other form of precipitation can find its way into the insulation if it was not properly installed or if there is a physical damage on the insulation either through regular trampling on the insulation or wears out by other mechanical means [23]. The water will find its way to the surface of the metal, if the metal is in operation at elevated temperature, the water will be heated up, and condenses back to the surface of the metal when it reaches the jacketing. This cycle will continue in a reflux pattern which has the tendency of dissolving chlorides within the insulation material, thereby increasing its concentration resulting in enhanced CUI. If the metal is out of service or operating under cold conditions, the water has the tendency of having prolonged contact with the metal surface which will also lead to increased CUI.

2.2.1) Mechanism of corrosion of carbon steel in sodium chloride solution

The corrosion of carbon steel in contact with insulation that is wetted with sodium chloride solution is an electrochemical reaction involving anodic dissolution of iron and cathodic reduction of oxygen. During CUI, chlorides could enter the insulated substrate externally through the surrounding fluid or it could be leached from the insulation itself. The presence of chloride around the environment of the metal have been reported to accelerate corrosion rate [24], induce pitting and creates an environment prone to stress corrosion cracking [25, 26]. The combination of products formed at the anode and cathode gives rise to ferrous oxide which oxidizes to ferric oxide in the presence of dissolved oxygen. The schematic representation of corrosion of insulated carbon steel is shown in Figure 2.7.

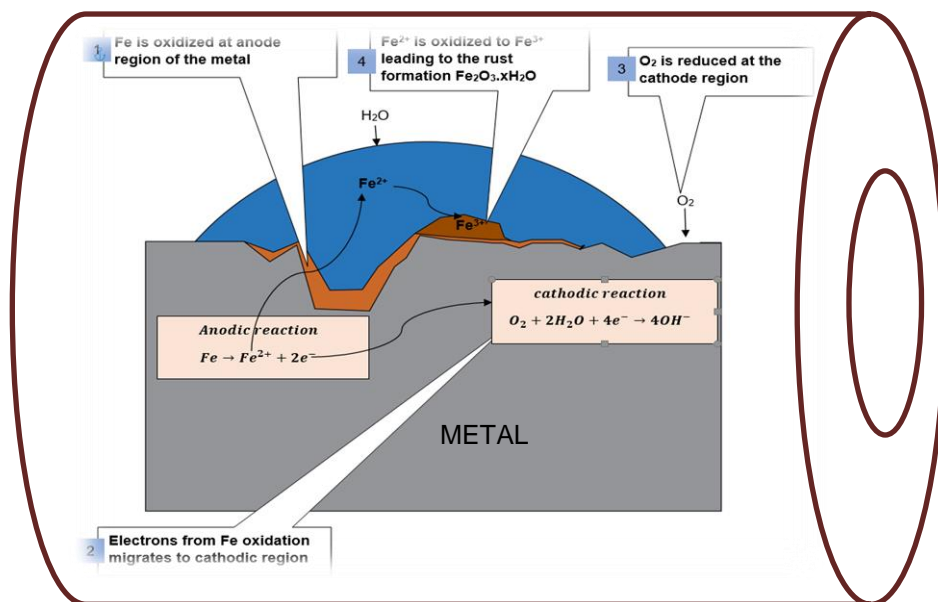


Figure 2.7: Schematic representation of corrosion under insulation in the presence of oxygen.

The surface of the metal has both anodic and cathodic sites. For localized corrosion, these sites tend to be fixed to certain region of the metal. Pitting has been identified as the most common form of localized corrosion where degradation of the metal is restricted to small areas as a result of the presence of salt particles, discontinuities in the coating or surface defects [3]. However, in the case of uniform corrosion, these sites are not restricted to a particular region of the metal but are constantly changing

depending on certain conditions. Areas of the metal where there is high availability of oxygen will serve as the cathode while the region with less oxygen will serve as the anode. The consistent change in anodic and cathodic areas on the surface of the metal results in uniform corrosion. At the anode, iron loses electrons to form ferrous ions, the electrons migrate to the cathode areas and reduces oxygen to hydroxyl ions. The ferrous oxide becomes oxidized to ferric oxide which is the corrosion product as shown in Figure 2.7.

2.3) Theory of galvanic corrosion

Galvanic corrosion is the corrosion occurring between two or more dissimilar metals in contact with an electrolyte. When two different metals are in contact with a conductive solution, the metal with the higher electronegativity will serve as the anode while the less electronegative metal will serve as the cathode (Figure 2.8). In this case, the metal that serves as the anode would rapidly corrode more than it would alone and the metal serving as the cathode would usually corrode less than it would alone [27]. The exposed area of the anode and cathode is an important factor in galvanic corrosion. A small anode to cathode area ratio would result in a rapid anodic dissolution due to the concentration of galvanic current on a smaller anodic area [28]. In addition, different techniques that have been employed to mitigate galvanic corrosion include isolating the two metals from each other, selecting similar materials or materials with close electrical potentials, or adding a corrosion inhibitor [29].

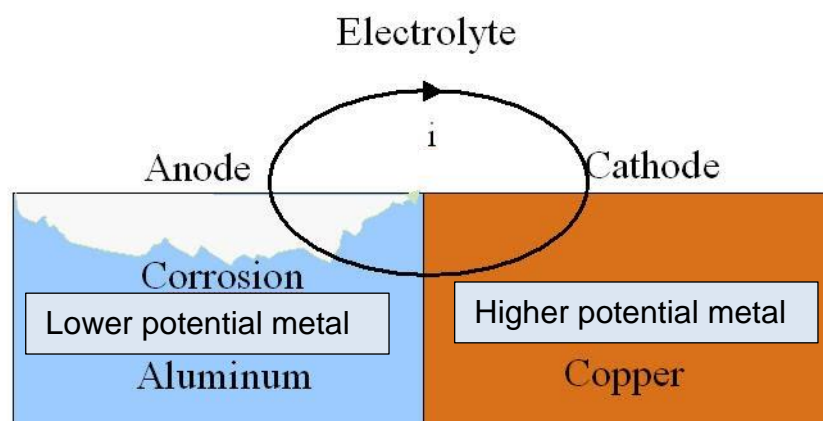


Figure 2.8: Galvanic corrosion of aluminium/copper couple.

2.4) Fundamental concepts on insulation dry out using galvanic current measurement.

Galvanic current is the current that flows between dissimilar metals when they are electrically connected and in contact with an electrolyte [3]. The dissimilar metals must have different electrode potentials and the metals should be electrically connected to each other [30]. In this section, the discussion about the use of galvanic current to measure insulation drying times will be restricted to aluminium-copper galvanic couple in contact with mineral wool insulation that is wetted with 1 wt % NaCl solution. This represents the system that was studied in this research; hence, it will provide the required understanding to the methodology and results presented herein. The schematic representation of the flow of electrons across a Cu/Al galvanic couple in contact with the electrolyte in the insulation is shown in Figure 2.9, while the electrical equivalent circuit for the ring electrode system is shown in Figure 2.10.

The concept of determining the degree of wetness of insulation lie in the fact that when the insulation is dry, there will be no flow of galvanic current; however, when it is wet, a measurable current is produced. A pair of dissimilar metals (Cu and Al) serving as a sensor are used to create a galvanic cell, the resulting current (I_g) produced when the metals are in contact with the wet insulation is measured using a multimeter. The opposition to the flow of current (resistance) due to the presence of a liquid film at the surface of the metal is referred to as solution resistance. This is caused by the interaction of ions with each other, which prevents the directed movement of ions between the electrodes [31]. Within an insulated system, the solution resistance could indicate the drying out process of the insulation. For the Cu-Al galvanic couple (Figure 2.9), the magnitude of the galvanic current depends mainly on the solution resistance (R_s) which represents the ohmic resistance between the two electrodes. The magnitude of R_s depends on the geometry of the rings as well as the conductivity of the solution in the insulation.

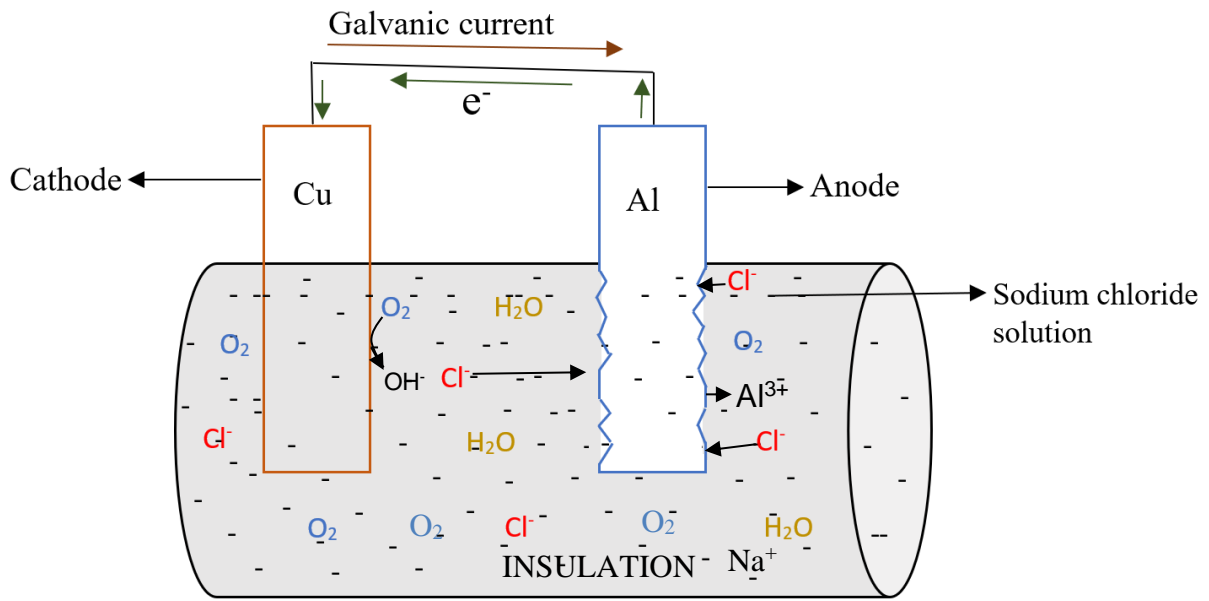


Figure 2.9: Schematic representation showing preferential corrosion of Al in an Al/Cu galvanic couple.

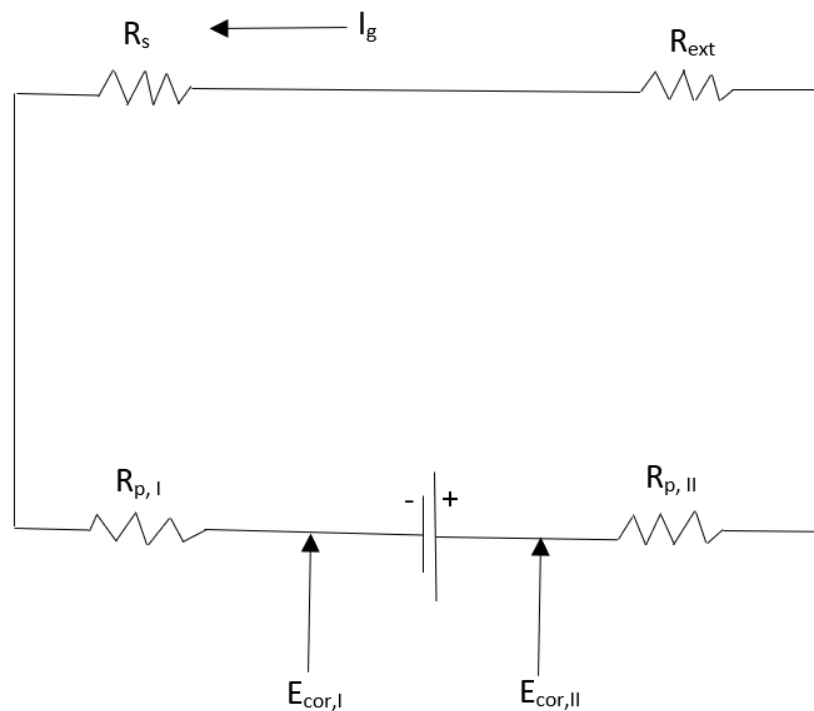


Figure 2.10: Equivalent circuit of the Cu-Al electrode system

This is an indirect method of determining the solution resistance (R_s) which is believed to relate to the degree of drying out in a reasonable way. This is because R_s is expected to increase as the insulation dries out due to the decrease in conductivity of

the solution. The galvanic couple used in this study consisted of copper and aluminium rings. When both metals are not connected, they will corrode independently, each having separate corrosion potentials, E_{cor} . The galvanic series of metals in sea water presented in Table 2.1 indicates that aluminium has a lower corrosion potential compared to copper. In other words, aluminium is less noble, hence, it will serve as the anode, while copper functions as the cathode where reduction of oxygen will occur according to the following reactions [32].

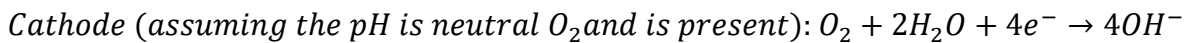
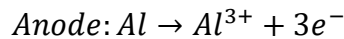


Table 2.1: Galvanic series of metals and alloys in seawater [32]

Metal/alloy	Potential range (V) vs SCE
Magnesium	-1.60 to 1.63
Zinc	-0.98 to -1.03
Aluminium	-0.70 to -0.90
Cadmium	-0.70 to -0.76
Cast iron	-0.60 to -0.72
Steel	-0.60 to -0.70
Brass	-0.30 to -0.40
Copper	-0.28 to -0.36
Lead-tin solder	-0.26 to -0.35
400 series stainless steel	-0.20 to -0.35
Lead	-0.19 to -0.25
Copper-Nickel (70/30)	-0.13 to -0.22
Silver	-0.09 to -0.14
Monel	
300 series stainless steel	-0.00 to -0.15
Titanium	+0.06 to -0.05
Platinum	+0.25 to +0.18
graphite	+0.30 to +0.20

On the other hand, when both metals are connected in the presence of an electrolyte, galvanic cells will form which can be represented by an equivalent circuit as shown in Figure 2.9. The magnitude of the solution resistance depends on the geometry of the

aluminium and copper rings as well as the conductivity of the solution in the insulation [33]. The external resistance (R_{ext}) is the resistance due to the external circuit and the measuring equipment (multimeter). The total resistance in the circuit (R_T) is the sum of the solution resistance (R_s), polarisation resistances ($R_{pI} + R_{pII}$) and the external resistance due to the measuring instrument (R_{ext}). The flow of current across an electrode will result in a shift in the potential of the electrode when compared to its potential when there is no current flow (open circuit potential). The resistance of a material to this shift in potential (polarisation resistance) is inversely proportional to the corrosion rate of the material [34].

The change in corrosion potential between the electrodes (ΔE_{cor}) represents the difference between the potentials of each electrode which is applied across all the possible resistances (R_s , R_{ext} , R_{pI} and R_{pII}) producing a galvanic current (I_g). This is in accordance with ohm's law as shown in equations 2.1 and 2.3 [35].

$$\Delta E_{cor} = I_g R_T \quad (2.1)$$

$$R_T = R_{pI} + R_{pII} + R_{ext} + R_s \quad (2.2)$$

$$I_g = \frac{\Delta E_{cor}}{R_{pI} + R_{pII} + R_{ext} + R_s} \quad (2.3)$$

Assuming the interfacial polarisation resistances (R_{pI} , R_{pII}) and the external resistance (R_{ext}) are quite small compared to the solution resistance (R_s), then equation 2.3 reduces to equation 2.4.

$$I_g = \frac{\Delta E_{cor}}{R_s} \quad (2.4)$$

Equation 2.4 corresponds to situation where ohmic control is dominant and suggests that the galvanic current is inversely proportional to the solution resistance. This implies that as the solution resistance increases towards infinity (∞) during the drying process of the insulation, the galvanic current (I_g) will tend to zero. However, this might only be accurate as the insulation continues to dry or as R_s increases. When the insulation is wet, the solution resistance may be relatively low, and the galvanic current may also be partly controlled by the polarisation resistances [35].

2.4.1) Theory of Electrochemical impedance technique in measuring insulation dry out

Electrochemical Impedance spectroscopy (EIS) is a frequency-based technique involving the application of a sinusoidal signal to an electrochemical system and measuring the resulting response due to this perturbation [36]. This can give insight to the mechanism of electrochemical reactions including transport properties of materials [37]. This technique has been useful in probing corrosion mechanisms and other electrochemical systems at different frequencies since the advent of potentiostats in the 1940's and frequency **analysers** in the 1970s [38]. EIS is **characterised** by a time dependent potential and current functions, a phase shift and a frequency. Impedance is the opposition to the flow of alternating current offered by an electric circuit [39]. This is represented in equation 2.5.

$$Z = \frac{E}{I} \quad (2.5)$$

Where E is the applied sinusoidal potential, and I is the measured AC current. This method can be used to study the metal/solution interface as well as the surface treatments [37]. The equivalent circuit of a metal-solution interface is shown in Figure 2.11.

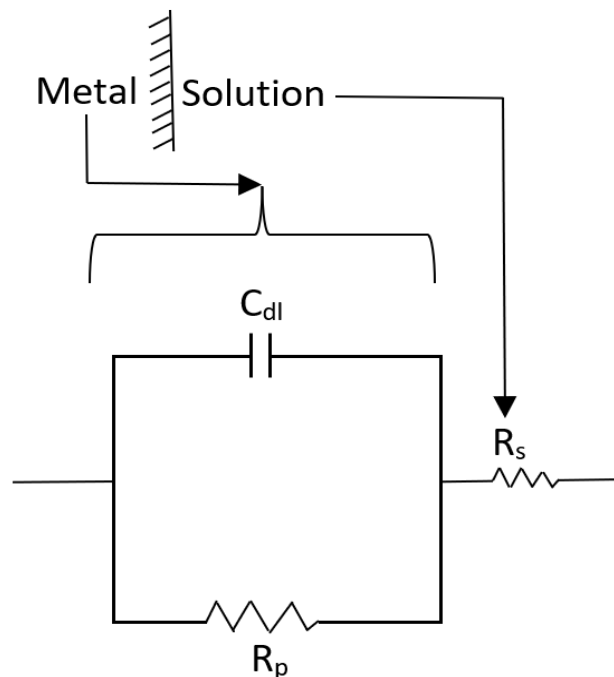


Figure 2.11: Equivalent circuit of a metal-solution interface [37]

The existence of two layers of electric charge at the metal-electrolyte interface having opposite polarities is referred to as double layer capacitance. The charge separation at this metal-solution interface helps to provide the driving force in terms of the potential drop for corrosion reactions [40]. Figure 2.11 shows that the polarisation resistance (R_p) and the capacitance of the electrical double layer (C_{dl}) of the metal-solution interface are in series with the solution resistance existing between the double layer and the reference electrode. Therefore, the overall impedance of the system depends on the contribution of all these components. Copper has been reported to possess good corrosion resistance in electrolytes such as sodium chloride [41]. Therefore, in this study, two copper rings were used as this is fairly noble and it is not expected to form surface films which would contribute its own impedance to the system; hence, it is suitable for this application. The main interest was to determine the solution resistance (R_s) between the rings. It was assumed that as the insulation dries out, the solution resistance will increase and approach infinity when the insulation is completely dry. The equivalent circuit of the two-ring system is shown in Figure 2.12.

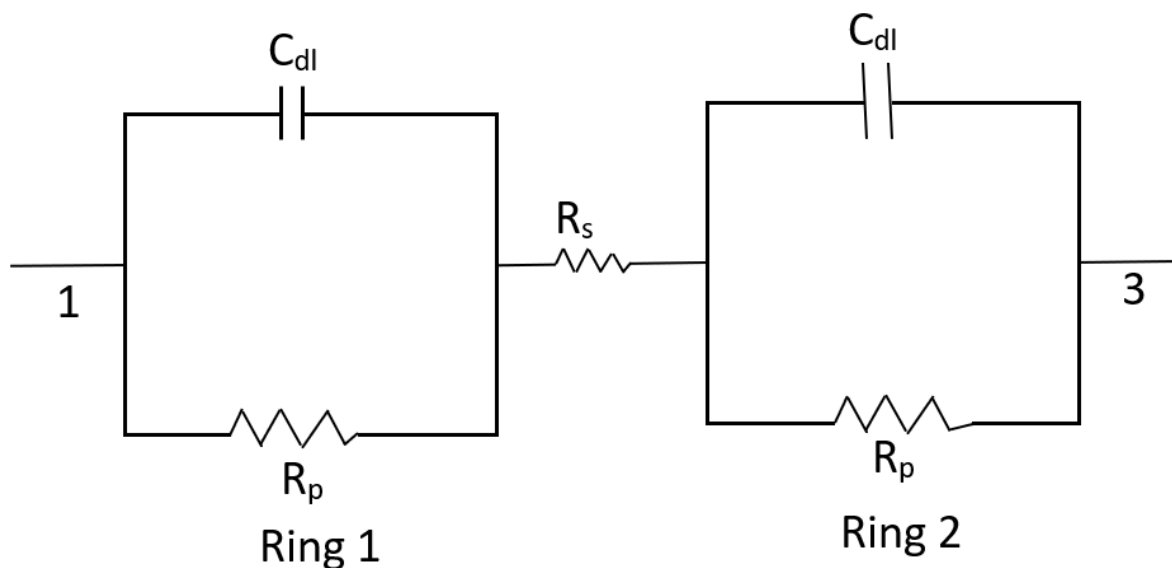


Figure 2.12: Equivalent circuit of the two-ring system used in this study

It should be noted that the polarisation resistance (R_p) and the double layer capacitance (C_{dl}) are the same for both electrodes. However, for simplicity, the equivalent circuit shown in Figure 2.11 will be used as it is relevant to this analysis. The impedance between points 1 and 3 is given in equation 2.6 [35].

$$Z = R_s + \frac{R_p}{1 + \omega^2 R_p^2 C_{dl}^2} - j \frac{\omega R_p^2 C_{dl}}{1 + \omega^2 R_p^2 C_{dl}^2} \quad (2.6)$$

Equation 2.6 can be rewritten as a complex number with imaginary and real components as in equation 2.7 [35].

$$Z = Z' + jZ'' \quad (2.7)$$

$$\text{Where } Z' = R_s + \frac{R_p}{1 + \omega^2 R_p^2 C_{dl}^2} \quad (2.8)$$

$$Z'' = -\frac{\omega R_p^2 C_{dl}}{1 + \omega^2 R_p^2 C_{dl}^2} \quad (2.9)$$

The resulting impedance (Z) obtained from the real and imaginary parts is shown in Figure 2.13.

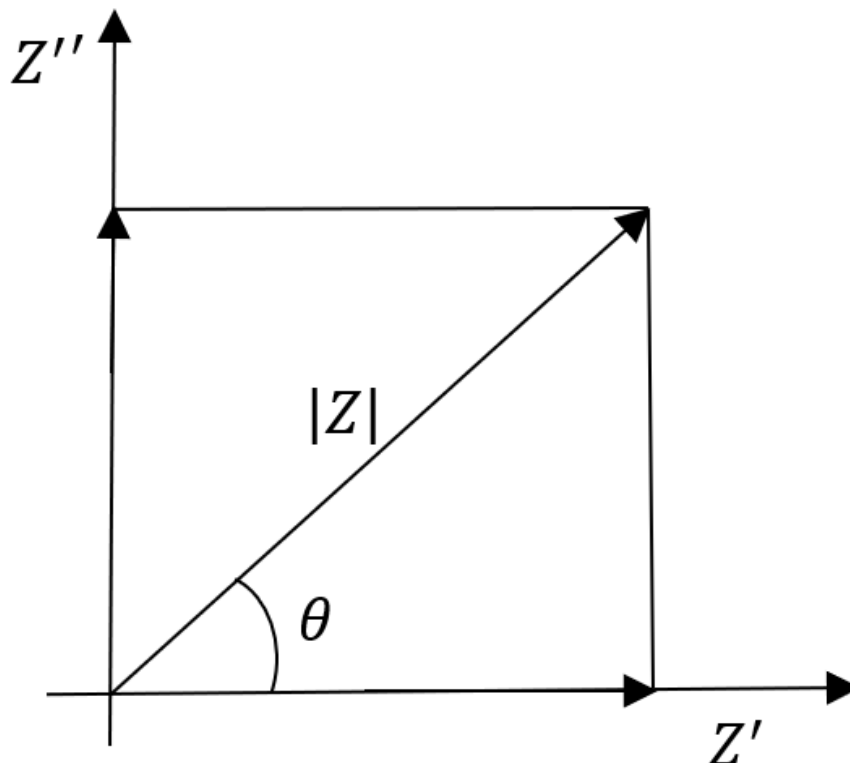


Figure 2.13: Representation of imaginary impedance, real impedance, and the absolute value of the impedance [42].

The absolute value of the impedance can be obtained from Figure 2.13 by applying the Pythagoras theorem.

$$|Z| = \sqrt{(Z'{}^2 + Z''{}^2)} \quad (2.10)$$

$$|Z| = \sqrt{\left(R_s + \frac{R_p}{1 + \omega^2 R_p^2 C_{dl}^2}\right)^2 + \left(\frac{\omega R_p^2 C_{dl}}{1 + \omega^2 R_p^2 C_{dl}^2}\right)^2} \quad (2.11)$$

Equation 2.11 shows that the total impedance depends on the various circuit parameters including the frequency. The dependence of impedance on the frequency is usually represented by the Bode plot. This is shown in Figure 2.14 for instance where the double layer capacitance (C_{dl}) is $10 \mu\text{Fcm}^{-2}$, polarisation resistance (R_p) is $1 \text{ k}\Omega$, and solution resistance is 100Ω .

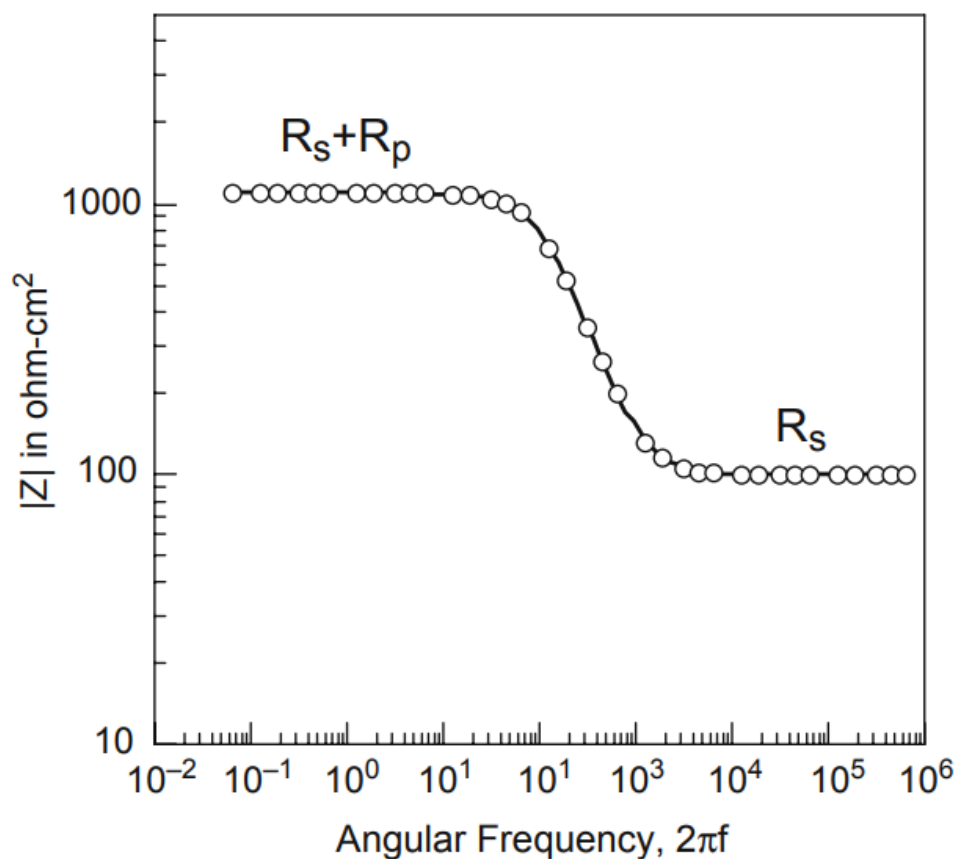


Figure 2.14: Typical Bode plot for an electrochemical surface [37]

Figure 2.14 shows that the polarisation resistance is prominent when a small value of the angular frequency is used. However, at high frequency of 1 kHz – 100 kHz, the measured absolute impedance is equal to the solution resistance (R_s). Therefore, in this study, the angular frequency of 1 kHz was used to ensure that the measured impedance reflects only the contribution of the solution resistance which was the primary target. In addition, the phase shift is another important parameter which shows the relationship between the AC current and voltage. This is illustrated in Figure 2.15.

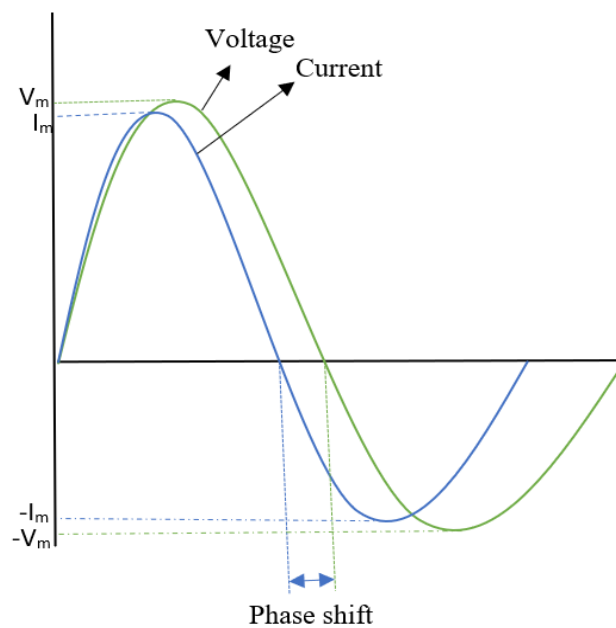


Figure 2.15: Schematic representation of the phase shift between current and potential operating at the same frequency.

In Figure 2.15, the potential and current are said to be in phase if at any instant in time in a complete cycle, both parameters reach the maximum, zero and minimum values at the same time even though the amplitude may be different; otherwise, they are said to be out of phase [39]. The potential and current are always in phase in a circuit containing only a resistor; but the current leads the voltage by 90° in a capacitor [39]. This is because the current (I_R) passing through a resistor (R) is directly proportional to the applied voltage (V), while the current (I_C) passing through a capacitor (C) is proportional to the rate of change of voltage. Therefore, in a capacitive circuit, the capacitor opposes a change in voltage and stores energy as an electric field, this

results in the current (I_c) leading the voltage by 90° [43]. Within the context of a corrosion system, the capacitive behaviour is observed at the electric double layer which exists at the electrolyte-metal interface [43].

When the total impedance is dominated by the solution resistance (R_s), the impedance is entirely resistive in nature and the measured phase angle is expected to be zero. This offers a means of confirming that the effects of other circuit components are negligible. It is expected that when the solution resistance is small (wet insulation), the effects of other components might be significant, and the phase angle might not be zero. However, as the insulation dries, the impedance continues to increase until it gets to very high values indicating significant drying out of the insulation. In this case, the phase angle and the measured impedance will be quite noisy and unreliable.

2.5) Theory of predictions using Artificial Neural Network

Artificial neural network (ANN) is a program that can be used to predict outcomes based on pattern recognition and classification acquired during training [44]. It is a biologically inspired program which mimics the activities of the biological neurone in the brain. A comparison of the activities of ANN and the neurone in the brain is shown in Figure 2.16. The input variables are compared to the dendrites, the hidden layer to the cell body, the output to the axon terminals [45]. Information is passed from the input layer to the hidden layer which processes it using an activation function and sends it to the output layer. This is similar to the impulse received at the dendrites, processed in the cell body and passed through the axon to the terminals where they are picked up by other cells.

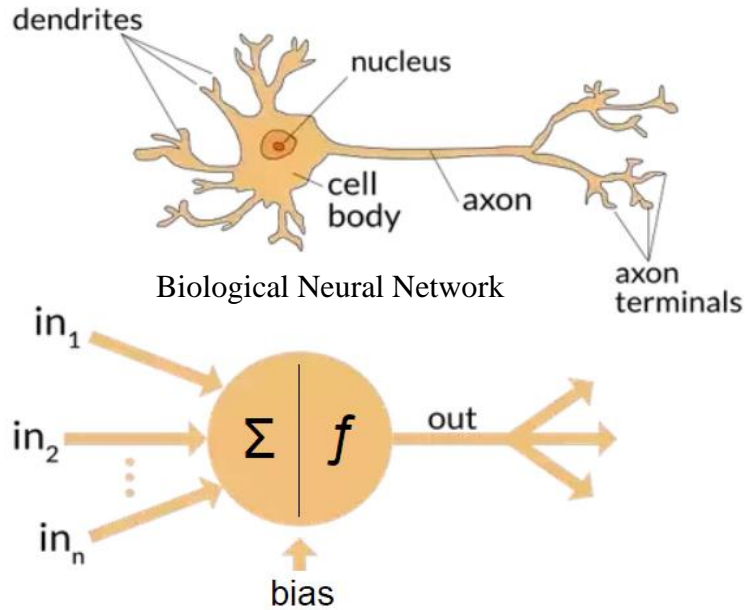


Figure 2.16: Comparison of artificial neural network with biological neural network [46]

ANN makes predictions by learning the patterns that exist in a set of complicated data. The ability to establish and recognize complex patterns is the reason why ANN has been quite useful in predicting the outcome of non-linear systems [47]. Prediction of the fate of chemical systems that are linearly related with the input parameters can easily be carried out using linear regression analysis; however, when they are non-linear, machine learning techniques such as artificial neural networks become the ideal tool in establishing patterns between the input and output variables.

Corrosion under insulation is affected by parameters such as temperature, electrolyte concentration, pH, inhibitors among others. These factors have a complex relationship with CUI rate, and it is quite difficult to establish the contribution of each of these parameters to the overall CUI rate. Moreover, it is almost impossible to control these factors in the field which further makes prediction of CUI rate quite difficult [48]. However, ANN is an ideal tool for studying non-linear relationships existing between these parameters (independent variables) and establish a pattern with the expected output [49]. Therefore, this section focuses on the background information on Artificial neural networks with the aim of providing the necessary understanding on its mechanism of operation. This will begin with the composition of ANN, followed by mechanism of prediction and limitations of ANN.

2.5.1) Components and classification of artificial neural network

ANN consists of three layers which include: the input, hidden and output layers [50]. The input layer contains the studied parameters affecting corrosion rate (independent variables), the hidden layer is where the calculations are carried out based on some activation functions and the output layer contains the expected outcome which is the corrosion rate (dependent variable). The input and output layers usually consist of a single layer while the hidden layer can be single, dual, or multiple hidden layers. The choice of the number of hidden layers for a particular prediction depends on the quantity and type of data [45]. Large industrial data might be difficult to process using a single hidden layer as it will make the network clumsy, slow, and difficult to train [51]. Therefore, dual, or multiple hidden layers might be used in such instance.

The number of neurons in any type of hidden layer chosen is also significant as choosing the appropriate number will enhance training and adaptability of the network. The architectural design of an artificial neural network as used in this study is shown in Figure 2.17. This represents the layout of a typical ANN design. This consists of the input layer which consists of the studied influencing factors on CUI rate. For an output that results from several related parameters, the higher the number of these factors incorporated into the network, the better the prediction, provided these parameters have some relationship with the expected output. It is important that these input parameters have some relationship with the expected output, if there is no relationship, the program will be difficult to train, and it will result in a reduced accuracy of prediction [52]. The hidden layer serves as the pivot that contains the activation functions. Some of the activation functions that have been used in artificial neural network include: Linear, identity, sigmoid, hyperbolic tangent, rectified linear unit functions (RELU) among others. ANN can be classified based on the number of layers, type of connections, direction of propagation and activation function as shown in Figure 2.18.

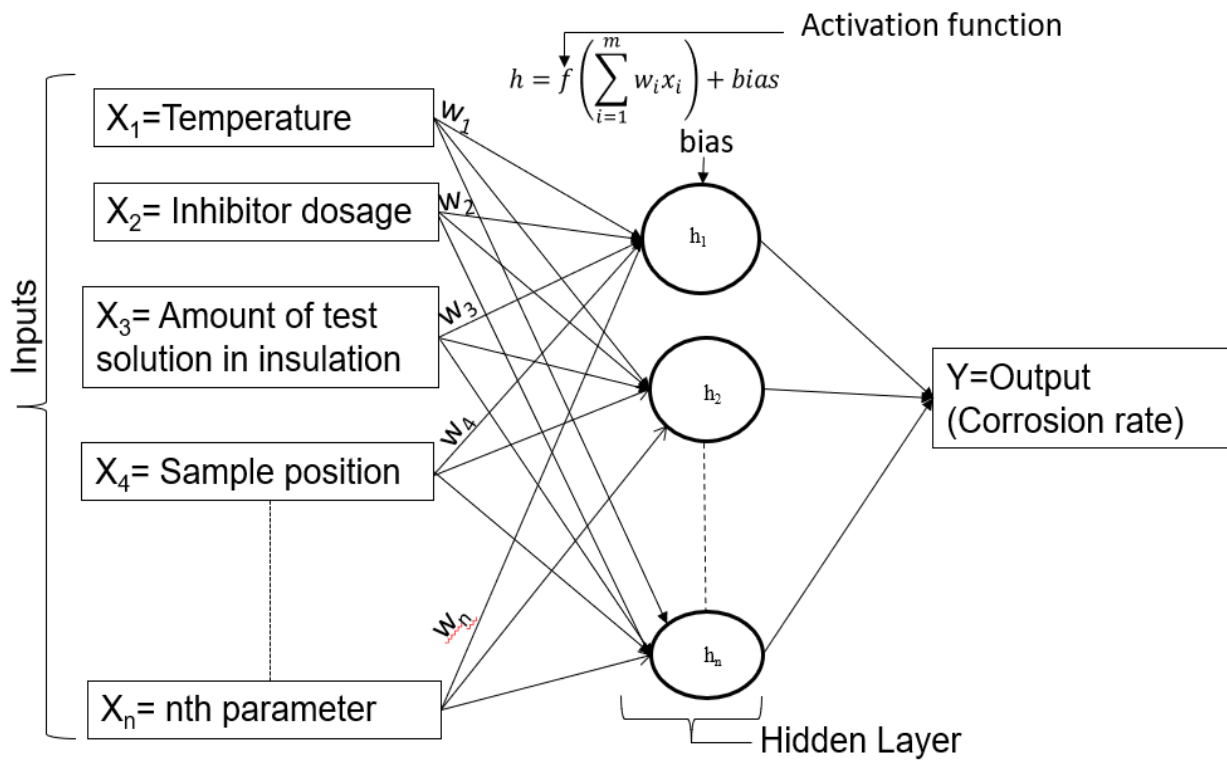


Figure 2.17: Components of ANN

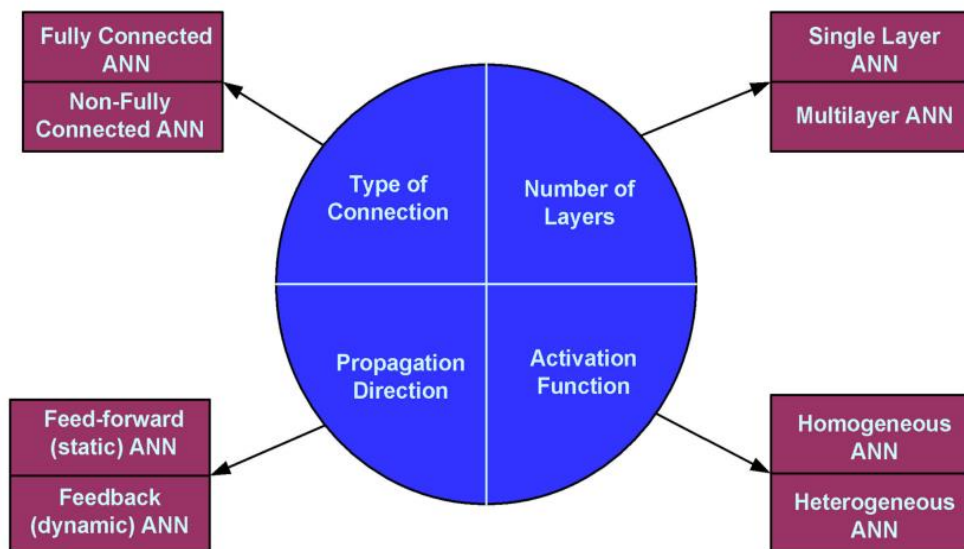


Figure 2.18: Classification of artificial neural network [52]

2.6) The role of activation functions in artificial neural network

Activation functions are mathematical functions that transform the input data fed into its node into an output [53]. During this process, it tries to suppress data that it

considers to be irrelevant, thus ensuring that only the important information is being processed. Activation function performs this task by using mathematical equations to decide whether the information in a certain neurone should be activated or not. The hidden layer is not exposed as the name implies. This means that the software performing this task does not explain what it is doing or how it arrives at the predicted output. This is probably the reason why many researchers working with artificial neural network hardly explains what the software is doing and how it arrives at the predicted output as seen in its absence in many publications. Nevertheless, the complex mathematical derivations associated with ANN predictions will be explained in the mechanism of prediction in the next section.

The primary purpose of activation functions to neural networks is to introduce non-linearity to the network so that complex patterns can be recognised [54]. Without an activation function, the output of the network will simply be a linear transformation of the input variables, and this will be independent of the number of hidden layers. Complicated data will be difficult to train under these circumstances and the network will reduce to a simple linear regression model. However, the presence of an activation function introduces non-linearity into the network which makes it easy to learn complex relationship existing between the input and output variables.

2.6.1) Types of Activation functions

Activation functions are grouped into linear and non-linear activation functions. The linear activation functions include linear, identity, and binary step function while non-linear functions include sigmoid, hyperbolic tangent, rectified linear unit, exponential linear unit, softmax, gaussian error linear unit, as well as Swish activation functions [55]. The non-linear activation functions used in this study include sigmoid and hyperbolic tangent functions; hence, these two functions will be the focus in subsequent discussions. For a mathematical function to be suitable to serve as an activation function in neural network, it must have a derivative that is differentiable so that adequate learning using gradient descent algorithm can take place [56]. Also, the function is expected to be symmetrical around 0 so that it does not shift the gradient to any direction in addition to being computationally feasible. The two significant types

of activation functions used in this study include the sigmoid and hyperbolic tangent functions and this will be discussed in detail.

2.6.1.1) Sigmoid activation function

Sigmoid activation function is a non-linear mathematical function which takes in any input data and processes an output that is restricted to 0 and 1 [57]. This implies that it is impossible to obtain a negative output or values higher than 1 when using a sigmoid activation function. All the possible variables that could be obtained is normalized within this range which means that the sigmoid activation function takes in all real numbers in its domain but produces an output that is more of a probability. This characteristic really fits CUI data since the impact of CUI is often evaluated in terms of probability of failure (PoF). The plot of a sigmoid function as well as its derivative is shown in Figure 2.19.

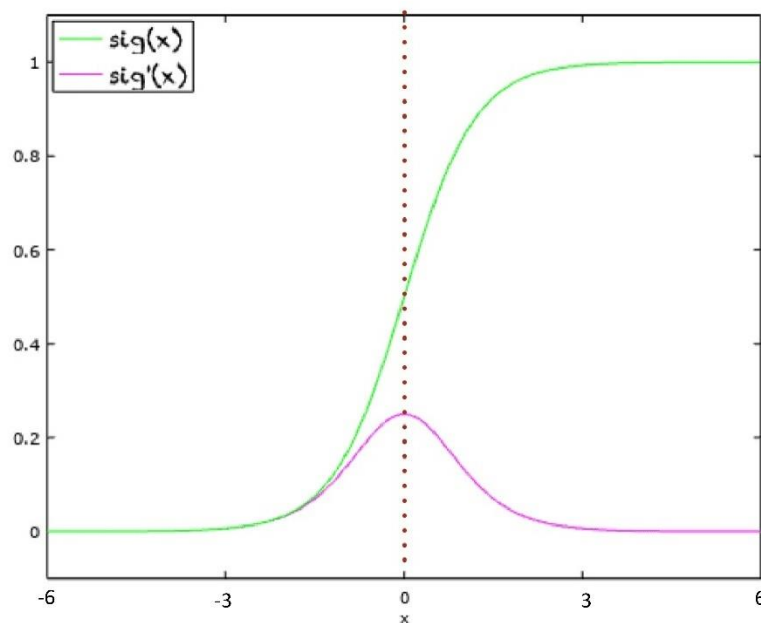


Figure 2.19: Representation of a sigmoid function and its derivative

The mathematical expression of the sigmoid function is given as

$$Sg(x) = \frac{1}{1 + e^{-x}} \quad (2.1)$$

$$Sg'(x) = f(x)(1 - f(x)) \quad (2.2)$$

The function $sg(x)$ is differentiable, and the gradient is smooth, which implies that it will not skip output values. This makes it desirable for neural network analysis [52]. However, the plot of the derivative of sigmoid function as shown in Figure 2.19 indicates that the gradient is only important for the output values of -3 to 3. The curve flattens out at other x values. This is the so called 'gradient vanishing problem' [58]. What this means for neural network modelling is that during the training process where the network computes the derivative of $sg(x)$ in order to adjust the weight and bias values via the mechanism of backpropagation which will be discussed in detail in subsequent section, the network will stop learning as the gradient is close to 0. Besides, the curve of sigmoid function is not symmetric around 0 which will also affect the learning rate.

2.6.1.2) Hyperbolic tangent activation function

The hyperbolic tangent function also has real numbers in its domain but the output falls within the range of -1 to 1 as shown in Figure 2.20. This implies that large input values will tend to approach 1 while smaller input values will approach -1. Hyperbolic tangent function is zero centred; hence, it makes the learning process during training easy unlike sigmoid function. The mathematical expression of hyperbolic tangent activation function and its derivative are given in equations 2.3 and 2.4 respectively [59].

$$\tanh(x) = \frac{e^x - e^{-x}}{e^x + e^{-x}} \quad (2.3)$$

$$\tanh'(x) = 1 - \tanh^2(x) \quad (2.4)$$

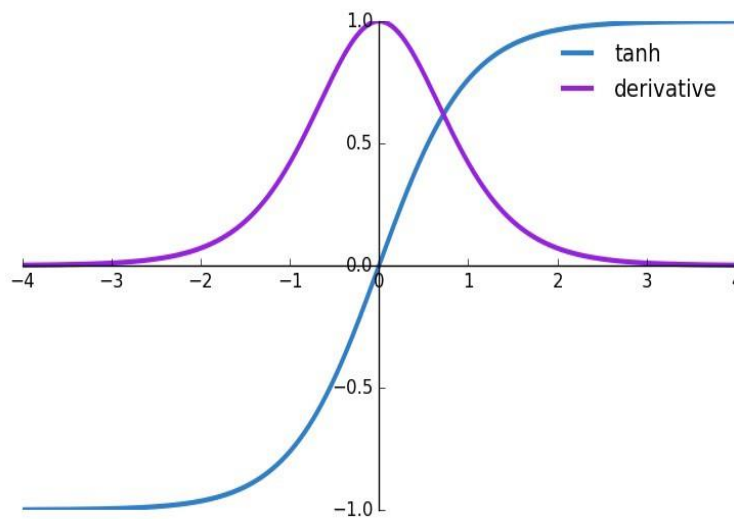


Figure 2.20: Representation of hyperbolic tangent function and its derivative

Although the gradient of the hyperbolic tangent function is symmetric around 0 which improves the learning rate, it still experiences the gradient vanishing problem around -3 to 3. Nevertheless, the gradient has no restriction in terms of which direction it should go which makes it preferable over sigmoid activation function.

2.7) Mechanism of prediction

In this section, the steps utilized by ANN in making its predictions are described. Prior to ANN analysis, the data needs to contain two different parts for it to be possible to be analysed using ANN. The first part involves variables affecting the expected output (independent variables), while the second aspect is the output itself. In terms of corrosion under insulation, the corrosion rate represents the output, while the different variables affecting CUI rate (temperature, quantity and distribution of electrolyte in the insulation, presence of inhibitor, among others) represent the independent variables. The mechanism of prediction involves two types of data propagation. This include feedforward propagation which involves feeding the weighted input variable into the hidden layer containing the activation function where the output is being processed [58]. The other type is called backpropagation which involves feeding the error between the predicted output and actual output back into the hidden layer and assessment of the input variable with the highest error and makes the necessary

adjustment to its weight and bias values [58]. At the input layer, no computation is carried out, the input variables are assigned weights and bias values randomly during the feedforward propagation mode. The hidden calculations to arrive at the predicted output is shown below [59].

$$\text{Let } I = \begin{pmatrix} x_1 \\ x_2 \\ x_3 \\ \vdots \\ x_n \end{pmatrix}, \quad w_i = \begin{pmatrix} w_1 \\ w_2 \\ w_3 \\ \vdots \\ w_n \end{pmatrix} \quad b_i = b, \quad \text{Actual output} = x_a, \quad I \text{ represent the input}$$

parameters, w_i and b represent the weights and bias respectively.

The linear combination of the input parameters as reported by IBM [59] is given as:

$$L_i(x_i) = b + \sum_{i=1}^m w_i x_i \quad (2.5)$$

The function $L_i(x_i)$ is passed to the hidden layer where it becomes transformed by the sigmoid and hyperbolic activation functions.

$$\text{Activation function: Sigmoid } f(x) = \frac{1}{1+e^{-x}} \quad (2.6)$$

$$\text{Predicted output } (y_o) = f(L(x)) = \left(\frac{1}{1+e^{-(b+\sum_{i=1}^m w_i x_i)}} \right) \quad (2.7)$$

It is worth noting that the first predicted output (y_o) was obtained by random assigning of weights and bias values to the input variables. The network will then compute the error and identify the degree of deviation of the first predicted output with the original output.

$$\text{Mean Square Error}(MSE_i) = \frac{1}{N} \sum_{i=1}^N (x_a - y_o)^2 \quad (2.8)$$

Where x_a is the actual output and y_o is the predicted output.

The software will then compute the error due to the weights and bias through the back propagation mechanism and initiates the gradient optimization algorithm to correct the old random weights and bias values [60].

$$W_{new} = W_{old} - y_o \times \text{gradient} \quad (2.9)$$

$$b_{new} = b_{old} - y_o \times \text{gradient} \quad (2.10)$$

The new weights and bias are then applied on the input variables and the entire process is repeated several times until the predicted output converges to the minimum specified error. The different steps employed by ANN in obtaining predicted outputs from data sets are shown in Figure 2.21.

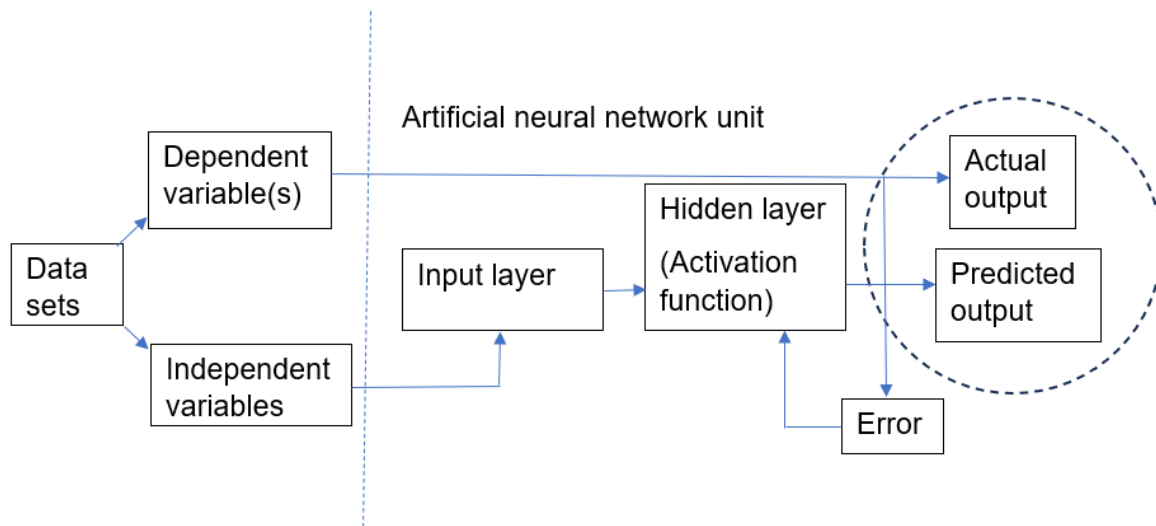


Figure 2.21: Mechanism of prediction using ANN

2.8) Limitations of artificial neural network

Artificial neural network has some drawbacks which limits its application despite the aura accorded to the technique as being among the top 5 within the field of predictive modelling [61]. One of which is that performance increases with number of input variables. This suggests that it tends to require the data for all the causal effects in order to obtain improved accuracy [62]. This is significant for outputs such as corrosion rate that results from a combination of parameters. In addition, ANN has been criticised to behave like a 'black box' in its predictions [63], which means that sometimes it presents an output that cannot be justified, in addition to being time consuming. However, these criticisms were applicable to the early ANN models, the calculations at the hidden layer are now known and the modelling time is now in minutes and no longer several hours. Nonetheless, the architectural network of ANN is designed for a particular application and may not be applicable in solving other

problems [62, 63]. This means that it presents the hassle of designing a new network architecture for each problem.

2.9) Summary

Corrosion under insulation is an external degradation of metals that is caused by the presence of water, moisture, oxygen, and other contaminants such as chlorides beneath the insulation. This occurs if the protective jacketing is breached leading to CUI which has enormous economic and safety concerns. CUI is affected by factors such as type of metal, condition of operation such as temperature, humidity, pH among others. The study of CUI is important in scheduling early maintenance and inspection plans to avoid unexpected failure.

The mechanism of corrosion of ferrous metals include: anodic dissolution of the metal with the release of electrons which migrates to the cathode where it reduced oxygen to hydroxide ions. The combination of the anodic and cathodic products results in the formation of ferrous oxide which can be oxidized to ferric oxide. The resulting corrosion could be said to be uniform if the degradation occurs over the entire or significant area of the metal surface. This is possible because the anodic and cathodic sites are not localized to a particular region of the metal. A uniform corrosion results from mobile anodic and cathodic sites with areas of high levels of oxygen likely to be the cathode, while the region with less oxygen will likely be the anode. Failure analysis of CUI incidences have revealed that a breach of the jacketing due to poor installation or damage which allows water to enter the insulation are the main causes of failure.

The use of galvanic current to determine the drying times of insulation has relied on the fact that as drying proceeds, the solution resistance increases which results in the galvanic current decreasing; thus, making it possible to monitor the drying process. The initial increase in temperature prior to reaching the target value, the galvanic current also increases. When the temperature stabilizes the galvanic current also tends to stabilize and starts decrease as the insulation dries out due to decrease in conductivity of the solution. On the other hand, the impedance decreases as temperature increases due to increased conductivity of the solution and stabilizes when the target temperature was reached. Then the resistance starts increasing even

though the temperature is still maintained at the target temperature due to the electrolyte in the insulation drying out. Moreover, when the quantity of electrolyte in insulation is very low or it has completely dried out, the galvanic current tends to 0 while the resistance becomes very high.

Artificial neural network uses patterns observed in data obtained from different influencing variables to make predictions by subjecting the variables to some non-linear activation functions and mapping to an output. The difference between the predicted and the actual output is computed and fed back to the hidden layer containing the activation function. This is iterated several times till the predicted output conforms to the specified minimum error. This has been useful in predicting the corrosion rates of metals since CUI depends on different variables such as temperature, quantity of electrolyte in the insulation as well as the presence of corrosion inhibitor in the insulation.

ANN prediction is based on these input parameters and the choice of activation functions as well as the network parameters such as number of hidden layers and nodes in each layer. Sigmoid and hyperbolic tangent activation functions have been widely used for corrosion predictions because they accept all real numbers in their domain and processes outputs that can be interpreted in terms of probabilities which is suitable for describing CUI data. Despite its usefulness, the fact that there is no universal network design that can solve all problems implies that each design is tailored to solve a particular problem which is one of the limitations of the technique apart from requiring large number of input data and variables for improved accuracy.

Chapter References

1. Jiang, R. J. and Cheng, Y. F. (2013). Mechanism of electrochemical corrosion of steel under water drop. *Electrochemistry communications*, 35:8-11.
2. Zhao, W., Zhang, T., Wang, Y., Qiao, J. and Wang, Z. (2018). Corrosion failure mechanism of associated gas transmission pipeline. *Materials*, 11:1935.
3. Pedferri, P. (2018). *Corrosion Science and Engineering*. 1st edition, Springer Nature, Switzerland, p. 212.

4. Lower, S. (2022). Electrochemical corrosion. Libretext Library, Simon Fraser University, U.S.A., pp 800-885.
5. Hilbert, L. R. (2006). Monitoring corrosion rates and localised corrosion in low conductivity water. *Corrosion Science*, 48:3907-3923.
6. Tan, Y., Aung, N. N. and Liu, T. (2012). Evaluating localised corrosion intensity using the wire beam electrode. *Corrosion Science*, 63:379-386.
7. Hayden, S. C., Chisholm, C., Grudt, R. O., Aguiar, J. A., Mook, W. M., Kotula, P. G. *et al.* (2019). Localized corrosion of low-carbon steel at the nanoscale. *Materials Degradation*, 3:17.
8. Cao, C. and Cheung, M. M. S. (2014). Non-uniform rust expansion for chloride-induced pitting corrosion in RC structures. *Construction and Building Materials*, 51:75-81.
9. Nestic, S. and Xiao, Y. (2004). A quasi 2D-localized corrosion model. NACE publications, paper number 04628.
10. Brossia, C. S. and Cragolino, G. A. (2000). Effect of Environmental Variables on Localized Corrosion of Carbon Steel. *Corrosion*, 56(5): 505-515.
11. Perry, S. C., Gateman, S. M., Stephens, L. I., Lacasse, R., Schulz, R. and Mauzeroll, J. (2019). Pourbaix diagrams as a simple route to first principles corrosion simulation. *Journal of the Electrochemical Society*, 166(11):3186-3192.
12. Berverskog, B. and Puigdomenech, I. (1996). Revised Pourbaix diagrams for iron at 25-300 °C. *Corrosion Science*, 38(12):2121-2135.
13. Caines, S., Khan, F. and Shirokoff, J. (2013). Analysis of pitting corrosion on steel under insulation in marine environments. *Journal of Loss Prevention in the Process Industries*, 26:1466-1483.
14. Burhani, N. R. A., Muhammad, M., Mokhtar, A. A. and Ismail, M. C. (2016). Application of logistic regression in resolving influential risk factors subject to corrosion under insulation. Proceedings of the 2016 International Conference on Industrial Engineering and Operations Management, Kuala Lumpur, Malaysia.
15. Pojtanabuntoeng, T., Machuca, L. L., Salasi, M., Kinsella, B. and Cooper, M. (2015). Influence of drain holes in jacketing on corrosion under thermal insulation. *Corrosion*, 71 (12):1511–1520.

16. Rana, A. R. K., Yang, M., Umer, J., Veret, T. and Brigham, G. (2022). Influence of robust drain openings and insulation standoffs on corrosion under insulation behaviour of carbon steel. *Corrosion*, 77(6):681-692.
17. Delahunt, J. F., 2003. Corrosion under thermal insulation and fireproofing, an overview. NACE publication, paper number 03022.
18. Mokhtar, A. A., Ismail, M. C., Zainordin, A. B., and Shahid, S. (2014). A framework for estimating piping reliability subject to corrosion under insulation. *Matec web of conferences*, 13:1-5.
19. Winnik, S. (2016). Corrosion under insulation (CUI) guidelines. 2nd edition, Woodhead Publishing.
20. Javaherdashti, R. (2014). Corrosion under Insulation (CUI): A review of essential knowledge and practice. *Journal of Material Science and Engineering*, 2(1):1-8.
21. Tsai, Y. H., Wang J., Chien, W. T., Wei, C. Y., Wang, X. and Hsieh, S. H. (2019). A BIM-based approach for predicting corrosion under insulation. *Automation in construction*, 107(102923): 1-14.
22. Cao, Q., Pojtanabuntoeng, T., Esmaily, M., Thomas, S., Brameld, M., Amer, A., Birbilis, N. A. (2022). Review of Corrosion under Insulation: A Critical Issue in the Oil and Gas Industry. *Metals*,12:561.
23. De Vogelaere, F. (2009). Corrosion under Insulation. *Process progress safety*, 28:30-35.
24. DNV (2022). - Maintenance management-corrosion under insulation (CUI). Report No. 2021-4107, 2nd Revision, Norway. p. 2.
25. Babakr, A. and Al-Subai (2006). Under Insulation Stress Corrosion Cracking of Process Piping. NACE Publications, 61st annual conference and exposition, Houston, Texas, paper number 06500.
26. Caines, S., Khan, F., Shirokoff, J., and Qiu, W. (2015). Experimental design to study corrosion under insulation in harsh marine environments. *Journal of Loss Prevention in the Process Industries*, 33:39-51.
27. Guo, B., Song, S., Chacko, J. and Ghalambor, A. (2005). Flow Assurance, offshore pipelines, Elsevier, pp 169-214.
28. Popov, B. N. (2015). Electrochemical kinetics of corrosion. Elsevier, pp 93-142.
29. Sotoodeh, K. (2022). Galvanic Corrosion. Case studies of material corrosion prevention for oil and gas valves. Elsevier, pp 271-286.

30. Shifler, D. A. (2006). Understanding and modelling galvanic corrosion in marine environments. NACE publications, paper number 06283.
31. Dobrego, K. V., Chumachenko, M. A., Boiprav, O. V., Grinchik, N. N. and Pukhir, H. A. (2020). Measurement of electrical resistance of liquid electrolytes and materials containing them. *Journal of Electromagnetic Analysis and Applications*, 12:7-14.
32. Dexter, S. C. (1999). Galvanic corrosion. Marine Advisory Publications, University of Delaware, U.S.A, pp 642-4261.
33. Blackwood, D. J. and Chong, A. S. L. (2013). Pitting corrosion on aluminium in absence of chloride. *British Corrosion Journal*, 33:219-224.
34. Klassen, R. D. and Roberge, P. R. (2004). Self linear polarisation resistance-theory and examples. *Journal of Applied Electrochemistry*, 34:723-727.
35. Landolt, D. (2007). Corrosion and surface chemistry of metals. 1st edition, EPFL press, Lausanne, Switzerland, p. 286.
36. McCafferty, E. (2010). Introduction to corrosion science. 1st edition, Springer New York, NY., U.S.A. pp 73-262.
37. Lasia, A. (2020). Electrochemical impedance spectroscopy and its applications. Springer Science and Business Media, New York, p. 15.
38. Macdonald, D. D. (2006). Reflections on the history of electrochemical impedance spectroscopy. *Electrochimica Acta*, 51:1376-1388.
39. Traficante, D. D. (1989). Impedance: What it is and why it must be matched. *Concepts in Magnetic Resonance*, 1:73-92.
40. Morgado, J. (2022). Modulation of the electrical double layer in metals and conducting polymers. *Scientific Reports*, 12:307.
41. Toparli, C., Sarfraz, A., and Erbe, A. (2015). A new look at oxide formation at the copper-electrolyte interface by in situ spectroscopies. *Physical Chemistry Chemical Physics*, 17:31670-31679.
42. Lasia, A. (2014). Electrochemical impedance spectroscopy and its applications. Springer Verlag, New York, U.S.A. pp1-367.
43. Khaled, K. F. (2011). Studies of the corrosion inhibition of copper in sodium chloride solutions using chemical and electrochemical measurements. *Materials Chemistry and Physics*, 125:427-433.

44. Zhang, G., Patuwo, E. and Hu, M. Y. (1997). Forecasting with artificial neural networks: The state of the art. *International Journal of Forecasting*, 14:35-62.
45. Dongare, A. D., Kharde, R. R., Kachare, A. D. (2012). Introduction to Artificial Neural Network. *International Journal of Engineering and Innovative Technology*, 2:189-195.
46. Nagyfi, R. (2018). The differences between biological and artificial neural networks. A web post published in Towards data science, <https://towardsdatascience.com/the-differences-between-artificial-and-biological-neural-networks-a8b46db828b7>, date accessed 10th November 2022.
47. Gupta, N. (2013). Artificial Neural Network. *Network and Complex Systems*, 3:24-30.
48. Caines, S., Khan, F., Shirokoff, J., and Qiu, W. (2015). Experimental design to study corrosion under insulation in harsh marine environments. *Journal of Loss Prevention in the Process Industries*, 33:39-51.
49. Vera, R., and Ossandon, S. (2014). On the prediction of atmospheric corrosion of metals and alloys in chile using artificial neural networks. *International Journal of Electrochemical Science*, 9:7131-7151.
50. Sharma, V., Rai, S. and Dev, A. (2012). A comprehensive study of artificial neural network. *International Journal of Advanced Research in Computer Science and Software Engineering*, 2:278-285.
51. Burhani, N. R. A., Muhammad, M. and Ismail, M. C. (2018). Corrosion under insulation rate prediction model for piping by two stages of artificial neural network. AIP Conference proceedings, paper number 030004.
52. Thike, P. H, Zhao, Z., Shi, P., and Jin, Y. (2020). Significance of artificial neural network analytical models in materials' performance prediction. *Bulletin of Material Science*, 43:211-233.
53. Sibi, P., Jones, S. A., Siddarth, P. (2013). Analysis of different activation functions using back propagation neural networks. *Journal of Theoretical and Applied Information Technology*, 47:1264-1269.
54. Feng, J. and Lu, S. (2019). Performance analysis of various activation functions in artificial neural networks. *Journal of Physics*, 1237:1-7.

55. IBM for Cloud Education (2020). Neural Networks. A post on What are Neural Networks? <https://www.ibm.com/uk-en/cloud/learn/neural-networks> , date accessed 11th November, 2022.
56. Farzad, A., Mashayekki, H., and Hassanpour, H. (2019). A comparative performance analysis of different activation functions in LSTM networks for classification. *Neural Computation and Application*, 31:2507-2521.
57. Lima, L. F., Vieira, A. L., Mukai, H., Andrade, C. M. G. and Fernandes, P. R. G (2017). Electric impedance of aqueous KCl and NaCl solutions: Salt concentration dependence on components of the equivalent electric circuit. *Journal of Molecular Liquids*, 241:530-539.
58. Cichocki, A., and Unbehauen, R. (1993). Neural Networks for optimization and signal processing. John Wiley and sons Limited, Chichester, England. pp. 67-162.47.
59. El-Abassy, M., Senouci, A., Zayed, T., Mirahadi, F., Parvizsedghy, L. (2014). Artificial neural network models for predicting condition of offshore oil and gas pipelines. *Automation in Construction*, 45:50-65.
60. Chung, N. T., Choi, S. R., and Kim, J. G. (2022). Comparison of response surface methodologies and artificial neural network approaches to predict the corrosion rate of carbon steel in soil. *Journal of the Electrochemical Society*,169:1-10.
61. McMahan, S. (2020). Artificial Neural Network Disadvantages. A post on Data Science, <https://www.datascienceexamples.com/artificial-neural-network-disadvantages/> , date accessed 11th November, 2022.
62. Jimenez-Come, M. J., Martin, M. L., Matres, V. and Balades, J. D. M. (2020). The use of artificial neural networks for modelling pitting corrosion behaviour of EN 1.4404 stainless steel in marine environment: data analysis and new developments. *Corrosion Reviews*, 38(4):339-353.
63. Sharma, V., Rai, S. and Dev, A. (2012). A comprehensive study of artificial neural network. *International Journal of Advanced Research in Computer Science and Software Engineering*, 2:278-285.

CHAPTER 3 : REVIEW OF RELATED LITERATURE

CHAPTER THREE

REVIEW OF RELATED LITERATURE

This chapter covers the study of the corrosion of metals under insulation. This includes water absorption studies, design of CUI test rigs, effects of temperature and inhibitors on the rate of CUI as well as predictive modelling of CUI rate using artificial neural network. The review is mainly focused on CUI systems that uses carbon steel as the metal substrate and mineral wool as the insulation, though reference is also made to other materials when needed. This is because carbon steel and mineral wool insulation are the most common materials used in the industry due to cost, availability, ease of installation, high thermal insulation properties, among others [1, 2, 3].

The purpose of the review is to assess the research that has been done within the field of corrosion of metals under insulation. This includes identifying gaps in the literature which this study is trying to fill and areas that still needs further research as well as linking up the research that has been carried out to assess the trend over the previous years. In addition, only a few researchers have shown interest in the corrosion of insulated metals, which is evident in the number of publications compared to uninsulated or immersion conditions. Therefore, this review will highlight technical challenges associated with measurement of CUI rates which will elicit discussions for solutions.

In addition, this section also assesses the water absorption capacity of different insulation materials with particular attention to mineral wool and different designs of test rig used for CUI studies as well as its limitations. Also, the effects of temperature and inhibitor on the corrosion rate of insulated carbon steel are covered. This is to ensure that there is not much deviation from the focus of the research as other metallic substrates has significantly different properties. The prediction of CUI rate using artificial neural network was assessed for both insulated and uninsulated conditions due to the dearth of publications on the CUI rate prediction using Artificial Neural Network.

There are interesting discussions on CUI in the literature ranging from water absorption capacity of insulation materials [4, 5, 6], inspection techniques [7, 8], failure analysis [9, 10], rate of CUI [11, 12], inhibitors [13, 14, 15], and theoretical predictions of CUI rate [16, 17]. Nevertheless, in this chapter, only discussions that are relevant to this research are included. This includes relevant water absorption studies, rate of CUI, inhibitors, and theoretical predictions using ANN. Therefore, the review begins with the study of the water absorption capacity of mineral wool insulation, including the effect of thermal treatment on water absorption capacity. This is followed by the study of the effect of factors affecting CUI rate such as temperature, including thermal cycling, and inhibitor. In addition, the available literature on electrochemical methods of measuring drying times of the insulation as well as the prediction of the rate of corrosion of carbon steel using ANN are assessed.

3.1) Available literature on the determination of the water absorption capacity of mineral wool insulation

The water absorption capacity of mineral wool insulation has been studied by some researchers in the literature in order to assess the moisture content and to understand the moisture transport properties within the mineral wool insulation. Investigations of the water absorption capacity of mineral wool insulation can be carried out over a short period in hours or over a long term like several days. It is important to study the degree of water absorption or repellency of mineral wool insulation as the quantity of water absorbed can influence the CUI rate of the underlying metal as well as the drying out time. For instance, Karamanos *et al.* [18] has explained that the fibres of mineral wool insulation are detached from each other under moist conditions as water separates the binders holding the fibres together. There are standard methods of determining the water absorption capacity of insulation materials; some of which involves full immersion of the insulation in water [19, 20], while some involve partial immersion of the insulation in water [21, 22]. A summary of the procedures for determining the water absorption capacity of insulation materials using these standards are presented in Table 3.1.

During the production of mineral wool insulation, some hydrophobic additives of organic or inorganic origin are usually added to improve the water repellency of the insulation material [23]. The thermal treatment of mineral wool insulation at temperatures as high as 250 °C has been reported to result in the degradation of the organic additives that impart hydrophobicity to the insulation culminating in enhanced water absorption properties of the insulation [23]. Moreover, the lifetime of these additives has been reported to reduce with increasing temperature resulting in a greater risk of water penetration to the insulation [24]. Organic binders may be in the form of polymeric resins from the family of esters or aromatic compounds.

The thermal decomposition products of the organic moiety in the resin as reported by Knop and Pilato [25] as well as the mechanism involved in the product formation are shown in Figure 3.1. The binder will decompose at temperatures greater than 175 °C to give lower chain structures such as dihydroxy benzophenone, which further breaks down to 2,4-xyleneol, which is a highly volatile compound and will likely escape from the insulation alongside CO₂. Although the fibres of mineral wool insulation have been reported to withstand high temperatures up to 1200 °C [26], the phenol formaldehyde resin that binds the fibres together as well as other organic compounds responsible for the hydrophobicity of the insulation have been reported to degrade when conditioned at 105 °C [27]. This would result in rapid uptake of water by the thermally degraded insulation allowing water to gain access to the insulation.

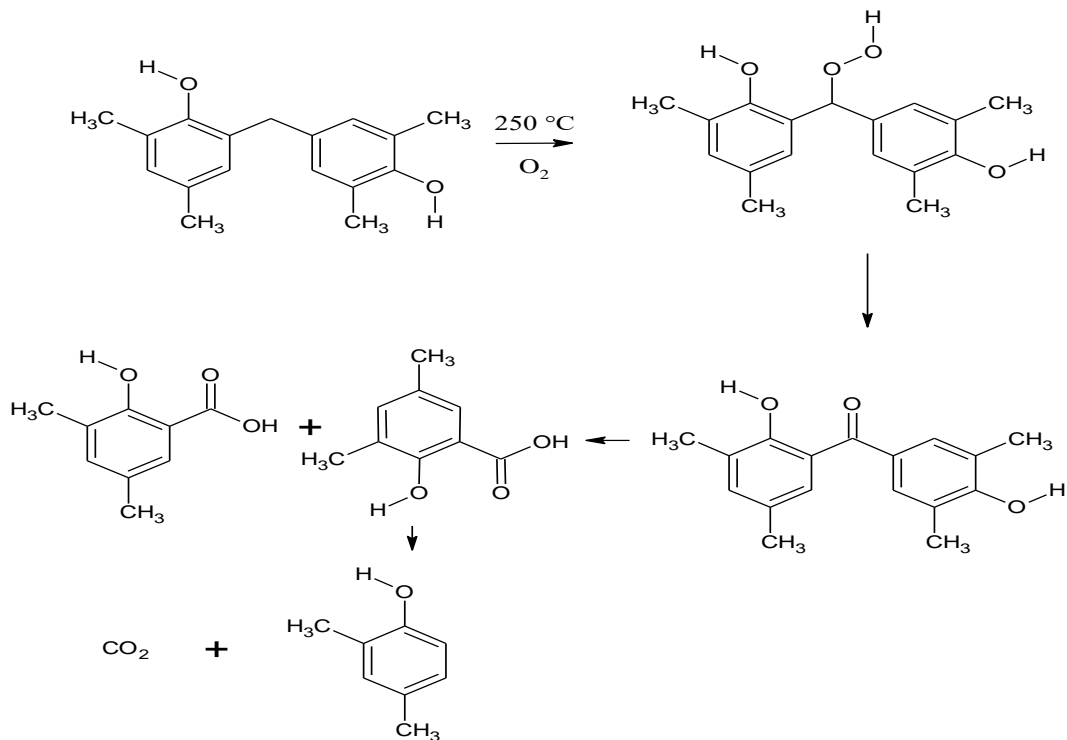


Figure-3.1: Thermal decomposition products of phenolic resin of mineral wool insulation [25].

In the literature, Zwaag and Rasmussen [28] investigated the effects of different hydrophobic additives on the water repellency of mineral wool insulation using both partial immersion method according to BS EN 13472 standard and full immersion technique reported in ASTM C1763 standard. The results in this report were presented as numbers in tables, this has been plotted for better visualization and it is shown in Figure 3.2.

Table 3.1 : Comparison of the four standards used in determining the water absorption characteristics of thermal insulation materials.

ASTM C1511 [2]	ASTM C1763 [3]	BS EN 13472 [4]	BS EN 1609 [5]
No conditioning of the specimen is required.	Pre-conditioning according to C870 standard is required.	Conditioning is required at 23 °C for 6h.	Conditioning is required at 23 °C for 6h.
Determines the absorption by full immersion	Determines absorption by full immersion	Determines absorption by partial immersion	Determines absorption by partial immersion
Distilled or deionized water is recommended as the immersion medium	Distilled or deionized water is recommended as the immersion medium	Tap water can be used as the immersion medium	Tap water can be used as the immersion medium
The sample drainage for 60seconds is recommended after immersion.	The specimen is weighed immediately after removal from water.	Drainage is recommended for 10 minutes after immersion.	Drainage is recommended for 10 minutes after immersion.
The immersion time is 15 minutes.	The immersion time is a minimum of 48 hours.	The immersion time is 24 hours.	The immersion time is 24 hours.
The Insulation is tested without a facing or a jacketing.	Not specified.	Any skin, facing or coating shall be retained.	Any skin, facing or coating shall be retained.

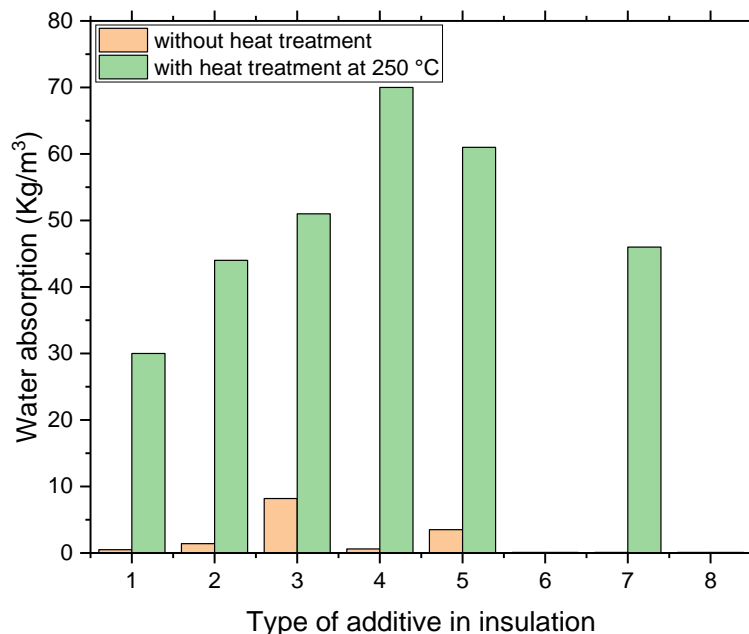


Figure 3.2: Water absorption of mineral wool samples with different hydrophobic additives using EN13472:2012 standard: samples 1-5 represent an insulation with a mineral oil-based additive, 6 and 7 represent an insulation with a silicone oil-based additive while sample 8 represent an insulation with an inorganic resin [28].

The sample numbers shown in Figure 3.2 represent the type of hydrophobic additive in the insulation as well as the region of purchase. Sample number 1-5 represent a mineral oil additive, while 6 and 7 represent silicone oil and 8 represents an inorganic resin. Samples 1 and 2 were purchased from the mainland Europe while 3-5 were purchased from North America. Samples 6 and 7 were obtained from the UK. The results show significant variability in water absorption for samples that were treated with the same type of hydrophobic additive. This may be due to differences in material properties due to different production recipes. The insulation samples with mineral oil additives that were aged at 250 °C were observed to show higher water absorption compared to insulation samples that were not aged. This is attributed to the fact that these additives are decomposed at a higher temperature thereby reducing the water repellency of the insulation material; hence, a higher water absorption is observed compared to unaged insulation samples.

It is interesting to observe that the water absorption of insulation samples with silicone oil and inorganic resins (samples 6 and 8) showed no difference in water absorption after heat treatment which indicates that the additives are yet to be decomposed at that temperature. However, the water absorption capacity of sample number 7 is questionable as the authors have declared that it was also made of silicone oil additive. The thermal stability limit of silicone oils has been reported to be 250 °C in a different study [23]. Therefore, it could be possible that slight temperature fluctuation beyond 250 °C might initiate decomposition of silicone oils leading to the reported water absorption value. Notwithstanding, the results reported by Zwaag and Rasmussen [28] (Figure 3.2) seems like a one-off measurement as no repeated measurements were reported which might not be representative of the true absorption capacity as significant deviations between replicate measurements have been reported by other researchers [29].

In another study, mineral wool insulation samples were aged at different temperatures (100 °C and 150 °C) for different aging times ranging from 1 h to 36 days. These temperatures are expected to degrade the organic additives in the insulation, while the silicone oil additives are expected to degrade at about 250 °C. In the report, the water absorption capacity of the insulation material was investigated using ASTM C1511 standard. This involved immersing the insulation samples in water at a temperature of

about 21 °C for 15 minutes after which the samples were removed and allowed to drain for a minute before it was reweighed. The authors presented the results in a table, this has been plotted to show the trend of thermal treatment and water absorption capacity of the insulation material.

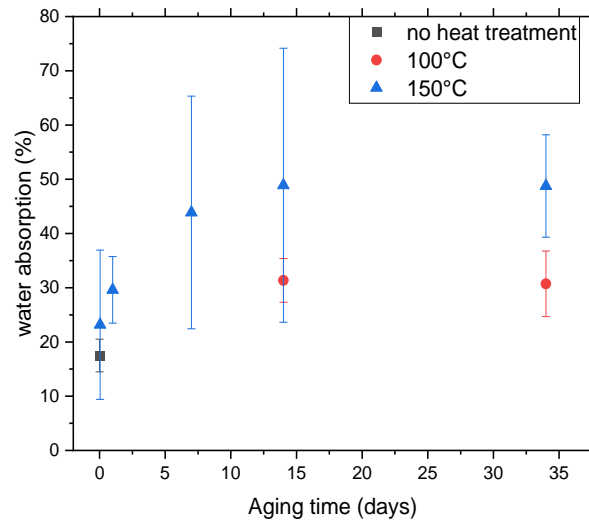


Figure 3.3 : Effect of thermal treatment on the absorption of water by mineral wool insulation using ASTM C1511 standard [29].

The result shown in Figure 3.3 also indicate an increase in water absorption as the temperature that the insulation was aged increases which agree with the result of [28]. This indicates decomposition of the binder and oily additives resulting in increased absorption of water by the insulation. Mineral wool insulation consists of polymeric binders that hold the fibres together and oily additives that impart hydrophobicity to the material. The slight increase in water absorption for samples aged at 100 °C for 15 and 35 days compared to samples that were not thermally treated suggests that only the polymeric binder was decomposed. Also, some polymeric resins from esters or aromatic origin have been reported to decompose at 175 °C [30], while phenyl formaldehyde resins have been reported to decompose at 105 °C [31]. Therefore, this suggests that the polymeric binder used in the research might be the first to decompose as it also imparts some hydrophobicity to the material in addition to the oily additive. Nevertheless, the results shown in Figure 3.3 indicates significant variability at some points as observed by the length of the error bars which according to the authors represent the standard deviation of several repeated measurements.

The long-term water absorption of mineral wool insulation was investigated by Kosinski *et al.* [32] and Williams and Evans [33] using EN ISO 12571:2013-12 standard. The results of their investigation are shown in Figures 3.4 and 3.5 respectively. Kosinski *et al.* [32] observed that the insulation continued to absorb water after a 22-day immersion period without saturation. This agrees with the findings of Williams and Evans [33], who also observed an increase in water absorption for 80 days without saturation. However, the absorption is continuous in their report, whereas the report of Kosinski *et al.* [32] contains some reduction in quantity of water absorbed as time increased which might be due to error during measurement. Moreover, in Kosinski's report, it is quite strange that when the medium was changed to sodium chloride solution, the insulation tends to saturate after 1 day. The authors did not provide any explanation for this behaviour, neither did they carry out repeated measurements to validate their results. It is important that repeated measurements be carried out when performing water absorption studies in order to observe repetitive trends which will provide an overall trend of water content with time. This would enable valid discussions and conclusions to be drawn which is more reliable than one-off measurements.

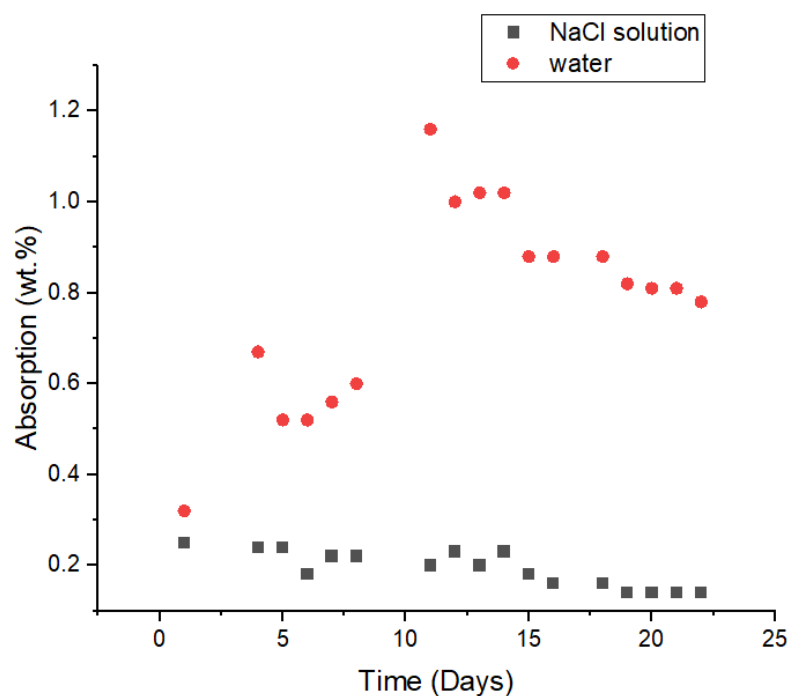


Figure 3.4 : The absorption capacity of mineral wool insulation in different media using EN ISO 12571:2013-12 standard [32].

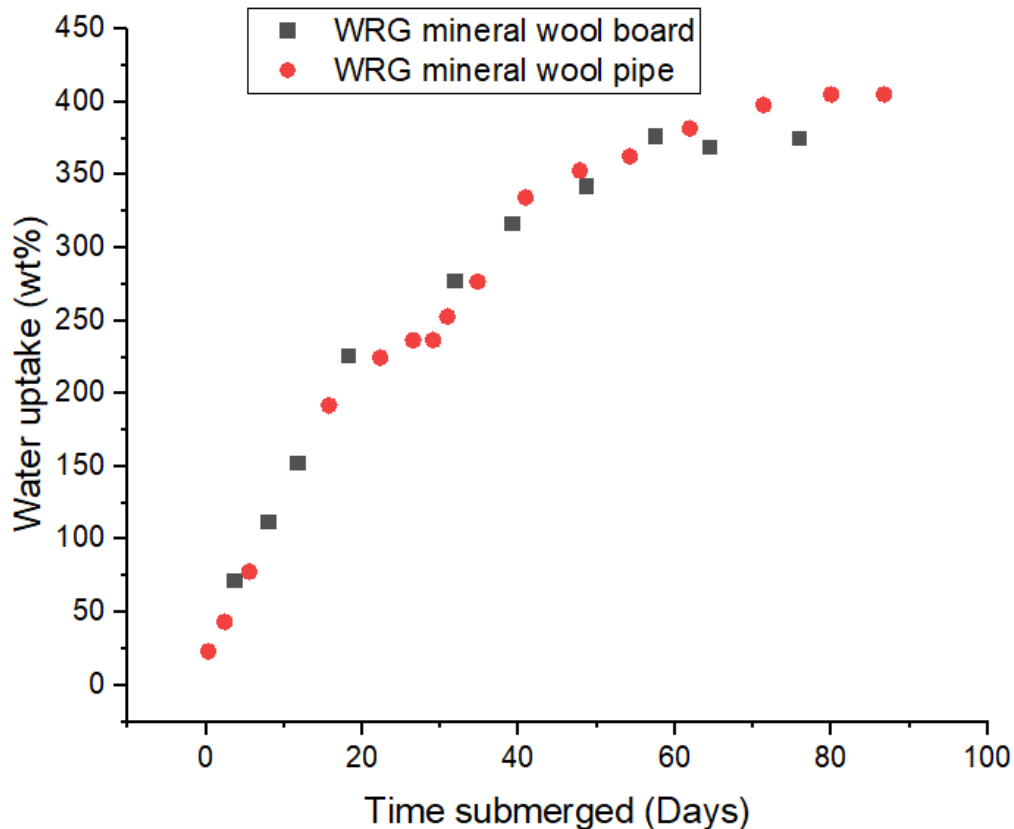


Figure 3.5 : The water absorption of mineral wool board and pipe [33].

3.2) Test rigs for studying the rate of CUI in the laboratory

There are a few test rigs that have been used in studying the rate of corrosion of insulated metals in the laboratory. This includes: the ASTM test rig [34], the rain chamber by Ayello and co-researchers [35], as well as other modified CUI test rigs based on the ASTM G189 standard by researchers at Curtin University, Australia [36], University of Alberta, Canada [37] and Safety and Risk Management group, Canada [38].

3.2.1) The ASTM CUI test rig

This is an advanced test rig for accelerating CUI in the laboratory. It has been the basis of most test rigs used in the literature due to its ability to simulate both isothermal and wet-dry cycles. The schematic representation of the ASTM test rig is shown in Figure 3.6.

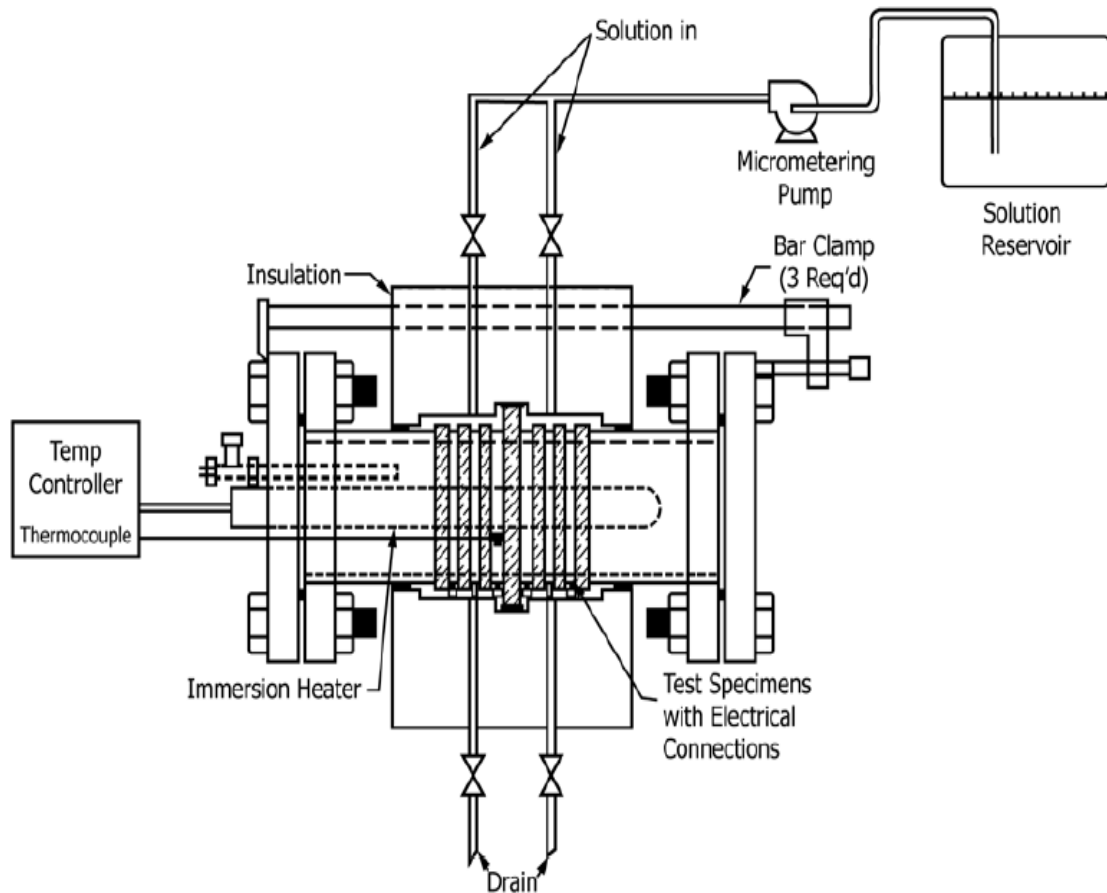


Figure 3.6 : Schematic representation of ASTM test rig [34]

The test rig consists of six metal ring samples separated from each other by PTFE spacers to prevent contact with each other which could interfere with electrochemical measurements. Even with the weight loss method, the ASTM standard still recommends that the metal rings be separated from each other using PTFE spacers. The six metal rings and spacers are polished with silicon carbide papers, rinsed with deionized water, alcohol and dried in an inert atmosphere, the cleaned rings are held together in a stack. At both ends of the stack are two end flanges that holds the stack together in position. The base metal plates, held together by a bar clamp are used to support the end flanges from where the inlet and outlet tubes are connected to allow the flow of oil in and out of the rig from a reservoir. An Immersion heater is inserted at the internal portion of the rig to maintain the temperature of the rings and the insulation is wrapped around the test area containing the rings, leaving a small annular space of about 0.5 cm to allow the flow of electrolyte around the test region. Electrolyte is

pumped into the test rig from a solution reservoir, which fills the annular space between the insulation and the ring and can be drained out at the bottom of the rig.

3.2.2) Limitations of the ASTM test rig

Although the ASTM test rig has been quite useful in simulating CUI in the laboratory, a few limitations have been identified by researchers that prompted the development of modified versions in order to better reflect the CUI situation in the field. For example, Pojtanabuntoeng *et al.* [36] had outlined some of the limitations of the ASTM test rig to include incorporation of a gap at the insulation-metal interface which does not simulate actual CUI situation, possibility of interruption during electrochemical measurements when the insulation fully dries out, the rig does not allow for investigation of the effect of climatic factors such as temperature changes.

In addition, each experimental run using the ASTM rig requires assembly, disassembly and re-assembly for subsequent experiments which is quite labour intensive. The researchers at Curtin University suggested the use of split rings which is easy to remove without disassembling the entire test rig [36]. However, the split ring system might be quite prone to oil leakage if not properly sealed. Besides, it is difficult to align the metal rings and spacers perfectly and reproducibly. Any misalignment during experiments could result in an oil leakage which means that the whole rig must be disassembled, cleaned, and reassembled.

These limitations pointed out by researchers at Curtin University seems valid especially the incorporation of a gap between the insulation and metal as engineers try to eliminate such gaps during installation so that it does not serve as conduit for water to infiltrate. Besides, circulating an electrolyte at the insulation-metal interface merely simulates an immersion condition rather than a CUI. Also, the ASTM test rig and most of the modified test rigs use immersion heaters to maintain constant temperature of the feed as well as the rings. Although this will provide reasonable CUI data as all the ring samples are being investigated under isothermal condition, this does not reflect the situation in the field. In industry, only the insulation is used to maintain the temperature of the pipe as the influent flow from one point to another, and no inner heating element is used across the entire length of the pipe. In addition,

the introduction of an electrolyte from the top and collected from the bottom does not actually wet the insulation. A typical CUI condition considers the entry of electrolyte at the top only in most cases due to damaged or poorly installed insulation, which is why CUI is always regarded as the more severe form of corrosion as water is trapped beneath the insulation and maintains contact with the metal for a long period.

3.3) The rain chamber

The rain chamber was developed to study how the response from different atmospheric conditions can be used to develop a reliable sensor network for the detection of CUI [35]. A schematic representation of the rain chamber is shown in Figure 3.7. This consists of an insulated loop in which the temperature is maintained by circulating a liquid either from the heating or cooling unit through the loop. Rain in the form of droplets is simulated using a pump and a steam generator. Also, different conditions such as drizzle, shower and dry can be simulated and corrosion detection sensors (s) and humidity sensors (H) were installed to detect any degradation of the underlying metal. However, Pojtanabuntoeng *et al.* [36] has pointed out that it may not be possible to achieve a significant CUI rate within a realistic timeframe as CUI takes a long time to occur if certain conditions have been met.

In addition, it seems the design is not operating under an accelerated condition. With the jacketing in place, the raindrops will merely run over it without penetrating or soaking the insulation. Even if a single drop eventually gets in by some means, the CUI rate obtained might just be negligible. The fact that the authors have not specified the route of entry of the water into the insulation makes it difficult to know how the insulation will get wet. Also, if the temperature of the pipe is not sufficient to degrade the insulation, then any rain drop that finds its way through the jacketing may not gain access to the surface of the metal. Besides, the design requires corrosion detection sensors to be attached throughout the insulated loop. This is expensive and unrealistic in real life application. This is because it might not be economically feasible to install sensors at every point on all the pipes in operation. Besides, it is possible that corrosion might initiate at a spot that has no corrosion sensor installed leading to leakage at that spot.

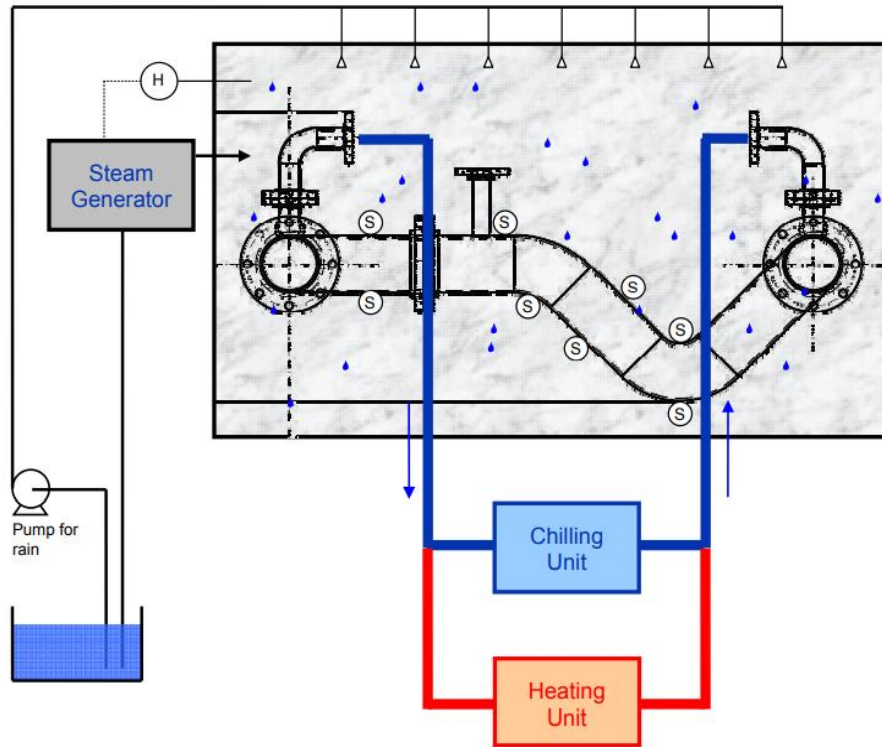


Figure 3.7 : A rain chamber for simulating CUI [35]

3.4) Other modifications of ASTM test rig

The ASTM test rig has served as the basis of most modified test rigs reported in the literature despite the limitations mentioned earlier. In this section, the focus will be on the modifications that each author has made instead of repeating the entire ASTM test rig for each modification. In 2015, researchers at Curtin university have reported a new experimental rig shown in Figure 3.8 to investigate CUI at different climate conditions which was used to accelerate CUI in the laboratory. The reported test rig contained a few adjustments from the ASTM G189 standard such as elimination of the gap between insulation and metal, pre-wetting of the insulation instead of pumping in the test solution into the rig, the use of split rings to compare corrosion rates at the top and bottom parts of the rings independently. This seems quite useful and eases the stress of the frequent disassembly and reassembly of the test rig for each experimental run. However, for this configuration, there is a high possibility of an oil leakage especially at the joints where the top and bottom rings meet.

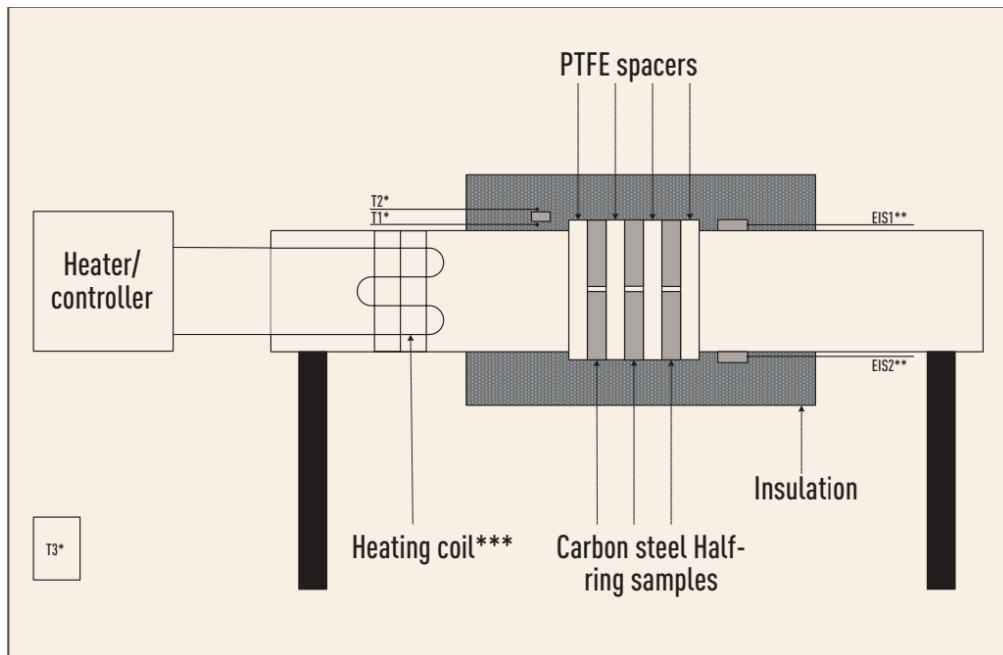


Figure 3.8: A modified CUI test rig by researchers at Curtin University [36].

In addition, the Safety and Risk Engineering group at the Memorial University of Newfoundland, Canada developed a CUI test rack to monitor the corrosion of insulated metals under field conditions as shown in Figure 3.9, in addition to the ASTM test rig that they used to monitor CUI under laboratory conditions. The CUI test rack looked quite promising; however, it will take an unrealistic time to obtain a reasonable CUI rate under field conditions as CUI is a slow process which may take years before a significant CUI rate can be obtained. This is the reason why accelerated conditions are usually employed in the laboratory. Other studies that have used the ASTM test rig without any significant modifications include *In situ* measurement of CUI by Yang and Liu [37], cyclic CUI testing by Zwaag and Rasmussen [4], effect of coatings, temperature variation and insulation types on CUI by Putra *et al.* [39] among others. Furthermore, Cao *et al.* [40] provided a report where a vessel was used to monitor the CUI of mild steel panels as well as the effect of dissolved metal ions. In their report, they soaked pieces of wet insulation in the vessel and immersed the metal panels inside the wet insulation. This merely represents an immersion condition rather than a corrosion under insulation environment.

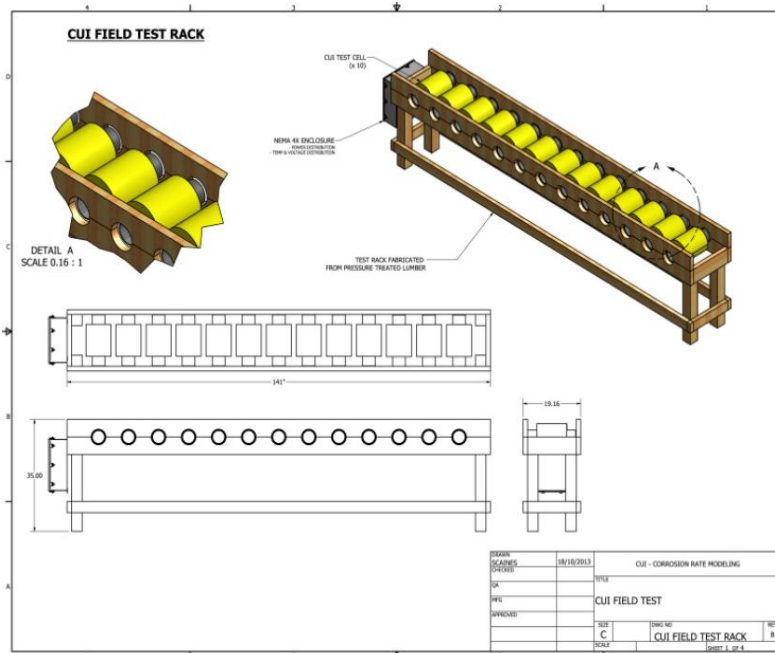


Figure 3.9: A CUI test rack for field studies [32].

In another study, a modified version of the ASTM test rig was reported by Essien and Neville [41]. The key modifications include the use of a single continuous pipe instead of metal rings, separation of the test area from the other pipe sections as well as different dimensions of the rig. A schematic representation of the modified test rig is shown in Figure 3.10. The design of the test rig is quite suitable for comparing two different conditions which may serve as test and control. For example, the corrosion rates of metals in an insulated and uninsulated environment or CUI with and without inhibitor since it is separated into two different compartments. However, a major drawback of the modified rig is that it has an operational limit of 90 °C which means it is not safe to operate at higher temperatures where CUI have been reported. Besides, the use of a single continuous pipe will present difficulty in quantifying the corrosion rate by weight loss across different sections of the pipe.

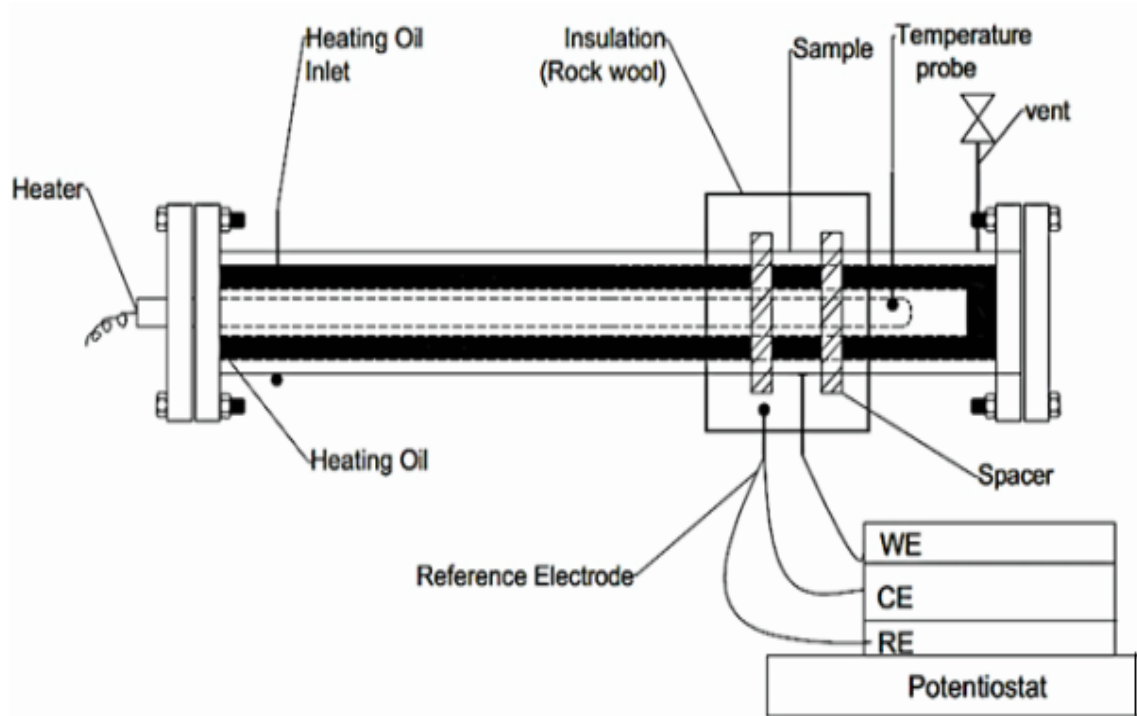


Figure 3.10: A modified CUI test rig by Essien and Neville [41]

3.5) The challenges and precautions associated with CUI test rigs

The challenges associated with CUI test rigs might likely be the reason for the disparity between published articles on corrosion under insulation in the literature and immersion conditions that do not require any test rig besides the vessel the samples will be immersed. Besides, the fact that the test rig needs to be disassembled after every trial in order to access the rings, clean and measure the weight loss and reassemble the test rig again for next experiments is enough demotivation for most researchers. Even though an advanced test rig has been provided by the ASTM standard as the basis by which other modified forms can be developed, most researchers don't see the need to talk about these challenges. This may probably be attributed to the fact that either they don't want to discourage researchers, or they assume it will devalue the research output. However, bringing these issues to limelight will enable researchers to take it into consideration when designing test rigs or modifying already established test rigs for CUI studies.

The challenges associated with the CUI test rigs will be discussed in relation to similar issues faced during this research. This will serve as the basis for discussions on

possible solutions. For the ASTM based rig, the common issue with the CUI test rigs is oil leakage during experiments [4, 36]. This may be caused by not tightening the bolts of the base metal plates properly or the PTFE spacers used to isolate the metal rings have become squashed. This implies that the experiment will be stopped, and the entire CUI set up would be disassembled, which can be quite laborious. To avoid this problem, it is important that the bolts of the base metal plates be tightened, and new PTFE spacers replaced frequently to avoid being squashed during experiments.

Another important issue associated with CUI test rig include aligning the metal rings and spacers perfectly. Failure to achieve this could result in an oil leakage, lack of contact of some parts of the rings with the insulation among others. To minimize this effect, it is necessary to machine both the metal rings and the spaces together so that both materials have equal and uniform diameter. This would ensure that the insulation contacts the metal without a gap. In addition, care must be taken into consideration during assembly and disassembly of the CUI test rigs. This is because the base metal plates, end flanges and the metal rings can cause serious harm if it fell on someone. Therefore, complete PPE must always be worn during experiments. Moreover, the hot circulating oil must be allowed to cool to a safe temperature before the rig can be disassembled.

3.6) Determination of CUI rate and effect of some influencing factors

The determination of the rate of CUI has been carried out mostly using weight loss method [36, 4, 30], linear polarisation resistance (LPR) technique [42, 40, 12, 37], and electrochemical noise [43, 44, 45]. The weight loss method involved determining the difference in weights of the metal samples before and after exposure to a corrosive environment. This can either be studied under isothermal condition where the pipe is gradually heated to a constant temperature, and it is maintained at that temperature for some time before cooling to room temperature or cyclic conditions involving gradual heating of the pipe to the target temperature, it is maintained at the temperature for a short period then it cools to a certain temperature and heats up again to the target temperature and the cycle continues.

For a cyclic CUI condition, the wet cycle involves measurement at temperatures that would allow the electrolyte to exist as a liquid in the insulation, while the dry cycle

consists of measurements at a temperature that the insulation is expected to dry out. In Figure 3.10, C-F and D-G represents an isothermal condition where the temperature is fixed for the entire duration of the tests. However, an initial ramping up to the target temperature is required prior to attaining the isothermal temperature. In the guideline, it has been suggested that the heating up stage to the target temperature should be about 1 h duration or less, the point at which the temperature is maintained can be as long as necessary, but the cooling down should not exceed 2 h and should reach 38 °C for the duration to be considered complete [34].

On the other hand, the cyclic condition (B-E) requires an intermittent change in temperature in which the insulation is expected to be wet at one temperature and dry out at the other temperature. The ASTM G189 standard recommends that the duration for the wet cycle be 20 h, while the duration of the dry cycle be 4h. However, it did not specify the temperatures that should be used for each cycle; instead, it suggested that the temperature should be specified by the user. The isothermal and wet dry cycles as used in most literatures are shown in Figure 3.11, while the 4 possible cycles specified by the ASTM standard and the minimum duration are presented in Table 3.2.

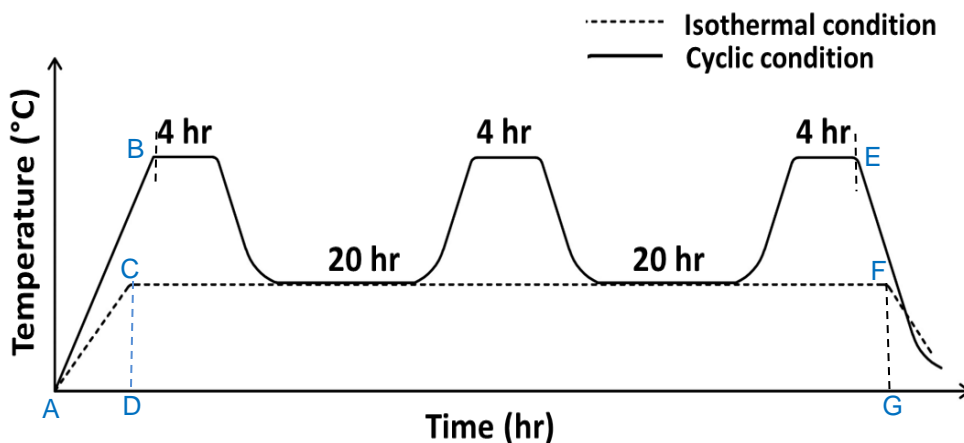


Figure 3.11: A plot showing the difference between an isothermal and a cyclic condition.

Table 3.2 : A plot showing the recommended times for isothermal and cyclic conditions [34]

Code	Description	Minimum Duration (h)	Cycle time (h)
IW	Isothermal-wet	72	NA
IWD	Isothermal-wet/dry	72	20 wet / 4 dry
CW	Cyclic-wet	96	24 hot / 24 cold
CWD	Cyclic-wet/dry	72	20 wet / 4 dry 20 cold / 4 hot

Rana *et al.* [42] investigated the effect of isothermal and cyclic conditions on the corrosion of carbon steel under mineral wool insulation. The isothermal condition was carried out at 100 °C for 24 h, while the cyclic condition consists of 40 °C for 20 h during the wet period and 100 °C for 4 h during the dry period. The results are shown in Figure 3.12. Comparing the isothermal wet/dry with the isothermal wet and cyclic wet/dry with cyclic wet conditions, the results indicated that the wet/dry and cyclic temperature cycles have higher corrosion rates than the isothermal wet and cyclic wet conditions. The authors suggested that cyclic temperatures involved the concentration of chloride ions especially during the dry cycle as well as higher concentration of dissolved oxygen at 40 °C compared to 100 °C, which tends to suppress anodic reactions but favours the cathodic reaction involving the reduction of oxygen to hydroxyl ions [42]. This agrees with the recent report of Cao *et al.* [40] who showed that CUI is aggravated in an equipment operating under wet/dry or thermal cyclic conditions. Although the distribution of dissolved oxygen within a liquid depends on the chemical composition of the study site, it has generally been established that dissolved oxygen levels is higher at the surface compared to the bulk of the liquid [46]. Therefore, corrosion which occurs at the metal-solution interface is expected to be aggravated.

However, the cyclic wet/dry condition had a significantly lower corrosion rate compared to an isothermal wet/dry condition both in the presence and absence of drain holes. It is only when there was no contact between the insulation and the rings and there was drain holes that the isothermal wet/dry condition was less than the cyclic wet/dry condition. Besides, the duration of thermal cycling (96 h) was higher than the isothermal wet/ dry condition (72 h) which makes the results a bit strange. Moreover, the authors did not explain the reasons for the choice of the temperature especially

the reason why 40 °C was chosen for both isothermal and cyclic conditions. The choice of temperature when simulating isothermal and cyclic CUI conditions is quite important and should be justified.

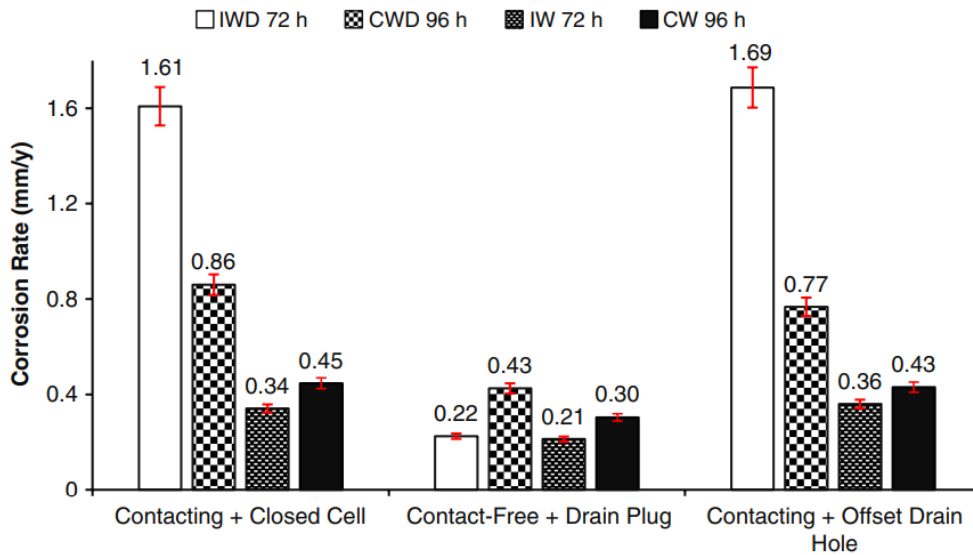


Figure 3.12: The corrosion rate of carbon steel under mineral wool insulation for isothermal and cyclic conditions [42].

Notwithstanding, the results presented by [42] also agree with the findings of Yang and Liu [37] who investigated the CUI of carbon steel under wet/dry and cyclic temperature conditions. In their report, the corrosion rate of carbon steel under mineral wool insulation was assessed at 50 °C for 20 h under wet condition and 93 °C for 4 h under dry conditions, as well as isothermally at 50 °C and 93 °C. Their results are shown in Figure 3.13. This also indicated a higher CUI rate during the thermal cycling compared to the isothermal condition at both temperatures. However, when considering the effect of increasing temperature on CUI, it would be expected that the corrosion rate at 50 °C should be reasonably lower than the corrosion rate at 93 °C. This is because corrosion rate is expected to increase with temperature and the drying out effect of the insulation is not expected to be dominant at 50 °C yet. This is because an increase in temperature is expected to increase the mass transport of ions and/or influence the kinetics of the reactions. However, this is expected to dominate at lower temperatures as other competing factors such as decreasing dissolved oxygen levels

and increased drying out of the insulation which would likely result in a decreasing corrosion rate tends to dominate as the temperature is increased.

However, only a slight difference in corrosion rate is observed between the isothermal conditions at 50 °C and 93 °C which is quite unusual, and the authors have not provided any explanation to this effect. Moreover, Cottis *et al.* [47] had asserted that corrosion data is inherently variable, this has reflected in the large error bars of corrosion data reported in the literature; however, the corrosion rates reported by Yang and Liu [37] seems quite reproducible from the length of the error bars unlike a typical corrosion data that has always shown significant variability.

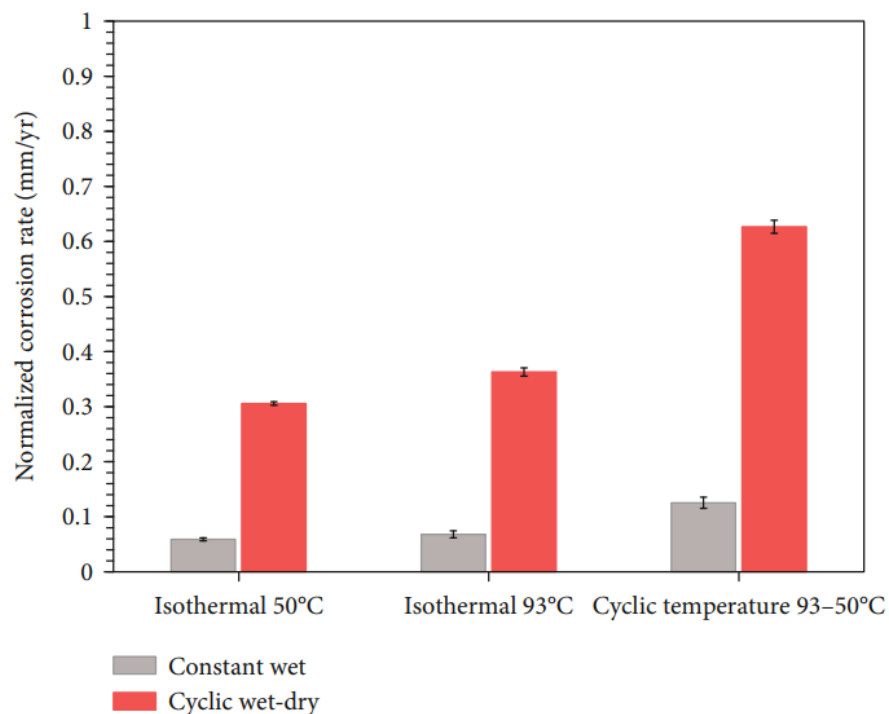


Figure 3.13: CUI rate under isothermal and cyclic conditions [37]

The laboratory investigation of the effect of temperature on corrosion of metals under insulation have been limited to the isothermal and cyclic conditions. There are other studies that are discussed in the result chapter (Chapter 5) of this thesis which focuses on these two conditions only. In addition, there has been field studies also discussed in Chapter 5 that have attempted to show the trend of CUI rate with temperature. It should be noted that the determination of the effect of temperature on CUI rate in the field cannot be relied upon. This is because it is difficult to control the temperature in

the field, but it can be controlled in the laboratory. To the best of our knowledge, there has been no laboratory report showing the trend of CUI rate with temperature apart from a couple of temperature points which does not exceed 3 temperature points as in the work of Putra *et al.* [39]. These few points are not sufficient to form a reliable trend of temperature with CUI rate. Also, most of the trends reported in the literature are based on field studies and some standards for example API 581 standard [48, 49], and ASTM standard [34], which are discussed in detail in the result section of this thesis (Chapter 5). As earlier stated, the two temperature points used in studying wet and dry cycles are not sufficient to form a trend of CUI rate with temperature. Therefore, this is one of the objectives of this research to investigate the CUI rate dependence on temperature in order to fill the gap which is lacking in the literature.

3.7) Effectiveness of inhibitors in mitigating corrosion under insulation

The use of inhibitors is one of the viable means of mitigating the effect of corrosion of insulated metals. These inhibitors may be classified based on the mechanism of inhibition as anodic, cathodic, or mixed inhibitors [50]; or they may be classified based on the state of the inhibitor as liquid or vapour phase inhibitors [51], or its chemistry such as organic or inorganic inhibitors [52]. The anodic inhibitors mitigate corrosion by forming a protective oxide layer on the metal surface that blocks the anodic sites resulting in a reduced corrosion rate, while the cathodic inhibitors slow down the reduction reaction at the cathode by blocking these sites through precipitation [53]. For an insulated metal, some important features to be taken into consideration when investigating the effectiveness of inhibitors for the mitigation of CUI include: the method of application which should ensure uniform spread of the inhibitor on the metal, the dosage required which will help in balancing cost and performance, as well as the temperature limits of the inhibitor which specifies the temperature range at which the inhibitor can be used.

In the literature, the corrosion inhibition efficiencies of some inhibitors in mitigating the CUI of metals have been reported to vary depending on the inhibitor used and the experimental conditions. It might not be possible to make comparisons of inhibition efficiencies between different reports due to differences in inhibitors, as well as the experimental conditions. Notwithstanding, one should be able to draw conclusions

from each report if every detail regarding the inhibitor and the experimental conditions are reported. However, this is not usually the case, for instance, Hou *et al.* [43] reported that 2mL of an undisclosed volatile inhibitor was effective in mitigating the corrosion of carbon steel under mineral wool insulation that has been wetted with artificial sea water at 80 °C for 14 days. The results are shown in Figure 3.14, the inhibitor seems to be effective in mitigating CUI only at the top parts of the rings but seems not to cause any change at the bottom part of the rings which is quite unusual, and no explanation have been given regarding this effect. Moreover, more corrosion was reported for the top rings compared to the bottom rings which contradicts the previous results reported by the same research group in 2015 as shown in Figure 3.15 [43].

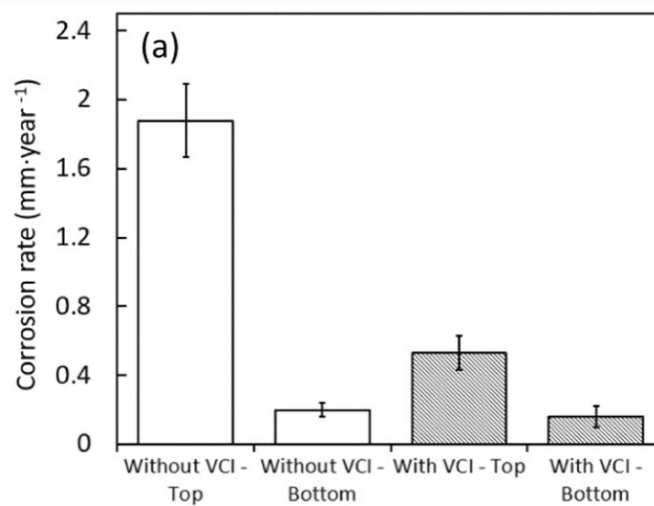


Figure 3.14: The effectiveness of a commercial volatile inhibitor in mitigating the corrosion under mineral wool insulation wetted with an artificial sea water at 80 °C for 14 days [43].

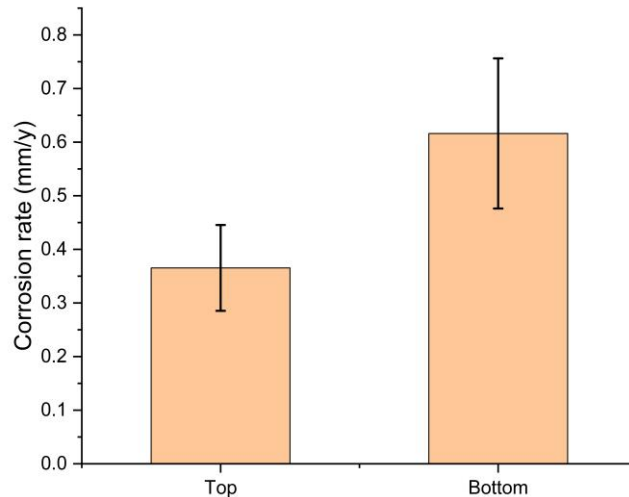


Figure 3.15: A comparison of the corrosion rate of carbon steel for the top and bottom rings under mineral wool insulation [36].

In another study, Cullin *et al.* [54] investigated the effectiveness of a sodium bentonite inhibitor which is a clay material that impedes moisture propagation by swelling along the metal surface. The inhibitor was injected into the insulation-metal interface and its effectiveness in mitigating CUI of carbon steel was assessed at temperatures of 60 °C, 71.1 °C and 82.2 °C. The results showed an average inhibition efficiency of 50.9 %. The authors did not report the dosage of their inhibitor, neither did they assess the inhibition efficiency as a function of dosage which would have provided additional information whether the applied dosage was sufficient.

Bavarian and co-researchers have provided two different reports published in 2015 and 2020 on the effectiveness of vapour phase corrosion inhibitors (VpCI 658) and an undisclosed vapour phase inhibitor respectively in mitigating API 5L X65 steel pipes [55, 56]. The authors showed that VpCI 658 was effective in mitigating CUI by reducing the initial corrosion rate from 0.96 mpy to 0.03- 0.04 mpy. However, the undisclosed inhibitor was only assessed under immersion condition and visual inspection only which makes it difficult to conclude for CUI. Also, it was interesting to realize that the undisclosed inhibitor was the same inhibitor used in this research. This information was obtained through communication with the company (Cortec Corporation) that Bavarian and co-researchers worked for. This was a new molybdate based inhibitor that the company carried out a preliminary investigation to assess its effectiveness

under immersion condition. Therefore, it would be interesting to assess its effectiveness under a CUI condition which is discussed in the result section (chapter 5) of this thesis.

3.8) Prediction of CUI rate using Artificial Neural Network (ANN)

Theoretical predictions of the corrosion rate of metals using ANN have mostly been carried out using data obtained from uninsulated metals or immersion conditions. To the best of our knowledge, only one research publication by Burhani *et al.* [16] regarding prediction of corrosion of metals under insulation using ANN was found. The same author had revised the available prediction methods for CUI in 2014 without including Artificial Neural Network [17], which suggests that it is likely that no research has been carried out in predicting CUI using ANN prior to this time.

The prediction carried out by Burhani *et al.* [16] was based on two input parameters, elapsed time and temperature, and the corrosion rate as the output parameter. The network involved a single hidden layer with a sigmoid activation function. The results of the prediction indicated 85-91 % accuracy as shown in Figure 3.16. When assessing accuracy from Figure 3.16, it should be noted that the scales on both axes are not the same even though it tends to show a good fit. Therefore, improvement in the prediction accuracy is still required which could be obtained if more input parameters affecting CUI are included in the model.

Moreover, the output was obtained from a one-off prediction. It is important that these predictions be repeated using the same network architecture to ensure a reliable output. In addition, the effect of different network architectures such as number of hidden layers, number of input parameters and the choice of activation function for CUI are missing in the literature. Studying these parameters will provide information on the network designs that could be useful in building a neural network to solve a CUI problem.

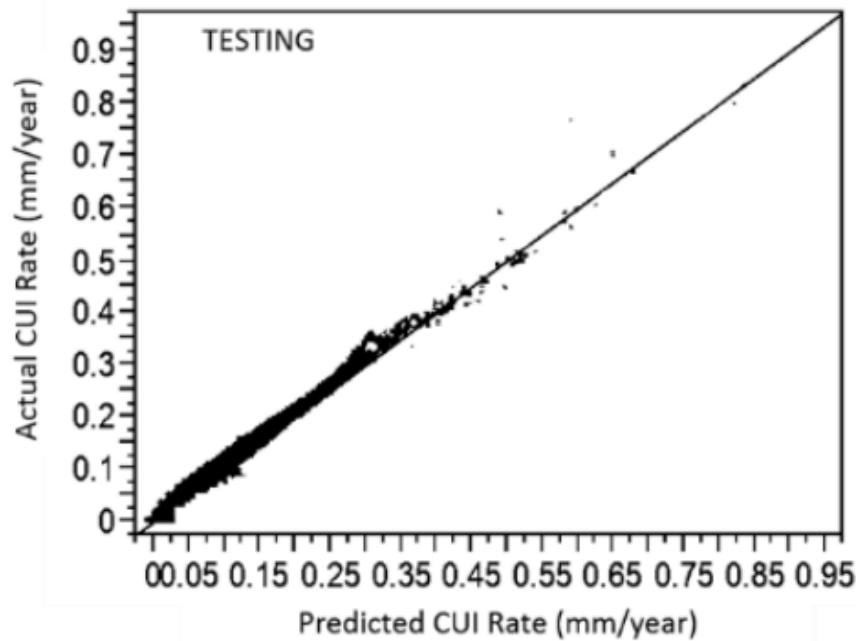


Figure 3.16: A comparison of the actual and predicted CUI rates using ANN [16].

The prediction of atmospheric corrosion of uninsulated carbon steel using ANN have been carried out by [57]. The network architecture consisted of two input parameters: temperature and time as well as the corrosion rate as the output variable. In addition, the network consisted of one single hidden layer containing a sigmoid activation function. The outcome of the prediction is shown in Figure 3.17. This compares the predicted and actual corrosion rates at different temperatures. The results indicated that only very few points had good accuracy. Most of the points have been underpredicted which may be attributed to the fact that just two input parameters have been used in the model to train the network. Cottis *et al.* [47] had noted this deficiency in neural networks by stating that ANN predictions cannot be relied upon when the conditions of the input data are different from the conditions used in the training process. The input data is usually obtained from laboratory experiments involving different factors that are supposed to serve as the input variables in neural networks; however, selecting a few parameters to train the neural network might lead to a reduced accuracy of prediction.

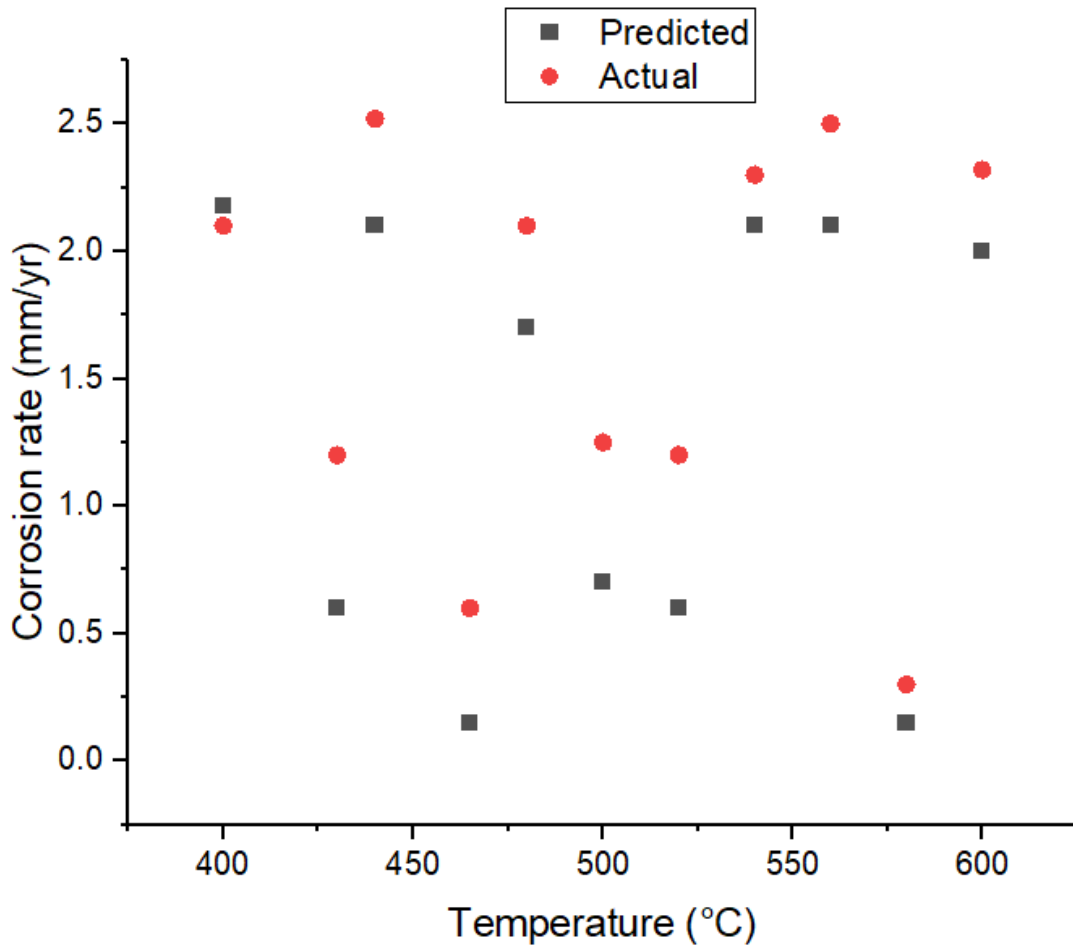


Figure 3.17: A plot showing the prediction accuracy for atmospheric corrosion of carbon steel using ANN [57].

In a different study, Kenny et al. [58] used 10 input variables to predict the atmospheric corrosion rate of an uninsulated carbon steel. The input variables are shown in Figure 3.18, while the predicted and actual outputs are shown in Table 3.3. It should be noted that the ten input parameters reported in the study were not arranged according to priority even though an independent importance analysis would have provided the contribution of each input parameter to the overall corrosion rate. However, the authors did not carry out this investigation. Hence, the entries are just a list of the input variables used in the prediction of corrosion rate.

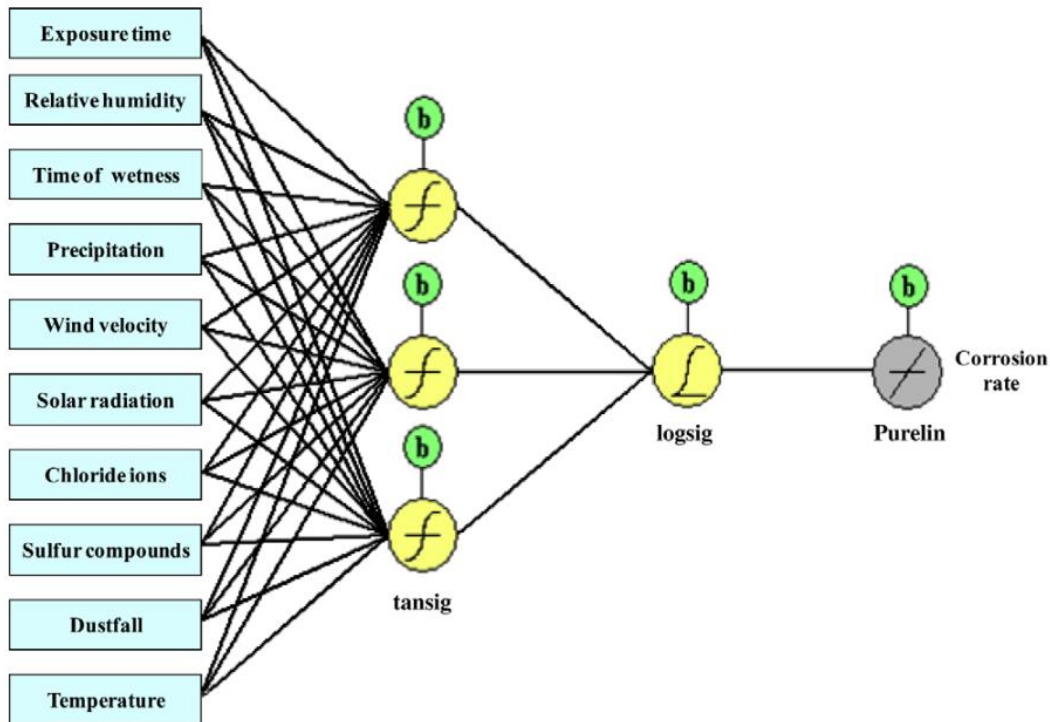


Figure 3.18: An ANN architecture showing the input variables [58].

Table 3.3: A comparison of the predicted and experimental corrosion rates [58]

Specimen	Corrosion rate ($\mu\text{m}/\text{yr}$)		
	Laboratory	Predicted	Error (%)
Validation 1	79.88	80.32	0.6
Validation 1	24.57	23.78	-3.2
Test 1	23.16	24.24	4.6
correlation	0.999		
Validation 2	169.53	169.46	0.0
Validation 2	19.68	20.59	4.6
Test 2	164.53	159.67	-3.0
Correlation	0.997		
Validation 3	19.78	19.78	0.0
Test 3	21.77	19.06	-12.5
Correlation	0.999		

In Table 3.3, the data were split into three groups, validation 1, 2 and test groups. This might be confusing as the first validation group should be correctly named as the training group. Nevertheless, there were good agreement between the predicted and the experimentally determined corrosion rates. This is evident in the low prediction error which varies between 0 % and 12.5 %. This suggests that inclusion of more input

parameters will likely improve the accuracy of prediction. This is supported by the work of Pintos *et al.* [59] who also observed a good prediction accuracy (90 %) when 6 meteorological variables (humidity, temperature, precipitation, chloride deposition rate, sulphate deposition rate and time of wetness) were used as the input variables to predict the corrosion rate of carbon steel.

3.9) Summary

In summary, the water absorption reports in the literature has indicated that mineral wool absorbs water for a long time without saturation. The results obtained from replicate measurements have indicated that the water absorption capacity is quite variable which is evident in the length of the error bars representing the standard deviation from triplicate measurements. Also, the effect of thermal treatment of the insulation has revealed that mineral wool insulation that has been thermally treated at temperatures exceeding 250 °C absorbs water more readily than the insulation that has not been thermally treated. This is because the hydrophobic additives are degraded allowing water to penetrate the insulation.

The study of corrosion under insulation of metals have mostly been carried out using the ASTM G189 test rig. This has been useful in simulating isothermal as well as cyclic temperature and wet/dry cycles. However, a few limitations have been pointed out by some researchers, one of which is the incorporation of a gap between the insulation and the metal rings to supply sufficient volume of electrolyte which resembles an immersion condition rather than a CUI condition. Moreover, the rain chamber reported by Ayello *et al.* [14] was also found not to be able to yield the required results in a reasonable time. The difficulty associated with the frequent assembly and disassembly of the test rigs as well as issues such as oil leakage during experiments have been identified as a likely reason associated with less publications on CUI compared to immersion conditions.

CUI has been reported to be worse when cyclic conditions are used compared to isothermal conditions. This has been attributed to the fact that cyclic conditions increase the concentration of chloride in the system as a result of the repetitive condensation of water which dissolves the chlorides in the insulation and transports it to the metal surface. Moreover, CUI rate has been measured at two different points

where water is expected to exist as a liquid and when it is expected to dry out. However, these measurements cannot be used to form a trend of CUI rate with temperature, this shows the need for the investigation of CUI rate at different temperatures. The vapour phase corrosion inhibitors (VpCI 658) have been shown to be effective in mitigating the CUI of carbon steel. However, in the literature, the new commercial inhibitor (VpCI 619) was only assessed under immersion conditions and visual inspection rather than CUI condition. Therefore, it would be interesting to assess the effectiveness of VpCI 619 inhibitor in mitigating corrosion of carbon steel under insulation.

Theoretical prediction of the CUI rate from the report of [60] has shown good prediction prospects which could be observed from the accuracy which was about 85-91% despite the fact that only two input parameters were used. ANN usually requires large input data and inclusion of more parameters affecting CUI rate is likely to result in improved accuracy of prediction. A similar decrease in the prediction accuracy was reported by Almomani who also used two input parameters resulting in an accuracy of 92.3 %. It is important that more parameters affecting the expected output be included in the model in order to obtain reliable predictions with a good accuracy. In addition, it is suggested that researchers working on predictive modelling especially for application in corrosion studies carry out repetitive predictions just to ensure that reliable outputs are obtained.

Chapter References

1. Dwivedi, D., Lepkova, K. and Thomas, B. (2017). Carbon steel corrosion: A review of key surface properties and characterization methods. *RSC Advances*, 7:4580-4610.
2. Osarolube, E., Owate, I. O. and Oforka, N. C. (2008). Corrosion behaviour of mild and high carbon steels in various acidic media. *Scientific Research and Essay*, 3:224-228.
3. Bennett, T. M., Allan, J. F., Garden, J. A. and Shaver, M. P. (2022). Low formaldehyde binders for mineral wool insulation. *Global challenges*, 6:1-19.
4. Zwaag, C. and Rasmussen, S. N. (2018). Mineral wool and water repellency. NACE Publications, paper number 10929.

5. Zach, J., Hroudova, J., Brozovsky, J., Krejza, Z. and Gailius, A. (2013). Development of Thermal Insulating Materials on Natural Base for Thermal Insulation Systems. *Procedia Engineering*, 57:1288-1294.
6. Ahmed, A. and Qayoum, A. (2021). Investigation on the thermal degradation, moisture absorption characteristics and antibacterial behavior of natural insulation materials. *Materials for Renewable and Sustainable Energy*, 10:4-14.
7. Cao, Q., Pojtanabuntoeng, T., Esmaily, M., Thomas, S., Brameld, M., Amer, A., and Birbilis, N. (2022). A Review of corrosion under insulation: A critical issue in the oil and gas industry, *Metals*, 12:561.
8. Amer, A., AlShehri, A., Cunningham, V., Taie, I. (2018). Inspection challenges for detecting corrosion under insulation (CUI) in the oil and gas industry. NACE publications, paper number 12400.
9. Geary, W. (2013). Analysis of corrosion under insulation failure in a carbon steel refinery hydrocarbon line. *Case Studies in Engineering Failure Analysis*, 1:249-256.
10. Marquez, A., Singh, J. and Maharaj, C. (2021). Corrosion under insulation examination to prevent failures in equipment at a petrochemical plant. *Journal of Failure Analysis and Prevention*, 21:723-732.
11. Caines, S., Khan, F., Shirokoff, J. and Qiu, W. (2015). Experimental design to study corrosion under insulation in harsh marine environments. *Journal of Loss prevention in the Process Industries*, 33:39-51.
12. Kane, R. D. Chauviere, M., Chustz, K. (2008). Evaluation of steel and TSA coating in a corrosion under insulation (CUI) environment, NACE publication, paper number 08036.
13. Bavarian, B., Ikder, Y., Samimi, B., and Reiner, L. (2015). Protection of corrosion under insulation using vapour phase corrosion inhibitors, Corrologic VpCI-658. A report to Cortec Corporation, U.S.A. pp. 1-24.
14. Low, P. (2022). A Novel Methodology for Addressing Corrosion Under Insulation (CUI) Utilizing Corrosion Inhibitor Impregnated Self-Amalgamating Silicone Based Tape. AMPP Annual Conference, Texas, USA, Paper Number 17931.

15. Cullin, M. J., Birmingham, G., Srinivasan, R., Hailu, G. (2020). Injectable sodium bentonite inhibitors for corrosion under insulation. *Journal of pipeline Systems Engineering and Practice*,11(4):1-11.
16. Burhani, N. R. A., Muhammad, M. and Rosli, N. S. (2019). Combined experimental and field data sources in a prediction model for corrosion rate under insulation. *Sustainability*, 11(6853):1-13.
17. Burhani, N. R. A., Muhammad, M. and Ismail, M. C. (2014). Available Prediction Methods for Corrosion under Insulation (CUI): A Review. *Matec web of conferences* 13: 1-5.
18. Kramanos, A., Hadjaraku, S., Papadopoulos, A. M. (2008). The impact of temperature and moisture on the thermal performance of stone wool. *Energy and Buildings*, 40:1402–1411.
19. ASTM C1511 (2021). Standard test method for determining the water retention (repellency) characteristics of fibrous glass insulation (aircraft type), ASTM International, USA.
20. ASTM C1763 (2016). Standard test method for water absorption by immersion of thermal insulation materials. ASTM International, USA.
21. British Standard BS EN 13472 (2012). Thermal insulating products for building equipment and industrial installations. Determination of short-term water absorption by partial immersion of preformed pipe insulation. BSI, London.
22. British Standard BS EN 1609 (2013). Thermal insulating products for building applications. Determination of short-term water absorption by partial immersion. BSI, London.
23. Bennett, T. M., Allan, J. F., Garden, J. A. and Shaver, M. P. (2022). Low formaldehyde binders for mineral wool insulation. *Global challenges*, 6:1-19.
24. Williams, J, and Evans, O. (2010). The influence of insulation materials on corrosion under insulation. NACE Northern area western conference, pp. 1-24.
25. Knop, A. and Pilato, L. A. (1985). Phenolic resins. Springer-Verlag, Berlin Heidelberg, p.141.

26. Material Safety Data Sheet for Rockwool, Rocklap H and V pipe section, <https://www.rockwool.com/syssiteassets/rw-uk/downloads/msds/msds-rockwool-insulation-web.pdf>, date accessed 26th November, 2021.
27. Ivanic, A., Kravanja, G., Kidess, W., Rudolf, R. and Lubej, S. (2020). The influences of moisture on the mechanical, morphological and thermogravimetric properties of mineral wool made from basalt glass fibres. *Materials*, 13:2392.
28. Zwaag, C. and Rasmussen, S. N. (2018). Mineral wool and water repellency. NACE Publications, paper number 10929.
29. Pojtanabuntoeng, T., Kinsella, B., Ehsani, H., Brameld, M. (2017). Comparison of insulation materials and their roles on corrosion under insulation. NACE International, paper number 9287.
30. Knop, A. and Pilato, L. A. (1985). Phenolic resins. Springer-Verlag, Berlin Heidelberg, p.141.
31. Ivanic, A., Kravanja, G., Kidess, W., Rudolf, R., and Lubej, S. (2020). The influences of moisture on the mechanical, morphological, and thermogravimetric properties of mineral wool made from basalt glass fibres. *Materials*, 13(10):2392.
32. Kosinski, P., Brzyski, P. and Duliasz, B. (2018). Moisture and wetting properties of thermal insulation materials based on hemp fibre, cellulose and mineral wool in a loose state. *Journal of Natural Fibres*, 17(2):199-213.
33. Williams, J, and Evans, O. (2010). The influence of insulation materials on corrosion under insulation. NACE Northern area western conference, pp. 1-24.
34. ASTM G189-07 (2007). Standard guide for laboratory simulation of corrosion under insulation. ASTM International.
35. Ayello, F., Hill D., Marrion, S. and Sridhar, N. (2011). Integrated sensor networks for corrosion under insulation: monitoring, cost reduction and life extension strategies. NACE International, paper number 11281.
36. Pojtanabuntoeng, T. Machuca, L. and Salasi, M. (2015). New experimental rig to investigate corrosion under insulation at different climate conditions. *Corrosion and materials*, 46-51.

37. Yang, M., and Liu, J. (2022). *In situ* monitoring of corrosion under insulation using electrochemical and mass loss measurements. *International Journal of Corrosion*, 2022:1-12.
38. Caines, S., Khan, F., Shirokoff, J. and Qiu, W. (2015). Experimental design to study corrosion under insulation in harsh marine environments. *Journal of Loss prevention in the Process Industries*, 33:39-51.
39. Putra, R., Muhammad, Hafli, T., Islami, N., Apandi, A. (2022). Analysis of temperature variations, types of insulation and coating on corrosion under insulation on ASTM A53 pipes. *International Journal of Engineering, Science, and Information Technology*, 2(1):110-118.
40. Cao, Q., Pojtanabuntoeng, T., Esmaily, M., Thomas, S., Brameld, M., Amer, A., and Birbilis, N. (2022). A Review of corrosion under insulation: A critical issue in the oil and gas industry, *Metals*, 12:561.
41. Essien, G. and Neville, A. (2021). Redesign and construction of corrosion cell for improved measurement of corrosion under insulation (CUI). *American Journal of Engineering Research*, 10(1):307-315.
42. Rana, A. R. K., Yang, M., Umer, J., Veret, T. and Brigham, G. (2021). Influence of robust drain openings and insulation standoffs on corrosion under insulation behaviour of carbon steel. *Corrosion*, 77(6):681-692.
43. Hou, Y., Pojtanabuntoeng, T. and Iannuzzi, M. (2020). Use of electrochemical current noise method to monitor carbon steel corrosion under mineral wool insulation. *Materials degradation*, 4 (39):1-9.
44. Caines, S., Khan, F., Shirokoff, J. and Qiu, W. (2017a). Demonstration of increased corrosion activity for insulated pipe systems using a simplified electrochemical potential noise method. *Journal of Loss Prevention in the Process Industries*, 47:189-202.
45. Caines, S., Khan, F., Zhang, Y. and Shirokoff, J. (2017b). Simplified electrochemical potential noise method to predict corrosion and corrosion rate. *Journal of Loss Prevention in the Process Industries*, 47:72-84.
46. Jung, H., Kwon, K. J., Lee, E., Kim, D. G., and Yim, G. Y. (2011). Effect of dissolved oxygen on corrosion properties of reinforced steel. *Corrosion Engineering, Science and Technology*. 46(2):195-199.

47. Cottis, R. A., Qing, L., Owen, G., Gartland, S. J., Helliwell, I. A. and Turega, M. (1999). Neural network methods for corrosion data reduction. *Materials and Design*, 20(4): 169-178.
48. American Petroleum Institute API 581 (2016). Risk based inspection technology, 3rd edition.
49. De Vogelaere, F. (2009). Corrosion under Insulation. *Process progress safety*, 28:30-35.
50. Rostami, A. and Nasr-El-Din, H. A. (2009). Review and Evaluation of Corrosion Inhibitors Used in Well Stimulation. SPE International Symposium, paper number 121726.
51. Subramanian, A., Natesan, M., Muralidharan, V. S., Balakrishnan, K. and Vasudevan, T. (2000). An Overview: Vapor Phase Corrosion Inhibitors. NACE publication, 144-156.
52. Kadhim, A., Al-Amiery, A. A., Alazawi, R., Al-Ghezi, M. K. S. and Abass, R. H. (2021). Corrosion inhibitors: A review. *International Journal of Corrosion Scale Inhibition*, 10:54-67.
53. Dariva, C. G., and Galio, A. F (2014). Corrosion inhibitors-principles, mechanisms and applications. Intech open, pp 365-379.
54. Cullin, M. J., Birmingham, G., Srinivasan, R., Hailu, G. (2020). Injectable sodium bentonite inhibitors for corrosion under insulation. *Journal of pipeline Systems Engineering and Practice*, 11(4):1-11.
55. Bavarian, B., Ikder, Y., Samimi, B., and Reiner, L. (2015). Protection of corrosion under insulation using vapour phase corrosion inhibitors, Corrologic VpCI-658. A report to Cortec Corporation, U.SA. pp. 1-24.
56. Bavarian, B., Reiner, L., Avnessian, A. B., Miksic, B. (2020). Development of a new corrosion inhibitor for corrosion under insulation at elevated temperatures. NACE Publications, paper number C2020-14293.
57. Almomani, M.A., Momani, A. M., Abdelnabi, A. A. B., Al-Aqebah, R. S. and Al-Batah, M. S. (2022). Predicting the corrosion rate of medium carbon steel using artificial neural networks. *Protection of Metals and Physical Chemistry of Surfaces*, 58 (2):414–42.
58. Kenny, E. D., Paredes, R. S. C., de Lacerda, L. A., Sica, Y. C., de Souza, G. P. and Lazaris, J. (2009). Artificial neural network corrosion modelling for metals in an equatorial climate. *Corrosion Science*, 51:2266-2278.

59. Pintos, S., Quiapo, N. V., de Rincon, O. T., Rincon, A. and Morcillo, M. (2000). Corrosion Science, 42:35-52.
60. Burhani, N. R. A., Muhammad, M. and Rosli, N. S. (2019). Combined experimental and field data sources in a prediction model for corrosion rate under insulation. *Sustainability*, 11(6853):1-13.

CHAPTER 4 : EXPERIMENTAL AND PREDICTIVE MODELLING OF CUI

CHAPTER FOUR

EXPERIMENTAL AND PREDICTIVE MODELLING OF CUI

This chapter gives the detailed description of the methods used in studying the corrosion of carbon steel under mineral wool insulation. This begins with the study of water absorption capacity of mineral wool when the insulation has been thermally degraded at 250 °C. The purpose of carrying out the water absorption study was to assess the time it will take the insulation to be saturated with water as well as the reproducibility of measurements. This is important because the severity of CUI depends on the degree of water and contaminant intrusion to the insulation [1]. This is followed by the study of the effect of temperature ranging from 60 °C to 130 °C on the corrosion of carbon steel under insulation. This temperature range was selected based on the laboratory and field studies that have agreed that it is the range where aggressive CUI is usually observed [2]. Afterwards, the distribution of the test solution (1 wt % NaCl) between the top and bottom parts of the insulation as well as the ends and the centre of the insulation were investigated. This was to assess areas of the insulation that is more vulnerable to corrosion as well as relating it to the corrosion rates of carbon steel rings in these regions.

The effectiveness of a new commercial inhibitor (VpCI 619) in mitigating CUI at the targeted temperatures were also investigated. This was carried out to assess the effect of increasing temperature and dosage of the inhibitor in mitigating CUI of carbon steel. This could be useful in determining the effectiveness of the inhibitor at the temperature range where aggressive CUI have been reported as well as providing useful information on the performance when the dosage is reduced, which can be used for cost analysis. In addition, the rate of insulation dry out was investigated at different temperatures using galvanic current and electrochemical impedance measurements. This was based on the ability to measure the corrosion current across the Al-Cu couple which is in contact with the wet insulation as well as the resistance as the electrolyte in the insulation dries. The main purpose of this study was to assess the time it will take for the insulation to dry out at different temperatures which can be useful to explain the trend of CUI rate with temperature.

Furthermore, the model used to predict the corrosion rate of carbon steel under insulation using artificial neural network are also discussed. The purpose was to determine the effectiveness of the logistic sigmoid and hyperbolic tangent activation functions in predicting the rate of CUI of carbon steel. These functions were selected because they are non-linear and differentiable functions with a smooth gradient, which means they can learn the complex relationship between the factors (input variables) affecting the corrosion rate of metals under insulation and the rate of CUI (output variable). Also, both functions take all real numbers into their domain, which means that it permits wide input variables but processes output that can be interpreted in terms of probabilities (0 to 1) in the case of a logistical sigmoid function and a wider output (-1 to 1) in the case of a hyperbolic tangent function which is quite suitable for describing CUI data. Moreover, the study also aims at investigating the effect of number of input parameters, the number of hidden layers as well as the repeatability of predictions which could be useful in assessing the reliability of CUI rate predictions.

4.1) Determination of water absorption capacity of mineral wool insulation

This was carried out to assess the water absorption capacity of mineral wool insulation as well as the time of wetness which is believed to have significant influence on the corrosion of insulated metals. Corrosion under insulation is dependent on the amount of water or test solution that penetrates the insulation as well as the duration of contact. If the water absorption capacity of the insulation is low and it has a higher rate of insulation dry out, then the corrosion rate is likely to be low [3]. It is likely that the chemical composition as well as the properties of mineral wool insulation may influence its water absorption behaviour. In this study, mineral wool insulation (RockLap from Rockwool), having an inner diameter, an outer diameter and a wall thickness of 6.0 cm, 8.5 cm and 2.5 cm respectively and covered with an aluminium jacket was used for the trials (Figure 4.2). The properties and chemical composition of the insulation as reported in the product data sheet and Material safety data sheet are presented in Tables 4.1 and 4.2 respectively.

Table 4.1 : Properties of mineral wool insulation ('RockLap' from Rockwool) as described in the product data sheet [4].

Properties of mineral wool insulation	Value/units
Thermal conductivity (at 50 °C)	0.037 W/mK
Relative density	20-300 kg/m ³
Melting point	>1000 °C
Binder Decomposition temperature	175 °C
Maximum service temperature	250 °C
Odour	Odourless
Appearance	Grey-green/brown

Table 4.2 : Chemical composition of mineral wool insulation as described in the product data sheet [5].

Chemical composition	Percentage by mass (%)
Stone wool	95-100
Synthetic thermosetting binder	0-5
Mineral oil	0-0.5
Silicone oil/emulsion	0-0.5

There are standard methods that are available for determining the water absorption characteristics of insulation materials. These include ASTM C1511 which describes methods of determining the water absorption characteristics of fibrous insulation materials [6]. Another standard is the ASTM C1763 which specifies methods of determining the amount of water retained by flat specimen of thermal insulation materials after full immersion in water for a prescribed time interval under isothermal conditions [7]. Also, BS EN 13472 is a standard method that describes the short-term water absorption by partial immersion of a preformed pipe insulation [8]. Furthermore, BS EN 1609:2013 also measures the short-term water absorption of thermal insulating products used in building applications in order to simulate the absorption caused by a 24-hour raining period during construction work [9]. Details of the water absorption measurements provided in these standards are reported in Chapter 3 (Literature review).

In this study, the ASTM C1511 standard was chosen because it offers a more realistic way of assessing the water absorption characteristics when the protective barrier of the insulation is breached [6]. The water absorption characteristic of the insulation under this condition is important in deciding its performance when it is in a dilapidated state. Besides, this standard is specifically designed to assess the water absorption characteristics of fibrous insulation material especially those ones that are used in aircrafts to provide a measure of the potential weight increase due to water retention. In order to evaluate the water absorption characteristics, the standard (ASTM C1511) specifies that all facings and jacketing be removed from the insulation material prior to determination. This is to ensure that the water absorption capacity of the insulation is assessed under worst case scenario. The properties of the insulation material as described in the product data sheet is presented in Table 4.1.

Each mineral wool insulation was initially 100 cm in length, which was further cut into 10cm length. The foil covering the insulation was removed as specified in the standard (ASTM C1511). The bare sample was weighed in an electronic balance (Sartorius 27349) with a precision of 0.1 mg and placed on a 6.4 mm rigid screen in a tank of distilled water at 21 ± 2 °C. With the aid of some weight, the screen was slowly submerged until it rests on a support at a level that is 127 mm above it and 51 mm below as shown in Figure 4.1. The mineral wool insulation was submerged for 15 minutes, after which it was slowly removed from the test system and hanged on a spring clamp in a vertical position for 60 ± 5 s. Then it was reweighed and recorded. The percentage absorption by weight was calculated using equation 1:

$$\% \text{ absorption by weight} = \frac{w_2 - w_1}{w_1} \times 100 \quad (1)$$

Where w_1 is the weight before immersion in water and w_2 is the weight after immersion.

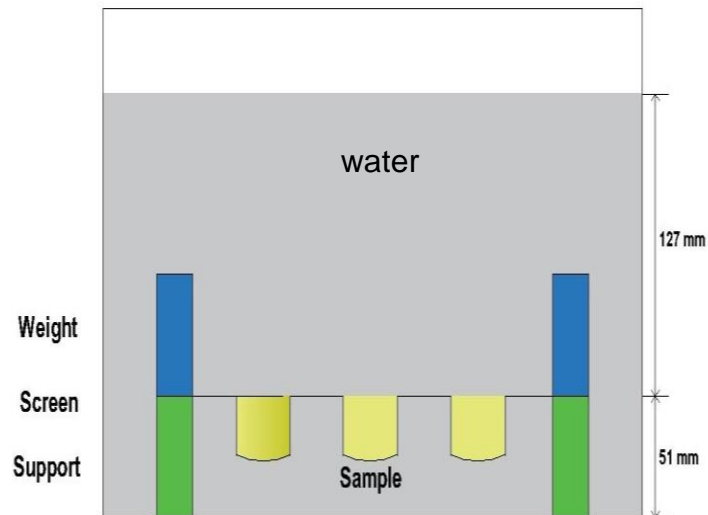


Figure 4.1 : Experimental set up for the determination of the water absorption capacity of mineral wool.

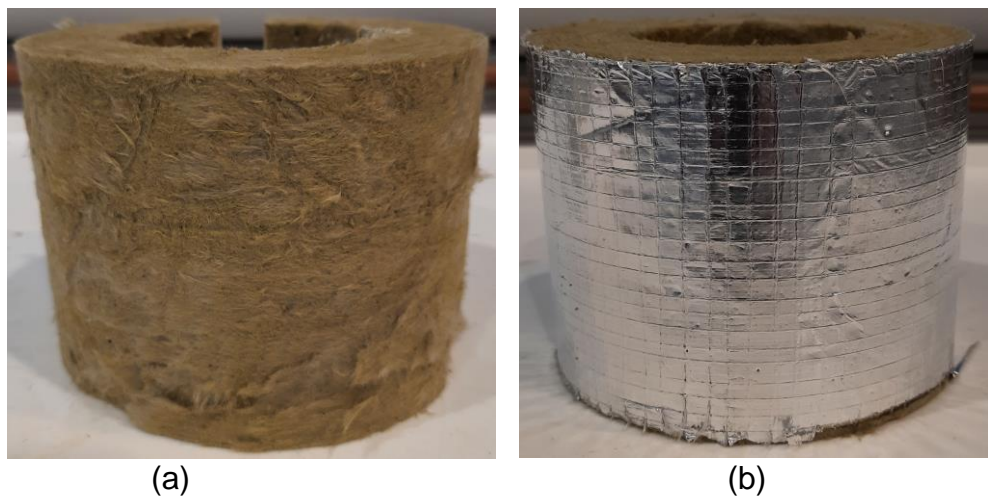


Figure 4.2 : Pictures of mineral wool insulation (a) with aluminium foil removed (b) with aluminium foil intact.

4.1.1) Other ways of determining the water absorption capacity of insulation materials

There are other methods of determining the water absorption capacity of insulation materials such as: BS EN 13472:2012 method which determines the short-term water absorption by partial immersion of preformed pipe insulation [8]. This method investigates the water absorption by partial immersion in water. It aims at determining the absorption characteristics of insulation material when exposed to rain for about 24

hours which is usually observed during installation. Here, the dry insulating material is first weighed and recorded. It is then placed in an empty tank, having the external surface of the material facing downwards and a sufficient load is placed on it to keep it in position as shown in figure 3. Water is carefully added to the tank and adjusted until the lowest point of the external surface of the insulation is 20 ± 2 mm. After 24 hours, the insulating material is removed from the test system and drained for 10 minutes by placing on a rigid mesh inclined at 45° . Then the insulating material is reweighed to determine the water absorption capacity.

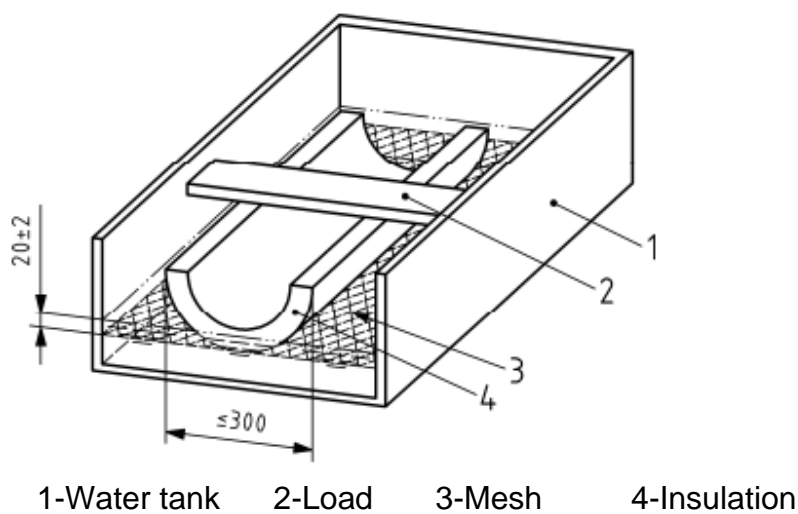


Figure 4.3: Experimental set up of BS EN 13472:2012 [8]

Another method of determining the water absorption capacity of insulation materials involves the BS EN 1609:2013 method which also measures the short-term water absorption by partial immersion [9]. This method is useful in determining the water absorption behaviour of insulating materials during construction work when exposed to rain for about 24 h. The insulating material is weighed to the nearest 100 mg to determine the initial dry weight. It is then placed in an empty water tank, and a load is placed on it to keep it in position as shown in figure 4. Water is carefully added until the insulating material is 10 ± 2 mm above. The water level required to keep the material partially immersed is maintained throughout the experiment. The insulating material is then removed after $24 \text{ h} \pm 30 \text{ min}$, it is held in a horizontal position and allowed to drain for 5 seconds and then reweighed.

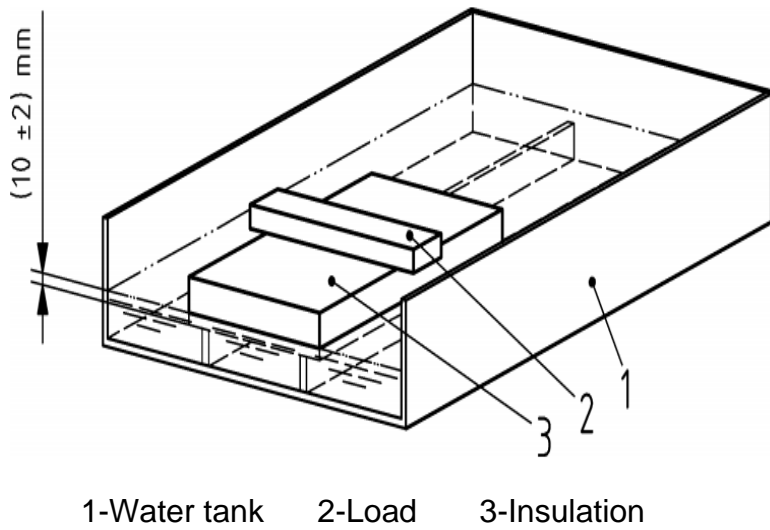


Figure 4.4: Experimental set up for BS EN 1609:2013 standard [9]

4.2) Design of corrosion under insulation test rigs

There are various test rigs to study the corrosion of insulated structures in the laboratory. This includes: the test rig originally developed by the Association of Standard Testing and Materials (ASTM) in 2007 [10], the rain chamber developed by Ayello and co-researchers in 2011 [11] and other modified test rigs based on the ASTM standard [12]. Details of these test rigs including their limitations have been documented in Chapter 3 of this thesis (Literature review). The design of the ASTM test rig is shown in Figure 4.5.

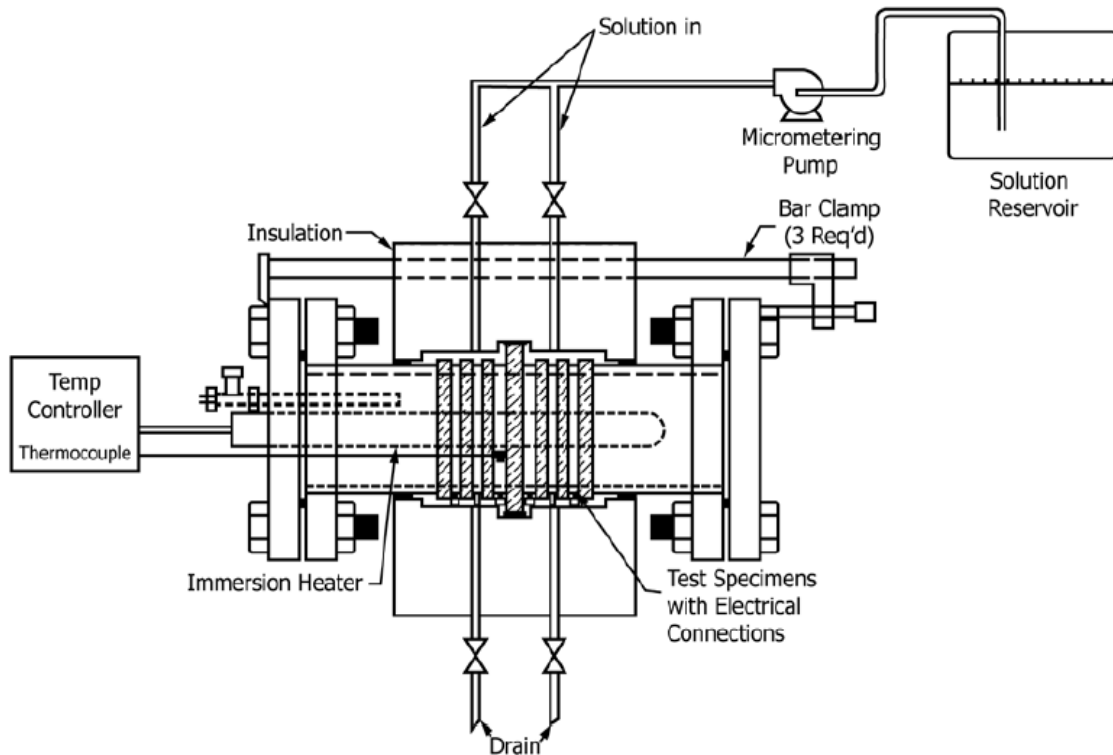


Figure 4.5 : A CUI test rig as designed by ASTM G189 [10]

4.2.1) Test rig used in this research for corrosion studies

The diagrams of CUI test rig used in this study as well as its schematic representation are shown in Figures 4.6 and 4.7 respectively. The entire CUI equipment including the work area is shown in Figure 4.8, while the arrangement of the rings and spacers is shown in Figure 4.9. This test rig is a modified version of the ASTM G189-07 previously described in Chapter 3 (Literature review). It is worth noting that although the ASTM test rig is still an advanced rig for simulating corrosion under insulation in the laboratory and have been widely used in the literature to accelerate CUI in the laboratory [13-16], a number of limitations associated with it have been pointed out by some researchers [17]. One of which is the incorporation of a gap between the insulation and the metal substrate to supply sufficient volume of electrolyte which closely reflects an immersion condition rather than corrosion under insulation. In industry, the insulation material is usually tight to the metal surface during installation in order to minimize the gap between the insulation and the metal substrate to help prevent the retention of water or electrolyte. Therefore, it was necessary to modify the ASTM standard in order to reflect CUI conditions in industry.

In the CUI set up used in this study, the insulation was made to be a tight fit with the carbon steel rings using aluminium tape to keep it in position thereby eliminating the gap between the insulation and the rings, reflecting actual CUI conditions. Besides, the introduction of the test solution from an external reservoir using a micrometering pump as specified in the ASTM standard did not really work with the CUI rig used in this study due to the hydrophobicity of mineral wool insulation. A report on the rig has revealed that an attempt to introduce the test solution into the rig from a reservoir resulted in the test solution running through the insulation and was collected at the bottom without wetting it as observed in industry. Therefore, it was necessary to thermally degrade the insulation at 250 °C and pre-soak it in the test solution for about 48 hours before installing on the test rig. This would accelerate the water absorption process and allow investigation of the CUI rate within a realistic timeframe.

The modified version of the test rig consists of six carbon steel rings (outer diameter 58 mm and thickness 0.5 mm) machined from a 2" schedule 80 API 5/A106 seamless pipe section which was purchased from M & T Pipeline Supplies Limited. The chemical composition of the carbon steel pipe is presented in Table 4.3. This material was chosen because it is commonly used in the construction of pipes and vessels for high temperature service in industry. Besides, this type of carbon steel pipe is highly recommended in the ASTM G189 standard [10]. The carbon steel rings were labelled 1-6 as shown in figures 4.7 and 4.9, and properly cleaned using 1200 grit silicon carbide papers (sourced from RS PRO Limited), rinsed with deionized water, isopropyl alcohol (Sigma Aldrich, 99.8% purity) dried with nitrogen gas and weighed as specified in the standard ASTM G1-03 [19].

The rings were held in a stack, separated by polytetrafluoroethylene spacers (0.5 cm thick and 6.0cm outer diameter). Although the PTFE spacers are particularly important when carrying out electrochemical measurements in order to electrically isolate the metal rings; nevertheless, to be compliant with ASTM G189 standard, the spacers were used even though they were not strictly necessary for weight loss measurements. In the study of Zwaag and Rasmussen [18], the PTFE spacers were removed to allow better sealing and to avoid oil leakage. The stack consisting of carbon steel rings and spacers were kept in position by two end flanges made of 304

grade stainless steel. At the end of the flanges are two base metal plates made of 304 grade stainless steel held together by threaded tie bars in order to hold the entire set up in position. Mineral wool insulation having an inner diameter of 60 mm and a thickness of 25 mm was pre-soaked in 1% by weight sodium chloride solution (prepared from NaCl, Sigma Aldrich, 99% purity) (pH 5.07) for about 48 hours, this was wrapped around the rings and held in place by an aluminium tape. A higher concentration of chloride proposed by the researchers at Curtin University [1] than the concentration (0.01 wt %) recommended by the ASTM standard was used in this study. This was to accelerate the test so that results could be obtained in a reasonable time.

End caps made of Delrin polymer were used at both ends of the insulation to keep the insulation in position and to prevent evaporation of the test solution at the ends. Although the end caps were very useful in holding the ends of the insulation and preventing evaporation at these regions, it presented its own challenges such as sticking to the end flanges at lower temperatures making it difficult to access the ends of the insulation. In order to overcome this, it was necessary to either adjust the end caps to the desired position when the end flanges are hot or if the pipe is already cold, it will require heating up the end flanges to release the end caps so that it can be adjusted to the desired position.

Hot silicone oil (Dow Corning 200/200 Cs fluid) from a temperature programmed bath (TXF 200, Grant instruments) is circulated through the internal portions of the pipe at different temperatures of 60 - 130 °C. The silicone oil enters the rig through end flange 1, passes across ring 1 to 6 and exits the rig at end flange 2 as shown in figure 4.7. The temperature of the rings was monitored by means of a K-type thermocouple connected to a digital voltmeter (Keithley 2110). The accuracy of the temperature measurement was estimated to be $\pm 1^\circ\text{C}$. Temperature program involved slow ramps from room temperature to the target temperature (60-130 °C), this was programmed to last for 1.5 h, and was maintained for 4 hours at the target temperature before cooling down to room temperature slowly for 1.5 h as shown in figure 4.10.

Prior to the start of experiments, it was necessary to allow the test rig to run for some time in order to check for silicone oil leakages. In some occasions, very minimal leaks

were observed and it was eliminated by either re-tightening the bolts of the base metal plates or replacing the PTFE spacers with new ones. Three experimental cycles were repeated with a fresh mineral wool pre-soaked in the test solution for the same amount of time (48 hours). It was quite difficult to install the wet insulation reproducibly for each run without losing some test solution. The estimated amount of test solution in the insulation before and after the CUI test for each experimental run was recorded, after which the test rig was dismantled, and the rings were removed from the test rig to be cleaned in order to determine the weight loss.

The corrosion product was removed from the carbon steel using standard methods reported in ASTM G1-03 [19]. The purpose was to ensure that the corrosion products are removed which would interfere with weight loss measurements without removal of the base metal. The etching solution required to remove the corrosion product as stated in the standard includes strong hydrochloric acid combined with antimony oxide and tin (II) chloride, this is the so-called Clarke's solution [19, 20]. The main role of the antimony oxide is to inhibit attack on the metal substrate during cleaning of the corrosion product, while the tin (II) chloride is used to reduce the ferric chloride produced by the rust solution to ferrous chloride. This is necessary because ferric chloride is suggested to increase corrosion whereas ferrous chloride appeared not to affect the carbon steel [20].

The test involved 50 ml of the Clarke's solution which was prepared by adding 2.5 g of tin (II) chloride (Sigma Aldrich, 98 % purity) and 1.0 g of antimony (III) oxide (Sigma Aldrich 99% purity) to 50ml of 37 % w/w hydrochloric acid (Sigma Aldrich). The corroded carbon steel samples were then immersed in the prepared etching solution for about 5-7 minutes. This time was selected to ensure that the corrosion products are completely removed with minimal attack on the base metal. It is important to rinse the carbon steel samples with large amounts of distilled water following cleaning in Clarke's solution as it has been reported that failure to rinse it will lead to surface contamination [20]. The ring samples were rinsed with large amounts of distilled water and further rinsed with isopropyl alcohol (Sigma Aldrich, 99.8 %) and dried with nitrogen gas and reweighed in an electronic balance (Sartorius AX 224) with a precision of 0.1 mg. The corrosion rate was then evaluated by weight loss following

equation 2 as described in the standard ASTM G1-03 [19]. The entire experimental cycle was repeated four times to determine the reproducibility of the experiments.

Table 4.3 : Chemical composition of the carbon steel pipe used in this study [21].

Element	Composition by weight (%)
Carbon	0.25
Manganese	0.27-0.93
Phosphorus	0.035
Sulphur	0.035
Silicon	0.10
Chromium	0.40
Copper	0.40
Molybdenum	0.15
Nickel	0.40
Vanadium	0.08

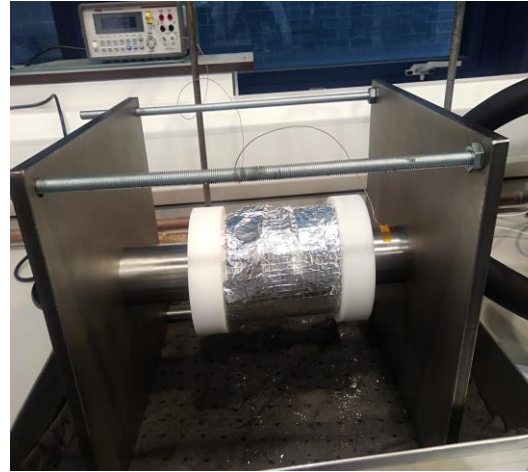
The corrosion rate was estimated using the following expression given in the ASTM G189 standard:

$$CR \left(\frac{mm}{yr} \right) = \frac{K \times \Delta W(g)}{T(hr) \times A(cm^2) \times \rho \left(\frac{g}{cm^3} \right)} \quad (2)$$

Where CR is the corrosion rate in mm/yr, K is a constant with the value 87600 which is a conversion factor from cm/hr to mm/yr, ΔW is the weight loss obtained from the difference between the initial and final weights of the carbon steel rings (g), A is the measured surface area of the rings (cm^2), ρ is the density of carbon steel which is 7.86 g/cm^3 and T is the duration of experiments (hours). It should be noted that the corrosion rate was estimated relative to the entire area of the carbon steel rings even though visible corrosion products were not uniform over the entire surface. Therefore, the estimated corrosion rate will best be termed relative corrosion rate.



(a)



(b)

Figure 4.6 : Pictures of CUI test rig used in this study (a) without insulation installed (b) with insulation and end caps installed.

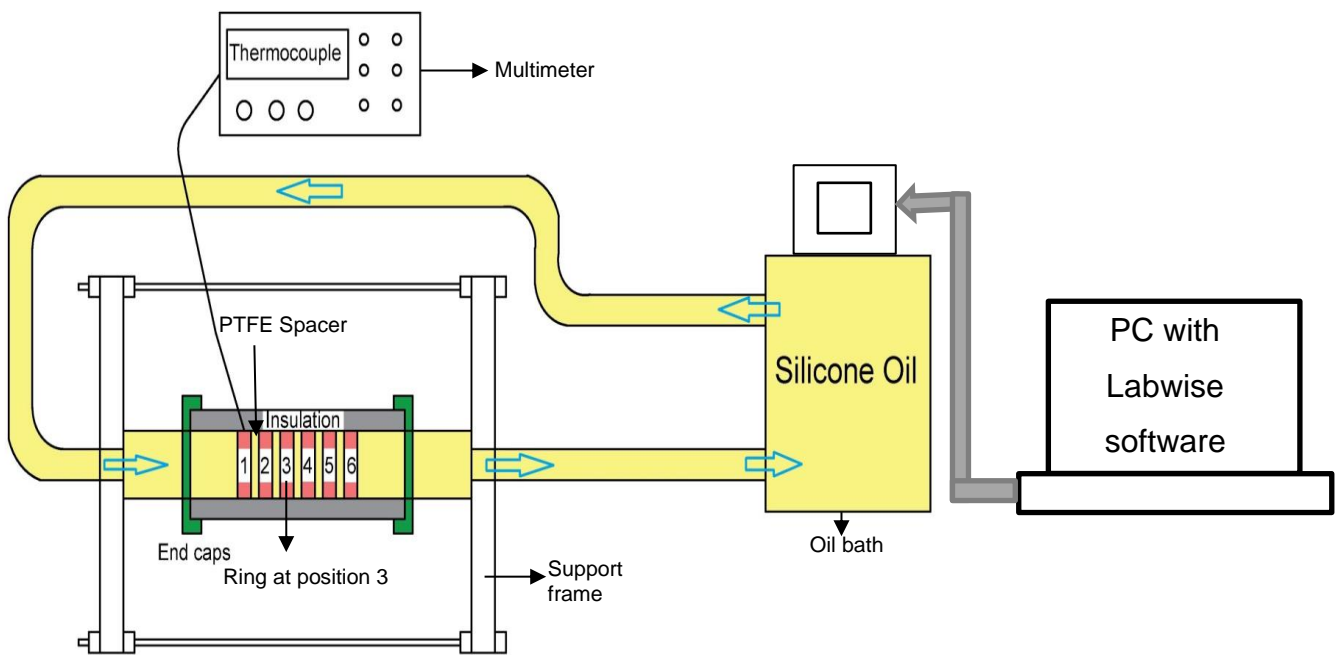


Figure 4.7: A schematic representation of the CUI test rig used in this study.



Figure 4.8 : Picture showing the complete set up of the CUI test rig

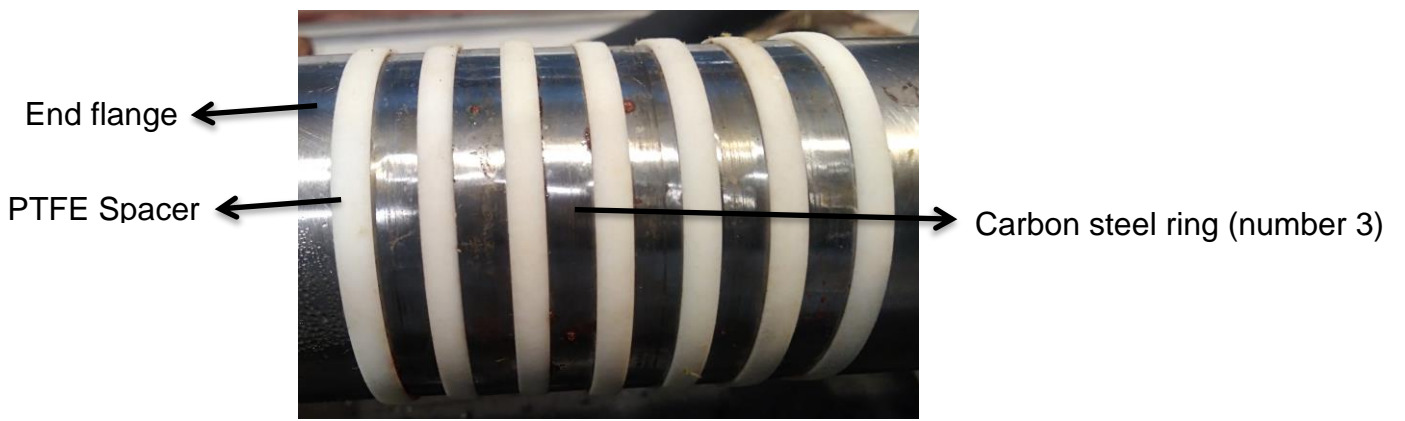


Figure 4.9: Picture of the test rig showing the arrangement of rings and spacers

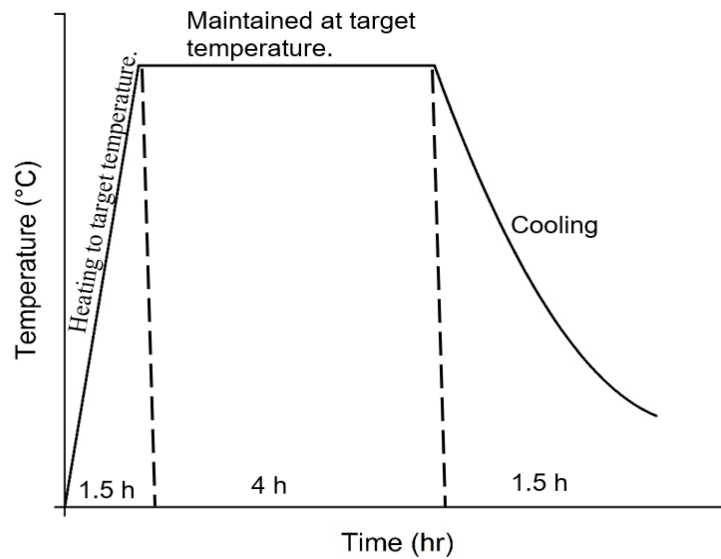


Figure 4.10 : Temperature program for each cycle used for CUI study.

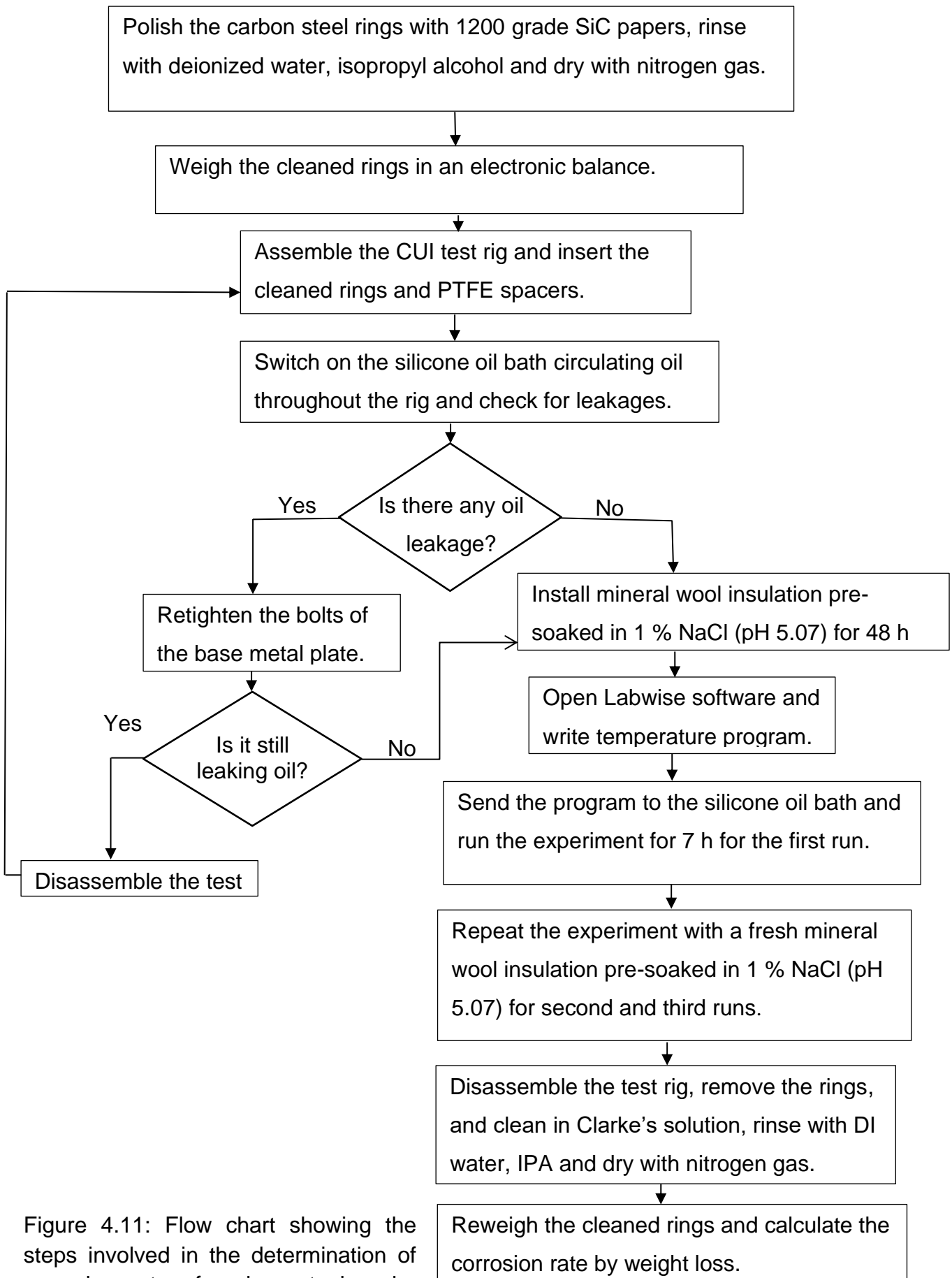


Figure 4.11: Flow chart showing the steps involved in the determination of corrosion rate of carbon steel under insulation by weight loss.

4.3) Distribution of test solution between the top and bottom sections of the insulation

These experiments were aimed at determining the quantity of test solution held by the top and bottom sections of the insulation to account for the reported differences in the corrosion rate between the top and bottom sections of the rings. The mineral wool insulation was sectioned into two halves representing the top and bottom sections (Figure 4.12) after soaking in the test solution (1 wt% NaCl, pH 5.07) for 48 hours. The two sections were weighed to determine their initial weight before the test. Both parts of the insulation were installed on the CUI test rig and measurements were carried out from 60 °C-130 °C for about 7 hours. On completion of the test, the insulation was removed and reweighed to determine the final weight of the insulation after test for both parts. The amount of test solution remaining in each part was calculated. The entire experiment was repeated three times to determine the reproducibility of the experiment.

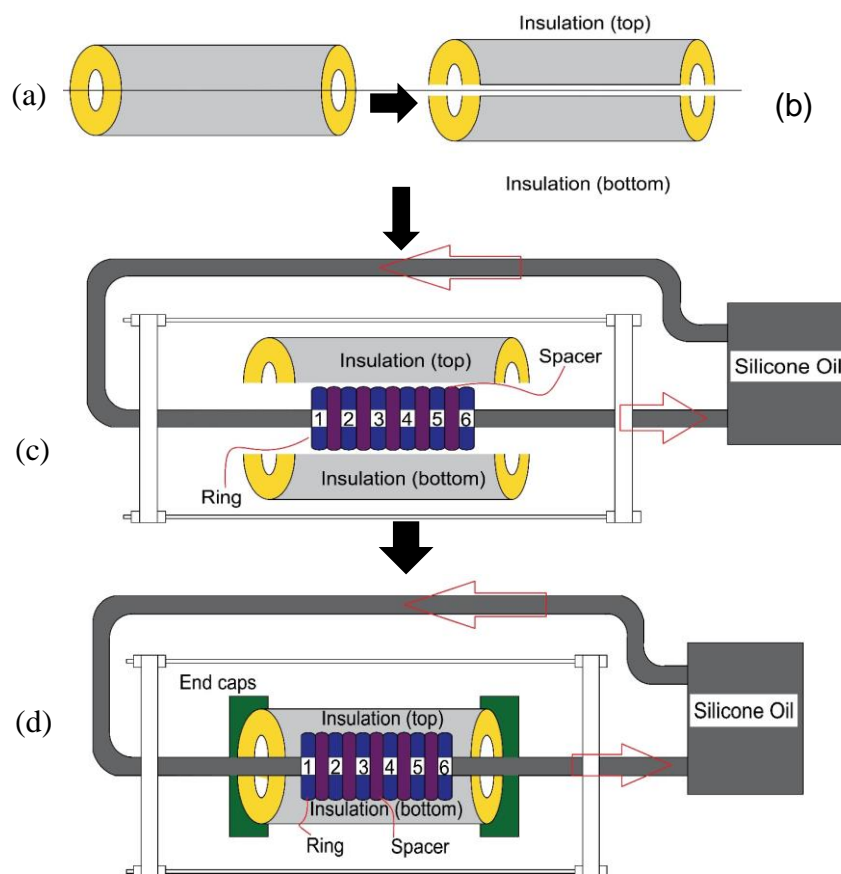


Figure 4.12 : Determination of the variation of test solution between the top and bottom parts of the insulation (a) An insulation showing the axis to be sectioned (b) An insulation sectioned into top and bottom parts (c) Insulation installed around rings (d) The complete set up including use of end caps to hold the insulation together.

4.4) Distribution of the test solution between the ends and centre of the insulation

The distribution of the test solution between the ends and centre of the insulation is shown in Figure 4.13.

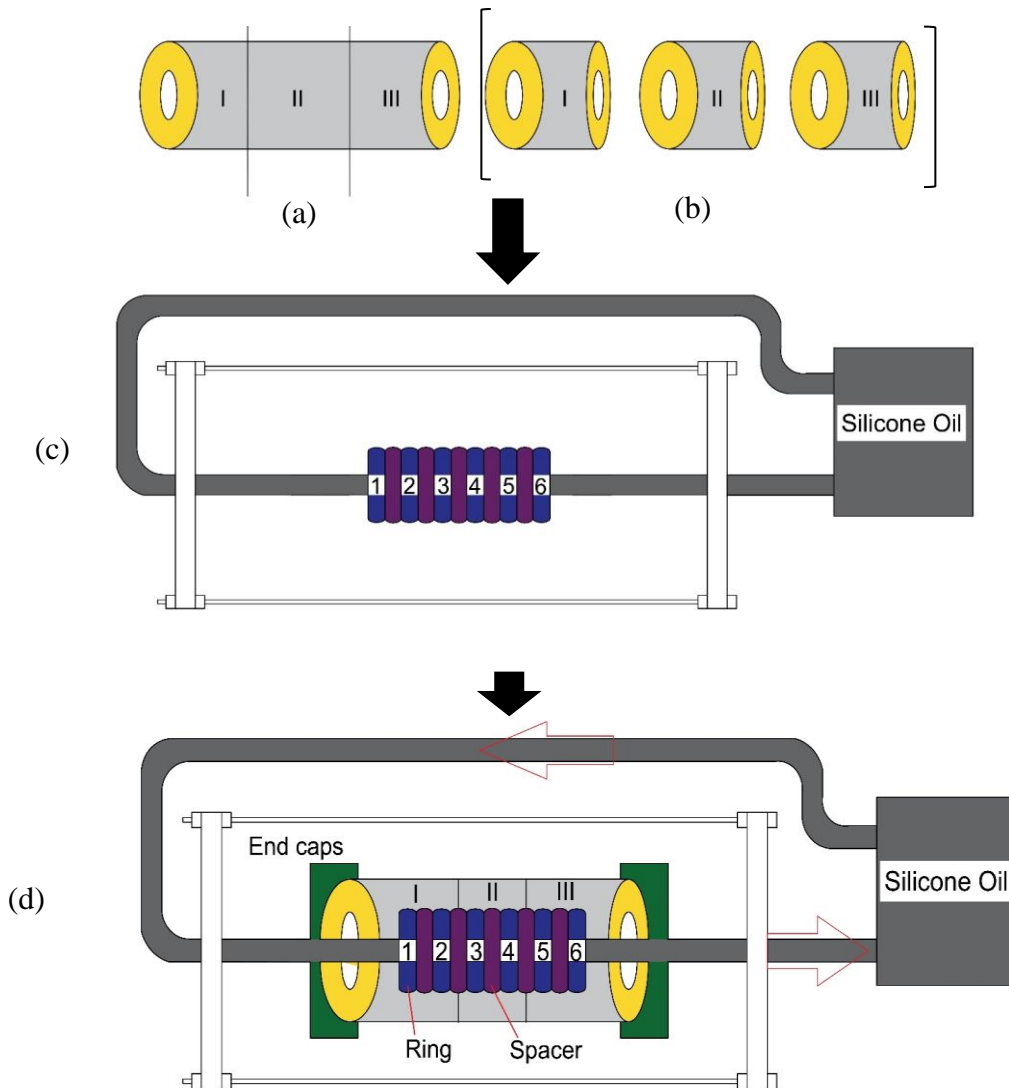


Figure 4.13: Determination of the variation in test solution between the ends and centre of the insulation (a) Full insulation showing the axis to be sectioned (b) An insulation sectioned into three pieces (c) A test rig without the insulation in place (d) A test rig with the three pieces of insulation installed.

This was carried out to determine the distribution of test solution between the ends and centre of the insulation in order to assess its influence on the degree of corrosion

across the six rings and to verify if the observed differences in corrosion rate across the six rings are due to end effects. In this method, a piece of mineral wool insulation was sectioned into three parts and labelled as w1 representing insulation wrapped around the inlet section (rings 1 and 2), w2 representing insulation around the middle rings (rings 3 and 4) and w3 representing insulation wrapped around the rings close to the outlet (rings 5 and 6) as shown in Figure 4.11. The three sections of the insulation were weighed separately and soaked in the test solution (1% by weight NaCl at a pH of 5.07) for 48 hours, after which they were removed and re-weighed to determine the quantity of test solution absorbed by each section. The three sections were installed on the CUI test rig using aluminium tape and experiments were conducted at different temperatures of 60-130 °C for about 7 hours. On completion of the experiment, the three sections of mineral wool were removed from the CUI test rig and re-weighed. This experiment was carried out in triplicate in order to assess its reproducibility.

4.5) Monitoring temperature variations across the six carbon steel rings

It is possible that there could be temperature variations across the six rings that may either influence the corrosion rate or affect the drying out time of different part of the mineral wool insulation. The test rig was arranged such that silicone oil enters the rig through ring1 and exits the rig through ring 6 as previously described and shown in Figure 4.7. This experiment was aimed at determining the temperature of each of the rings in order to correlate with the differences in corrosion rate across the rings. Six carbon steel rings labelled 1-6 from the inlet to the outlet end were used to set up the CUI test rig and mineral wool insulation was used to wrap around the rings. The temperature of each of the rings was monitored using a K-type thermocouple connected to a digital multimeter (Keithley 2110). The temperature of the silicone oil bath (TXF 200, Grant instruments) was set from 60 °C-130 °C and the temperature of each of the carbon steel rings was measured to an accuracy of ± 1 °C.

4.6) Quantifying the corrosion rate between the top and bottom parts of carbon steel rings

It has been reported that there is difference in corrosion rate between the top and bottom parts of the rings, with the bottom rings corroding more than the top as a result of test solution settling to the bottom due to gravity [12]. This assertion has previously been investigated in this study by assessing the content of test solution between the top and bottom sides of the insulation but not correlated with corrosion rate. Therefore, this study uses Lacomit lacquer purchased from Agar Scientific Limited to quantify the degree of corrosion occurring in the top and bottom parts of the carbon steel rings. The chemical composition of the lacquer as well as the remover as specified in the product data sheet is presented in table 4.5.

This product was used to assess and quantify the difference in the corrosion rate occurring between the top and bottom of the rings. This was carried out by masking the top parts of the rings with Lacomit lacquer using a paint brush. The masked rings were mounted on the CUI test rig and the experiment was carried out at 80 °C for about 7 hours, after which the test rig was disassembled, and the rings were removed and cleaned with Clarke's solution. For comparison, this was repeated with the varnish applied to the bottom parts and the corrosion occurring at the top was assessed at 80 °C for about 7 hours. At the end of the experiments, the rings were removed from the rig and the corrosion products were also removed.

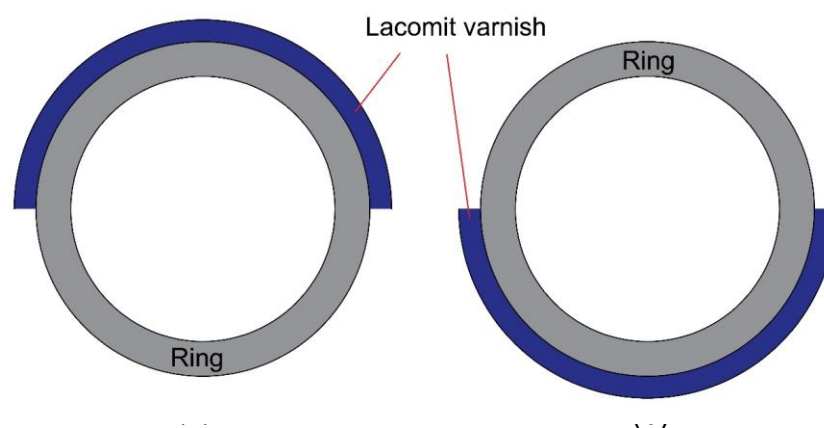
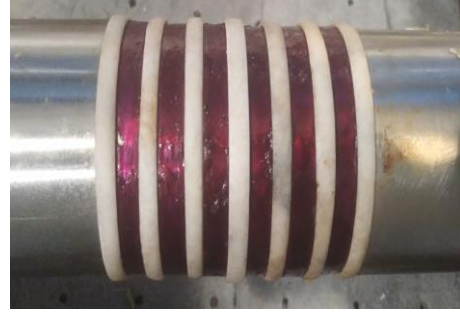


Figure 4.14: A schematic diagram showing the application of Lacomit lacquer to the carbon steel rings (a) Application of the lacquer to the top part of the ring samples (b) Application of the lacquer to the bottom part of the rings.



(a)



(b)

Figure 4.15: Top view images of the test rig showing (a) Lacomit lacquer applied to the bottom part of the rings (b) Lacomit lacquer applied to the top part of the carbon steel ring samples.

Table 4.4 : Chemical composition of Lacomit lacquer and remover [22].

Chemicals present	Lacomit lacquer	Lacomit remover
	Composition (%)	Composition (%)
Xylene	45	25
Acetone	3	75
Butyl acetate	15	-
Butan-1-ol	20	-
1-methoxy-2-propanol	3	-

4.7) Effectiveness of a new commercial inhibitor (VpCI 619) on corrosion rate

Vapour phase corrosion inhibitors (VpCIs) are volatile chemical compounds that form a stable bond with metallic surface preventing the formation of corrosion cells thereby significantly reducing corrosion in insulated structures [23]. Among the available inhibitors, VpCI 619 was chosen because it is specifically designed to protect metals under insulation and it has properties such as high temperature tolerance up to 600 °C, non-flammable and protects metals under insulation against corrosion in both wet and dry cycles.

As specified in the product data sheet [23], the vapour phase corrosion inhibitor purchased from Cortec Solutions made up of sodium molybdate (10-25 wt%), boric acid (2.5-5.5 wt%) and borax pentahydrate (≤ 2.5 wt%). The density of the inhibitor is

1.1 g/cm³, while the vapour pressure at 20 °C is 0.023 bar which is similar to the vapour pressure of water at the same temperature. Based on these characteristics, using the term 'vapour phase' with VpCI 619 inhibitor seems to be a misnomer as this is consistent with liquid phase inhibitors rather than vapour phase inhibitors. Notwithstanding, the insulation was applied to the internal parts of the insulation that was pre-soaked in the test solution for 48 hours. First, the area of the mineral wool insulation which is similar to the area of an open-ended cylinder was calculated. Since the coverage of the inhibitor per area of insulation as specified in the guide provided by Cortec is 3.68-4.9 l/m², the quantity of inhibitor required per area of insulation was calculated from this specified range. The detailed calculations and equations used are shown in the appendix.

The inhibitor was put in a weighed plastic spray bottle and the weight of the bottle with the inhibitor was taken. This was used to spray the internal portions of the wet insulation and it was weighed regularly to ensure that a similar quantity of inhibitor was used for all the trials. The treated insulation was then wrapped around the central portions of the CUI test rig containing carbon steel rings that was previously polished with silicone carbide papers, rinsed with deionized water, isopropyl alcohol, dried with nitrogen gas and weighed. Experiments were carried out at different temperatures of 80 °C, 95 °C, 110 °C and 130 °C for three different experimental runs. After the third run, the test rig was disassembled and the rings removed and cleaned in Clarke's solution, rinsed with deionized water and isopropyl alcohol and blown dry with nitrogen gas and re-weighed. In order to assess the effectiveness of the inhibitor, the corrosion rate obtained using the inhibitor was compared with the corrosion rate determined without the inhibitor (control), and the percentage inhibition was calculated using equation 3 reported by McCaferty [24].

$$\% \text{ Inhibition} = \frac{CR_o - CR_1}{CR_o} \times 100 \quad (3)$$

Where CR_o represents the corrosion rate without inclusion of the inhibitor and CR_1 is the corrosion rate with the use of inhibitor.

Table 4.5 : Properties of VpCI 619 inhibitor as reported in the safety data sheet [23]

State	Liquid
Colour	White
Odour	Characteristic
pH at 20 °C	8.2-8.7
Density at 20 °C	1.04-1.15 /cm ³

4.7.1) Effect of dosage of inhibitor on CUI of carbon steel

The effect of an increasing dosage of inhibitor in mitigating the corrosion of carbon steel under insulation was carried out to assess the effectiveness of different amounts of the inhibitor. Besides, it will also give some insight into the mechanism of inhibition. Therefore, in this study, different dosage of inhibitor ranging from 1.2 g/m², 3.6 g/m² and 5.2 g/m² was applied to the internal part of the insulation prior to installation on the test rig. After application of the inhibitor to the insulation, it was then installed on the test rig and experiments were carried out at 80 °C for a total of 21 h. On completion of experiments, the insulation was removed, and the test rig was disassembled. The rings were removed and cleaned in Clarke's solution, rinsed with deionized water, isopropyl alcohol and blown dry with nitrogen gas and re-weighed. The corrosion rate was determined, and the percentage inhibition was calculated.

4.8) Monitoring of drying out times of mineral wool insulation using galvanic current and impedance measurements

The time it takes for mineral wool insulation that has been wetted with 1 wt % NaCl solution to dry out at different temperatures was investigated using galvanic current and electrochemical impedance measurements. The purpose of this measurement was to assess the insulation dry out time and how it affects CUI rate. This is important because the severity of CUI depends on the time the metal is in contact with the electrolyte in the insulation [15]. Also, monitoring the insulation drying out time could also provide useful information on the moisture transport properties of the insulation which can be used in the characterization of the material [20]. The CUI test rig showing the connections for galvanic current and impedance measurement is shown in Figure 4.16, while the schematic representation of the connections is shown in Figure 4.17.

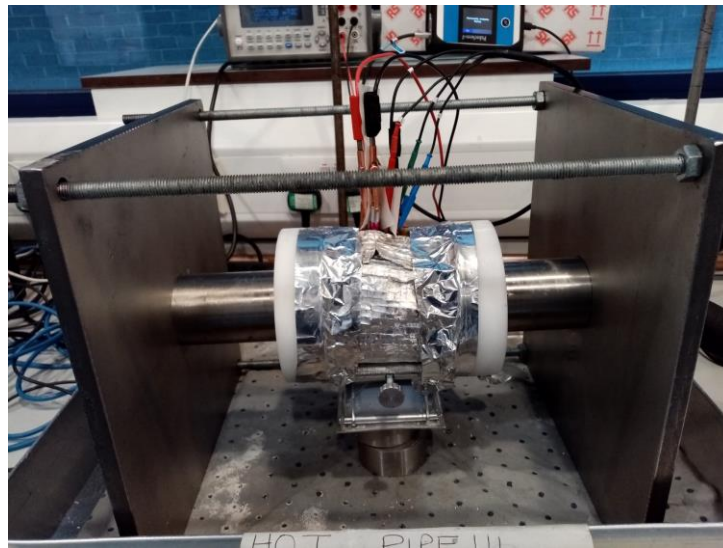


Figure 4.16: CUI test rig showing connections for insulation dry out using galvanic current and electrochemical impedance measurements.

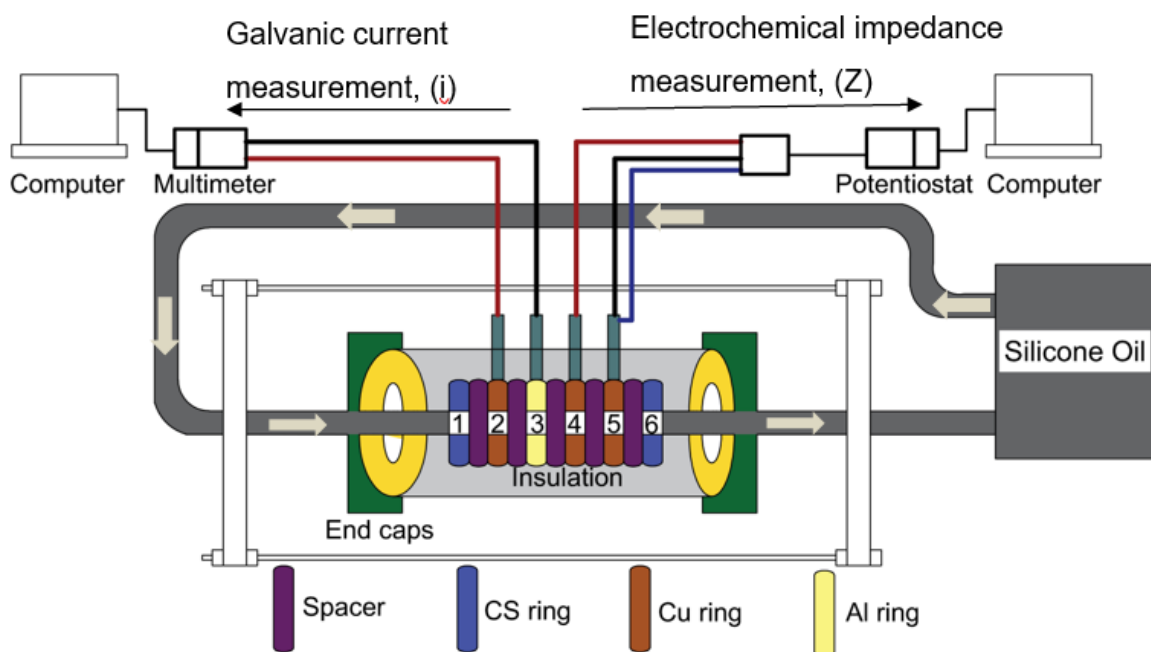


Figure 4.17: Schematic representation of the connections for measurements of insulation dry out using galvanic current and electrochemical impedance measurements.

In this study, rings 2 and 3 from the inlet end were replaced with copper and aluminium rings respectively. Aluminium is less noble than copper and it will preferentially corrode instead of copper (galvanic corrosion) as earlier discussed in chapter 2. Both metals were masked with Lacomit varnish leaving out a surface area of 0.5 cm^2 , the masked area was further covered with a tape to ensure that current flow is around the exposed area only and not the entire metal surface. A mineral wool insulation prewetted with 1 wt % NaCl solution was installed on the rig containing the Cu-Al couple for galvanic current measurement and Cu-Cu rings placed at positions 4 and 5 for impedance measurements as shown in Figure 4.15. The galvanic couple was connected to a digital multimeter (Keithley 2110). The 10mA DC current range was used with an internal resistance of 5.1Ω and a resolution of $0.1 \mu\text{A}$. The current-time data was sampled every 2 seconds using Labwise software. Impedance and phase data were recorded every 10 seconds at a fixed frequency of 1kHz and AC amplitude of 25 mV using a Palm Sens 4 potentiostat.

The galvanic current measurement records the current flowing through the exposed area as a function of time, while the two copper rings at positions 4 and 5 were connected to the potentiostat (PalmSens 4) for impedance measurements. The connections of the galvanic couple would result in the flow of galvanic current which was measured using a multimeter. The two copper rings were chosen for the impedance measurements because they will corrode without the formation of corrosion products under acidic condition which might cause additional impedance.

The drying out of the insulation was monitored at temperatures ranging from $70 \text{ }^\circ\text{C}$ to $130 \text{ }^\circ\text{C}$. These temperatures were selected so that complete insulation dry out can be obtained in a reasonable time and the results can be compared with the CUI rate previously measured at the same temperatures. The copper and aluminium rings were drilled halfway through to allow similar metal rod to be inserted for electrical connections. The rings were painted with the Lacomit lacquer leaving out a small area of 0.5 cm^2 to allow for contact with the wet insulation. A laboratory jack was used to ensure that adequate contact between the wet insulation and the bottom of the rings were achieved (Figure 4.16). Experiments were carried out at the target temperatures in triplicates to assess the reproducibility of measurement. Experiments were also repeated to assess the drying out at the top and sides of the metal rings.

4.9) Predictive Modelling of Corrosion of Carbon Steel under Insulation using Artificial Neural Network

The modelling of corrosion rate of carbon steel under insulation was carried out using artificial neural network (ANN) in SPSS software (version 13.0). The purpose of this investigation was to assess the accuracy of ANN in predicting laboratory CUI data based on the input parameters (temperature, dosage of inhibitor, quantity of electrolyte in insulation and sample position) studied in the laboratory as well as the effects of different network architectures such as number of hidden layers, the choice of activation functions on accuracy of prediction including precision of the predicted output. Artificial neural network uses the short-term data obtained from experiments to train itself on the pattern and determines the degree of relationship between each of the contributing parameters that influences the corrosion rate as studied in the laboratory and the observed output which is the corrosion rate.

In this study, the multilayer perceptron (MLP) was used, which is a more advanced modelling tool with a better prediction accuracy than the single layer perceptron. In addition, MLP offers more flexible options as number of neurons and hidden layers can be adjusted compared to radial basis function [25]. The modelling process starts by specifying the dependent variable (corrosion rate) and independent variables identified by the software as covariates (temperature, sample position, amount of test solution in insulation and dosage of inhibitor). Corrosion rate was fed into the output layer while the aforementioned independent variables were fed into the input layer of the ANN module. The data at the input layer was subjected to hyperbolic tangent and sigmoid activation functions in the hidden layer. The data at the input layer was partitioned into the training and test data sets. This was carried out exclusively by the software; however, the percentage of data classified into each set (training and test) can be adjusted manually by the user. In this study, a 70%:30% combination was used based on the reported prospects of better adaptability resulting in an enhanced prediction accuracy [26].

The comparative prediction accuracies of the neural network were assessed for both a single layer and a dual hidden layer. In the single layer configuration, the sigmoid and hyperbolic tangent activation functions were independently assessed, while in the dual hidden layer configuration, sigmoid and hyperbolic tangent activation functions

were used at each layer. In both configurations, the input and output layers which were both made of one layer each remained unchanged while the feedback error was set at 1%. The parameters such as temperature, quantity of test solution in the insulation, positional arrangement of the rings and dosage of inhibitor were used as input variables while the corrosion rate was used as the output variable.

The effect of the activation function on the prediction accuracy was assessed with a single layer configuration. In this case, two sets of prediction were carried out independently, the first set consists of a sigmoid function as the activation function while the second set consists of a hyperbolic tangent as the activation function. In both cases, the prediction was carried out three times to assess the repeatability of the prediction. A 70/30 % data splitting pattern as reported in other corrosion prediction reports [27] was adopted. Also, an independent variable importance analysis was carried out to assess the contribution of each of the input parameters to the predicted output. This is based on the estimation of the variations based on the patterns established between each input variable and the output (corrosion rate) and it could be a decisive factor in parameter prioritisation. The step-by-step process showing the modelling steps is shown in Figure 4.18.

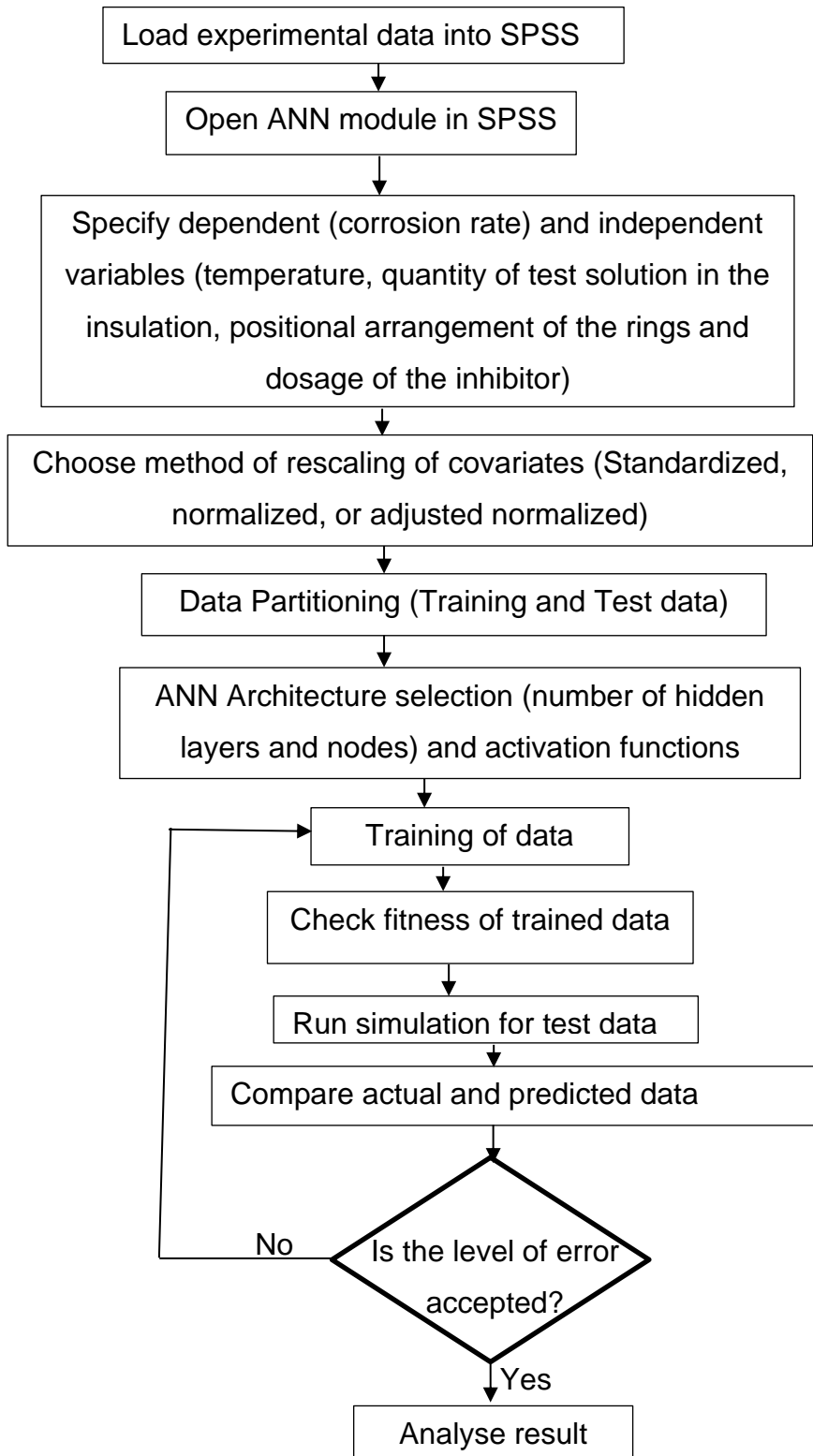


Figure 4.18: A flow chart showing the steps involved in the modelling process.

Chapter References

1. Pojtanabuntoeng, T. Laura, M. S., Mobin, S., Brian, K. and Martyn, C. (2015). Influence of drain holes in jacketing on corrosion under thermal insulation. *Corrosion*, 71(12):1511-1520.
2. De Vogelaere, F. (2009). Corrosion under Insulation. *Process progress safety*, 28:30-35.
3. Zwaag, C. and Rasmussen S. N. (2017). Cyclic CUI testing of Insulation materials, National Association of Corrosion Engineers publication, paper number 8877.
4. Product Data Sheet for Rockwool, Rocklap H and V pipe section, <https://p-cdn.rockwool.com/siteassets/rw-uk/downloads/datasheets/rocklap-hv-pipe-sections.pdf?f=20210202134822>, date accessed 15th May, 2021.
5. Material Safety Data Sheet for Rockwool, Rocklap H and V pipe section, <https://www.rockwool.com/syssiteassets/rw-uk/downloads/msds/msds-rockwool-insulation-web.pdf>, date accessed 26th November, 2021.
6. ASTM C1511 (2015). Standard test method for determining the water retention (repellency) characteristics of fibrous glass insulation. ASTM International.
7. ASTM C1763 (2016). Standard test method for water absorption by immersion of thermal insulation materials. ASTM International.
8. British Standard BS EN 13472 (2012). Thermal insulating products for building equipment and industrial installations. Determination of short-term water absorption by partial immersion of preformed pipe insulation. BSI, London.
9. British Standard BS EN 1609 (2013). Thermal insulating products for building applications. Determination of short-term water absorption by partial immersion. BSI, London.
10. ASTM G189-07 (2007). Standard guide for laboratory simulation of corrosion under insulation. ASTM International.

11. Ayello, F., Hill D., Marrion, S. and Sridhar, N. (2011). Integrated sensor networks for corrosion under insulation: monitoring, cost reduction and life extension strategies. NACE International, paper number 11281.
12. Pojtanabuntoeng, T. Laura, M. S., Mobin, S., Brian, K. and Martyn, C. (2015). Influence of drain holes in jacketing on corrosion under thermal insulation. *Corrosion*, 71(12):1511-1520.
13. Kane, R. D. Chauviere, M., Chustz, K. (2008). Evaluation of steel and TSA coating in a corrosion under insulation (CUI) environment, National Association of Corrosion Engineers publication, paper number 08036.
14. Caines, S., Khan, F., Shirokoff, J. and Qiu, W. (2015). Experimental design to study corrosion under insulation in harsh marine environments. *Journal of Loss prevention in the Process Industries*, 33:39-51.
15. Caines, S., Khan F., Shirokoff, J. and Qiu, W. (2017). Demonstration of increased corrosion activity for insulated pipe systems using a simplified electrochemical potential noise method. *Journal of Loss Prevention in the Process Industries*, 47:189-202.
16. Bai, X., Tang, J., Gong, J and Lu, X. (2017). Corrosion performance of Al-Al₂O₃ cold sprayed coatings on mild carbon steel pipe under thermal insulation. *Chinese Journal of Chemical Engineering*, 25(4):533-539.
17. Pojtanabuntoeng, T. Machuca, L. and Salasi, M. (2015). New experimental rig to investigate corrosion under insulation at different climate conditions. *Corrosion and materials*, 46-51.
18. Zwaag, C. and Rasmussen S. N. (2017). Cyclic CUI testing of Insulation materials, National Association of Corrosion Engineers publication, paper number 8877.
19. ASTM G1-03 (2011) Standard practice for preparing, cleaning and evaluating corrosion test specimens. ASTM International.
20. Reiser, A., Herrera-Avellanosa, D., Leonardi, E., Larcher, M. and Pfluger, R. (2021). Experimental measurement of material's drying coefficient for internal

insulation: New approaches for laboratory testing. *Earth and Environmental Science*, 863:1-9.

21. ASTM A106/A106M (2010). Standard specification for seamless carbon steel pipe for high temperature service. ASTM International.
22. Agar Scientific (2018). Safety Data Sheet for Lacomit varnish. [https://www.agarscientific.com/media/import/AGG371_Lacomit_Varnish_\(50_0ml\)_GB.pdf](https://www.agarscientific.com/media/import/AGG371_Lacomit_Varnish_(50_0ml)_GB.pdf), date accessed 26th November 2021.
23. Cortec Material Safety Data Sheet (MSDS) for VpCI 619, Hitek Electronic Materials Limited, <https://www.hitek-ltd.co.uk/msds-cortec>, date accessed 23rd November, 2020.
24. McCafferty, E. (2010). Introduction to corrosion Science, Springer Science, New York, U.S. A., pp.357-400.
25. Nelles, O. (2001). Non-linear system identification: From classical approaches to neural networks, fuzzy models and gaussian processes. 2nd edition, Springer, Switzerland.
26. Xu, Y., and Goodacre, R. (2018). On Splitting Training and Validation Set: A Comparative Study of Cross-Validation, Bootstrap and Systematic Sampling for Estimating the Generalization Performance of Supervised Learning. *Journal of Analysis and Testing*, 2:249–262.
27. Burhani, N. R. A., Muhammad, M., Ismail, M. C. (2018). Corrosion under insulation rate prediction model for piping by two stages of artificial neural network. The International conference on Production, Energy and Reliability, pp 1-6.

CHAPTER 5 : RESULTS AND DISCUSSION

Water absorption studies and rate of CUI of carbon steel

CHAPTER 5

RESULTS AND DISCUSSION

Water absorption studies and rate of CUI of carbon steel

This chapter covers the results showing the quantity of water absorbed by mineral wool insulation, the effect of temperature on corrosion of carbon steel under mineral wool insulation, and the effectiveness of a new commercial inhibitor (VpCI 619) in mitigating CUI rate of carbon steel. The water absorption study was carried out to determine the water absorption capacity of mineral wool insulation and the time required for the insulation to be saturated with water, which could be useful to assess the risk of CUI of metals operating at different temperatures. This is important because mineral wool insulation is usually impregnated with organic compounds predominantly silicone oil which consists of siloxanes, silicones and hydrocarbon chains linked together to impart hydrophobicity to the material [1, 2]. Also, the insulation consists of a phenyl formaldehyde resin which binds mineral wool fibres together, this also contribute to the hydrophobicity of the material [3].

However, when mineral wool insulation is installed on pipes that are intended to operate at high temperatures, these additives will likely decompose if the operating temperature exceeds its thermal stability limit, resulting in the loss of hydrophobicity. This could enhance water absorption leading to increased risk of corrosion under insulation. Therefore, this study was aimed at investigating the absorption capacity of mineral wool insulation under these conditions, as well as assessing the time it will take for the degraded insulation to be saturated with water and the variability associated with the trials. This was carried out without the protective jacketing as specified in ASTM C1511 standard, which could be useful in assessing the worst-case scenario that should be expected if the insulation is exposed to water.

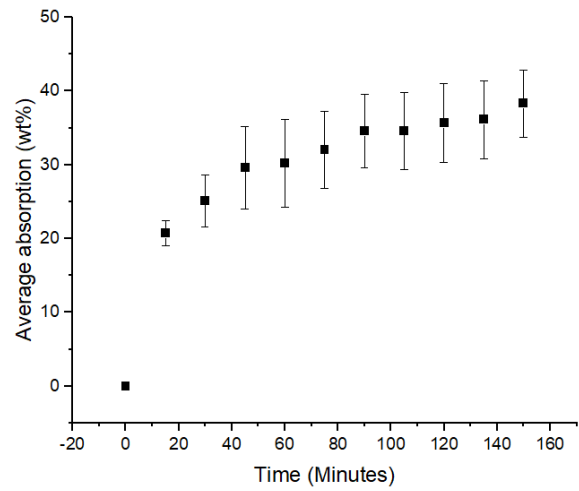
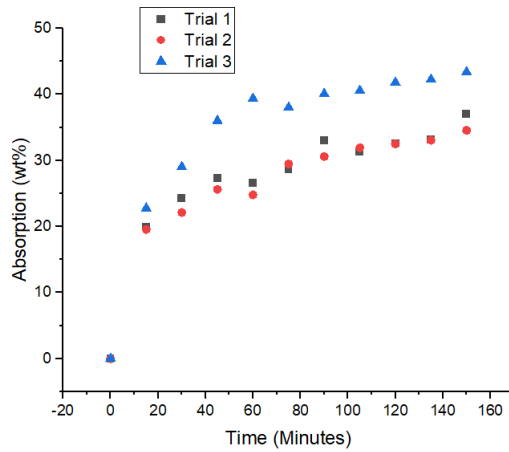
Afterwards, the effect of increasing the temperature of the pipe from 60 °C to 130 °C on the corrosion rate of carbon steel under mineral wool insulation is reported. This temperature range was selected because it has been reported to be the hotspots for aggressive CUI. Also, most chemical plants using insulated metals operate within this temperature range during service. Therefore, it was necessary to focus on this range

where the corrosion rate is expected to be high. It is worth noting that these results were obtained under an accelerated CUI conditions in order to obtain a meaningful CUI data within a realistic timeframe. This is because the corrosion of insulated metals is a slow process that could take several years before failure could be imminent depending on the operating conditions. Hence, it would be difficult and unrealistic to monitor the corrosion rate of insulated metals following the timescales typically observed in industry. Apart from the short exposure time compared to outdoor tests, accelerated conditions also offer the possibility of assessing the corrosion resistance of a material under controlled and stressed conditions. For these reasons, it was necessary to accelerate the corrosion process by deliberately saturating the insulation with water and increased concentration of sodium chloride relative to the ASTM G189 standard so that corrosion rate could be accelerated to facilitate testing in a reasonable time.

In addition, the effectiveness of a new commercial inhibitor in mitigating the corrosion of carbon steel under mineral wool insulation is reported. The effect of different dosage of the inhibitor is described as well as the effect of temperature at a fixed dosage is reported. This would enable the estimation of the cost and effectiveness in mitigating CUI in order to obtain a balance between both parameters which are important factors when choosing an inhibitor for insulated metals in a typical industrial process. The mechanism of inhibition of the main component of the inhibitor based on its chemistry is also described.

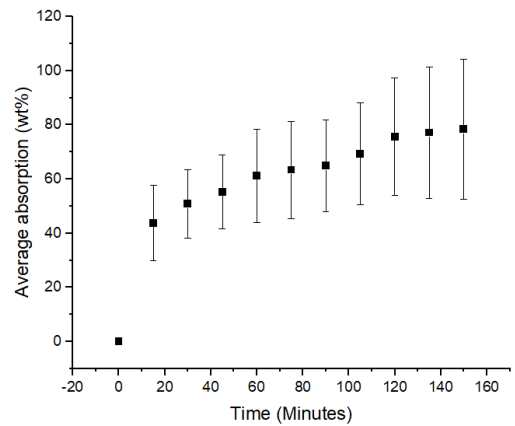
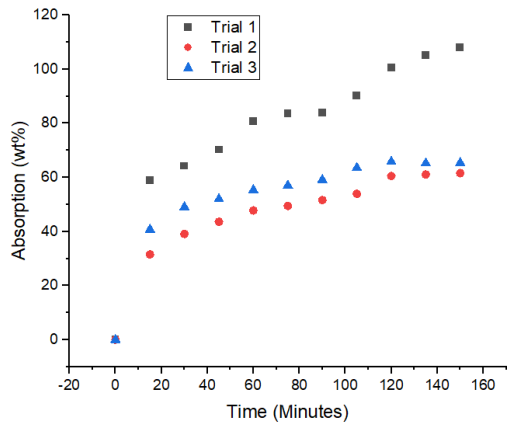
5.1) Water absorption capacity of mineral wool insulation

The results showing the water absorption capacity of mineral wool insulation for three replicates, the average absorption capacities, as well as the standard deviations computed from the repeated measurements are shown in Figure 5.1. These represent the results of three repeated measurements for the conditions where the insulation was untreated and when it was thermally treated at 250 °C for 3 h.



(a)

(b)



(c)

(d)

Figure 5.1: The water absorption profiles (a) Triplicate measurements without preheating the insulation (b) The average absorption of untreated samples (c) Triplicate measurements for insulation treated at 250 °C for 3 h (d) The average of treated samples.

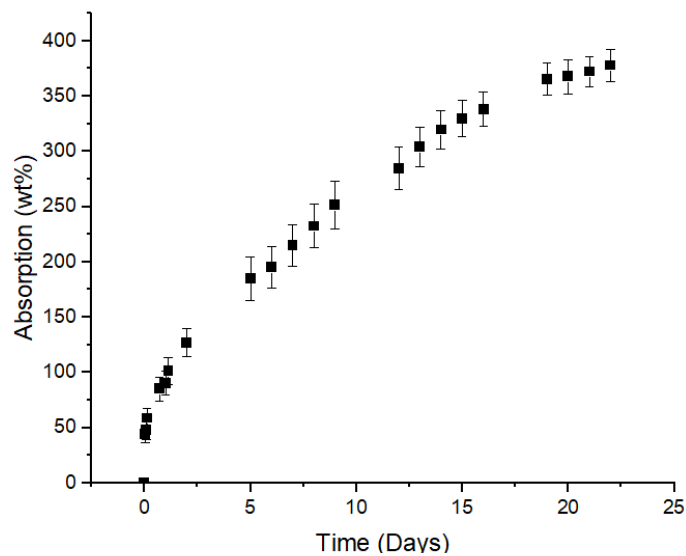


Figure 5.2 : Results showing the long-term water absorption test of mineral wool insulation

Figure 5.1a shows an increase in the water absorption with time for the three replicates. Even though all the replicates show a similar trend, the amount of water absorbed in the third replicate is different from the first two trials. The standard deviation of the replicate measurements which signifies variability are shown in Figures 5.1b and d. It is obvious that the third replicate is the main contributor to the overall variability. This was initially suspected to be due to the distribution of the hydrophobic additives since the three insulation parts used for the replicate measurements were from the same insulation material. However, Figures 5.1c and d which represent the water absorption capacities of the insulation after thermal decomposition of the organic additives have shown even more variability. This indicates that the differences in the replicate measurements might be inherent in the method used rather than differences in the hydrophobicity across the insulation. This is not unusual as other researchers have observed very high variability of about 52 % in the replicate measurement of the water absorption of mineral wool insulation that was thermally treated at 150 °C using the same ASTM standard [4].

Moreover, the relatively slow absorption at about 2 hours seemed that saturation may likely be attained if the time is further extended. This prompted further investigation of the absorption capacity over an extended period. However, the result of the 22-day

immersion tests shown in Figure 5.2 indicated continuous absorption of water instead of saturation. This suggested that saturation may not be attained within a reasonable time. This agrees with the report of Williams and Evans [5] who observed an increase in water absorption without saturation in mineral wool insulation immersed in water for 60 days. Comparison of the water absorption capacity of the insulation with and without heat treatment at 250 °C for 3 hours was carried out as a separate experiment where both materials were immersed in the same water under similar conditions. The result of the triplicate measurement is shown in Figure 5.3.

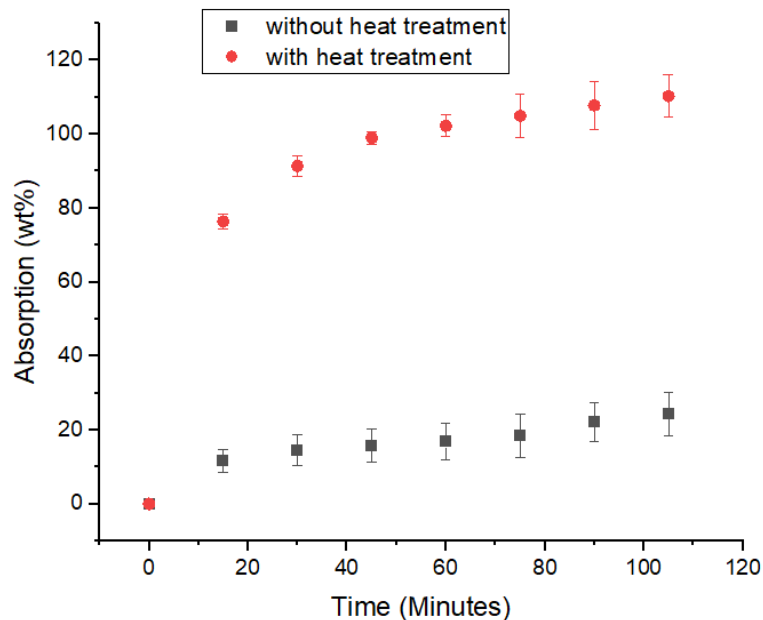


Figure 5.3: Results showing the water absorption capacity of mineral wool insulation with and without heat treatment at 250 °C for 3h.

In Figure 5.3, the quantity of water absorbed by the insulation that was thermally treated was higher than the untreated insulation. The amount of water absorbed has tripled as a result of the heat treatment. This may be attributed to the decomposition of the organic additives to volatile compounds, this renders the insulation vulnerable to water penetration. The additives are mainly silicone oils and phenolic resins [1,2]. From the material safety data sheet, the insulation contains 0-0.5 wt. % silicone oils and 0-5 wt. % organic binders [2], both chemical compounds contribute to the overall

hydrophobicity of the material. The organic binder has been reported to be stable up to 175 °C, while the silicone oil has a stability limit of 250 °C. However, both compounds will decompose if the operating temperature exceeds this value to give volatile products [1].

5.1.1) A comparison of the water absorption data with the available reports in the literature

The water absorption capacity of the untreated mineral wool insulation and the insulation that was thermally treated at 100 °C and 150 °C as reported in the literature is shown in Figure 5.4 [4]. For better comparison, the water absorption data in this study which was obtained using mineral wool insulation that was thermally treated at 250 °C for 3h is also shown in Figure 5.4.

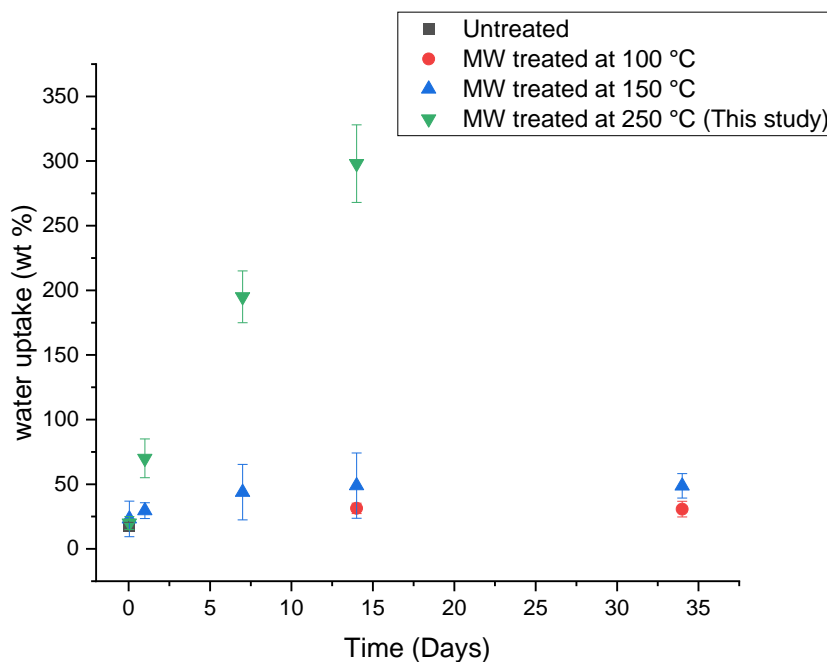


Figure 5.4: Results showing the long term water absorption of MW insulation obtained in this study and results reported in the literature [4]. All studies were conducted according to ASTM C1511 standard.

In Figure 5.4, the result indicates an increase in the water absorption for all the temperatures investigated. These were observed to be higher than the water absorption capacity of the untreated insulation. The absorption capacity of the

insulation treated at 150 °C is higher than the untreated and the treated insulation at 100 °C. In addition, the absorption capacity of the mineral wool insulation reported in this study which was treated at 250 °C is much higher than the absorption capacities reported by Pojtanabuntoeng *et al.* [4]. This significant difference may be attributed to the fact that the temperature used in this study has exceeded the stability limit of the organic binder and reached the point at which silicone oil is expected to start degrading (250 °C) resulting in an increased absorption of water, while the temperatures used to treat the insulation in the literature (100 °C and 150 °C) are below the stability limit of 175 °C which suggests that both the binder and the silicone oil may not be decomposed yet.

In another study, mineral wool insulation was thermally treated at 300 °C, and the water absorption capacity was assessed by immersion in water for 17 weeks instead of the 15 minutes specified by ASTM C1511 standard [5]. For better comparison, the results of the 22-day water absorption data obtained in this thesis has been overlaid with the data reported in this literature, this is shown in Figure 5.5. The results also indicated an increased absorption but at a slower rate than what is obtained in this study. However, the authors did not specify the duration of treatment of the insulation as well as the type of hydrophobic additive used in the insulation which would have been useful to explain the difference in absorption capacity shown in Figure 5.5. Notwithstanding, the important information from the study is that it took quite a long time before saturation was likely to be obtained. This is evident in the absence of a plateau after 60 days in the report by Williams and Evans, which agrees with the 22-day continuous absorption obtained in this study.

In addition, it should be noted that unlike organic additives, inorganic compounds used to improve hydrophobicity of insulation materials may require a higher temperature for a sustained period before degradation is imminent. This is evident in the report of Zwaag and Rasmussen [6], who observed that there was no difference in the water absorption of mineral wool insulation impregnated with inorganic resin before and after thermal treatment at 250 °C. This may be attributed to the fact that the inorganic resins were yet to be decomposed at that temperature. Nevertheless, the consensus found in these reports is that increasing the temperature used in treating the insulation reduces the hydrophobicity culminating in enhanced water absorption. In addition,

water absorption studies by mineral wool insulation show significant variability in replicate trials. Characterization of the different parts of a thermally treated mineral wool insulation using SEM/EDX by Ivanic *et al.* [3] has revealed the presence of a localized melt within certain parts of the insulation which opens up during thermal degradation allowing more water to be absorbed in this region than other areas of the insulation. This could possibly contribute to the observed differences in the water absorption capacity when the same insulation was cut into small parts and were immersed in the same solution under the same condition.

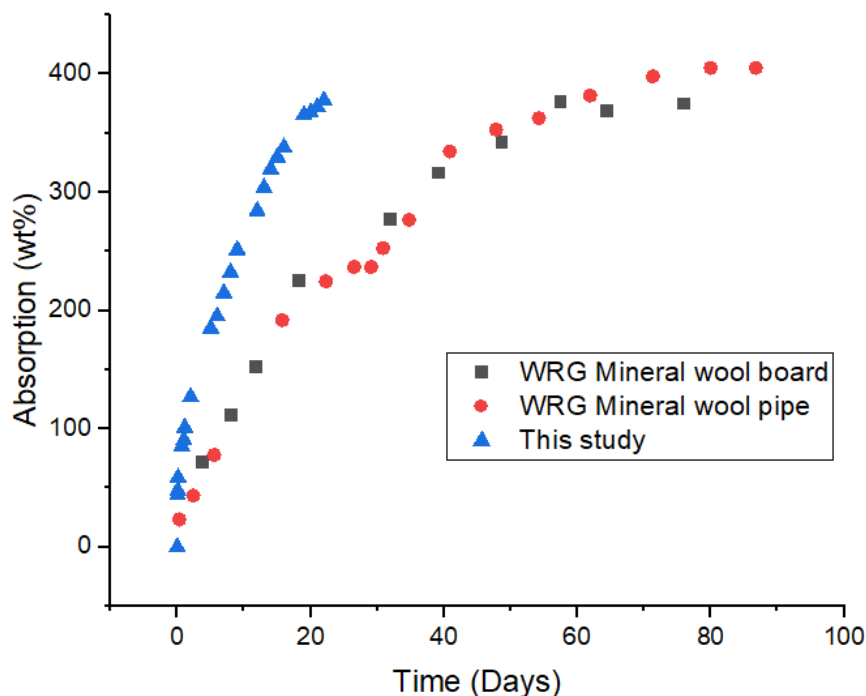


Figure 5.5: Comparison of water uptake of mineral wool board and cylindrical mineral wool used on pipe as reported by Williams and Evans [5] with the results obtained from this study.

These results indicate a significant increase in the water absorption when mineral wool insulation was subjected to thermal treatment due to the decomposition of the binder that account for the hydrophobicity of the material. The degraded insulation under these conditions was observed to absorb water for several days without reaching saturation. Other researchers also reported a continuous increase in the water absorption of a thermally treated mineral wool insulation for as long as 60 days [5].

Moreover, in this study, the mineral wool insulation treated at 250 °C was observed to absorb water continuously for 22 days without saturation. Considering the time constraint, it was necessary to discontinue the experiment and proceed with the measurement of corrosion rates using the CUI test rig. Nevertheless, a reasonable amount of time (2 days) where the insulation is known to absorb a well-defined and constant amount of water was chosen for CUI tests even though the insulation was not saturated within the chosen time.

5.2) Effect of temperature on corrosion rate of carbon steel under insulation

In this section, the results showing the effect of different pipe temperatures ranging from 60 °C to 130 °C on the corrosion rate of carbon steel under insulation are discussed. This temperature range was selected mainly because field data and failure analysis reports have indicated that corrosion under insulation is worse within this temperature range [7, 8]. In addition, scarcity of laboratory data showing the effect of temperature on corrosion rate of insulated metals have also been one of the reasons for initiating this research. The available CUI data showing the trend of corrosion rate with temperature were obtained from field studies. However, field data is not reliable, this is because the factors influencing CUI of metals as discussed in the introductory chapter are difficult to control under field conditions. This implies that laboratory data is required to validate the observed trend of CUI rate with temperature obtained from field studies.

Surprisingly, to the best of our knowledge, most of the laboratory report showing the trend of corrosion rate of insulated metals over different temperatures have focused on two extreme points and at most 3 points when testing coatings or inhibitors [9, 10]. However, this is not sufficient to show a reliable trend of CUI rate with temperature. In industry, the different temperatures of fluid flowing through insulated metals is known to have significant impact on the integrity of insulated metallic structures. Hence, it is important to assess and quantify the effect of temperature on CUI rate over a wider range to understand their contribution to corrosion of insulated assets. In this section, the results showing the effect of six different pipe temperatures selected between 60 °C and 130 °C on the corrosion rate of carbon steel under mineral wool insulation is hereby presented and discussed.

To enhance clarity, the process of obtaining the mean values is first explained. This involves the description of how the CUI rates of the 6 independent rings were analysed as well as the significance. This will be followed by presentation and discussion of the results for each mean value. The overall trend of the change in CUI rate with temperature is assessed using the global average of all the rings for the four replicates and the trend is shown and discussed accordingly. This is followed by the mechanism of CUI rate with respect to temperature which will focus on providing explanation to the observed trend reported in this study. Furthermore, the results will be compared with the field data reported in the literature. Finally, the effectiveness of a new commercial inhibitor in mitigating the corrosion of carbon steel under insulation as well as the mechanism of inhibition will be presented and discussed.

5.2.1) Averaging results of corrosion rate with temperature

The average corrosion rates of the metal rings were computed both horizontally across the six rings (inter-ring average) to obtain the average corrosion rate of all the rings for each replicate and vertically to obtain the mean CUI rate for each ring position for the four replicates (intra-ring average). Inter-ring average involved computing the mean corrosion rates of all the six rings at each temperature for each replicate, which provides information on the reproducibility of the data at each temperature, while intra-ring average involved averaging the corrosion rates of all the rings occupying the same position for each temperature. This provides the trend of CUI rate with temperature for each ring position as well as showing the deviation in the CUI rate across the different ring positions.

5.2.2) Inter-ring average of CUI data

The average CUI rate for the six carbon steel rings operating at different temperatures is shown in Figure 5.6. This shows an initial increase of corrosion rate with temperature up to a maximum temperature of 80 °C, further increase in temperature resulted in a decrease in corrosion rate up to 130 °C. In addition, the replicates seem to show a similar rate of increase in the corrosion rate with temperature as indicated by the steepness of the curve, though with slightly different values especially at 70 °C. The maximum corrosion rate is observed at 80 °C for all the replicates and the values of

the corrosion rate at this threshold are reasonably similar for replicates 1, 2 and 4. Ideally, the curves would be expected to be quite close to each other in addition to showing a similar shape. However, there are slight differences in the corrosion rates measured at each temperature, which may be attributed to the stochastic nature of corrosion as well as the difficulties associated with assembling the CUI rig reproducibly for each replicate measurement. Some of the field data also follows similar trend of initial increase in corrosion rate with temperature up to some maximum point, then it decreases as the temperature is further increased. The reason for this behaviour as well as the chemical reactions involved will be explained under the mechanism section.

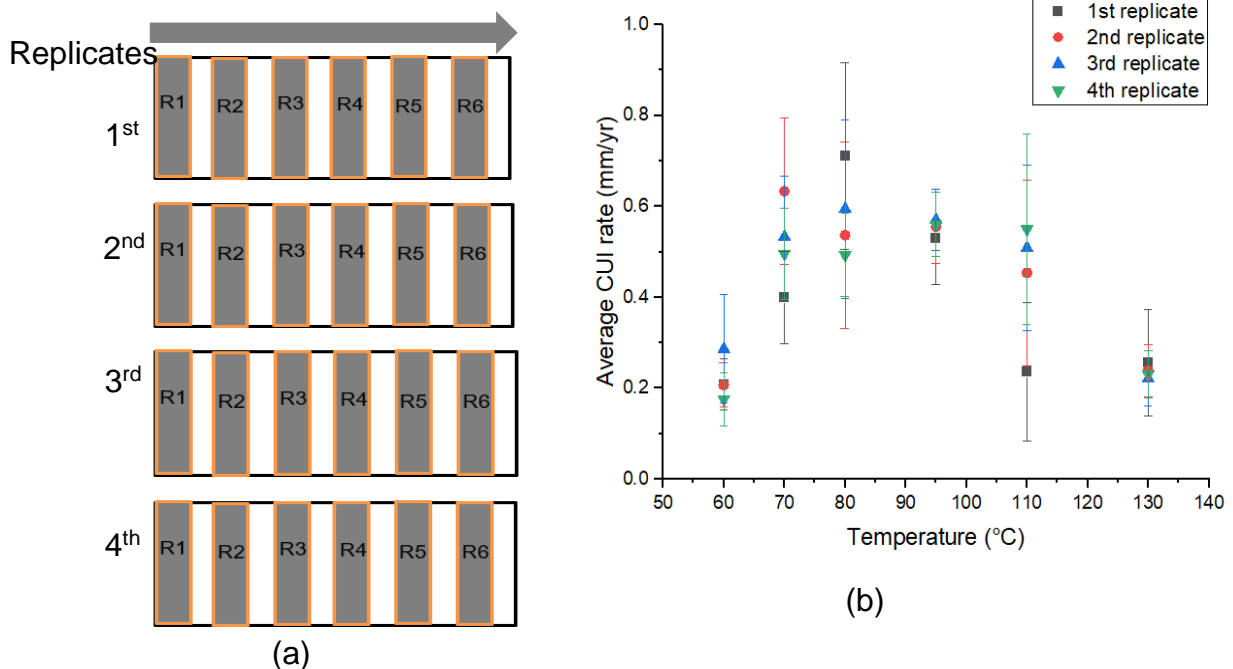


Figure 5.6: (a) Arrangement of the six carbon steel rings (b) Inter-ring average of the corrosion rate across the six rings at all the temperatures investigated. Error bars represent the standard deviation of four replicate measurements.

The average CUI rate across the six rings is based on the assumption that the difference in the corrosion rate at each ring position is negligible for each replicate measurement at the temperatures studied. This assumption was tested statistically by subjecting the mean CUI rate of each replicate to one way analysis of variance at 95 % confidence interval using SPSS (version 15). The null hypothesis stated that there

is no difference between the mean CUI rate of each replicate at the temperatures investigated, while the alternative hypothesis stated otherwise. The computed f-value (0.55) was observed to be less than the critical f-value (3.07) which implies that there is no statistically significant difference in the mean CUI rate of each replicate across the six temperature points, hence, the null hypothesis is not rejected. This is evident in the variability of the CUI rates of each replicate observed for each temperature cycle as shown in Figure 5.6. The experimental data which represents four replicates at each temperature has shown to be fairly close to each other at most of the temperature points investigated which indicates agreement between replicate measurement.

Other studies have observed significant variability in replicate measurement of CUI rate as shown in the reports of the researchers from Curtin University shown in Figures 5.7 and 5.8 and other researchers (Figure 5.9). The researchers reported the average corrosion rate and standard deviation of triplicate measurements of CUI rate for the top and bottom metal ring samples insulated with mineral wool at 80 °C (Figure 5.7), the results showing the effects of jacketing and drain holes on CUI rate (Figure 5.8) and the influence of chloride concentration on the CUI rate. The results provided in these reports show significant variability as indicated by the large error bars. This is not surprising as it is expected that there will be more variability in the corrosion rate obtained from metals under insulation compared to immersion methods. This is clearly observed in Figure 5.9 where the uninsulated metal had the lowest corrosion rate compared to the metals under insulation. This is due to the difficulty in obtaining a consistent quantity of electrolyte in the insulation wrapped around the test area where the CUI rate is being monitored as well as other challenges involved in re-assembling the CUI test rig reproducibly during each replicate measurement.

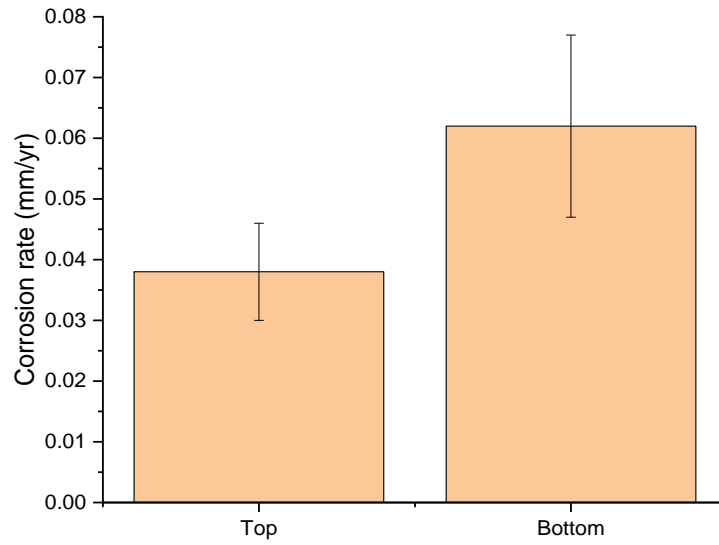


Figure 5.7: Average corrosion rate of carbon steel under mineral wool insulation at 80 °C [11]

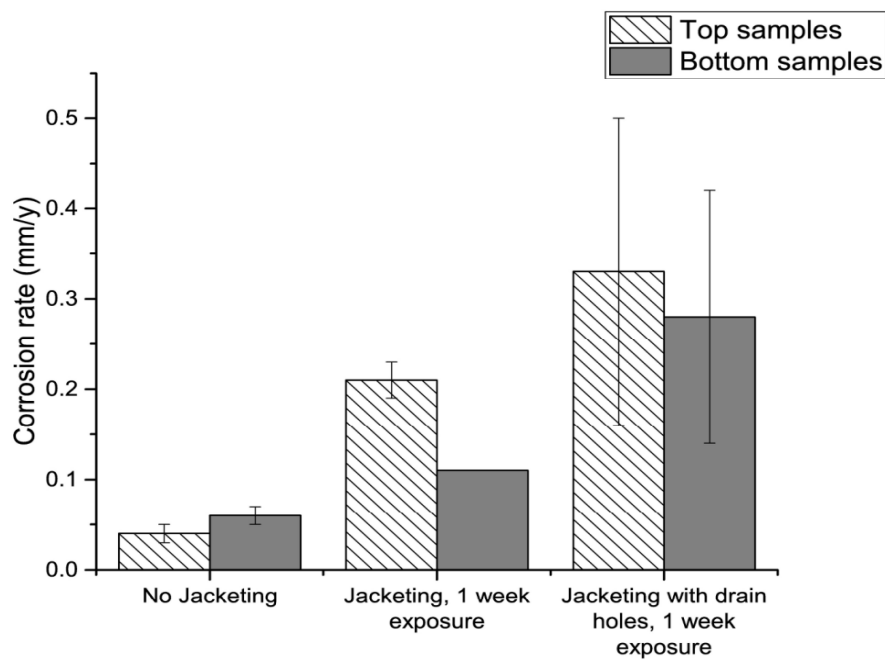


Figure 5.8: Average CUI rate of carbon steel under mineral wool insulation at 80 °C [12].

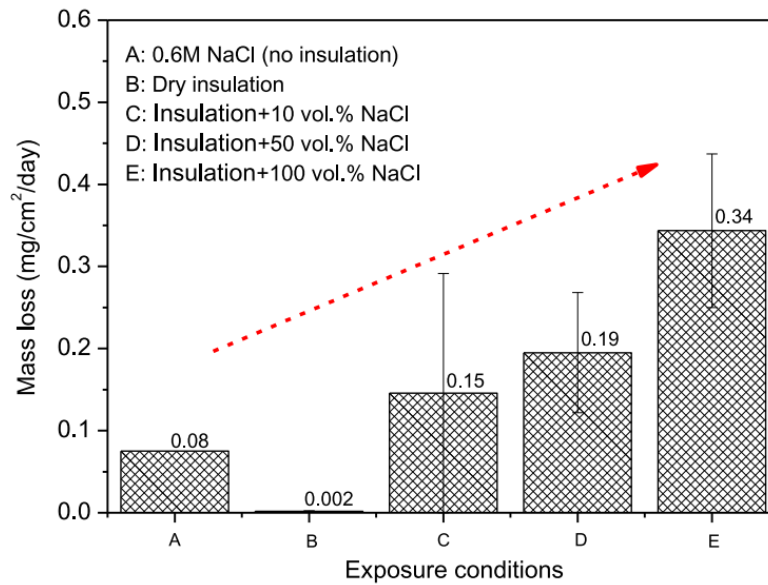


Figure 5.9: Corrosion of mild steel under mineral wool insulation [13].

Table 5.1 : Available laboratory data showing the corrosion rate of carbon steel under mineral wool insulation at a fixed temperature

Temp. (°C)	Electrolyte used	Time (h)	CUI rate (mm/yr)	References
24	Salt fog	336	0.02	[9]
60			0.05	
80			0.05	
80	1.0 wt % NaCl	336	0.61	[11]
80	1.0 wt % NaCl	168	0.10	[12]
80	4.0 wt % NaCl	336	2.08	[14]
82	100 ppm NaCl	480	0.25-1.0	[15]
30	Sea water	336	0.03	[13]
50	Sea water	336	0.06	[13]
70	Sea water	336	0.07	[13]

5.2.3) Intra-ring average of CUI data

The corrosion rate of the metal rings was also assessed by computing the average of the four replicates of each ring at different temperatures as shown in Figure 5.10. In this case, the average corrosion rate of the metal rings occupying the same position for the four replicates were computed. This was used to assess the degree of variability of the CUI rate across the six ring positions as well as the trend of CUI rate of each ring position with temperature. Results revealed that the corrosion rates of all the ring positions showed a similar initial increase with temperature and a subsequent decrease as temperature exceeds 80 °C. However, there are slight differences in the values of the corrosion rate at each ring position. The first ring tends to have the lowest corrosion rate compared to other ring positions. Ideally, it would be expected that the corrosion rate should slightly decrease with ring position. This is because the measurement of temperature of the rings showed a slight temperature difference of about 1-2 °C between the first ring and the last ring (Figure 5.11), which may be due to the heat loss as the oil flows through the pipe. The fact that the corrosion rate across the six ring positions does not follow this trend suggests that there are other factors that may contribute to the observed corrosion rate besides temperature.

One of such factors could be the distribution of the test solution in the insulation. Preliminary water absorption test of mineral wool insulation earlier discussed in this study showed a high variability in the water absorption with replicate trials. The reason for this increased variability even when the same insulation was used in repeated measurement has been suggested by Ivanic *et al.* [3] to be caused by the presence of localized melt inserts in the insulation which tends to open up during thermal treatment absorbing more water than other areas with good binding strength [3]. Therefore, this could influence the quantity of electrolyte in the insulation around each ring, which has a significant effect on the rate of corrosion across the ring positions. Hence, further investigation to determine the distribution of test solution in the insulation wrapped around the inlet rings (positions 1 and 2), middle rings (3 and 4) and the outlet rings (5 and 6) was necessary to assess the content of test solution across these regions which will be discussed in the subsequent chapter.

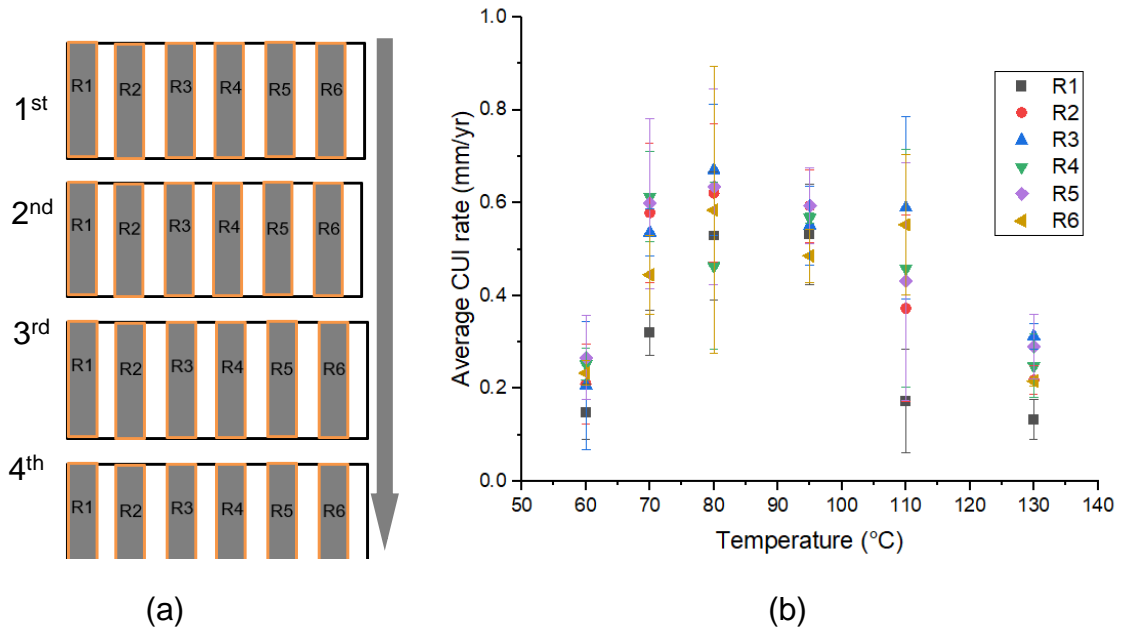


Figure 5.10: (a) Arrangement of six carbon steel rings (b) Average corrosion rate at each metal ring position for all the temperatures investigated (error bars represent the standard deviation of the four replicates)

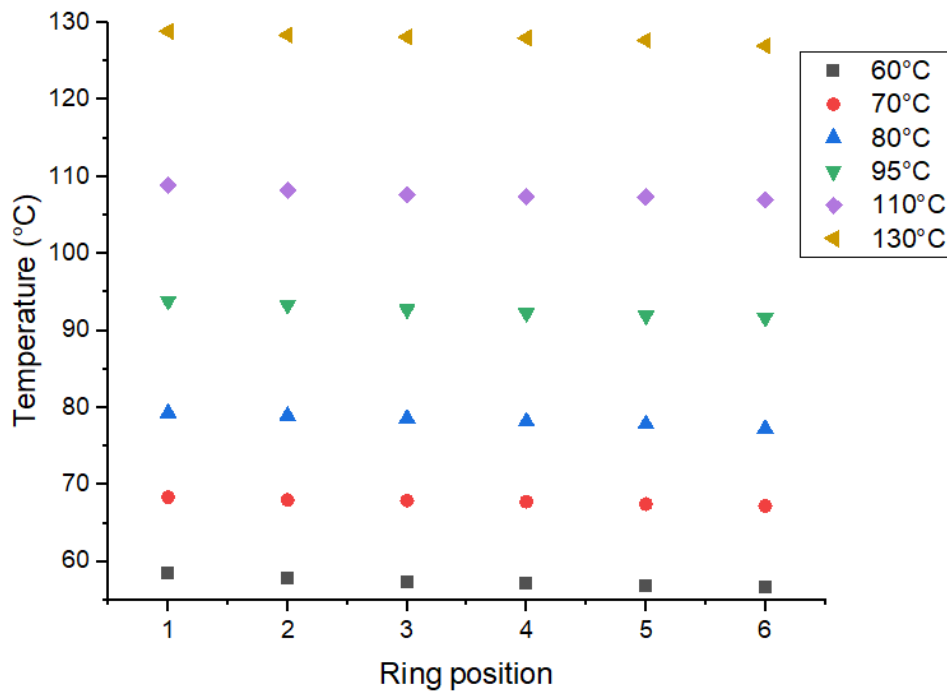


Figure 5.11: Temperature variation across the six ring samples

5.3) Overall trend of CUI rate with temperature

An overview of the variation of corrosion rate with temperature can be estimated by computing the global average of the corrosion rates of all the six metal rings for all the four replicates as well as the standard deviation. This was carried out at each temperature (60 °C - 130 °C). The result is presented in Table 5.2 and shown in Figure 5.12.

Table 5.2 : Global average and standard deviations of corrosion rate with increasing temperature

Temperature (°C)	Average CUI rate (mm/yr)	Standard deviation
60	0.22	0.08
70	0.52	0.15
80	0.58	0.19
95	0.55	0.12
110	0.44	0.12
130	0.24	0.07

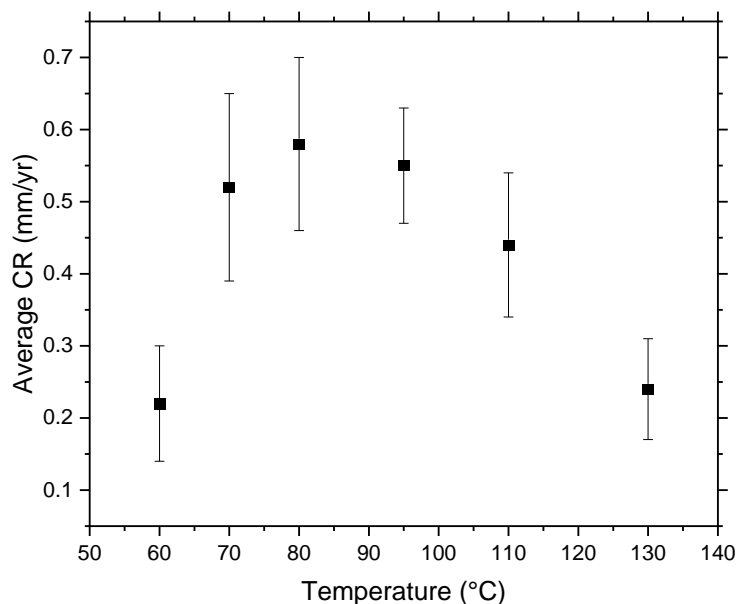


Figure 5.12: Global average corrosion rates of all the four replicates for the six metal rings (Error bars represent the standard deviation of all the replicates for the six metal rings).

The data presented in Table 5.2 and shown in Figure 5.12 represent the global average of all the six rings for the four replicates, while the error bars represent the standard deviation of the four replicates. In addition, the data obtained from replicate measurements in corrosion studies have been reported to have significant deviations due to the stochastic nature of corrosion. Results shown in Table 5.2 reveal an increase in the corrosion rate as the temperature is increased up to 80 °C. Further increase in temperature beyond this threshold results in a decrease in the corrosion rate as shown in Figure 5.12. The reason for this trend will be explained using the mechanism of corrosion in the next section.

5.3.1) Mechanism of CUI of carbon steel

The variation of corrosion rate with temperature observed in this study will be discussed in three aspects. First, the region of increasing corrosion rate with temperature will be explained. This will be followed by the region of decreasing corrosion rate with temperature, while the third part will consist of explanation of the observed corrosion rate at temperature as high as 130 °C when no liquid film is expected to be present as shown in Figure 5.13 below.

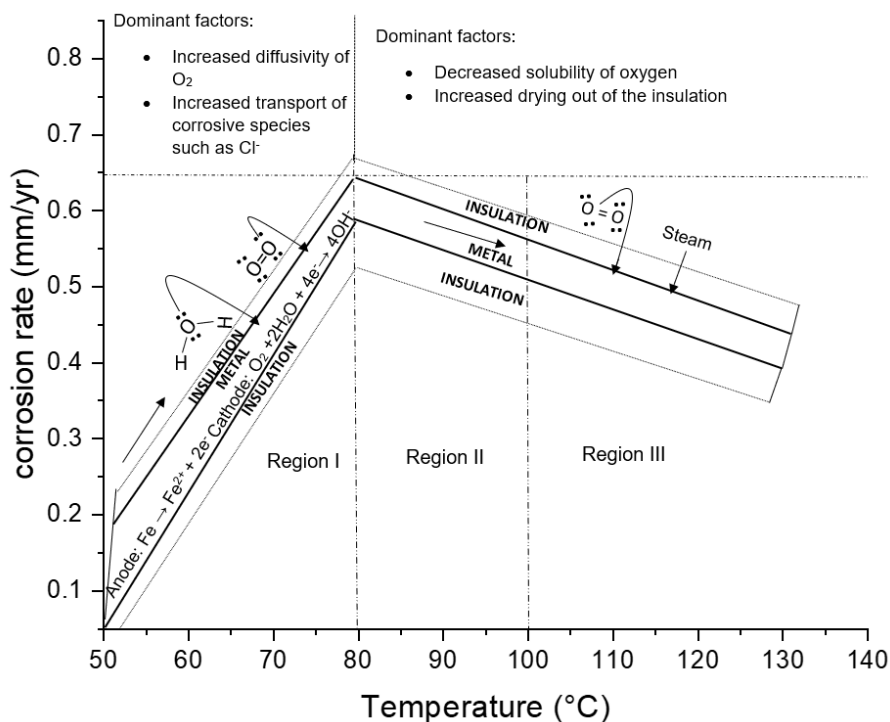


Figure 5.13: Mechanism of corrosion of insulated carbon steel at different temperatures

In Figure 5.13, the variation of corrosion rate with temperature across the wet and dry regions representing temperatures below and above 100 °C respectively is described. The wet region consists of two parts (A and B) consisting of the region of initial increase of CUI rate with temperature up to 80 °C (part A), while the second part (B) consists of the area of decreasing corrosion rate with temperature even when liquid water is still expected in the insulation (80-100 °C). On the other hand, the dry region consists of temperatures greater than 100 °C, where liquid water is not expected in the insulation. The dependence of corrosion rate with temperature is based on the fact that either the anodic reaction involving metal dissolution and cathodic reaction involving oxygen reduction are rate controlled or there is mass transport control which influences the diffusivity of oxygen required to initiate the cathodic reaction [16].

Region I shows an increase in the corrosion rate with temperature which reaches a maximum point during the transition into region II. The existence of this point suggests that there are different factors having opposite effects on CUI rate. For instance, increase in temperature is likely to increase the diffusivity of oxygen required for cathodic reactions resulting in initial increase in corrosion rate, which dominates at low temperatures. However, as temperature increases above 80 °C, other opposing effects such as a decrease in the solubility of oxygen as temperature increases and increased drying out of the test solution becomes dominant resulting in the existence of a maximum point as shown in the transition from region I into II. This continues up to region III where the decreased solubility and drying out of the insulation are dominating factors resulting in a reduced CUI rate.

In addition, it might be expected that the metal will not corrode within the dry region as shown in Figure 5.13 due to the absence of a liquid film. However, a low corrosion rate was still observed at temperature as high as 130 °C. Other researchers that have investigated CUI rate under cyclic conditions have also noted that insulated metals corrode at a slow rate under a dry cyclic condition of about 120 °C [15]. In another report, Kane *et al.* [17] expected the corrosion rate of carbon steel insulated with mineral wool to fall to zero when the insulation dried out; however, the corrosion rate reduced to a steady value of 0.002 mm/yr. The possibility of obtaining a reduced corrosion rate when there is no electrolyte at high temperatures has been described as dry corrosion in the literature [18]. However, the corrosion rate observed within the

dry region in this study is greater than what should be expected from 'dry corrosion' and the temperature is not as high as temperatures where a typical dry corrosion is usually observed. Therefore, the reduced corrosion rate observed at 130 °C could likely be attributed to the short period of wetness prior to the complete insulation dry out as well as existence of steam when the target temperature was reached.

5.4) Comparison of laboratory CUI results with field data

The results showing the trend of corrosion rates with increasing temperature for insulated carbon steel reported in this study was compared with the report provided in the American Standard Testing and Materials (ASTM G189-07) [19], American Petroleum Institute standard (API 581) [8] and other field data reported by researchers in the literature. This is important to validate the observed trend of corrosion rate with temperature reported under field conditions. Therefore, the data obtained from this study is overlaid with the available field data for adequate comparison.

5.4.1) Comparison of laboratory CUI data with field data reported in the ASTM standard

The data showing the effect of temperature on the CUI rate as obtained in this study is overlaid with some field data reported in ASTM G189-07 standard as well as some trends of the corrosion rate with temperature that would be expected from close and open systems as shown in Figure 5.14. In an open system, oxygen is free to escape as the system is not sealed, whereas oxygen is trapped in a closed system and cannot easily escape as it is sealed. This will likely lead to differences in the corrosion rate of both systems as oxygen is a major reactant required at the cathode to obtain a complete corrosion reaction. Therefore, this comparison would allow assessment of the trend of CUI rate with temperature for field data reported in the ASTM standard as well as the laboratory data reported in this study.

Figure 5.14 shows that for a closed system, the corrosion rate would be expected to increase linearly with temperature, while for open systems, the corrosion rate tends to initially increase with temperature and reaches a maximum value, then decreases with further increase in temperature. It should be noted that a CUI system will experience the effects of the water enclosed within the pores of the insulation material (absorbed

water) and the condensed water held between the jacketing and the insulation material (trapped or adsorbed water), which would have significant influence on the estimated corrosion rate.

The field CUI data reported in the standard tends to show a linear increase of CUI rate with temperature up to 80 °C. This trend is similar to the laboratory CUI data obtained in this study for measurements carried out from 60 °C to 80 °C; however, the laboratory CUI data shows a decrease in the CUI rate as the temperature exceeds 80 °C, resembling an open system rather than a closed system. This is similar to the corrosion of iron in water in systems exposed to the atmosphere as shown in Figure 5.15 [18]. Unfortunately, the field CUI data in the ASTM standard has not recorded any data above 80 °C which would have been useful in comparing with the laboratory CUI data. Therefore, the trend of CUI rate obtained from this study resembles an open system when the temperature exceeds 80 °C rather than a closed system where oxygen and water are likely to escape with increase in temperature resulting in a decrease in the corrosion rate.

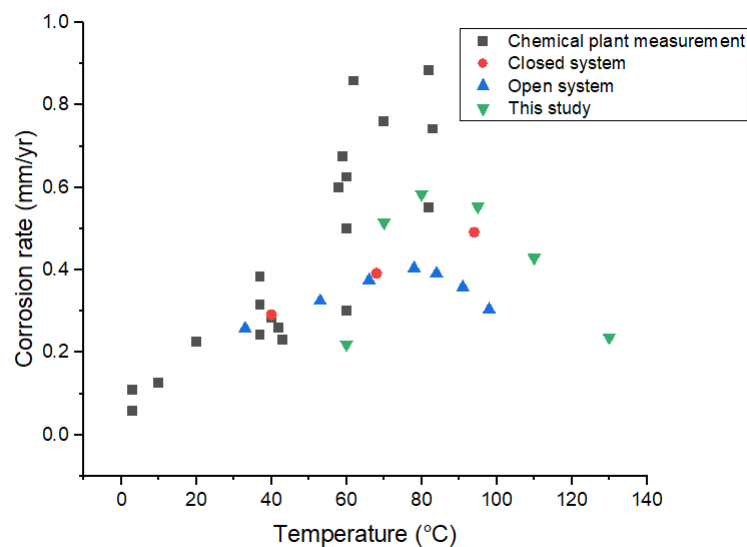


Figure 5.14: Comparison of CUI data from this study with the field data showing the effect of temperature on corrosion of metals as reported in ASTM G189 standard [19].

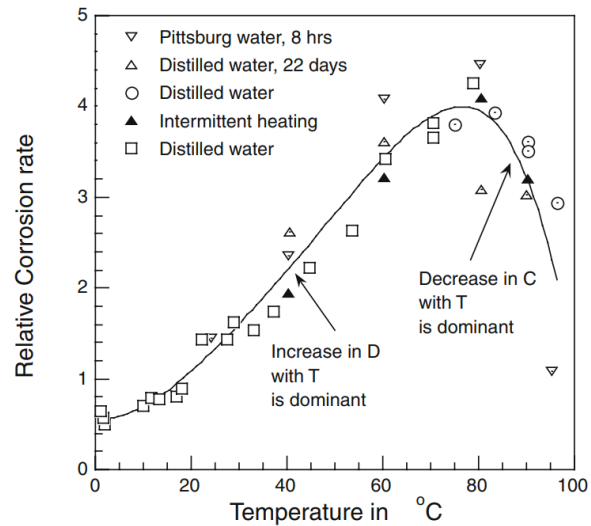


Figure 5.15: Effect of temperature on corrosion of iron in water [18].

5.4.2) Comparison of laboratory CUI results with the field data reported in the API 581 standard

The laboratory CUI data obtained by taking the global average of the corrosion rates of all the six rings for the four replicates is overlaid with the field data reported in API 581 standard and shown in Figure 5.16. This was necessary to compare the trend and to assess the dependence of rate of CUI with temperature obtained from field studies. This was important because temperature, in addition to other parameters are difficult to control in the open field. Therefore, it was necessary to assess the relationship in the laboratory over a certain temperature range in order to observe the trend and assess the degree of deviation of the data in this study from the field data from API 581 standard.

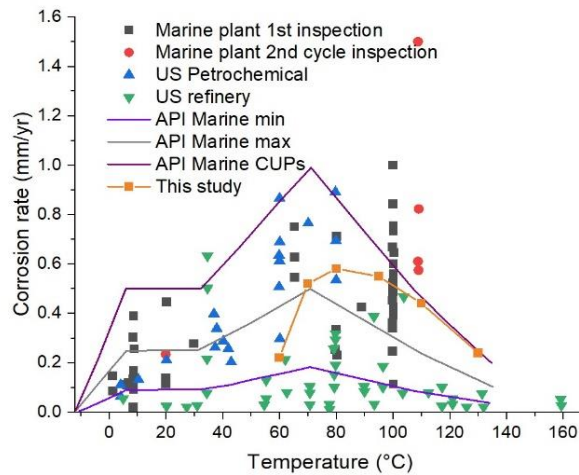


Figure 5.16: Comparison of the laboratory CUI data from this study with the field CUI data reported in API 581 standard [8]

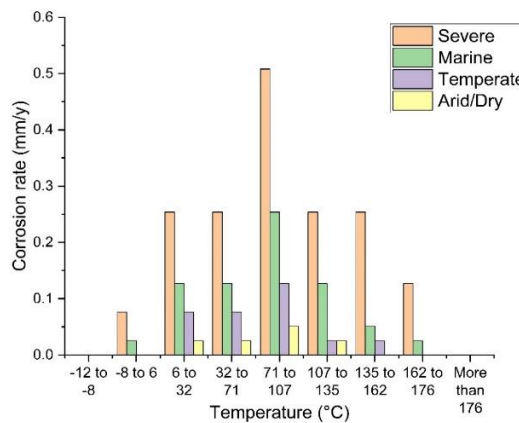


Figure 5.17: Relationship between the CUI of carbon steel and the operating temperature [8, 20].

The field data reported in API 581 standard (Figure 5.16) are quite scattered, this may be as a result of the different factors that influences CUI rate in the field besides temperature. Notwithstanding, the corrosion rates reported in this study are within the range of the reported CUI rates from field studies. In addition, the maximum corrosion rates tend to lie between 60 °C and 100 °C, while the other data points have much lower corrosion rates despite the further increase in temperature. This also suggest an initial increase in corrosion rate with temperature to a maximum value observed between 60 °C and 100 °C, which starts to decrease as the temperature increases further. It should be noted that corrosion is still observed at a slower rate at

temperatures as high as 130 °C which agrees with the findings of this study. Also, a similar trend of increasing corrosion rate with temperature up to a maximum value of 0.51 mm/yr was observed for the field data shown in Figure 5.17. Although temperature and quantity of test solution in the insulation have been identified as the key factors that can influence corrosion rate of insulated metals [21], other contributing factors such as the type of insulation and the concentration of contaminants can also have a significant effect on the corrosion rates of insulated assets [22].

5.4.3) Comparison of Laboratory CUI data with other field data reported in the literature

The field data showing the effects of temperature on corrosion rate as a function of different qualities of insulation as well as the corrosion depth has been reported by De Vogelaere [23] and Matsuda *et al.* [24] respectively. These are shown in Figures 5.18 and 5.19 respectively. In the report of De Vogelaere [23], an unspecified insulation is grouped into three categories, such as good, which indicates that the jacketing in addition to the insulation are in good condition devoid of damages which could give access to water intrusion. Also, average quality is another category which represents a minimal damage to the jacketing and the insulation, while poor quality represents the condition in which the jacketing is damaged giving access to water intrusion into the insulation. It should be noted that these classifications are based on field experiences and not on the standard grading of insulation performance. The corrosion rate profile shows a similar trend of an initial increase in the corrosion rate with temperature with a maximum point obtained at 90 °C for the three categories of insulation. In addition, the corrosion rate is observed to increase with a decrease in the quality of the insulation as would be expected.

Although the insulation used in this study was completely immersed in the test solution prior to carrying out experiments rather than deliberately damaging the jacketing, the maximum corrosion rate (0.51 mm/yr) obtained for the insulation with poor quality indicating an unrestricted access of water and contaminants to the insulation can be compared to the maximum corrosion rate obtained in this study. However, no corrosion has been observed at 120 °C as shown in Figure 5.19, but a significant corrosion has been reported at 110 °C, which also agrees with the fact that there will

still be corrosion at temperatures exceeding the boiling point of water where a liquid film is not expected to be present. This observation is different from the findings of Matsuda *et al.* [24] who reported that no corrosion was observed at 110 °C for carbon steel insulated with calcium silicate insulation and there was no obvious temperature dependence on the corrosion rate as the points were scattered (Figure 5.19). This suggests that the type of insulation could also contribute to the variation of CUI rate with temperature across different reports.

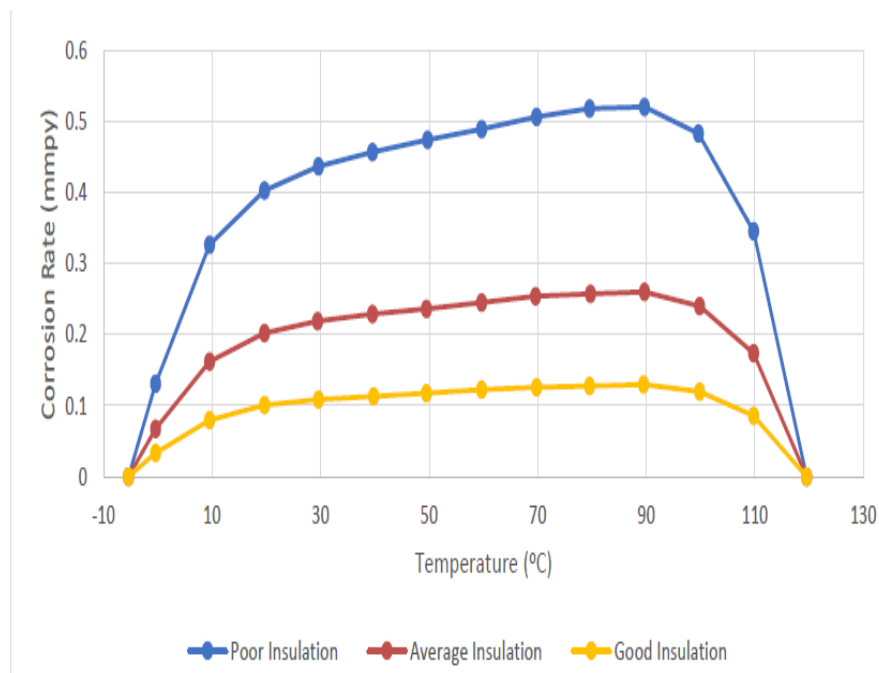


Figure 5.18: Corrosion rate as a function of temperature and condition of insulation [23]

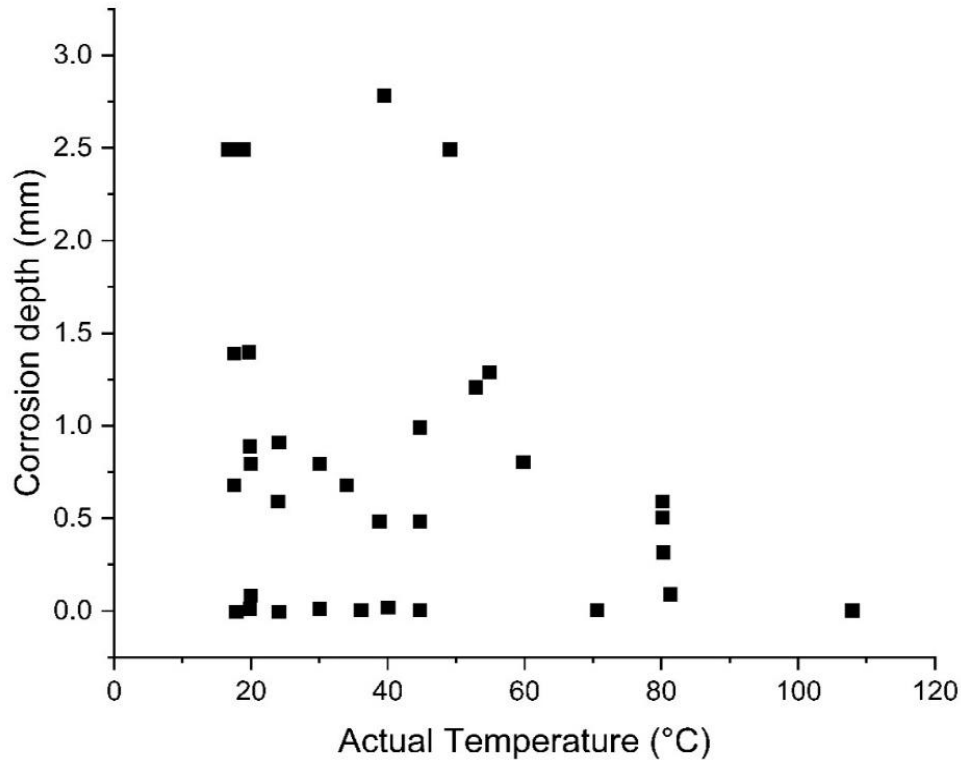


Figure 5.19: Variation of corrosion depth of carbon steel pipe under calcium silicate insulation with temperature [24].

5.5) Risk Based Assessment of CUI

Risk assessment is one of the CUI management strategies to qualitatively assess the probability of failure using available CUI data. This is necessary to make informed decision on the level of risk as well as suggest options to mitigate unacceptable risks. It is necessary that the important factors contributing to the overall risk of failure be included in the risk model in order to obtain a reliable output. In this study, the main risk factors include water absorption capacity of the insulation (water wetting barrier), presence of jacketing which serves as barrier (design barrier) and corrosion resistance of carbon steel (material barrier). Other important factors such as temperature and quantity of electrolyte in insulation are sub-factors which may be categorised under material and water wetting barriers respectively. The risks associated with these factors have been assessed as a function of temperature in the report of Wiggen [25], this is shown in Figure 5.20.

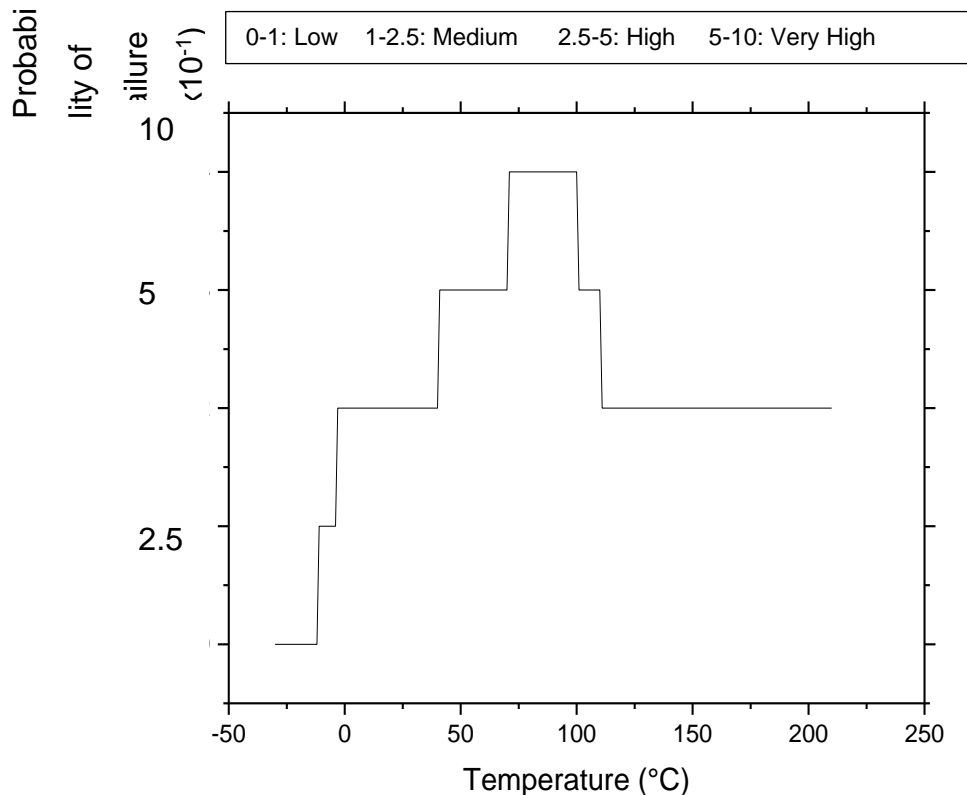


Figure 5.20: Probability of failure of material barrier as a function of temperature [25]

Figure 5.20 shows the risk rating for a carbon steel pipe operating at different temperatures. The temperature range used in this study (60 °C-130 °C) starts from the high-risk zone, passes through the maximum risk zone to the medium risk range observed at high temperatures. It is important to note that the highest corrosion rate obtained in this study which was observed at 80 °C falls within the maximum risk zone (70 °C-100 °C) in the Wiggen’s model. Moreover, as the temperature increases further, the probability of failure reduces to medium at about 120 °C and it is maintained at this level for temperatures as high as 210 °C. This corresponds to the observed decrease in the corrosion rate as the temperature is increased to 130 °C as obtained in this study. It should be noted that the risk level did not fall to 0 at temperatures exceeding 100 °C where liquid water is not expected in the insulation, which agrees with the low corrosion rate at 130 °C observed in this study. This implies that even at elevated temperatures where water is not expected, it is important to monitor the integrity of

insulated structures as corrosion is still possible, though the corrosion rate would be expected to be quite low with a reduced likelihood of failure.

5.6) Effectiveness of the corrosion inhibitor (VpCI 619) at different temperatures

In this section, the results showing the effectiveness of a commercial inhibitor (VpCI 619) in mitigating the corrosion of carbon steel under insulation at different temperatures (80 °C, 95 °C, 110 °C, and 130 °C) are presented and discussed. These temperatures were selected based on previous measurements where no inhibitor was used, which would allow the estimation of inhibition efficiency within the temperature range where CUI has been reported to be severe. In addition, this study was aimed at assessing the performance of the new inhibitor (VpCI 619) in mitigating the corrosion of carbon steel under mineral wool insulation. This was achieved by assessing the inhibition efficiency as a function of temperature, investigating the effectiveness of the inhibitor at different dosages which could provide useful information on the mechanism of inhibition and cost analysis as well as comparing its performance with other available commercial inhibitors used to mitigate CUI in the literature.

Due to the complexity of CUI systems, it is not surprising that there has been scarcity of data assessing the performance of inhibitors for CUI. A handful of reports investigating the effectiveness of inhibitors in mitigating CUI include: the performance of vapour phase inhibitor (VpCI 658) on insulated API X65 steel operating between 120 °C-140 °C [26], the effectiveness of sodium bentonite inhibitors on an insulated steel [27], the effectiveness of a volatile corrosion inhibitor in mitigating the CUI of carbon steel under mineral wool insulation [14] and more recently, the performance of self-fused silicone inhibitors impregnated on tapes for the mitigation of CUI of steel at 175 °C [28]. The CUI data reported in these literatures are summarized and comparison made with the present work.

Although these reports have tried to provide some data showing the performance of certain inhibitors under CUI conditions, the effectiveness of the inhibitors are either assessed at a single temperature point or are not quantified but observed by mere visual inspection. Moreover, there has been no report showing the effectiveness of inhibitors over different temperature ranges where CUI is expected to be severe. A

preliminary investigation of the effectiveness of the new inhibitor (VpCI 619) used in this study was only assessed qualitatively for Cortec Corporation in 2018 using a visual inspection technique, this was later published in 2020 [29]. However, no data quantifying the degree of performance of the inhibitor under CUI condition were reported. The available corrosion data reported in the publication were obtained by boiled immersion test rather than CUI.

Therefore, the need to provide adequate scientific data that validates the effectiveness of the 'new' inhibitor (VpCI 619) under CUI conditions was necessary and has been the drive for this study. Hence, this study was aimed at providing laboratory data that assesses and quantifies the effectiveness of VpCI 619 inhibitor for the mitigation of CUI of carbon steel operating between 80 °C and 130 °C. First, the results showing the corrosion rates of the inhibited and uninhibited CUI systems at the temperatures investigated are presented and discussed. Then, the mechanism of inhibition will be explained based on the composition of the inhibitor as well as the effects of temperature and dosage on the inhibition efficiency. Furthermore, the results obtained from this study is compared with the available CUI data in the literature to assess its performance in relation to the available reports.

5.6.1) Effectiveness of the inhibitor at different operating temperatures

The effectiveness of the inhibitor (VpCI 619) in mitigating CUI of carbon steel was assessed by computing the difference between the inhibited and uninhibited corrosion rates and expressing the result as a percentage of the uninhibited CUI rate which gives the inhibition efficiency as shown in equation 5.1. The chemical composition of the inhibitor comprises of sodium molybdate (10-25 wt.%), boric acid (2.5-5.5 wt.%), and borax (< 2.5 wt.%). The density of the inhibitor is 1.1 g/cm³, while the vapour pressure at 20 °C is 0.023 bar which is similar to the vapour pressure of water at the same temperature. Based on these characteristics, the term 'vapour phase' seems to be a misnomer as this is consistent with liquid phase inhibitors rather than vapour phase inhibitors. However, the focus of this research is not on the state of the inhibitor, but on the performance in mitigating CUI of carbon steel. The composition of the inhibitor suggests that molybdate ion is the main inhibiting component, while boric acid and borax may also contribute or just serve as a buffer. This is necessary because

molybdates require a stable pH, which may be neutral or alkaline for an effective corrosion inhibition. The inhibition efficiency at each operating temperature was used as the performance indicator, this is presented in Table 5.3 and shown in Figure 5.21.

Table 5.3 : Comparing the average corrosion rates in the presence and absence of the inhibitor as well as inhibition efficiencies.

S.P.	Corrosion rates (mm/yr) and inhibition efficiencies (I %) at different temperatures											
	80 °C			95 °C			110 °C			130 °C		
	CR _o	CR	I(%)	CR _o	CR	I(%)	CR _o	CR	I(%)	CR _o	CR	I(%)
1	0.5	0.08	84	0.5	0.07	89	0.2	0.04	81	0.1	0.02	82
2	0.6	0.06	89	0.6	0.07	88	0.4	0.05	85	0.2	0.04	80
3	0.6	0.07	89	0.5	0.06	88	0.6	0.05	90	0.3	0.04	87
4	0.5	0.04	91	0.6	0.06	83	0.5	0.04	89	0.2	0.04	84
5	0.6	0.06	89	0.6	0.06	89	0.4	0.05	88	0.3	0.04	86
6	0.6	0.06	90	0.5	0.07	88	0.5	0.03	94	0.2	0.04	79

S.P.= Sample Position, CR_o = corrosion rate in the absence of inhibitor (mm/yr), CR=corrosion rate in the presence of inhibitor (mm/yr), I=inhibition efficiency (%).

$$\text{Inhibition efficiency (\%)} = \frac{CR_o - CR}{CR} \times 100 \quad (5.1)$$

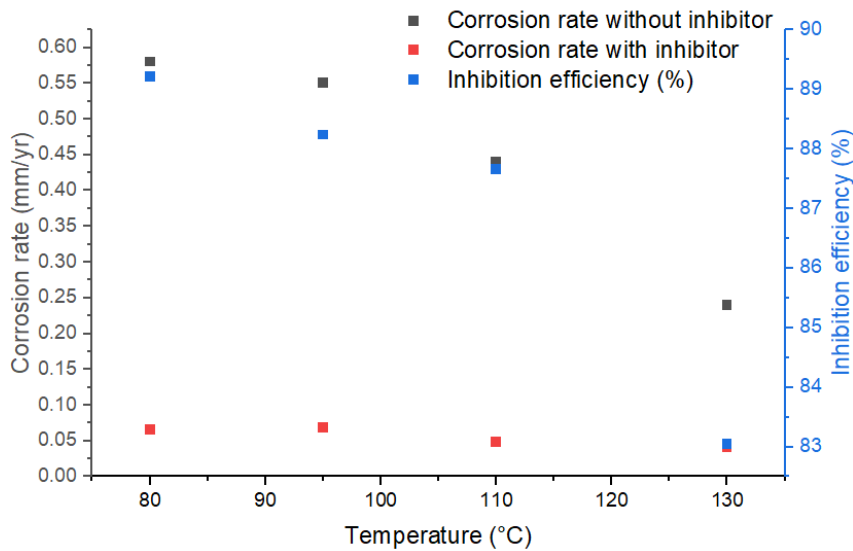


Figure 5.21: Plot of mean corrosion rate of insulated carbon steel and inhibition efficiency of VpCl 619 as a function of temperature.

The data presented in Table 5.3 and Figure 5.21 show a significant decrease in the corrosion rate when the inhibitor was used compared to the absence of inhibitor. The pictures of the corroded rings in the absence of the inhibitor and inhibited metal rings where no visible corrosion products were observed is shown in Figure 5.22. The effectiveness of the inhibitor can be quantified in terms of the inhibition efficiency as shown in Figure 5.21. In this study, high inhibition efficiencies were observed across all temperatures investigated which ranges from 81.3 % to 94.3 %. Similar inhibition efficiencies were observed at temperatures of 80 °C to 110 °C; however, a slight decrease in the inhibition efficiency is observed as the temperature is increased to 130 °C. In the material safety data sheet of the inhibitor, it was stated that the inhibitor could be used on pipes operating at high temperature up to 600 °C [30]. It is likely that the inhibition efficiency will continue to decrease as the operating temperature increases to this threshold.

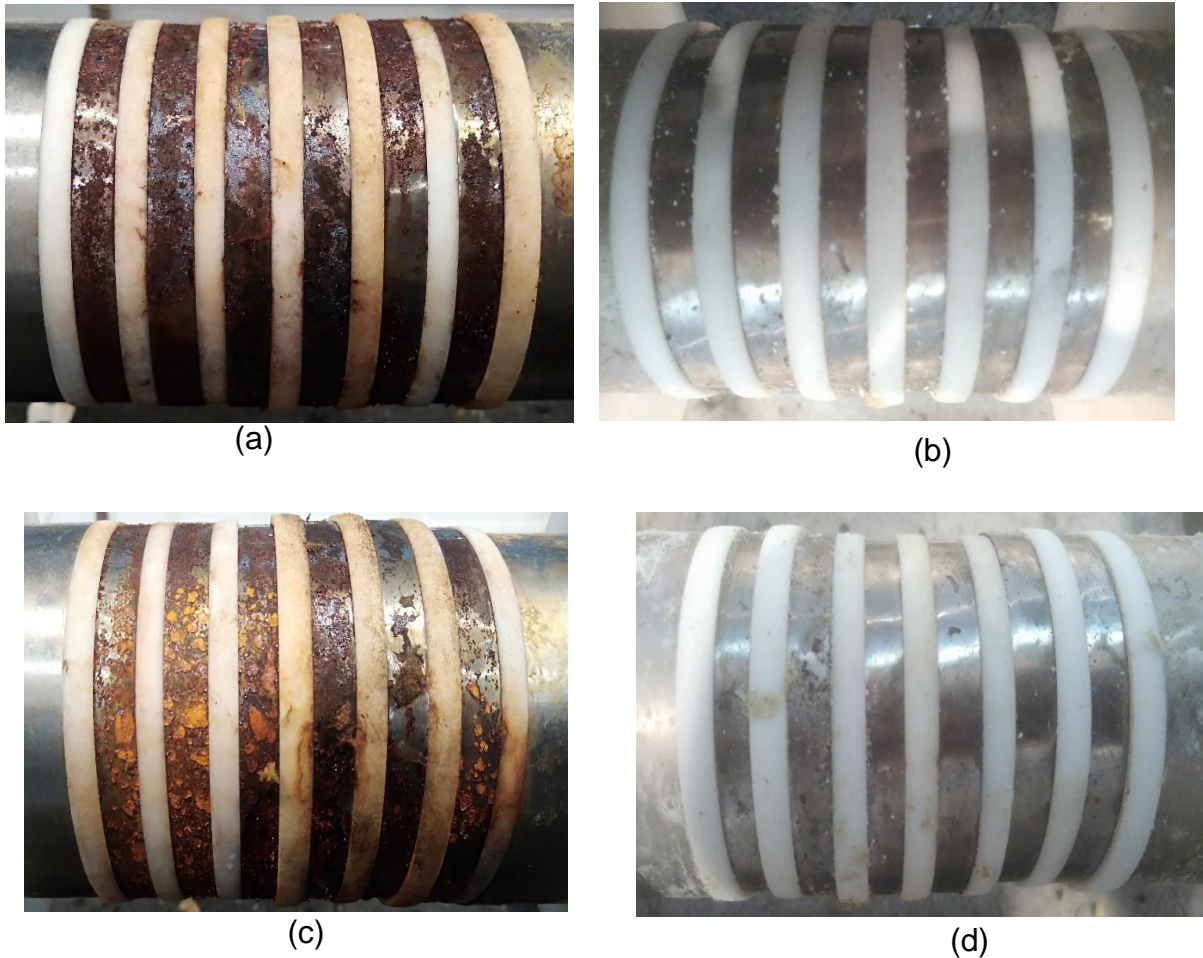


Figure 5.22: Images of carbon steel rings showing the degree of corrosion at 80 °C (a, b) and 95 °C (c, d). Inhibitor was only used in b and d, no inhibitor was applied in a and c.

5.6.2) Effect of varying dosage of inhibitor

This was carried out to assess the performance of the inhibitor at different dosages. This could be useful when carrying out cost analysis as inhibitors with reduced dosage, but having a high inhibition efficiency would be highly desirable in industry. The manufacturer's suggested the quantity of the inhibitor per area of the insulation to be 3.6-5.2 g/m² [30]. However, it was necessary to calculate the cost of the specified dosage as well as reduced dosages of the inhibitor and assess its performance in mitigating CUI. Therefore, in this study, the internal area of the cylindrical insulation was calculated and the weight of the inhibitor corresponding to the target range recommended by Cortec as well as reduced dosages and the difference in performance between the upper limit of the recommended dosage and the reduced

dosages were determined. The effectiveness of the inhibitor in terms of the measured corrosion rate at different dosages compared to the control experiment where no inhibitor was used is presented in Table 5.4 and shown in Figure 5.23, while the cost of the inhibitor as a function of the dosages is presented in Table 5.5.

Table 5.4 : Average corrosion rate (mm/yr) of carbon steel with different dosage of inhibitor

Dosage of inhibitor (g/m ²)	Corrosion rate (mm/yr)	S.D.	Inhibition efficiency (%)
0.0	0.58	0.19	-
1.3	0.14	0.03	76.16
2.6	0.09	0.03	83.80
5.2	0.06	0.02	89.23

The result of the effectiveness of VpCl 619 inhibitor in mitigating CUI of carbon steel at 80 °C is presented in Table 5.4. The results indicate an increase in the inhibition efficiency as the dosage of the inhibitor increases, resulting in a corresponding decrease in the corrosion rate. The assessment of the effectiveness of dosage of a new commercial inhibitor in mitigating CUI is basically aimed at analysing the cost in order to maintain balance between inhibition efficiency and the cost, these are presented in Table 5.5.

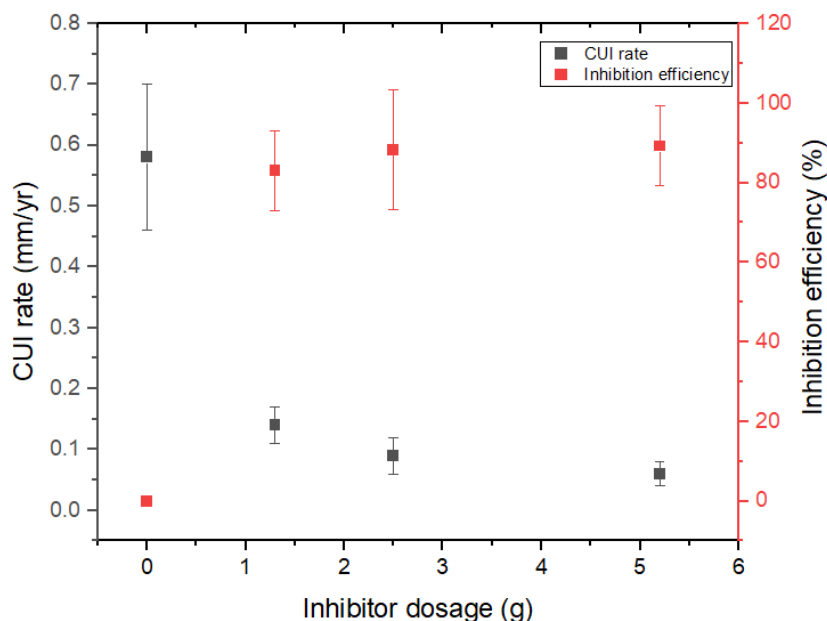


Figure 5.23: Effect of inhibitor dosage of CUI rate

Table 5.5: Cost analysis of the inhibitor for a given area of the insulation

Dosage of inhibitor (g/m ²)	Estimated area of insulation (m ²)	Cost (£)
1.3	500	19.4
2.6	500	38.8
5.2	500	77.5

The upper limit of the dosage recommended by Cortec was 5.2 g/m². This has been observed to significantly reduce the degree of corrosion, with a high inhibition efficiency of 89.20 %, 88.23 % and 83.04 % observed at 80 °C, 110 °C, and 130 °C respectively. When the dosage was halved, there was a decrease in inhibition efficiency of about 6 %. Further decrease in the dosage of the inhibitor led to a significant decrease in the inhibition efficiency which was estimated to be 14.6 %. The cost evaluation shown in Table 5.5 was computed from the total cost of a 20 L pail which was £656 including tax. The volume of the inhibitor was converted to weight in kilograms by multiplying it with density. The corresponding cost of the dosages used in this study were computed from the 23.2 kg inhibitor. Results showed a significant increase in the cost as dosage increases. The cost saving between the minimum and maximum dosage limit per area of the insulation is 78 % which suggests that it is important to consider the cost at the planning stage to maintain balance between cost and performance of the inhibitor. In addition, the inhibition efficiency of VpCI 619 was compared with other vapour phase corrosion inhibitors and this is presented in Table 5.6.

Table 5.6 : Performance of inhibitors for CUI

Inhibitor	Composition	^a Dosage of inhibitor, ^b concentration of test solution and ^c temperature	Maximum Inhibition Efficiency (%)	References
VpCI 658	Naphtha, 3- butoxy propan- 2-ol, and alkyl triazole	^a NR, ^b 200 ppm NaCl, ^c Temperature: 45 °C and 120-140 °C.	98.63	[26]
Sodium bentonite	Sodium bentonite	^a NR, ^b Synthetic seawater, ^c 60 – 82.2 °C	50.9	[27]
VCI	NR	^a 660 mL/m ³ , ^b artificial seawater, ^c 80 °C.	66.8	[14]
VpCI 619	Sodium molybdate and boric acid	^a 1.3 – 5.2 g/l ^b 1 wt % NaCl ^c 80-130 °C	94.27	This study

NR-Not reported

The effectiveness of the new commercial inhibitor used in this study in mitigating CUI was compared with other commercial inhibitors used for a similar purpose. Although all the inhibitors show different inhibition efficiencies, this is only meant to provide an overview of the performance of these inhibitors in different CUI environments. It might not be reasonable to make direct comparison in terms of the inhibition efficiencies of these inhibitors. This is because the CUI systems, the dosage of the inhibitors including the conditions which the investigation were carried are quite different. At best, the information provided in Table 5.6 might be useful in assessing the composition of each inhibitor as well as the corresponding inhibition efficiency under the conditions which it was investigated. This would be important in evaluating the cost, eco-friendliness and performance in mitigating CUI which are key factors to be taken into consideration when choosing inhibitors for a specific application.

5.6.3) Mechanism of Inhibition

In this section, the mechanism of inhibition as well as the chemical reactions involved during inhibition and in the absence of the inhibitor will be discussed. Based on the chemical composition of the inhibitor, it would be reasonable to assume that sodium molybdate is the main contributor to the overall inhibition efficiency. Boric acid-borax combination mainly serves as a buffer to ensure that the pH is kept constant. A preliminary characterization of API 5L X65 steel pipe treated with the VpCI 619 inhibitor using SEM/EDX has revealed the formation of a molybdenum rich compound without any trace of ferric oxide [29]. This suggests the incorporation of molybdenum to the protective film, which would be expected to reflect on the proposed mechanism.

Molybdate inhibitors are known to inhibit the corrosion of carbon steel by slowing down metal dissolution at the anode thereby passivating the metal in non-CUI systems [30]. Although oxygen is an essential component required for corrosion to occur, molybdate inhibitors also require oxygen to initiate spontaneous passivation due to their weak oxidizing property [31]. The mechanisms of inhibition using sodium molybdate and the formation of the passive oxide film on the surface of the metal are shown in Figures 5.24.

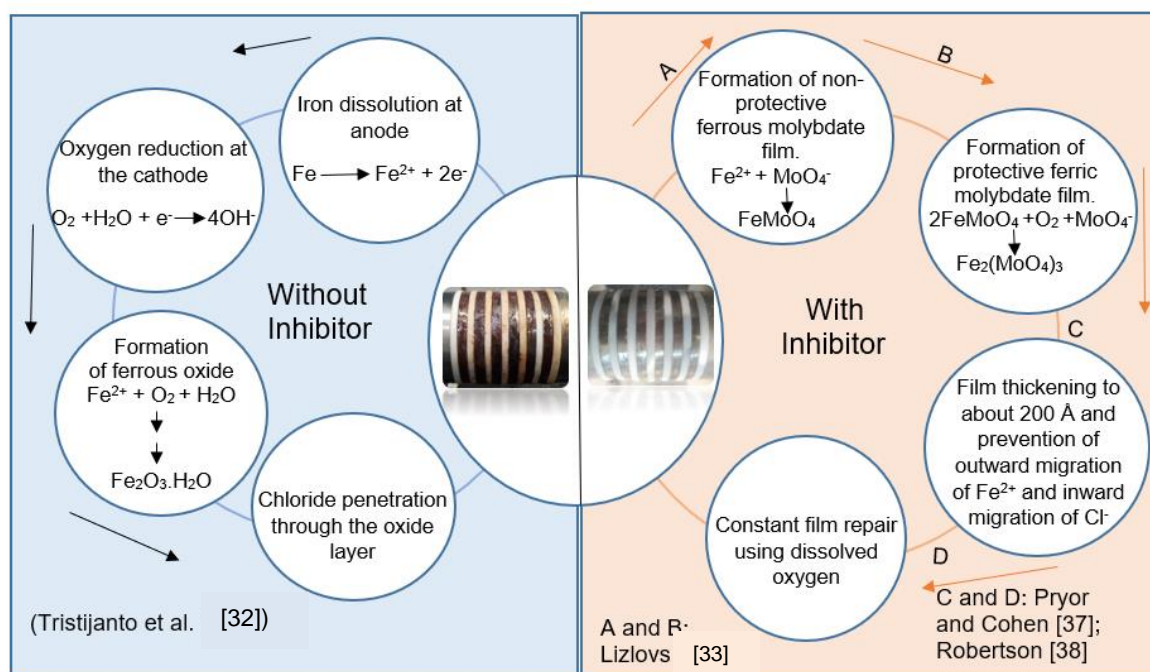


Figure 5.24: The mechanism of inhibition of corrosion of insulated carbon steel

For the uninhibited system shown in Figure 5.24, the anodic reaction involves the dissolution of iron to give ferrous ions (Fe^{2+}) giving out electrons in the process. At the cathode, oxygen accepts the electrons generated from the anodic reaction and it is reduced to hydroxyl ions. The resulting anodic and cathodic products culminate in the formation of a ferric oxide layer on the metal surface. Moreover, the hydrated ferric oxide film formed on the surface of the metal without the inhibitor is anion selective, this would allow the transfer of corrosive species (Cl^-) to the metal surface. However, in the presence of a molybdate inhibitor, the molybdate ions react with the ferrous ions to form ferrous molybdate, which can be oxidized by dissolved oxygen to form an insoluble and protective ferric molybdate film. Furthermore, the presence of a molybdate ion makes the film to be cation selective, which will therefore be fully protective as it will prevent an inward transfer of aggressive anions (Cl^-) to the metal surface as well as preventing the outward migration of metal ions into the solution [36]. This will reduce the susceptibility of the steel to corrosion.

5.7) Conclusions

In conclusion, this study indicates an increased water absorption when the insulation was thermally treated at 250 °C for 4 h compared to the untreated samples. This may be attributed to the decomposition of the organic additives and silicone oil that are responsible for the hydrophobicity of the insulation [37]. In addition, it was observed that the insulation absorbed water continuously for 22 days without saturation, which indicates an increased risk of CUI if water penetrates the system. Other researchers have also observed a continuous absorption of water by mineral wool insulation soaked for 60 days without saturation [5]. In addition, variable water absorption capacities for triplicate measurements were observed which is similar to other reports in the literature [4]. This has been attributed to the presence of localized melts in the insulation which opens during thermal degradation absorbing more water than other parts of the insulation [3].

Mineral wool insulation wetted with 1 wt % of NaCl solution when installed on carbon steel pipe was observed to result in the corrosion of the metal. The corrosion rate

initially increased with temperature up to 80 °C where maximum CUI rate was observed. The existence of a maxima could be attributed to a combination of an increased drying, decreasing solubility of oxygen as temperature increases which has opposite effects to the increased diffusion of oxygen as temperature increases. This agrees with the observation of Pedefferri [3] who reported that the trend of corrosion rate with temperature is neither linear nor exponential as reported in routine chemical reactions, but it is determined by the prevailing factor of either decreased solubility of oxygen as the temperature increases or an increased diffusion coefficient of ions. In this study, further increase in temperature up to 130 °C resulted in a decrease in the corrosion rate due to the dominating effects of insulation dry out and the decreasing solubility of oxygen.

The available field data on the dependence of corrosion rate on temperature reported in the literature either showed no trend [24] or tends to increase to a certain threshold, then decrease on further increase in temperature as observed in this study and reported by De Vogelaere [23]. The differences in the effect of temperature on CUI in these reports may likely be attributed to the differences in the field as well as the experimental methods and conditions which the investigation was carried out. Moreover, some of the field data and laboratory reports agree with what is observed in this study that it is possible to have corrosion of insulated metals at temperatures greater than 100 °C. The maximum corrosion rate of about 0.58 mm/yr obtained at 80 °C in this study agrees with Wiggen's risk assessment model which suggests an increased risk of failure for pipes operating between 70 °C and 100 °C compared to pipes operating at much lower or higher temperatures.

The new commercial inhibitor (VpCI 619) was observed to be effective in mitigating CUI at the temperatures investigated (80 °C-130 °C). The maximum inhibition efficiency was about 89 % which was observed at 80 °C when the recommended dosage as specified by Cortec was used. Although reduced dosages of the inhibitor were still effective in protecting the metal, the inhibition efficiencies were reduced compared to the recommended dosage. It is reported that corrosion inhibition using molybdates is caused by the formation of a passive ferric molybdate film on the surface of the metal, which restricts the penetration of aggressive species such as chlorides resulting in an enhanced protection. The incorporation of molybdate to the protective

oxide layer on the surface of the inhibited metal has already been reported using SEM/EDX [29]. This provides a technical guidance for design and material selection to prevent failure of insulated metallic structures.

Chapter References

1. Bennett, T. M., Allan, J. F., Garden, J. A. and Shaver, M. P. (2022). Low formaldehyde binders for mineral wool insulation. *Global challenges*, 6:1-19.
2. Cortec Material Safety Data Sheet (MSDS) for VpCI 619, Hitek Electronic Materials Limited, <https://www.hitek-ltd.co.uk/msds-cortec>, date accessed 23rd November, 2020.
3. Ivanic, A., Kravanja, G., Kidess, W., Rudolf, R. and Lubej, S. (2020). The influences of moisture on the mechanical, morphological and thermogravimetric properties of mineral wool made from basalt glass fibres. *Materials*, 13:2392.
4. Pojtanabuntoeng, T., Kinsella, B., Ehsani, H., Brameld, M. (2017). Comparison of insulation materials and their roles on corrosion under insulation. NACE International, paper number 9287.
5. Williams, J, and Evans, O. (2010). The influence of insulation materials on corrosion under insulation. NACE Northern area western conference, pp. 1-24.
6. Zwaag, C. and Rasmussen S. N. (2017). Cyclic CUI testing of Insulation materials, National Association of Corrosion Engineers publication, paper number 8877.
7. Wilds, N. (2017) Corrosion under insulation. Trends in oil and gas corrosion research and technologies, Woodhead publishing series in energy, pp 409-429.
8. American Petroleum Institute API 581 (2016). Risk based inspection technology, 3rd edition.
9. Fuad, M. F. I. A., Razak, K. A., Alias, N. H., Othman, N. H. and Ab Lah, N. K. I. N. (2017). Thermal spray coating for corrosion under insulation (CUI) prevention. AIP Conference Proceedings, 120008:1-6.
10. Putra, R., Muhammad, Hafli, T., Islami, N., Apandi, A. (2022). Analysis of temperature variations, types of insulation and coating on corrosion under

- insulation on ASTM A53 pipes. *International Journal of Engineering, Science, and Information Technology*, 2(1):110-118.
11. Pojtanabuntoeng, T., Machuca, L., Salasi, M., Kinsella, B. and Cooper, M. (2015a). New experimental rig to investigate corrosion under insulation at different climate conditions. *Corrosion and materials*, 40(6):46-51.
 12. Pojtanabuntoeng, T., Machuca, L. L., Salasi, M., Kinsella, B. and Cooper, M. (2015b). Influence of drain holes in jacketing on corrosion under thermal insulation. *Corrosion*, 71 (12):1511–1520.
 13. Cao, Q., Esmaily, M., Liu, R. L., Birbilis, N. and Thomas, S. (2020). Corrosion of mild steel under insulation-the effect of dissolved metal ions. *The International Journal of Corrosion Processes and Corrosion Control*, 55:322-330.
 14. Hou, Y., Pojtanabuntoeng, T. and Iannuzzi, M. (2020). Use of electrochemical current noise method to monitor carbon steel corrosion under mineral wool insulation. *Materials degradation*, 4 (39):1-9.
 15. Bai, X., Tang, J., Gong, J. and Lu, X. (2017). Corrosion performance of Al–Al₂O₃ cold sprayed coatings on mild carbon steel pipe under thermal insulation. *Chinese Journal of Chemical Engineering*, 25(4): 533-539.
 16. Takasaki, S. and Yamada, Y. (2007). Effects of temperature and aggressive anions on corrosion of carbon steel in potable water. *Corrosion Science*, 49:240-247.
 17. Kane, R. D., Chauviere, M., Chutz, K. (2008). Evaluation of steel and TSA coating in a corrosion under insulation (CUI) environment. NACE International, paper number 08036.
 18. McCafferty, E. (2010). *Introduction to corrosion Science*, Springer Science, New York, U.S. A., pp.357-400.
 19. ASTM G189-07 (2007). *Standard guide for laboratory simulation of corrosion under insulation*. ASTM International.
 20. Khan, M. M., Mokhtar, A. A., Hussin, H., Muhammad, M. (2018). Prediction for CUI in piping systems using fuzzy logic with sensitivity analysis of corrosion producing factors, MATEC web of conferences, 225, paper number 06002.
 21. Mizushima, K. Satake, N., Sakai, M., and Miyashita, J. (2019). Factors for selecting thermal insulation materials to prevent corrosion under insulation. NACE International, paper number 12952.

22. Swift, M. (2019). Corrosion under insulation on industrial piping-a holistic approach to insulation system design, NACE International, Paper number 13042.
23. De Vogelaere, F. (2009). Corrosion under Insulation. *Process progress safety*, 28:30-35.
24. Matsuda, H., Ishikawa, Y. and Sakai, J. (2015). Application of effective maintenance for CUI (Corrosion under insulation) of pipes in chemical plants. NACE International, Paper number 5757.
25. Wiggen, F. (2020). Risk based management of corrosion under insulation. *Inspectioneering Journal*, 26(3):2-8.
26. Bavarian, B., Ikder, Y., Samimi, B. and Reiner, L. (2015). Protection effectiveness of vapour corrosion inhibitor for corrosion under insulation. NACE International, Paper number 5448.
27. Cullin, M. J., Birmingham, G., Srinivasan, R., Hailu, G. (2020). Injectable Sodium Bentonite Inhibitors for Corrosion under Insulation. *Journal of pipeline Systems Engineering and Practice*, 11(4):1-11.
28. Low, P. (2022). A Novel Methodology for Addressing Corrosion Under Insulation (CUI) Utilizing Corrosion Inhibitor Impregnated Self-Amalgamating Silicone Based Tape. AMPP Annual Conference, Texas, USA, Paper Number 17931.
29. Bavarian, B., Reiner, L., Avanesian, A. B. and Miksic, B. (2020). Development of a new corrosion inhibitor for corrosion under insulation at elevated temperatures. NACE International, Paper number C2020-14293.
30. Cortec Material Safety Data Sheet (MSDS) for VpCI 619 (2018), Hitek Electronic Materials Limited, <https://www.hitek-ltd.co.uk/msds-cortec>, date accessed 23rd November, 2020.
31. Stranick, M. A. (1984). The corrosion inhibition of metals by molybdate. NACE, 40(6): 296-301.
32. Trisjanto, H., Ilman, M. N., Iswanto, P. T. (2020). Corrosion Inhibition of Welded of X-52 Steel Pipelines by Sodium Molybdate in 3.5% NaCl Solution. *Egyptian Journal of Petroleum*, 29(2):155-162.
33. Lislovs, E. A. (1976). Molybdates as corrosion inhibitors in the presence of chlorides. *Corrosion*, 32(7): 263-266.

34. Pryor, M. J. and Cohen (1953). The inhibition of the corrosion of iron by some anodic inhibitors. *Journal of the Electrochemical Society*, 100:203-215.
35. Robertson, W. D. (1951). Molybdate and tungstate as corrosion inhibitors and the mechanism of inhibition. *Journal of the Electrochemical Society*, 98:94-102.
36. Lu, Y. C., Clayton, C. R., and Brooks, A. R. (1989). A bipolar model of the passivity of stainless steels-II: The influence of aqueous molybdate. *Corrosion Science*, 29(7):863-880.
37. Knop, A. and Pilato, L. A. (1985). Phenolic resins. Springer-Verlag, Berlin Heidelberg, p.141.

CHAPTER 6 : RESULTS AND DISCUSSION

**ELECTROLYTE DISTRIBUTION IN INSULATION AND RATE OF DRYING USING
GALVANIC CURRENT AND ELECTROCHEMICAL IMPEDANCE
MEASUREMENTS**

CHAPTER 6
RESULTS AND DISCUSSION
ELECTROLYTE DISTRIBUTION IN INSULATION AND RATE OF DRYING USING
GALVANIC CURRENT AND ELECTROCHEMICAL IMPEDANCE
MEASUREMENTS

In this chapter, the results showing the distribution of test solution (1 wt % NaCl) in the insulation as well as the time taken for the insulation to dry at different temperatures ranging from 70 °C to 130 °C as measured using galvanic current and electrochemical impedance measurements are presented. The purpose of the electrolyte distribution study was to assess how the test solution is distributed between the top and bottom parts as well as the ends and centre of the insulation and how it relates with CUI rate within these regions. In addition, a Cu-Al galvanic couple was used as a sensor to monitor the drying times of the insulation at different temperatures.

This is based on the fact that the presence of an electrolyte in contact with the galvanic couple would induce the flow of electrons from the metal with a lower potential (aluminium) to the metal with a higher potential (Cu). This electron flow due to the potential difference existing between the two metals will lead to the preferential corrosion of aluminium (galvanic corrosion). However, the focus of this study was not on galvanic corrosion but taking advantage of the corrosion current between the dissimilar metals when it is in contact with the wet insulation to monitor the rate of drying of the insulation at different temperatures. This was carried out to validate the drying out effects of the insulation which was assumed to dominate at high temperatures leading to a reduced CUI rate earlier discussed in the previous chapter of this thesis.

The estimation of the drying times using galvanic current and electrochemical impedance measurements were based on the ability to measure the corrosion current (i_{corr}) between the galvanic couple as well as the resistance as the insulation dries. This is important because the severity of CUI is influenced by the contact time of an insulated metal with the electrolyte. The longer the time a metal contacts an insulation that has been wetted with an electrolyte, the greater the severity of CUI [1, 2, 3].

Besides, the drying process provides information on the moisture transport as the insulation reverts to the dry state which gives useful insight to the characterization of insulation materials [4]. Also, the efficiency of the drying process as well as the time required for mineral wool insulation to revert to a completely dry state is quite significant in industry [5, 6], especially for monitoring the structural integrity of insulated pipes. Therefore, the study of the drying process will help to assess if the observed decrease in the CUI rate as the temperature increases which was discussed in the previous chapter is due to the drying out of the insulation or some other effect.

In this study, the distribution of electrolyte in the insulation was estimated gravimetrically by calculating the quantity of water absorbed by the different parts of the insulation (top, bottom, ends and centre) after pre-soaking for 48 h, as well as the remaining water after each experimental cycle. In addition, the drying out times at each temperature was estimated from the current-time and impedance-time profiles which were obtained at about the same time. The results showing the electrolyte distribution will be discussed in two parts; the first part consists of the distribution of the test solution between the top and bottom sections of the insulation while the second part consists of the distribution of the electrolyte between the ends and centre of the test area of the rig. Thereafter, the results showing the drying out times estimated from the current-time and impedance-time profiles will be presented and discussed.

6.1) Results showing the insulation dry out at different temperatures

The drying of the insulation was assessed for both the top and bottom parts as well as ends of the insulation versus the centre. This was carried out to observe areas with high susceptibility to CUI. It has been reported that increase in the quantity of test solution within a specific region will culminate in an increased CUI rate within that area [1, 2]. The non-uniform distribution of an electrolyte in the insulation implies that the corrosion rate will vary with position. Therefore, it is important that the quantity of electrolyte across different parts of the insulation be investigated to assess its contribution to CUI.

6.1.1) Results showing the insulation dry-out between the top and bottom parts and effect on CUI rate

The results showing the average quantity of the electrolyte lost at each temperature is shown in Figure 6.1, while the distribution of the electrolyte in the insulation before and after experiments at 80 °C and the corrosion rate measured at the same temperature are shown in Figures 6.2 and 6.3 respectively. The corrosion test results shown in Figure 6.3 has been overlaid with the results reported by Pojtanabuntoeng et al. [1]. The data represents the percentage of electrolyte lost relative to the initial quantity of electrolyte in the insulation, while the error bars represent the standard deviation of three replicates. This was obtained by a quick ramp to the target temperature and then held at the temperature for 4 hours to observe the quantity of the test solution lost at each temperature.

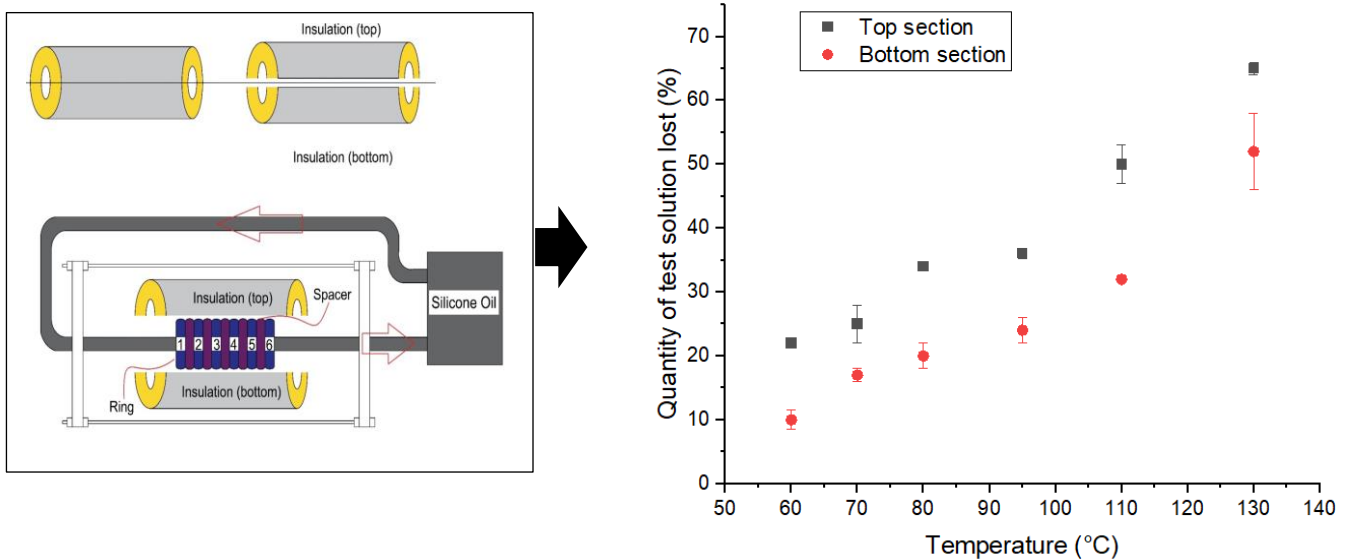


Figure 6.1 : Quantity of test solution lost between the top and bottom parts of the MW insulation at different temperatures.

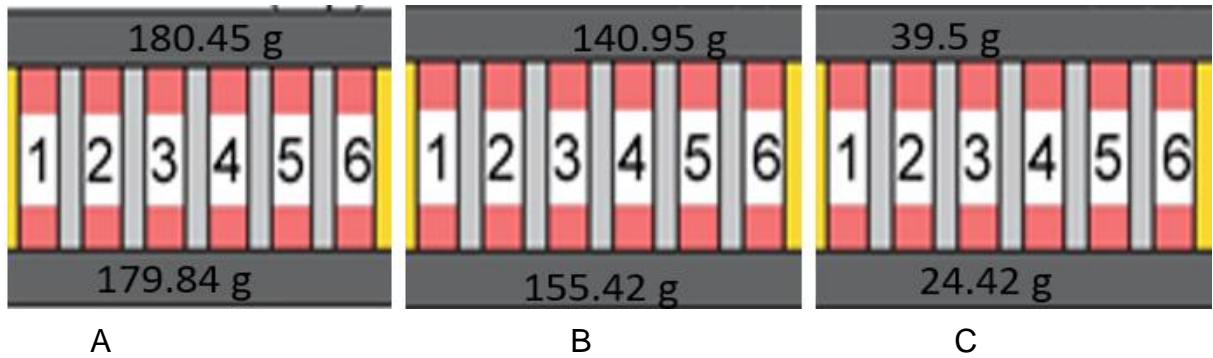


Figure 6.2: Distribution of test solution at the top and bottom parts of the insulation at 80 °C (A) initial weight of insulation (B) Weight after experiment (C) Quantity of test solution lost.

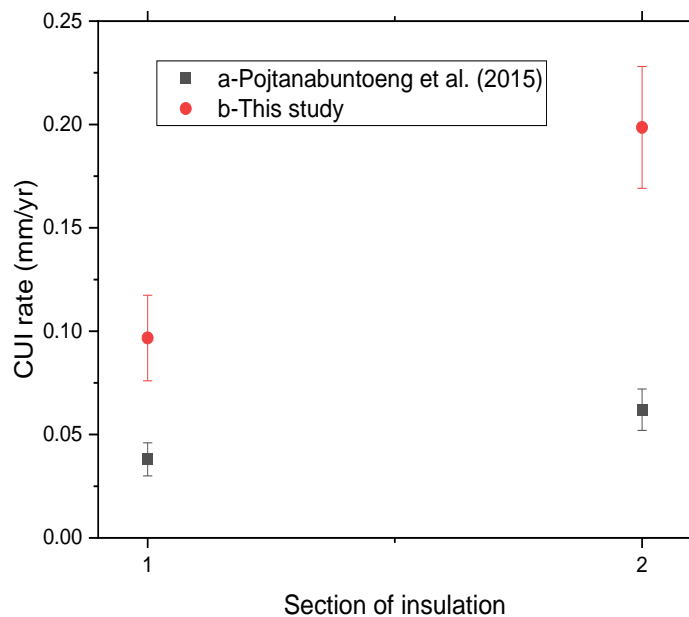


Figure 6.3: Comparison of the top (section 1) and bottom (section 2) CUI data of Pojtanabuntoeng et al. [1] with the average CUI rate obtained in this study which was carried out at 80 °C. Error bars represent the standard deviation of three replicates.

The results shown in Figure 6.1 indicates that more test solution is lost at the top section compared to the bottom for all the temperatures investigated. The bottom part

of the insulation was observed to hold more test solution than the top. This may be attributed to the fact that the test solution settles down quickly to the bottom part of the insulation. This results in an increased corrosion rate at the bottom part of the rings compared to the top as shown in Figure 6.2. This results also agree with the report of Pojtanabuntoeng *et al.* [1] who also observed a higher quantity of electrolyte in the insulation wrapped around the bottom of the half-ring samples compared to the insulation at the top of the rings. This also resulted in a higher corrosion rate for the half rings that were at the bottom compared to the top as shown in Figure 6.2. This implies that a higher corrosion rate would be expected for the bottom section of the insulated metal due to the increased settling of electrolyte as a result of gravity.

However, this is not always the case as another report from the same research group has shown that the top part of the insulation dries out faster than the bottom parts of the insulation. The two contradictory results reported from the same research group is shown in Figure 6.4. In both studies, the same grade of carbon steel (UNS G10220) and mineral wool insulation were used. However, a significant difference in the corrosion rate of the half ring samples at the top was observed compared to the bottom ring samples [7]. This contradicts the results earlier reported by Pojtanabuntoeng *et al* [8] who observed that the bottom ring samples corroded more than the top.

In these reports, the authors had explained that the settling of the test solution to the bottom of the solution in addition to the delayed drying out of the insulation at the bottom parts of the rings may be the reason for the increased corrosion rate observed with the half ring samples at the bottom of the rig. However, Hou *et al.* [7] has neither provided any explanation why a higher corrosion rate was observed at the top parts compared to the bottom ring samples nor is there any information regarding the water distribution in the insulation around both rings.

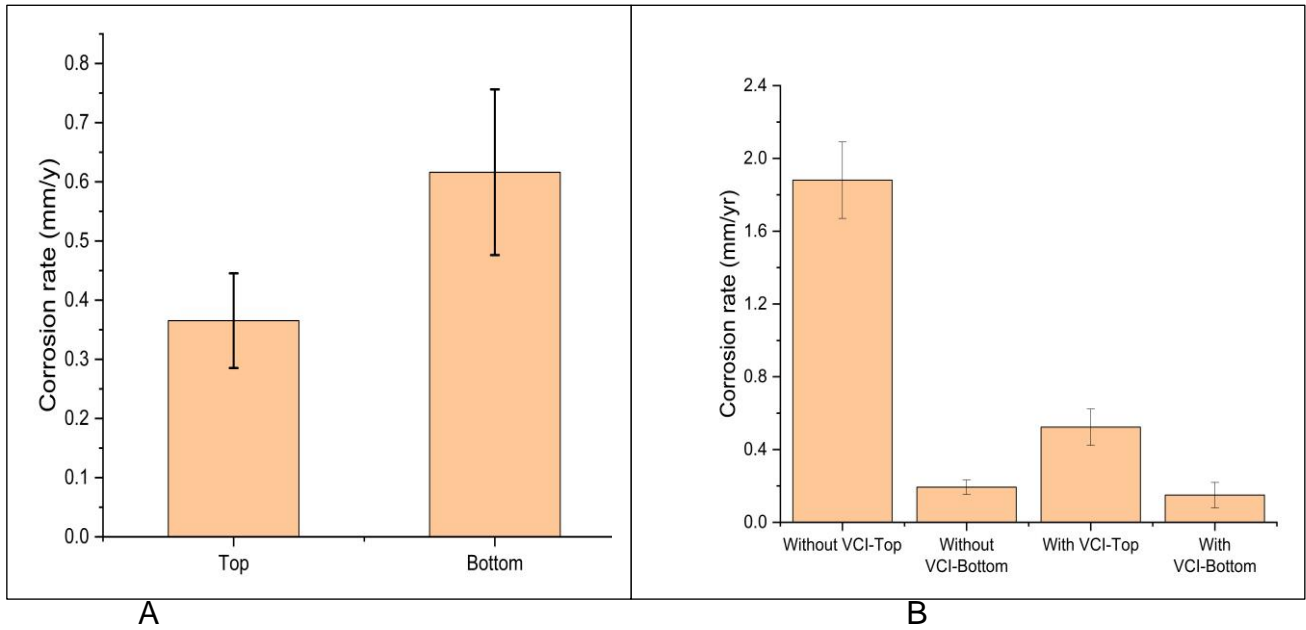


Figure 6.4: Results showing the corrosion rate at the top and bottom parts of the carbon steel pipe (UNS G10220) under mineral wool insulation. (A) Pojtanabuntoeng *et al.* [8] (B) Hou *et al.* [7].

6.1.2) Results of insulation dry out between the ends and middle sections

The results showing the quantity of the test solution lost in the insulation covering the inlet rings (1 and 2), the middle rings (3 and 4) and the outlet rings (5 and 6) as shown in Figure 6.5 are presented and discussed. Each data point represents the average of three replicates and the error bars represent the standard deviation.

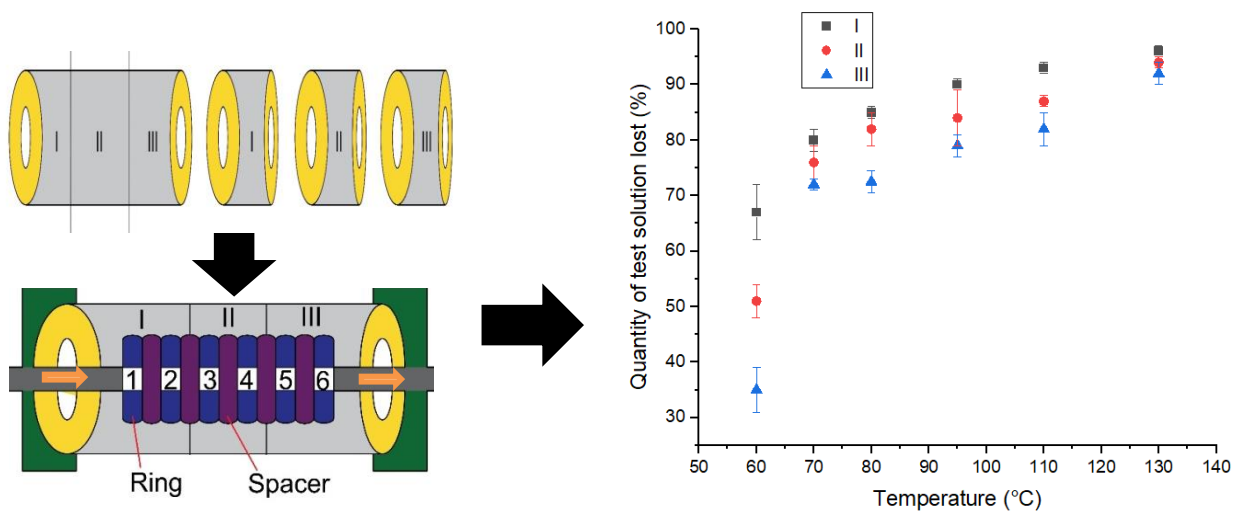


Figure 6.5: Quantity of test solution lost in the inlet (I), middle (II) and the outlet (III) regions of the mineral wool insulation.

The distribution of the test solution across the three sections of the insulation consisting of the inlet where silicone oil enters the rig, the middle and outlet regions where the oil leaves the rig is shown in Figure 6.5. The results indicate an increase in the quantity of the test solution lost with temperature for all the three sections of the insulation due to drying out as the temperature increases. However, a decrease in the quantity of the test solution lost from the insulation was observed across the inlet end to the outlet end for all the temperatures studied. This could partly be attributed to the slight temperature gradient across the six rings as shown in Figure 6.6. Nevertheless, the statistical test results using one way analysis of variance discussed in the previous chapter (chapter 5) has indicated that these temperature deviations across the six rings and quantity of test solution across the three sections of the insulation is statistically insignificant.

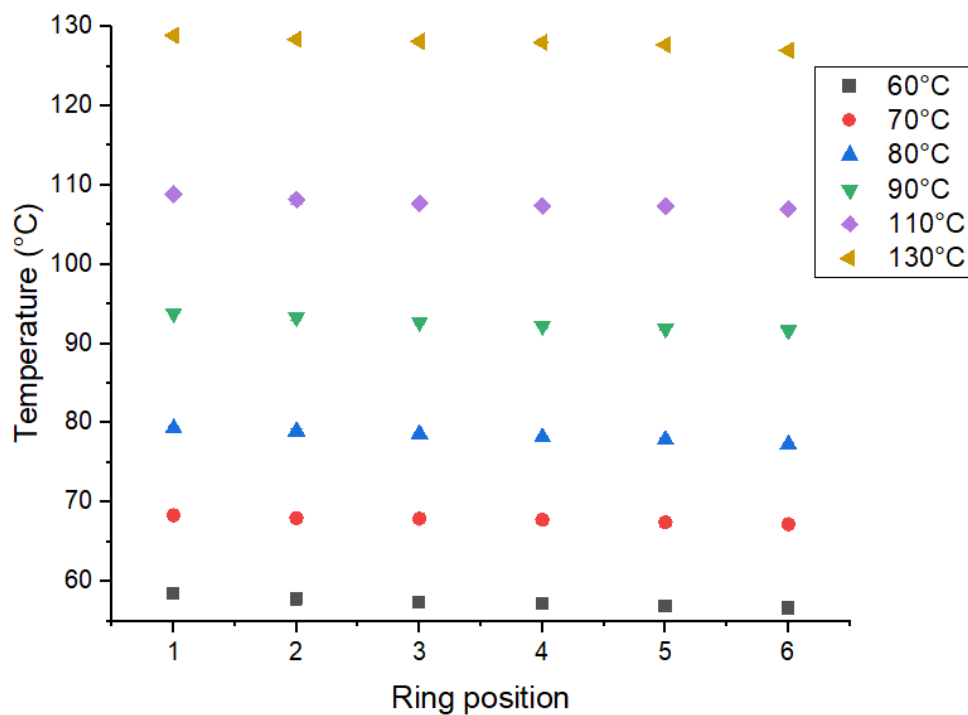


Figure 6.6 : Temperature variation across the six rings

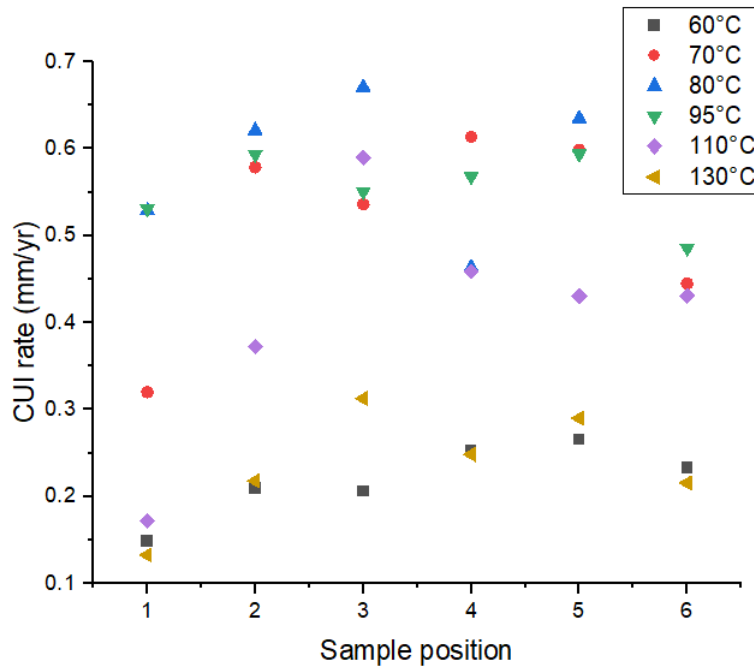


Figure 6.7: A plot of the corrosion rate as a function of the sample position at the different temperatures investigated.

The results of the corrosion rate of the metal rings as a function of the sample position is shown in Figure 6.7. This indicates significant fluctuations in the corrosion rates across different positions of the rings. The first two rings tend to have lower corrosion rates compared to the rest of the rings in most cases, this may likely be due to increased drying out within these regions as Figure 6.6 has shown a slight temperature gradient across the six rings with rings 1 and 2 being at a higher temperature compared to the rest of the rings. However, this is not reflected at the other ring positions as there is a significant variation in the corrosion rate across the other ring positions. This suggests that temperature is not the only factor affecting the corrosion rate of the metal, other contributing factors include, distribution of electrolyte at different region of the insulation.

Moreover, Figure 6.6 shows a slight decrease in temperature across the six sample positions. Comparing Figures 6.5 and 6.6, it would be reasonable to assume that the three data points at each temperature in Figure 6.5 would have been quite close to each other as observed at 70 °C and 130 °C if the difference in the quantity of the test solution lost in the three sections was exclusively controlled by the temperature gradient. This is because a temperature difference of about 1-2 °C is not expected to

cause much deviation in the quantity of the test solution lost as observed at some of the temperatures like 60 °C and 80 °C. The significant deviations at these data points may be attributed to the random errors during installation of the wet insulation on the rig as well as during its removal to determine the final weights. Therefore, electrochemical techniques consisting of galvanic current and electrochemical impedance measurements were carried out to monitor the drying out in real time without the need to remove the insulation.

6.2) Drying out profile of insulation using galvanic current measurements

In this section, the current-time profile obtained at different temperatures are presented and discussed. The results obtained from this study are also compared with other reports in the literature. Estimation of the drying times is important because the severity of CUI is also determined by the time of wetness [9,7]. Therefore, the main purpose was to assess the time it takes the wet insulation to dry out at different temperatures which would explain the observed decrease in the CUI rate as temperature was increased up to 130 °C. The drying times were evaluated at initial, mid, and late stages represented by 0%, 50% and 90% at all the temperatures investigated. These values were chosen to monitor the progress of the insulation dry out, which represents initial, mid, and late stages of insulation dry out respectively which will enable comparison to be made with the CUI rate data obtained at those temperatures. The reference point (t_0) represents the time at which the galvanic current starts drifting towards the horizontal axis. The mid and late drying stages were then calculated from the reference current (I_0) and the corresponding times for 50 % and 90% decrease in I_0 were estimated as shown in Figure 6.8.

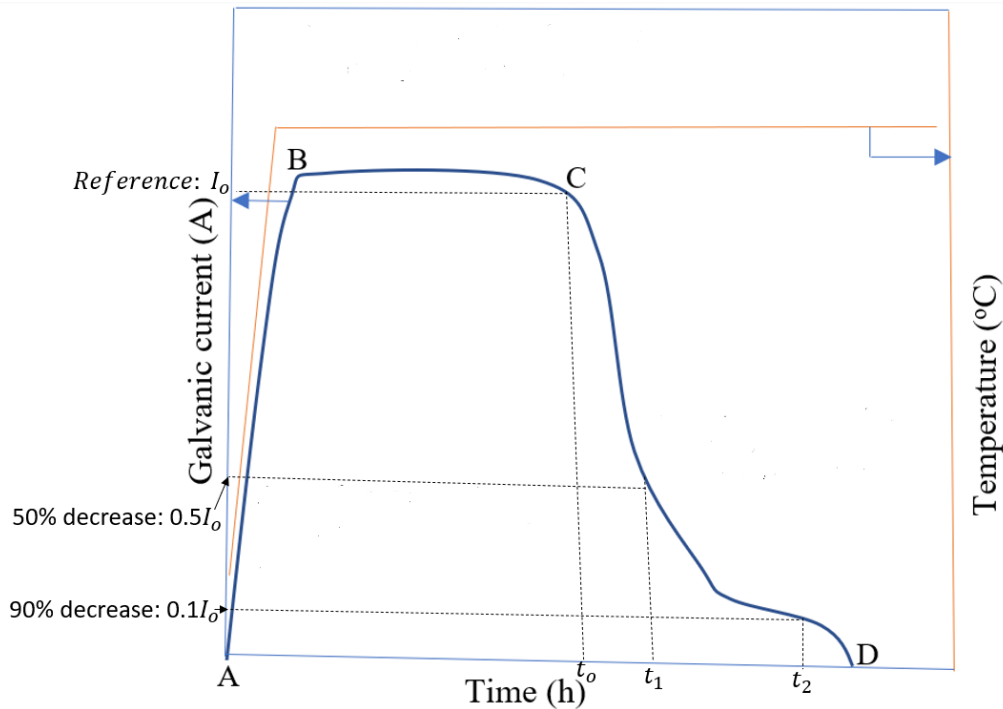


Figure 6.8: Estimation of initial (t_0), mid (t_1) and late drying stages (t_2)

The galvanic current-time profile obtained in this study is shown in Figure 6.9. The initiation of the drying process is shown by the vertically dotted lines which represents the point at which the curve starts dropping to the horizontal axis. The entire area under the plot could be divided into two regions. The region before the dotted lines may be regarded as the wet region, where the metal is in contact with the wet insulation without an insulation dry out being initiated. The region after the dotted lines may be considered as the drying region, where the insulation dry out gradually begins. The colours of the dotted lines should be matched with the colours of the plot when assessing these two regions. Each plot represents the three trials at the temperature under investigation. The reproducibility of the plot (wet and dry region) was not excellent. This is observed by the variability of each of the trials measured at one temperature. The differences in replicate measurements may be attributed to the fact that galvanic current across the small area of the electrodes is quite sensitive to any small changes in contact between the wet insulation and the metal.

The water absorption was quite variable as earlier discussed in the previous chapter (chapter 5). The insulation holding the higher quantity of the test solution will be expected to dry longer than the insulation with the less amount when measured at the

same temperature. Nevertheless, the triplicate measurements at each temperature shown in Figure 6.8 was necessary to observe the variability associated with each trial which will indicate the reliability of the technique as a sensor in monitoring insulation dry out. In Figure 6.8, there are four aspects of interests which forms the basis of discussion. The area of increasing galvanic current with temperature, which is uniform across all trials, the aspect of variable current density during the wet region, the estimated point in which the curve starts moving towards the horizontal axis and the final point at which the galvanic curve is negligible or 0.

Despite the variability, the plot shows an initial increase in the galvanic current with time for all the temperatures under investigation. This might be attributed to the fact that the temperature shown in the secondary axis increases initially from room temperature to the target temperature. This results in an increase in the galvanic current as the temperature increases which is uniform across the three trials at each temperature. However, as the temperature stabilizes and it is maintained, the current tends to drift towards the horizontal axis. This initial drift does not represent drying out but an attempt to attain a stable value of the corrosion current. The variability in this region may be attributed to the sensitivity of the technique to slight changes in contact between the insulation and the metal.

The estimated point at which the curve starts drifting towards the horizontal axis and actually reaches it is quite reproducible at some trials for example, the last two trials at 70 °C, the first two trials measured at 80 °C, and all the trials measured at 110 °C. This is the estimated point at which the drying out process is initiated. As the insulation starts to dry out, the solution resistance increases which reduces the galvanic corrosion current. The solution resistance continues to increase as the drying process continues till it reaches the point where the galvanic current is negligible or 0 as shown in Figure 6.9. It can be observed that the time at which the galvanic current reaches 0 decreases with temperature. This is as expected as an increase in temperature enhances the drying process by driving out the test solution rapidly compared to the lower temperatures.

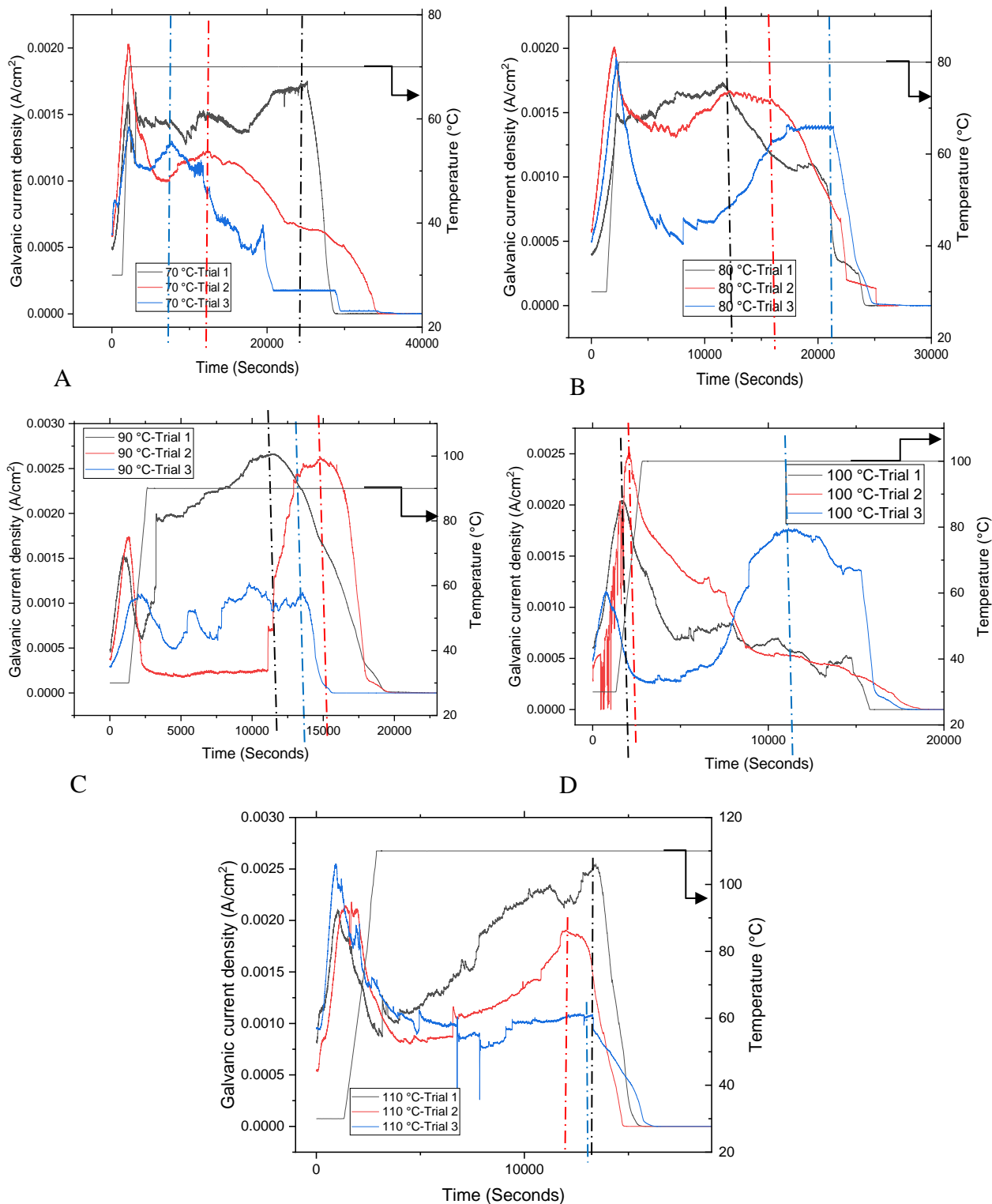


Figure 6.9: A plot of galvanic current density (A/cm²) against drying time (seconds) at different temperatures (primary axis) and temperature ramp against time (secondary axis). The vertically dotted lines of each colour correspond to the colour of each trial, which represents the estimated time where drying of the insulation is initiated.

To obtain a better picture of the drying process, it was necessary to estimate the average drying times for each temperature including the standard deviation represented as error bars. This is presented in Table 6.1 and shown in Figure 6.10.

Table 6.1 : Drying times (minutes) of insulation at different temperatures

Temperature (°C)	Replicates	t_0 ($\times 10^3$) (seconds) (0%)	t_1 ($\times 10^3$) (seconds) (50%)	t_2 ($\times 10^3$) (seconds) (90%)
70	Trial 1	25.01	27.16	28.15
	Trial 2	12.06	26.11	33.60
	Trial 3	8.04	16.09	22.09
80	Trial 1	11.64	20.89	24.25
	Trial 2	12.31	21.04	24.17
	Trial 3	2.13	22.77	24.37
90	Trial 1	11.69	15.92	17.92
	Trial 2	15.00	17.27	19.22
	Trial 3	13.59	14.38	14.98
100	Trial 1	10.57	13.29	15.65
	Trial 2	7.60	9.58	17.24
	Trial 3	11.15	15.62	16.13
110	Trial 1	13.49	14.35	14.99
	Trial 2	12.11	13.72	14.57
	Trial 3	12.89	14.67	15.68

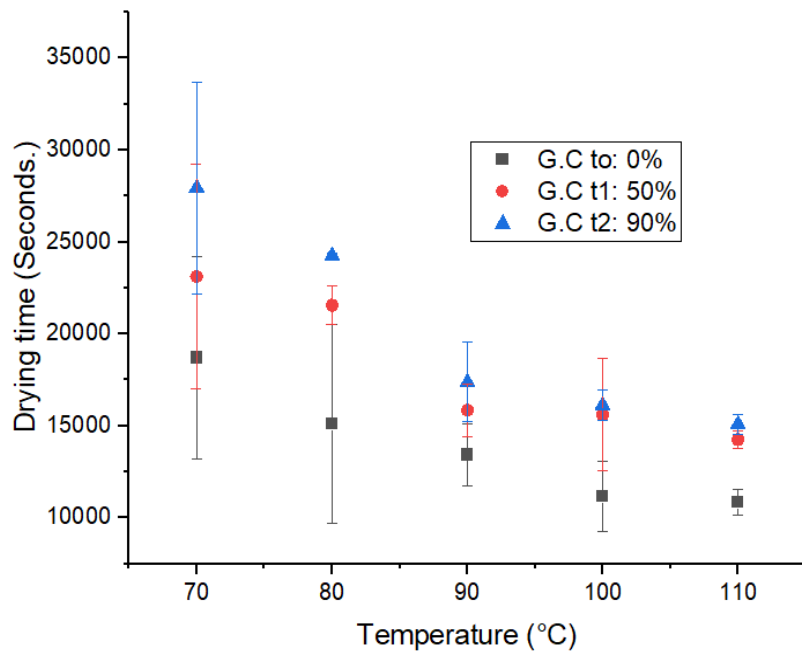


Figure 6.10: Average drying times estimated from the galvanic current density-time profile at different temperatures.

The drying times shown in Figure 6.10 is an average of the triplicate measurements presented in Table 6.1. This will be discussed in two directions, vertically, representing the differences in the data points at each temperature and horizontally, representing the differences in the estimated points across the temperatures for each plot. For the estimated data points at each temperature, the distance between t_0 , t_1 and t_2 indicates the progress of the insulation dry out. This gap is observed to decrease with temperature which indicates that an increase in temperature enhances insulation dry out. The significant decrease in the insulation dry out observed at 110 °C explains the decrease in the corrosion rate observed at 110 °C compared to 80 °C as discussed in the previous chapter.

The galvanic current density-time plot for the top and bottom sections of the insulation obtained at 100 °C is shown in Figure 6.11. The drying profile begins with an increase in the corrosion current with time for all the temperatures studied. This could be attributed to an initial increase in temperature till the target temperature was reached. Thereafter, the temperature was maintained for hours till the drying was completed, which is evidenced by the corrosion current dropping to 0 before the pipe was allowed to cool down to room temperature. The initial increase in temperature will result in an increase in the corrosion current (I_{corr}) which also reflects the result observed with an increase in the corrosion rate as the temperature is increased up to 80 °C. Therefore, the gradual increase in the corrosion current prior to reaching the target temperature observed in this study could be attributed to the gradual increase in the temperature of the insulated couple (Al-Cu).

The drying times of the insulation at the top, sides, and bottom parts at different stages is shown in Figure 6.11. The results indicate that the top and lateral sections of the insulation dries out more quickly than the bottom section of the insulation. This could be attributed to the fact that more test solution settles to the bottom of the insulation which takes time to dry out. Moreover, this agrees with the result of the distribution of test solution in the insulation between the top and bottom parts as well as the corrosion rate data estimated for these two regions. The estimated drying times at different stages (t_0 : 0 %, t_1 :50 % and t_2 : 90%) is shown in Figure 6.12 below.

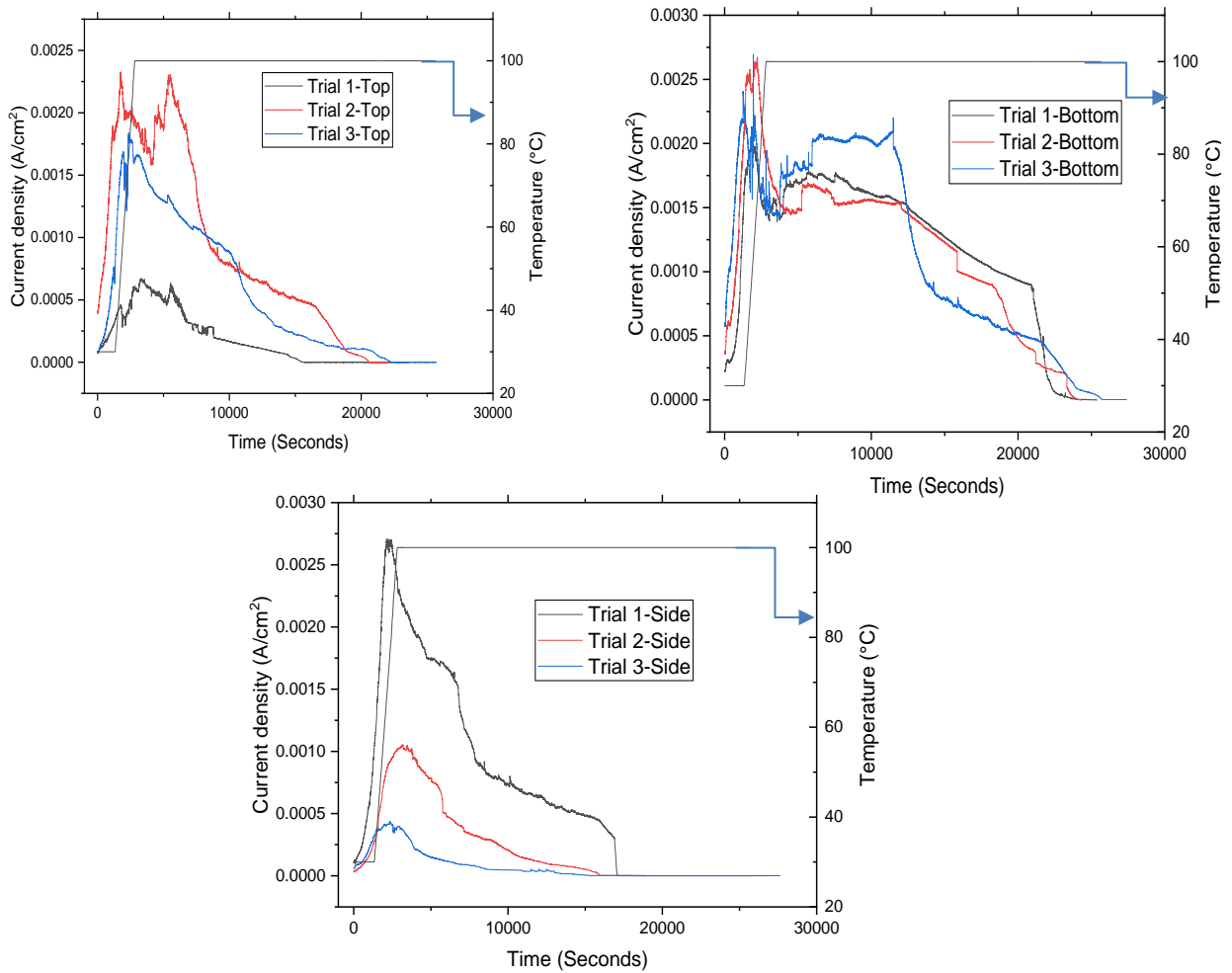


Figure 6.11: Galvanic current density-time profile for the top, bottom and lateral sections of the insulation at 100 °C.

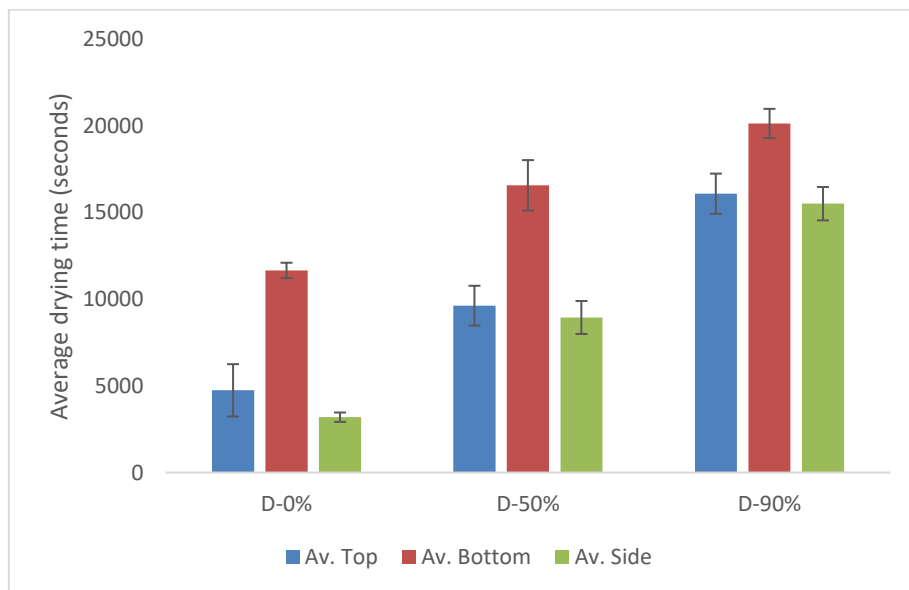


Figure 6.12: Average drying time estimated from the galvanic current density-time profile in Figure 6.7.

Figure 6.11 shows the estimated drying times (D) at different stages such as t_0 : 0 % to t_2 : 90%. The fact that more test solution settles to the bottom and takes a longer time to dry out implies that the corrosion rate will be expected to increase at the bottom parts of the metal compared to the top and sides. This supports the previous results shown in Figures 6.1 and 6.2.

6.2.1) Drying out profile of the mineral wool insulation using Electrochemical impedance measurements

In this section, the results showing the drying out times of the mineral wool insulation at different temperatures as obtained from the electrochemical impedance measurements is presented. The purpose was to investigate the drying process of the mineral wool insulation wetted with 1 wt% NaCl, which would also help in validating the reduced CUI rate obtained in the previous chapter as the temperature increases beyond 100 °C. The fact that the solution resistance changes as the insulation dries out makes it possible to monitor the progress of insulation dry out at different temperatures.

It has been reported that the ability to monitor the electrochemical impedance of electrolytes beneath the insulation could lead to an indirect detection of the CUI activities as well as the associated risks [8]. Therefore, this result will also help in monitoring the degree of wetness and the time it takes for the insulation to dry. Similar to the galvanic current measurements, the estimation of the mid (t_1) and late drying stages (t_2) representing the time it takes to obtain 50 % and 90 % increase in the reference impedance (Z_o) where drying is believed to be initiated as evident in the gradual increase in the impedance were calculated. The estimation of the different drying stages is shown in Figure 6.13.

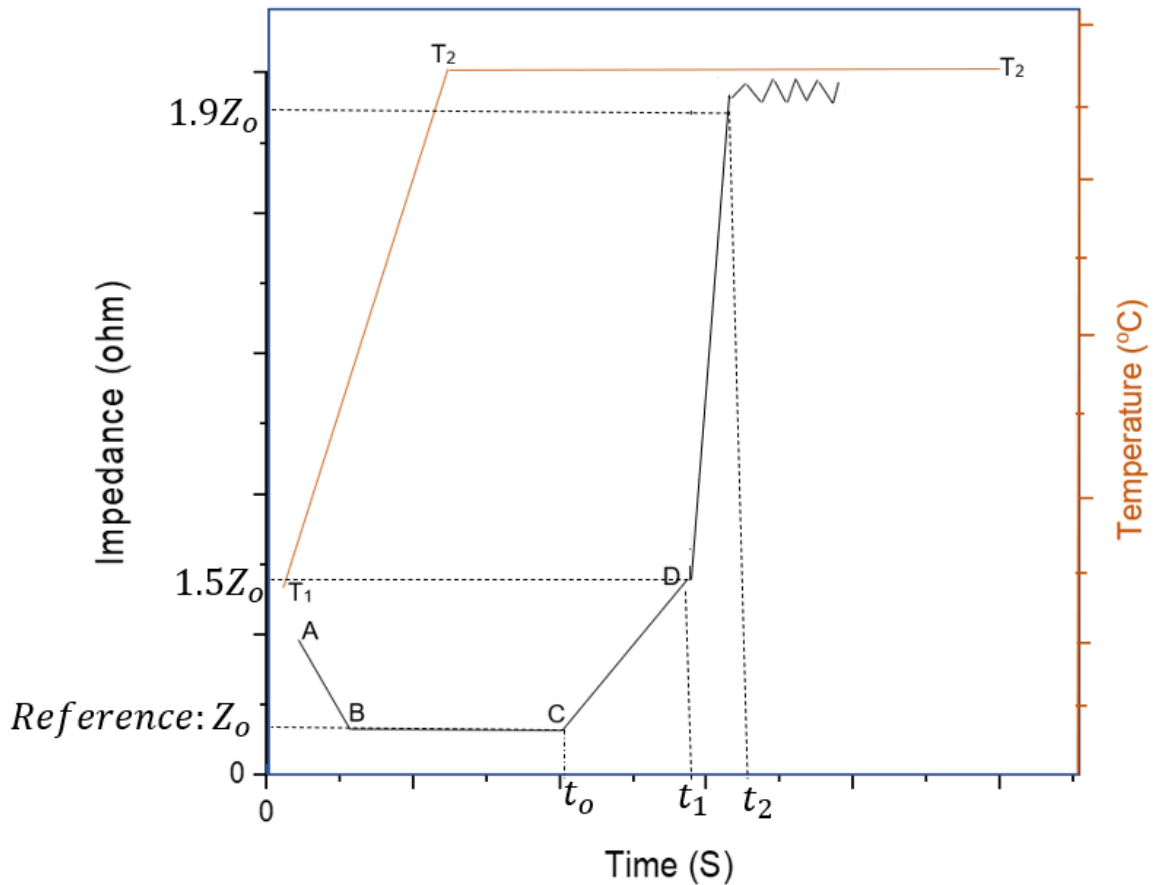


Figure 6.13: Impedance-time plot showing an estimation of the different drying times.

The drying out profiles obtained from the impedance measurements are shown in Figure 6.14, while the different stages of drying ranging from 0% to 90 % extracted from the plots are shown in Figure 6.15. Figure 6.14 shows the impedance-time data at different temperatures. The results indicate an initial decrease in impedance which corresponds to the time at which the electrolyte is heated up to the target temperature as shown by the vertically dotted arrows in green. The temperature program involved a rapid ramp to the target temperature at about 30 minutes. This is indicated by a decrease in impedance as a result of an increased conductivity of the solution. Also, an increased temperature will result in a decrease in the solution resistance [9, 10]. When the target temperature is reached, the temperature is maintained for at least 7 hours as shown by the horizontally dotted arrows in green till the insulation dries out. Within this range, the impedance tends to stabilize initially before it gradually starts increasing slightly due to the gradual drying out of the insulation at the target temperature.

As the solution dries out, the solution resistance dominates, and the impedance increases. This continues until there is a sudden increase in the impedance to the point where the potentiostat cannot measure the signal beyond a certain threshold (1 M Ω) due to the extremely high impedance. At this point, the solution resistance is quite high resulting in a noisy data which reflects either complete insulation dry out or negligible amount of test solution in the insulation as shown in Figure 6.14. The initial stages where the impedance decreases with increasing temperature is an indication that there are other contributing factors other than the solution resistance. However, as the insulation continues to dry out at constant temperature, the dominant nature of the solution resistance is reflected in the phase difference which tends to zero.

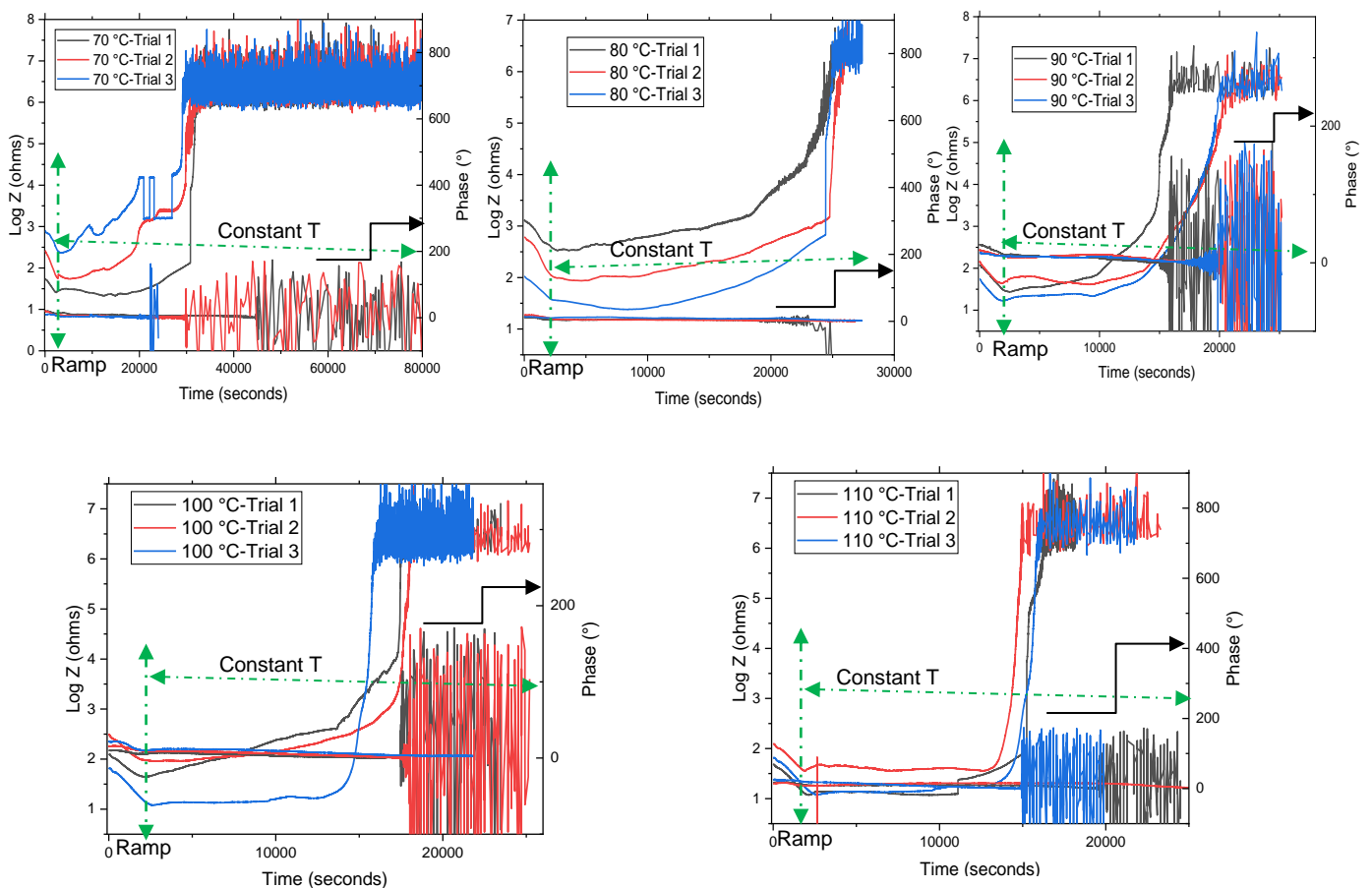


Figure 6.14: Impedance-time plot and phase versus time plot at different temperatures (T).

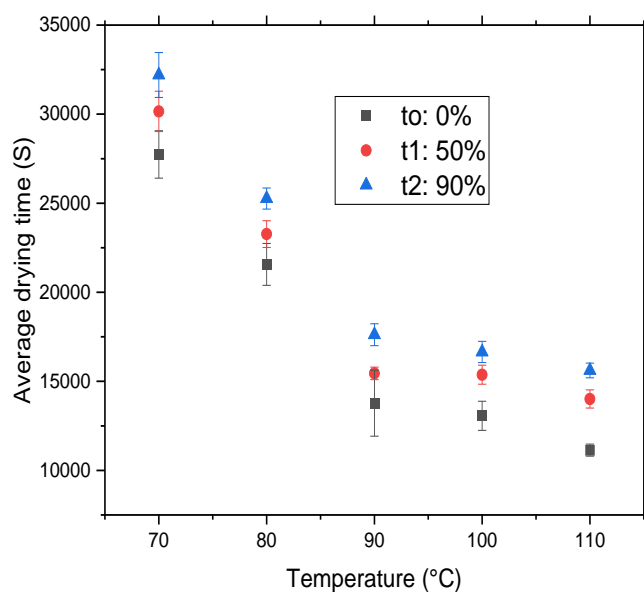


Figure 6.15: Plot showing the drying stages at different temperatures

Figure 6.15 shows the different drying stages (0%, 50% and 90%) extracted from the plots in Figure 6.14. This indicates a decrease in the drying time as the temperature increases up to 110 °C as would be expected. In addition, Figure 6.13 also indicates that for all the temperatures studied, the initial increase in the drying time from 0% to 50 % dry out seems greater than the late drying stages (50% to 90%) especially at high temperatures of 100 °C and 110 °C. This agrees with the gradual rate of insulation dry out followed by the rapid drying phase as shown in Figure 6.15. Although it is difficult to know the exact quantity of electrolyte around the test area as this might affect reproducibility, the triplicate measurement obtained in this study was quite reproducible compared to the galvanic current method.

These results are comparable to the report of [10] as shown in Figure 6.16, who also observed an initial decrease in the impedance with time for the mineral wool insulation that was wetted with 0.5 M NaCl solution and water. This continued until the drying of the insulation sets in resulting in a sharp increase in the solution resistance. This is further supported by the work of Pojtanabuntoeng *et al.* [11] who investigated the drying out of mineral wool insulation using electrochemical impedance spectroscopy as well as the resultant effect on corrosion under insulation. They reported that low impedance values were obtained when there was a sufficient quantity of electrically

conductive water in the insulation. They also observed a reduced corrosion damage when holes were drilled at the bottom of the insulation to remove excess water from the bottom of the insulation.

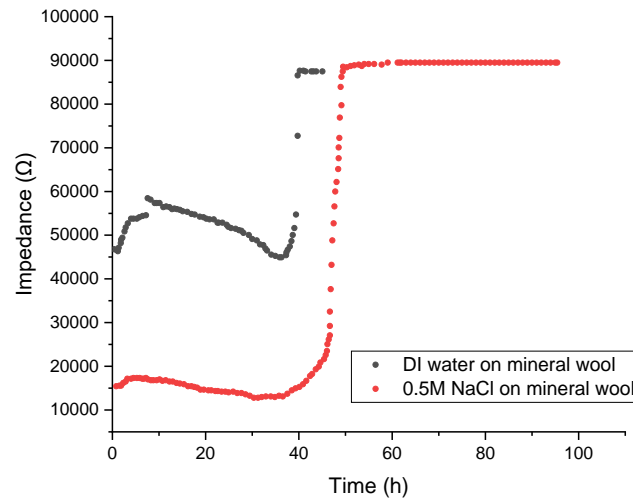


Figure 6.16: An impedance-time plot for mineral wool insulation wetted with 0.5 M NaCl and water at 40 °C at a frequency of 100 kHz [10].

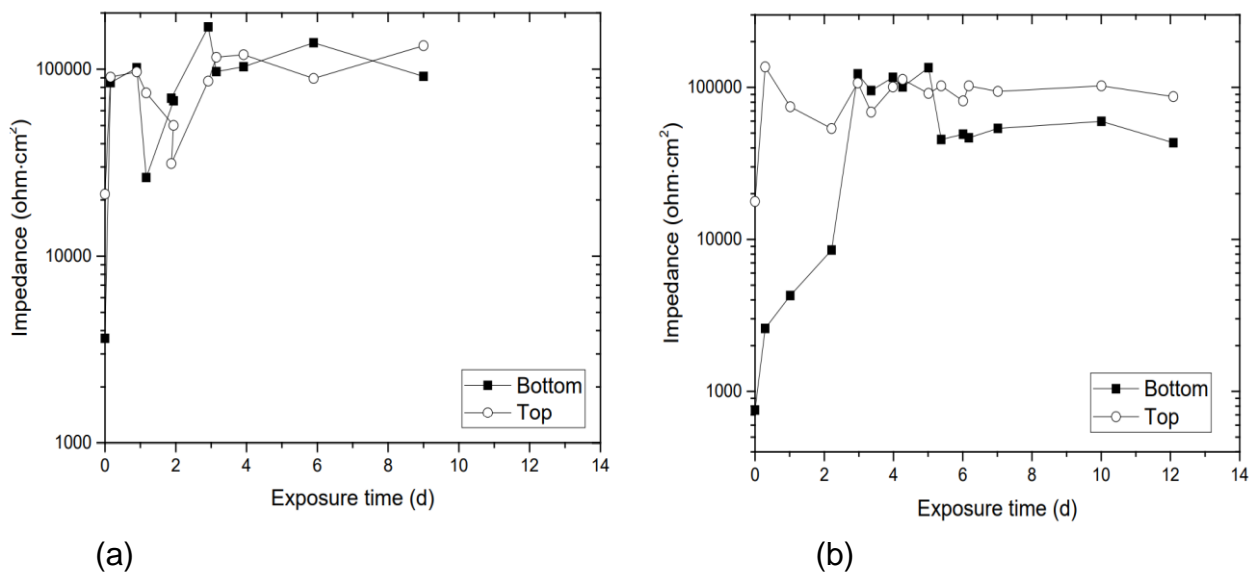


Figure 6.17: An electrochemical impedance plot showing the drying times of wet mineral wool insulation installed on carbon steel rings at a frequency of 10 kHz (a) without drain holes (b) with drain holes [11]

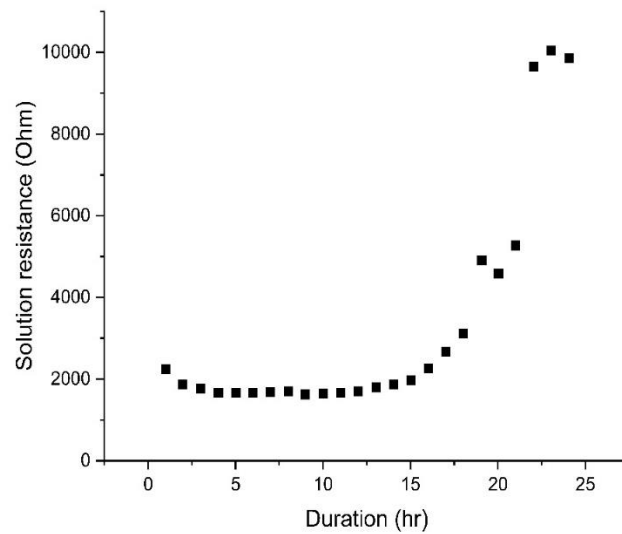


Figure 6.18: Solution resistance values showing the drying of mineral wool insulation [12].

The results obtained in this study also agree with the reports of Pojtanabuntoeng and co-researchers shown in Figure 6.17 and 6.18, who investigated the drying times of wet mineral insulation occurring at the top and bottom parts of carbon steel rings with and without drain holes to remove water from the insulation. The results indicated a rapid increase in impedance as the solution dries out. The effect of drain holes seems pronounced for both the top and bottom parts of the insulation. The insulation without drain holes is still showing evidence of wetness after the initial increase in impedance, while the insulation with drain holes tend to show stable impedance values after some days which suggests less drainage of the water from the insulation [11]. The top parts of the insulation indicated a rapid increase in impedance which later remained constant, whereas the impedance at the bottom parts of the insulation showed some delay by 2 or 3 days, which suggests that the drying out step is slow at the bottom parts of the insulation compared to the top.

6.3) A Comparison of the drying times of galvanic and impedance measurements

In this section, the drying times obtained from galvanic current and impedance measurements have been compared to assess the difference between both methods. The drying times of both methods were collected as a function of temperature and the

calculated degree of insulation dry out (0%-90%). The result is presented in Table 6.1 in the appendix and plotted in Figure 6.19.

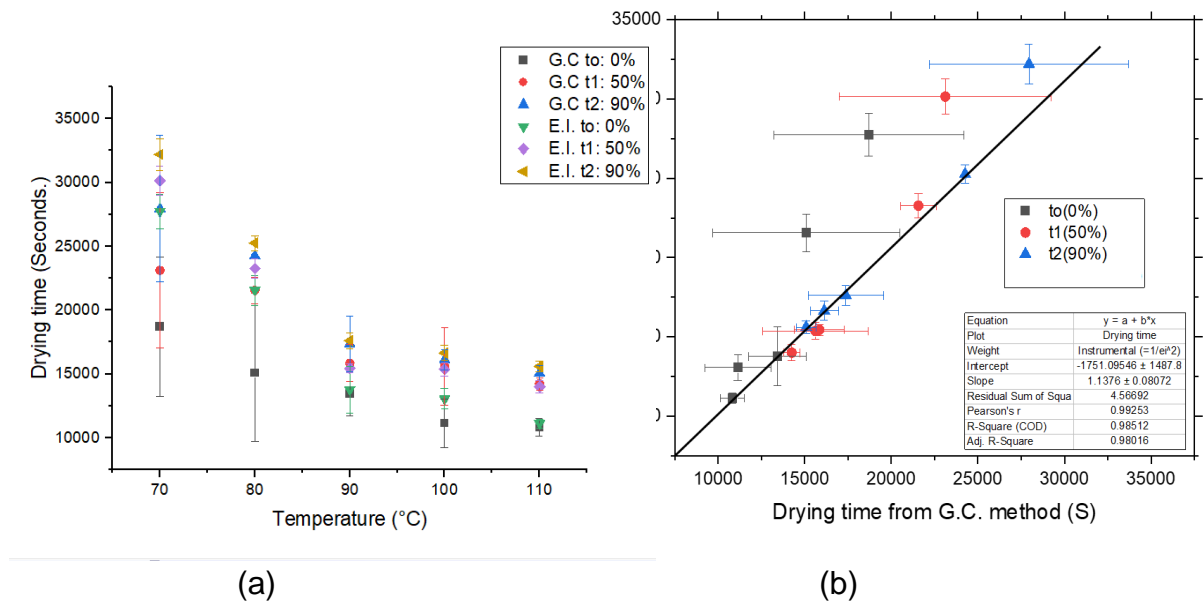


Figure 6.19: A comparison of the drying times of the galvanic current (G.C.) and impedance measurements (E. I.).

The estimated drying times from the galvanic current and electrochemical impedance measurements shown in Figure 6.19a indicates a similar trend with temperature but quite different in the values estimated at the same temperature (Figure 6.19b). The drying time falls more rapidly at 70 °C and 80 °C but seems not to cause much change at 100 °C and 110 °C. Both shows a decrease in the drying time as the temperature is increased. However, in Figure 6.19b, the variability associated with the replicate measurements at each temperature for galvanic current method is seen by the large difference in the horizontal error bars at some of the data points compared to the vertical error bars. This significant variability associated with the galvanic current method may likely be attributed to the sensitivity of galvanic current measurements to slight changes in the degree of contact of the insulation with the metal rings. The impedance method seems quite reproducible across the studied temperature range and the values of the replicate measurements shown in Figure 6.19b does not show much difference compared to the galvanic current method.

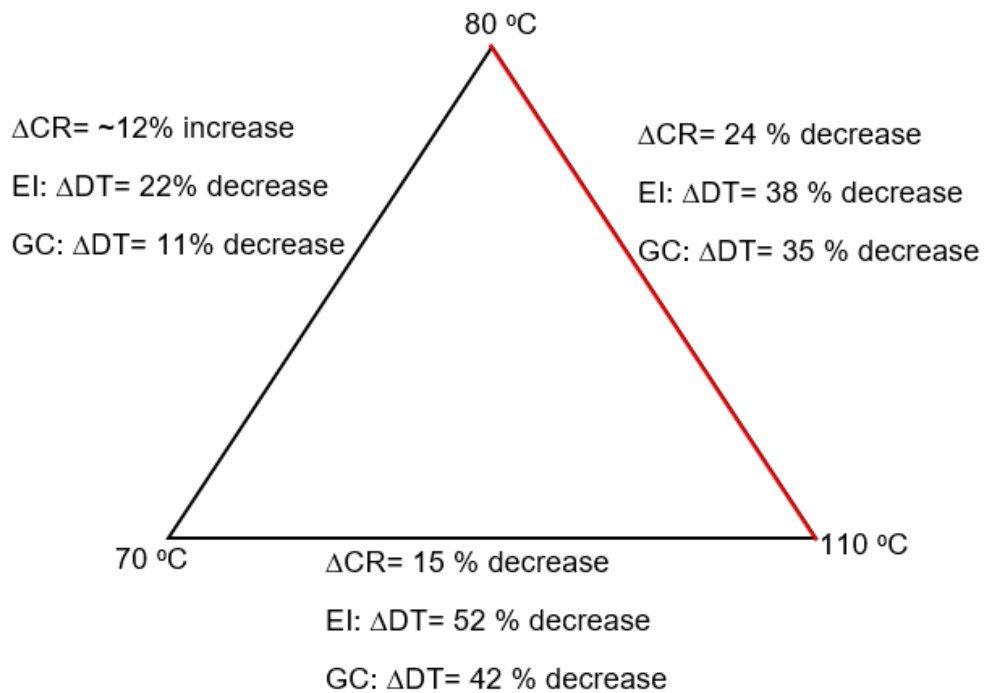


Figure 6.20: A comparison of the change in drying times of both galvanic current and impedance methods with the change in corrosion rate at 70 °C, 80 °C and 110 °C.

In Figure 6.20, the change in drying times is assessed with respect to the corresponding change in the corrosion rate. The red axis represents the temperature range that is believed to be exclusively dominated by an insulation dry out. The decrease in the drying times (t_2) of both the electrochemical impedance and galvanic current methods from 70 °C to 110 °C are 52 % and 42 % respectively. The change in corrosion rate within this temperature range was observed to be 15 %. The drying out times within this range cannot account for the observed change in the corrosion rate, this could probably be caused by the fact that insulation dry out is not dominant at 70 °C as observed by the time it takes to reach an impedance of 1 M Ω (Figure 6.14). This is also the case with the drying times and corrosion rates within 70 °C to 80 °C where the corrosion rate increases even when there is a 22 % decrease in the drying time. This suggests that within this temperature range, insulation dry out is not the dominant factor.

However, within the temperature range (80 °C to 110 °C) where the insulation dry out is believed to be dominant, the decrease in the drying time for E.I and G.C. methods

were obtained as 38 % and 35 % respectively. In this temperature range, the corrosion rate is observed to decrease by 24 %. The decrease in the drying time also corresponds to a significant decrease in the corrosion rate even though it is not exactly at the same rate. The non-linear dependence of the CUI rate with temperature implies that the drying times could only be used to account for the change in corrosion rate within the temperature range in which the insulation dry out is the dominant factor.

6.4) Conclusions

The distribution of electrolyte in mineral wool insulation was assessed at different temperatures in terms of the amount lost within the top and bottom sections as well as the ends and centre of the insulation. This was carried out to identify areas with high susceptibility to CUI as the rate of CUI depends on the quantity of electrolyte around each region of the metal. Results indicated that more test solution was lost at the top section compared to the bottom section of the insulation. This agrees with the work of [1] who also observed more CUI damage around the bottom ring samples compared to the top due to an increased settling of the test solution to the bottom part due to gravity. This suggests that the bottom part of the insulation may likely be more susceptible to CUI damage compared to the top. In addition, the ends and centre of the insulation did not show much deviation in the quantity of water lost between the inlet, middle and outlet ends of the insulation. The slight temperature gradient of about 1-2 °C between the inlet and outlet end of the rig may likely be a contributing factor. However, this could not account for the variability of CUI rate across the six ring positions. This is probably because there are other factors such as variability in the distribution of test solution in the insulation used in different trials, difficulty aligning the rings and spacers reproducibly for each trial among other reasons.

The drying out times of mineral wool insulation was investigated using galvanic current and electrochemical impedance measurements using an Al-Cu galvanic couple and Cu-Cu connection respectively which would serve as a sensor in monitoring the drying out of the mineral wool insulation. It was observed that it took a longer time for the bottom part of the insulation to dry out compared to the top and the sides which agrees with the water distribution results as well as the estimated corrosion rate results reported in this thesis and by Pojtanabuntoeng *et al.* [1]. This implies that more test

solution occupies the bottom part of the insulation and might likely cause more corrosion within this area compared to other regions.

Both galvanic current and electrochemical impedance methods showed a similar trend in the drying times at the temperatures under investigation (70 °C-110 °C). The drying times of both methods decreased as the temperature increased. Replicate measurements of the drying times showed a higher variability with the galvanic current method compared to the electrochemical impedance method. Both methods showed that an increased drying out of the insulation resulted in a decreasing corrosion rate. However, the fact that the decrease in the drying out times of both methods was not exactly at the same rate as the decrease in corrosion rate within the temperature range where the drying out was believed to be dominant (80 °C-110 °C) implies that other factors such as the availability of oxygen, steam, among others may still have some effect on the CUI rate within this temperature region.

References

1. Pojtanabuntoeng, T., Machuca, L. L., Salasi, M., Kinsella, B. and Cooper, M. (2015a). Influence of drain holes in jacketing on corrosion under thermal insulation. *Corrosion*, 71 (12):1511–1520.
2. De Vogelaere, F. (2009). Corrosion under insulation, *Process safety progress*, 28(1): 30-35.
3. Hou, Y., Pojtanabuntoeng, T. and Iannuzzi, M. (2020). Use of electrochemical current noise method to monitor carbon steel corrosion under mineral wool insulation. *Materials Degradation*, 4 (39):1-9.
4. Jirickova, M., and Cerny, R. (2006). Effect of hydrophilic admixtures on moisture and heat transport and storage parameters of mineral wool. *Construction and Building Materials*, 20(6):425-434.
5. Ojanen, T. (2017). Moisture performance of mineral wool insulation products in highly insulated structures. *Energy Procedia*, 132:795-800.
6. Loboda, B. and Szurman, F. (2019). Thermal conductivity coefficient research on mineral wool after partial immersion in water and drying to constant mass. *IOP Conference Series: Material Science and Engineering*, 471:1-10.

7. Hou, Y., Pojtanabuntoeng, T. and Iannuzzi, M. (2020). Use of electrochemical current noise method to monitor carbon steel corrosion under mineral wool insulation. *Materials degradation*, 4 (39):1-9.
8. Pojtanabuntoeng, T. Machuca, L. and Salasi, M. (2015). New experimental rig to investigate corrosion under insulation at different climate conditions. *Corrosion and materials*, 46-51.
9. Caines, S., Khan, F., Shirokoff, J. and Qiu, W. (2015). Experimental design to study corrosion under insulation in harsh marine environments. *Journal of Loss Prevention in the Process Industries*, 33:39-51.
10. Ayello, F., Hill, D., Marion, S., and Sridhar, N. (2011). Integrated sensor networks for corrosion under insulation: monitoring, cost reduction, and life extension strategies. NACE publications, paper number 11281.
11. Pojtanabuntoeng, T., Kinsella, B., Ehsani, H., Brameld, M. (2017). Comparison of insulation materials and their roles on corrosion under insulation. NACE International, paper number 9287.
12. Pojtanabuntoeng, T., Machuca, L. L., Salasi, M., Kinsella, B. and Cooper, M. (2015b). Influence of drain holes in jacketing on corrosion under thermal insulation. *Corrosion*, 71 (12):1511–1520.

CHAPTER 7 : RESULTS AND DISCUSSION

PREDICTIVE MODELLING OF CORROSION RATE OF CARBON STEEL UNDER INSULATION USING ARTIFICIAL NEURAL NETWORK

CHAPTER 7
RESULTS AND DISCUSSION
PREDICTIVE MODELLING OF CORROSION RATE OF CARBON STEEL UNDER
INSULATION USING ARTIFICIAL NEURAL NETWORK

This chapter covers the results of prediction of CUI rate using artificial neural network (ANN) which was carried out using SPSS software. First, the results of dimensional reduction of data using principal component analyses (PCA) tool are presented. This is followed by sensitivity analyses involving assessment of percentage contribution of each of the input parameters, as well as accuracy and precision of predicted CUI rate. In addition, the effect of different network designs such as number of input parameters and hidden layers as well as choice of activation function (logistic sigmoid and hyperbolic tangent functions) were investigated. This study was aimed at assessing the accuracy and precision of CUI rate predictions from artificial neural network and the architectural network designs that could enhance accuracy of predictions.

This is important because corrosion of insulated metals is hidden beneath the insulation, which means that corrosion can proceed unnoticed till final consequences are severe. Therefore, accurate prediction of CUI rate would enable adequate inspection and maintenance schedule to be executed prior to failure which have enormous cost and safety implications. Although damage and probability of failure functions have been developed for CUI and non-CUI applications [1, 2, 3, 4], this was based either on the tendency of failure of protective coatings or fitting a single degradation measurement to failure-time distribution models in situations where field CUI data cannot be obtained. Theoretical prediction of the rate of CUI is difficult due to the fact that the interactions between different factors affecting CUI is quite complicated. For this reason, ANN has been the most suitable predictive tool compared to linear regression models since it specializes in identifying non-linear relationships between different interrelated variables and can be used to predict the behaviour of complex systems [5]. To the best of our knowledge, there has been scarcity of data assessing different neural network combinations that could enhance accuracy and precision of CUI rate predictions using ANN.

Most prediction of corrosion rates reported in the literature were carried out for uninsulated metals [6, 7]. In fact, the only available study on prediction of CUI rate using ANN after a thorough search on different search engines were the works of Burhani *et al.* [8] who utilized the machine learning module of JMP software to predict CUI rate as well as the prediction of wetness and CUI damage for above ground pipelines by Erickson *et al.* [3]. However, these were just one-off predictions, there was no data showing ways of improving accuracy and precision of prediction in these reports. Therefore, this study was carried out to provide a broader perspective to CUI rate prediction by assessing the accuracy of different network designs which would serve as a guide when choosing network parameters for improved accuracy and precision of CUI rate predictions.

The prediction of CUI rate of carbon steel was carried out using patterns mapped between the experimental CUI rate as the dependent variable and the parameters that influenced CUI such as temperature, quantity of test solution (1 wt % NaCl) in insulation, dosage of inhibitor injected to insulation and arrangement of the metal rings as the input variables. These were parameters measured in the laboratory and their significance to CUI have already been discussed in Chapters 3 and 5. The mapping process is based on the variations captured between the input variables and the expected output variables which is used during the training step to establish a relationship between both variables. The training process involves assigning of weights and bias values to the input variables and subsequent implementation with an activation function to yield the first predicted output, the error obtained by computing the difference between the predicted and observed outputs are evaluated and minimized by adjusting the weights and bias iteratively till a minimum specified error ($\leq 1\%$) was obtained [9].

Furthermore, it should be noted that theoretical predictions using ANN is not restricted to these parameters only; in fact, more measurable input parameters having effect on CUI can be added which may likely result in improved adaptation of the network during training [10]. The input variables were subjected to both logistic sigmoid and hyperbolic tangent functions using single and double hidden layers to compare the accuracy and precision of both network designs. The input data was split into training and test sets comprising of 70% and 30% respectively. The percentage of data assigned to each

set was user controlled, and the percentages were chosen based on the generally accepted criteria for data partitioning for ANN analysis [8, 11]. However, the assigning of specific data to each set was strictly software controlled which would eliminate human bias.

Therefore, to enhance clarity, this result is organised and presented in four parts. The first part consists of evaluation of the relationship between the input parameters (independent variables) and the output which is CUI rate (dependent variable) using PCA and importance module of ANN. The second part consists of the results showing the effect of architectural design of ANN (single and double hidden layers), this is followed by prediction accuracy of logistical sigmoid and hyperbolic tangent activation functions as well as precision of the predicted output. Detailed explanation of the choice of network parameters including description of the calculations behind the training process and predictions have been provided in the Fundamentals chapter. It is expected that this study will provide useful information on the choice of network parameters and design of neural architecture for CUI rate predictions as well as clarify the degree of consistency of logistical sigmoid and hyperbolic tangent activation functions in making reproducible predictions of CUI rate. This could be useful in making informed decision on the state of insulated metals without the need to remove the insulation which has enormous cost implications.

7.1) Relationship between the input parameters with CUI rate

The existence of relationship between the input parameters used in this study such as temperature, dosage of inhibitor, quantity of test solution in insulation and sample position with CUI rate was assessed using principal component analysis and artificial neural network. This was to ensure that the data satisfy certain criteria such as existence of some correlation between each of the input parameters and the expected output. This is important because ANN relies on this relationship in making predictions. Therefore, input parameters that has no relationship with the expected output may not be suitable for predictions using ANN, as it will be difficult to train the software [8]. As a matter of fact, the greater the number of input parameters with some relationship with the expected output, the greater the adaptability of the network during training in making predictions. Also, the Scree and orthogonal component plots derived from

principal component analysis of CUI data are good data screening tools used in this study prior to carrying out CUI rate prediction.

7.1.1) Principal Component Analysis (PCA) Results of CUI Data

Principal component analysis (PCA) is one of the multivariate data analytical techniques that is mostly used in converting large datasets into units called components with a decreasing order of variations captured in each component [12]. The main purpose of PCA is to reduce the dimensions of many interrelated variables through a transformation to a newly ordered data set such that most of the variations of the original data are retained in the first few components [13]. This is important because ANN makes prediction based on the pattern that the software has learned from existing data. Therefore, narrowing the data to dimensions with highest variations would improve the training process resulting in improved predictions. Moreover, improved accuracy of corrosion rate prediction has been reported with PCA transformed data compared to the data without PCA transformation [14].

Therefore, it is necessary that the data used for training and predictions be subjected to PCA analysis to ensure that only the most significant data are included in the model for CUI rate prediction by capturing the significant variations in transformed data sets called components. Hence, this ensures that parameters with negligible variations are removed prior to making predictions. The outputs of PCA analysis used in this study include the orthogonal component and Scree plots which explains the relationship between the input parameters and the significance of each component respectively. This is presented and shown in Table 7.1 and Figure 7.1 respectively.

Table 7.1 : PCA table showing the correlation coefficients between each component and the variables studied

Parameters	Component 1	Component 2	Components 3-5
Corrosion rate (CR)	-0.901	-0.278	Discarded
Dosage of inhibitor (DI)	0.868	-	
Temperature (T)	0.850	-	
Quantity of test solution (TS)	-0.582	0.218	
Sample position (SP)	-	0.959	
Variations (%)	80.5	16.65	2.85

The total number of components derived from the PCA result corresponds to the total number of the input and output variables as presented in Table 7.1. The order of significant groups based on the captured variations are arranged into components (1-5); hence, the name principal component analysis. The most significant variation is captured in the first component, which represents the dimensions by which maximum spread out of the data is achieved. The next significant variation is captured in the second component, which represents the linear combination of the observations having a maximum variation in an orthogonal direction to the first principal component [12]. The less significant data are filtered into components 3 to 5, but these are excluded from further analysis due to the low contribution to the total variations of the original data set. According to Jolliffe [13], a single component is insufficient to describe the total variations in a data set and inclusion of components with negligible contributions would negatively affect the accuracy of predictions. Therefore, only the first two components were chosen for further analysis. The positive and negative numbers in both columns represent the correlation of each component with the original data for each parameter studied. The higher the value irrespective of the sign, the stronger the correlation.

In addition, it is worth noting that the components are uncorrelated with each other, and the most significant correlations are filtered into the first component. This makes up 80.5 % of the total variations, while the second component accounted for 16.65 %

of the total variations. In total, both components accounted for 97.15% of the original variations, while the 2.85% spread across the three remaining components were discarded. The results shown in Table 7.1 indicates that the first principal component is strongly correlated with the corrosion rate, dosage of the inhibitor and temperature but moderately correlated with the quantity of the test solution in the insulation. However, the corrosion rate and the quantity of the test solution in the insulation have negative signs while temperature and dosage of the inhibitor have positive signs. This implies that an increased dosage of the inhibitor would result in a decrease in the corrosion rate, while an increase in the quantity of test solution in the insulation would result in an increased corrosion rate.

On the other hand, the sample position has less significant effect on the corrosion rate as shown by the near perpendicular orientation with the CUI rate in Figure 7.1a. This may be attributed to the fact that the distance between the first ring and the last ring was just 6 cm; therefore, no significant difference in the corrosion rate would be expected. This agrees with the statistical test of hypothesis reported in chapter 5 of this study which indicated that there was no significant difference in the corrosion rate across the sample positions. This explains why no correlation has been established between the positional arrangement of the metal rings and the first component representing the most significant variation. Nevertheless, some of the important variations have also been filtered into the second component accounting for 16.65 % of the total variation.

In addition, the relationship between the studied parameters is shown by the orthogonal component plot in Figure 7.1a, while the eigen values associated with each component is shown as a scree plot in Figure 7.1b. The orthogonal component plot is interpreted in terms of the position of each of the parameters in the quadrant, the distance from the origin as well as the presence of clusters. The interpretation of the correlations of the principal component result shown in Figure 7.1a will be carried out with respect to the corrosion rate as the reference point since this is the expected output. On the other hand, the scree plot shown in Figure 7.1b will be interpreted in terms of the significance of each of the components which is indicated by the eigen values and the contribution of each of the components to the total variation.

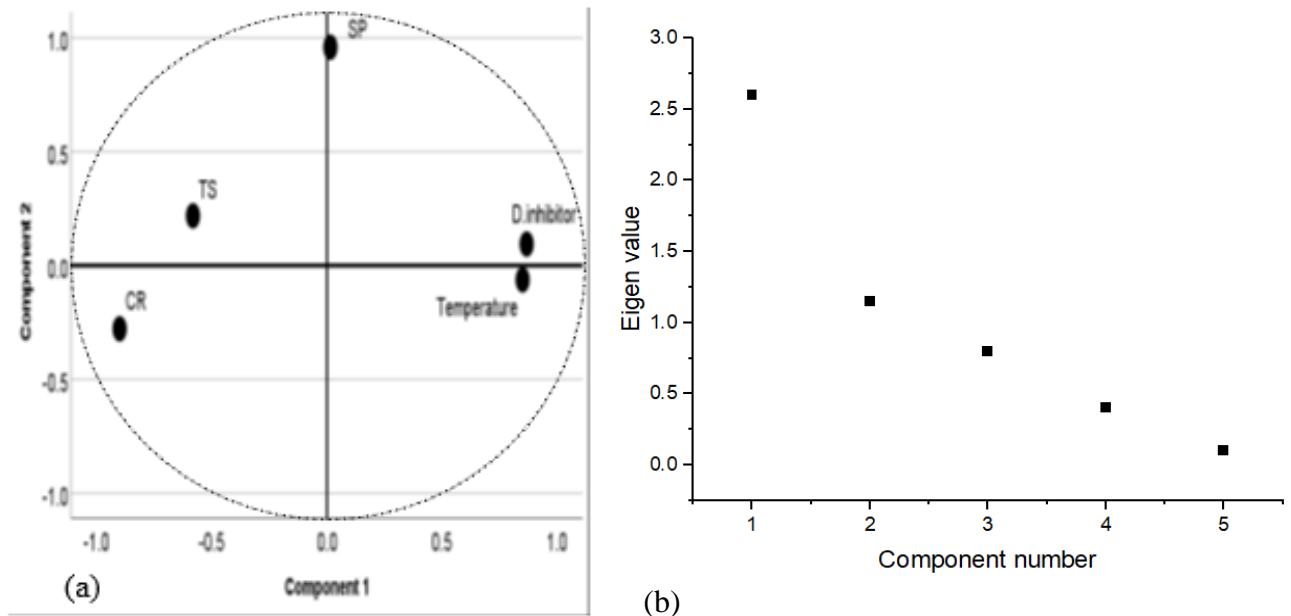


Figure 7.1 : (a) An orthogonal component plot of the CUI data (b) A Scree plot showing the decreasing order of significant data in each component

An overview of the relationship of each of the input parameters with the expected output (CUI rate) is shown in Figure 7.1a. The dosage of the inhibitor shows a good negative relationship with the corrosion rate, this is supported by the fact that both values lie on the opposite side of the quadrant, which shows that an increased dosage of the inhibitor would result in low corrosion rates. In addition, the temperature also shows a near opposite correlation with the corrosion rate as shown by the proximity of the temperature to the opposite quadrant of the corrosion rate. This behaviour may be attributed to the initial increase in corrosion rate with temperature up to 80 °C and a subsequent decrease of corrosion rate when temperature was further increased to 130 °C as discussed in chapter 5. Also, the quantity of test solution in the insulation shows an average positive relationship with the CUI rate. This could be attributed to the fact that the trend of an increase in the corrosion rate as the quantity of the test solution in the insulation increases is less significant due to the presence of the inhibitor.

On the other hand, the sample position indicated a weak relationship with the corrosion rate compared to the rest of the parameters as shown by the near perpendicular orientation with the corrosion rate. This is evident in the lack of correlation with the

component with the highest variation (component 1). Nevertheless, it has a good positive correlation with the second component representing the component with the next significance after the first component. Although it has been suggested that the input parameters with negligible relationship with the expected output should be removed from the model in the bid to enhance prediction accuracy of the CUI rate [8], it is important that the contribution of these input parameters be quantified prior to making predictions to assist with the choice of parameters to be included in the prediction. This was carried out using the normalized importance module of the artificial neural network which will be discussed in the next section.

Furthermore, the degree of variation captured by each component is shown on the Scree plot shown in Figure 7.1b. In this figure, each component represents the dimensional variable space showing the best least squares approximation. The degree of variation decreases as the number of component increases. This implies that the most significant variation is captured by the first component (PC1) as indicated by the highest eigen value, this is followed by the second principal component (PC2). The general rule of thumb relating to component selection is to choose components with an eigen value of at least 1 [15, 16]. This implies that only the first two components satisfy this criterion, and this will be sufficient to provide the required information expected from the input data. In predictive modelling, a single principal component may not be sufficient to model the variability existing in a set of data [12]. Therefore, it was important to choose the first two components as inclusion of more insignificant components will affect the accuracy of prediction. Further confirmation of this relationship was carried out using the normalized importance module of the artificial neural network.

7.1.2) Percentage contribution of input parameters using ANN

The contribution of the input data to the prediction of the expected output was assessed using the normalized importance module of the artificial neural network. This estimation was based on the degree of the relationship between the input variables and the output, which could be useful in determining if a parameter should be excluded from the model or not. This is important because it might be difficult to train the software using data sets that has a negligible trend with the expected output.

Moreover, it is likely that such data could be the main cause of error during prediction. Therefore, to ensure reliability of the predicted output, it is advisable to assess the importance of each of the input variables in terms of the degree of the relationship of each input parameter. Artificial neural network assesses the contribution of each independent variable by normalizing the importance values of each of the input variables to the parameter with the highest importance and further expresses it as a percentage. The result could also be useful in verifying the output of the principal component analysis. The ANN result is presented in Table 7.2 and plotted in Figure 7.2.

Table 7.2 :Normalized importance of the input variables

Input parameters	With inhibitor (VpCI 619)	Without Inhibitor
	Normalized Importance (%)	Normalized Importance (%)
Dosage of inhibitor (DI)	100	-
Temperature	60.2	98
Sample position (SP)	40.5	16
Amount of test solution (TS)	26.3	100

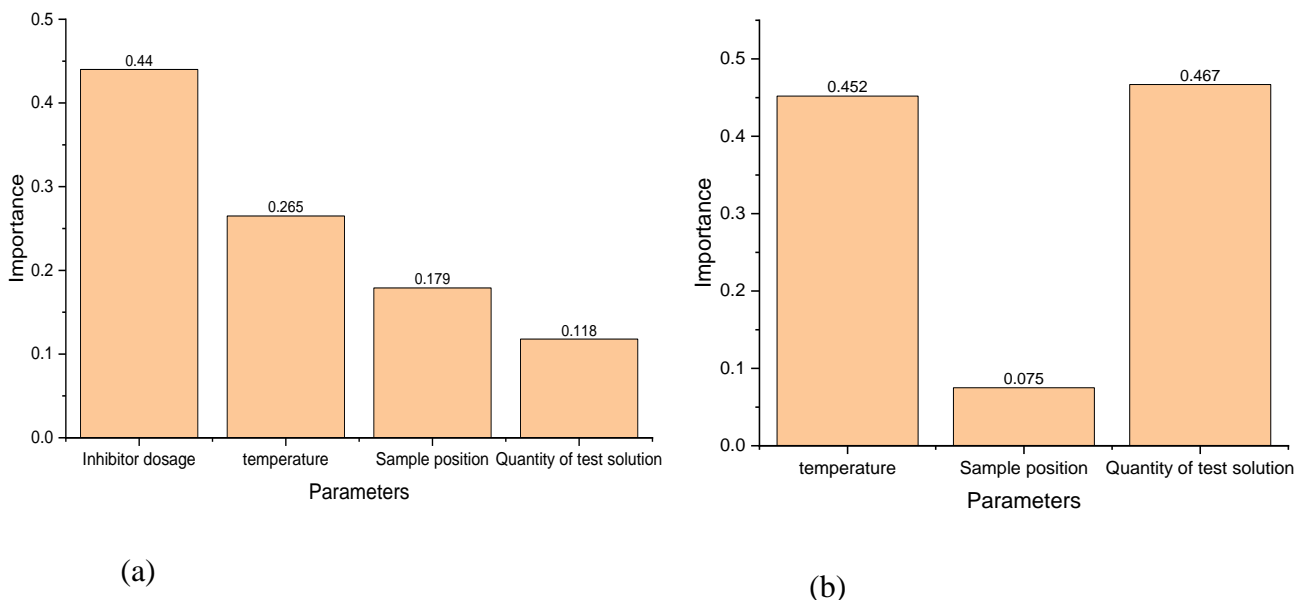


Figure 7.2 : Significance plot of the input parameters (a) Data sets including inhibitor (b) data without inhibitor

The importance analysis is computed based on the significance of each of the input parameters to the prediction of the rate of CUI. The data presented in Table 7.2 and shown in Figure 7.2a indicates that the dosage of the inhibitor has the highest contribution in predicting the final value of the corrosion rate. Therefore, other parameters are normalized to this value. This is followed by temperature, which is also observed to have a good trend with the expected output. These results agree with the output of the principal component analysis. The quantity of the test solution in the insulation is observed to show the least relationship which may be attributed to the presence of the inhibitor. This is confirmed in Figure 7.2b where no inhibitor was used, the importance value for the quantity of electrolyte in the insulation became the most significant, which suggests that the effect of the quantity of electrolyte on the CUI rate was minimized by the inhibitor. On the other hand, sample position was observed to have low importance values independent of the presence of the inhibitor. The importance of the input parameters based on the mapped pattern with the experimental output is shown below.

With inhibitor: Dosage of inhibitor > Temperature > Sample position > Test solution

Without inhibitor: Test solution > Temperature > Sample position

This indicates that the dosage of the inhibitor had the most significant effect on the predicted values of the rate of CUI. This implies that it has the strongest trend by which the network can learn in establishing the relationship between the experimentally determined input and output variables. In addition, the temperature is observed to be the next significant parameter that would also contribute significantly to the overall predicted corrosion rate. This shows the importance of monitoring the temperature of insulated pipes as it has a significant contribution to the overall corrosion rate predicted by the model. The least contributing factor to the corrosion rate was observed to be the amount of test solution in the insulation when the inhibitor was used but it became the most prominent factor when inhibitor was excluded. This indicates that the effect of test solution on corrosion rate has been minimized by the inhibitor indicating its effectiveness in mitigating CUI.

7.1.3) Mapping of input parameters

In this section, a brief description of the network architecture used in estimating the degree of the relationship of input variables with the CUI rate which would form the basis of understanding the result presented herein. Detailed explanation of the ANN layout employed in the CUI rate prediction in this study have already been provided in the Fundamentals chapter. The main calculations carried out during training and actual predictions including the transfer of input data through the synapse involves only the functions used in the hidden layer. In this study, the sigmoid and hyperbolic tangent functions were used as the activation functions. These two functions were chosen based on specific characteristics which served as a good fit for corrosion data. For instance, logistic sigmoid function has domain values which are well defined across the real line plane and produces output as probabilities (0-1) which is quite useful in describing corrosion data. Similarly, the hyperbolic tangent function also has properties such as: non-linearity and wide domain values (all real numbers), but has a broader output range (-1 to 1). The prediction accuracies of these functions have been reported to be size dependent with an evidence of a reduced mean square error [17]. However, the ideal size or the minimum size required for predictive modelling has not been specified in the literature which makes the definition of sample size quite vague. In this study, a sample size of 36 was used for both the training and the prediction regimes.

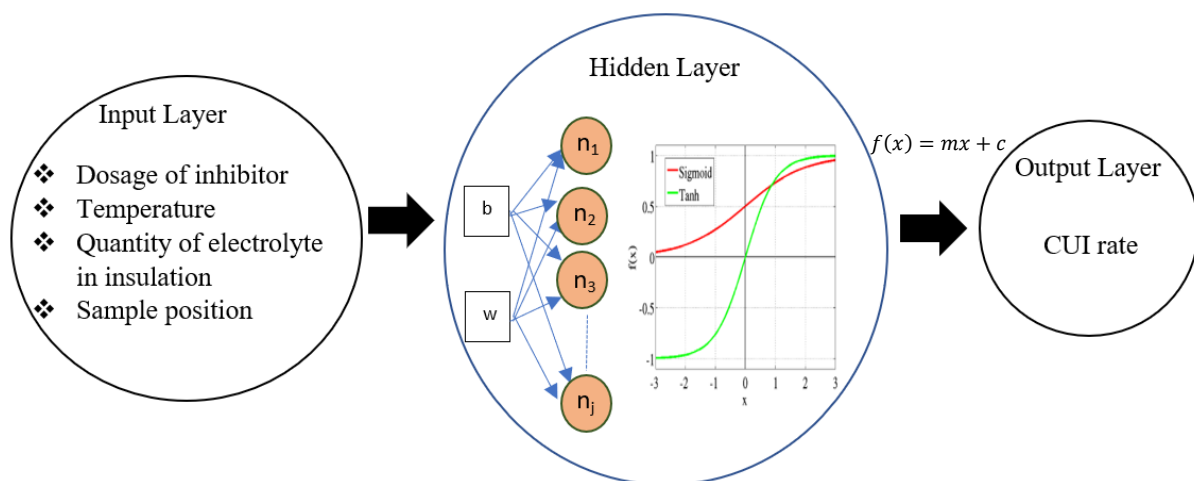


Figure 7.3 : Feedforward ANN architecture with a single hidden layer with j nodes used in this study (b =bias, w = synaptic weight, n =nodes).

Figure 7.3 shows the three important layers of ANN which include the input, hidden, and output layers. Experimental data were fed into the input layer and the network parameters were selected prior to initiation of the training program. This involved initial estimation of the output using the sigmoid and hyperbolic tangent functions on separate trials, this was followed by feeding the deviation between the predicted and experimentally determined outputs back into the hidden layer through a backpropagation mechanism. The weights and bias values were assigned to each variable and repeatedly adjusted by means of series of iterations until an accepted predefined error was obtained as shown in equations 7.1 and 7.2. Weights represent the coefficient of the equation which the model is trying to solve, while the bias is an offset used to achieve an improved generalisation of the neural network model. The magnitude of the weights is an indication of the direction of mapping in each of the nodes. The nodes in the hidden layer are connected to the input layer by blue and grey lines which is referred to as synapse. For each node in the hidden layer, the positively and negatively mapped synapses are represented by blue and grey colours respectively.

$$p(x)_{model} = f\left(\sum_{i=1}^m w_i x_i\right) + b \quad (7.1)$$

$$MSE_i = \frac{1}{N} \sum_{i=1}^N (p(x)_{experiment} - p(x)_{model})^2 \quad (7.2)$$

Where $p(x)$ is the predicted output, f represents the activation function, w_i is the synaptic weight of the i th parameter, x_i is the i th input parameter, b and m are the bias and maximum number of the input parameter respectively, MSE represents the mean square error. The mathematical expressions of the activated functions used in this study is given as:

$$\text{Logistic sigmoid function: } Sg(x) = \frac{1}{1 + e^{-x}} \quad (7.3)$$

$$\text{Hyperbolic tangent function: } \tanh(x) = \frac{1 - e^{-2x}}{1 + e^{-2x}} \quad (7.4)$$

In addition, the functions used in mapping the variables in the hidden layer to the output layer in Figure 7.3 can be a linear function or an identity function. The reason

is that the calculated variables at the hidden layer is supposed to be either a linear combination of the variables in the output layer or identical to the output variables. However, the properties of linear functions such as presence of gradient and intercept implies that there might be deviations between the calculated variables at the hidden layer and the variables at the output layer. Both linear and identity functions have real numbers in their domain but linear function produces an output (real number) which is different in value to the input variable in its domain, while identity function produces an output which is identical to the variable in its domain as shown in equations 7.5 and 7.6.

$$\text{Linear function: } f(x) = mx + c \quad (7.5)$$

$$\text{Identity function: } Id(x) = x \quad (7.6)$$

Where x represents any real number, m represents the gradient associated with the input variable, c is the intercept.

7.1.4) Relationship of the input parameters with the CUI rate

The reliability of the predicted output may likely be influenced by the degree of the relationship between the activation function and the variables in the input layer. In this study, this was estimated from the thickness of the synapse as shown in Figures 7.4 and 7.5 respectively. The results shown in Figure 7.4 indicate that the temperature, quantity of test solution in the insulation and dosage of the inhibitor had good relationships with the output as evident in the thickness of the lines. However, the sample position was observed to have faint connecting lines for both activation functions in the hidden layer which is an indication of a weak relationship with the CUI rate. These results agree with the output of the principal component analysis which mapped the dosage of the inhibitor and temperature to the component of highest significance (component 1), but only mapped the sample position to the second component without including any of the data in component 1.

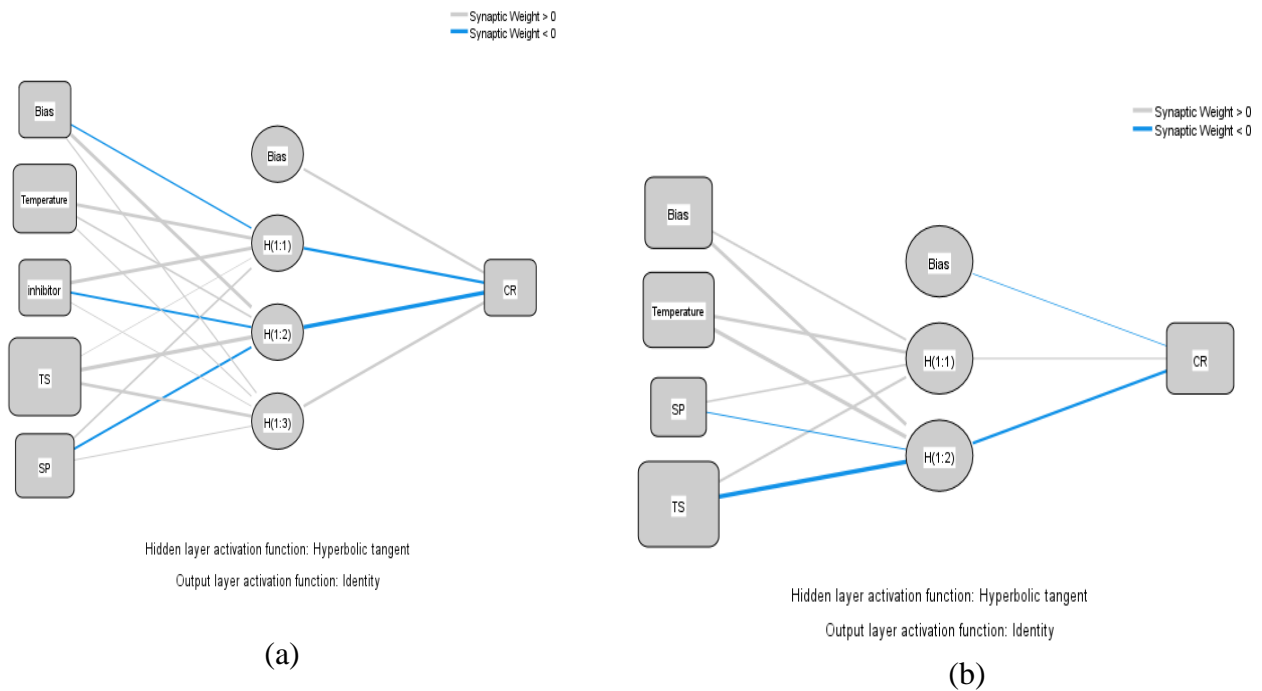


Figure 7.4 : Relationship between the input parameters and the hidden layer for hyperbolic tangent activation function (a) with inhibitor (b) without inhibitor

On the other hand, the relationship existing between the input variables and the hidden layers for a logistic sigmoid function is shown in Figure 7.5. In this figure, the synapse of the quantity of test solution in insulation at the input layer without the use of inhibitor are thicker than the synapse of the same input parameter in the presence of the inhibitor. This is also observed for hyperbolic tangent activation functions as well. This suggest that the quantity of test solution (1 wt % NaCl) in the insulation is more significant when no inhibitor is used than when inhibitor is applied to the insulation. The effect of the network architecture involving two hidden layers was also investigated and the results will be compared with a single hidden layer in subsequent section. This is aimed at determining the best criteria for improved accuracy in predicting the rate of corrosion of carbon steel under mineral wool insulation.

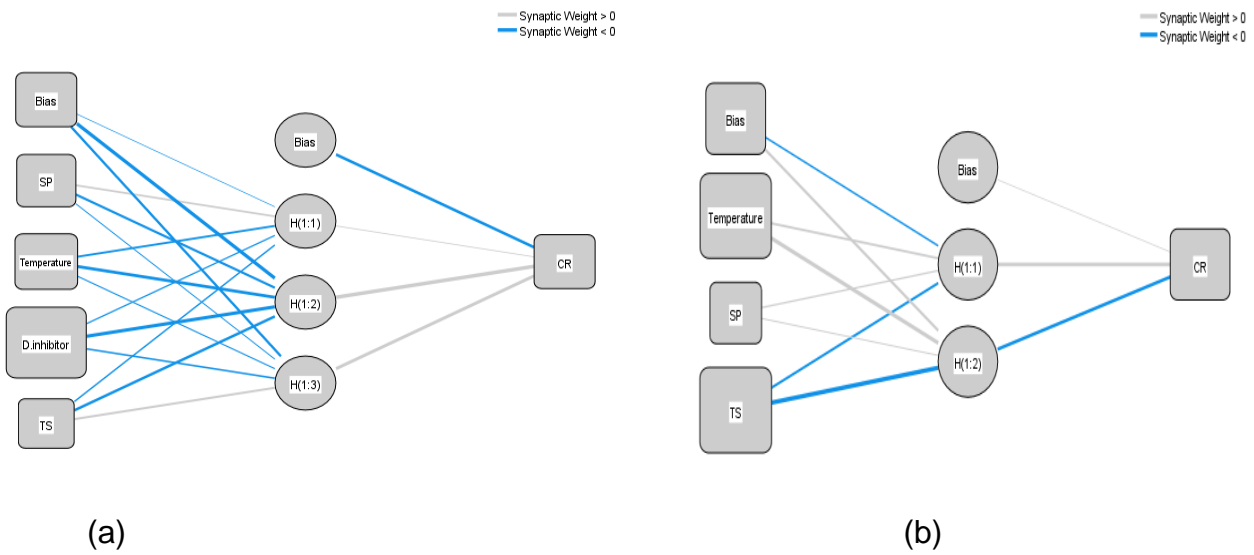


Figure 7.5 : The relationship of the input parameters at the input layer for a logistic sigmoid activation function (a) with inhibitor (b) without inhibitor

7.2) Results showing the accuracy of ANN in predicting the CUI rate of carbon steel

The prediction accuracy of ANN for the theoretical estimation of the CUI rate based on the patterns observed in the experimental data is presented and discussed in this section. For each of the studied parameters earlier mentioned, the best prediction will be decided by assessing the linearity of the predicted and experimentally determined CUI rates based on the proximity of the coefficient of determination (r^2) to 1. The closer the predicted and experimentally determined outputs, the better the prediction. This is because a perfect prediction would imply that the predicted output is equal to the experimentally determined output as shown in equation 7.7. However, corrosion rate is stochastic; hence, it is quite unrealistic to obtain an output with an ideal prediction. This implies that the network design that yields an output with a coefficient of determination (r^2) close to unity and the least prediction error would be the best design suitable for the theoretical prediction of the CUI rate. Therefore, in this section, the effect of different neural network parameters on the prediction accuracy is hereby discussed.

$$Ideal\ prediction: CUI\ rate_{model} = CUI\ rate_{experiment} \quad (7.7)$$

7.2.1) Comparison of the prediction accuracy between Logistic sigmoid and hyperbolic tangent activation functions

The accuracy of logistic sigmoid and hyperbolic tangent functions in predicting the CUI rate based on the observed pattern in the experimental data are shown in Figures 7.6 and 7.7 respectively. The logistic sigmoid function makes prediction by converting all real domain values into an output that lie between 0 and 1. This makes the interpretation of output derived from a logistic function a probability. Likewise, hyperbolic tangent function also has sigmoidal properties (s-shape) and has a domain of real numbers just like the logistic sigmoid function. However, the hyperbolic tangent function has a broader output range (-1 to 1) with a steeper derivative. These properties would suggest that both activation functions are suitable for mapping CUI data due to the nature of the output. However, corrosion rate data are always positive real numbers and though it might not be expected to differ significantly from the output of a logistic function, it has the tendency of predicting an output outside the probability range for which CUI data is based.

Figures 7.6 and 7.7 show a similar trend between the predicted and the experimentally determined outputs for both logistic and hyperbolic tangent functions. Even when the number of parameters were reduced according to the least significant parameters earlier assessed with the principal component analysis and the importance module of artificial neural network, both functions still indicated a similar trend in all cases. Also, both functions showed comparable prediction accuracies when the same number of input parameters were compared. The slight improvement in the correlation coefficient was observed with the predicted output obtained from the sigmoid function. This may be attributed to the fact that sigmoid function is strictly a probabilistic function and does not make predictions that lie outside 0 and 1, unlike a hyperbolic tangent function that has the possibility of predicting negative outputs.

Figures 7.6 (a-c) and 7.7 (a-c) have indicated an improved prediction accuracy as the number of input parameters increased as would be expected for both activation functions. The accuracy of the predicted outputs when all the four input parameters were used is much better than the accuracy of the output obtained from the two input parameters with the highest significance (7.6c and 7.7c). This suggests that the accuracy of prediction of CUI rate should not just be based on the main parameter

having the highest contribution. The gradual decrease in the prediction accuracy as the number of input parameters decreased is an indication that the rate of corrosion of metals under insulation is a consequence of a combination of different factors rather than a single or dual factors. Therefore, it might be concluded that for CUI data and other data obtained from non-linearly correlated variables, the greater the number of input parameters having some relationship with the expected output in the model, the better the prediction accuracy.

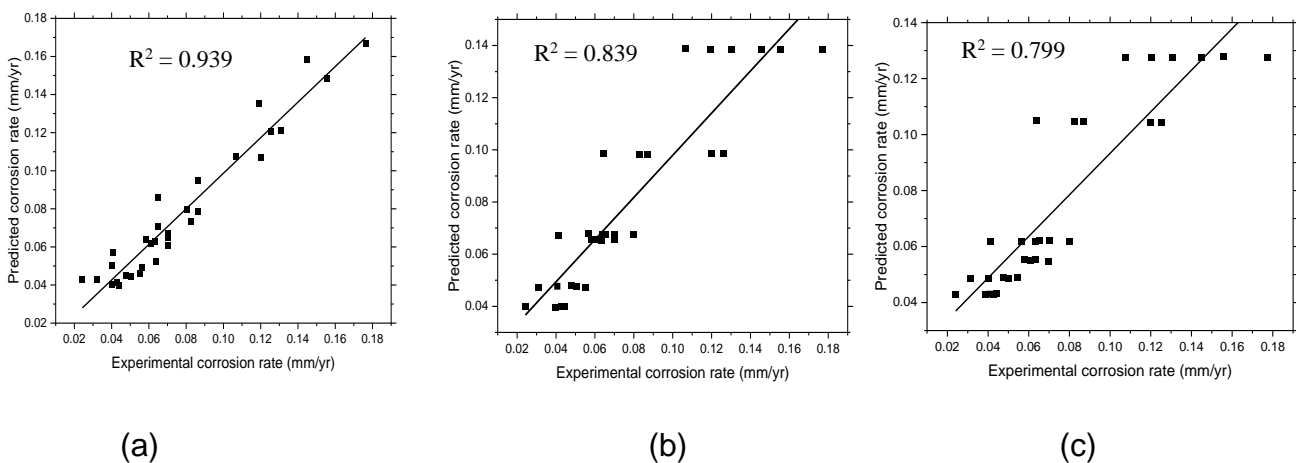


Figure 7.6: A comparison of the predicted and experimentally determined CUI rates estimated using logistic sigmoid activation function (a) 4 input parameters (DI, T, TS and SP), (b) 3 input parameters (DI, T, TS), (c) 2 input parameters (DI and T).

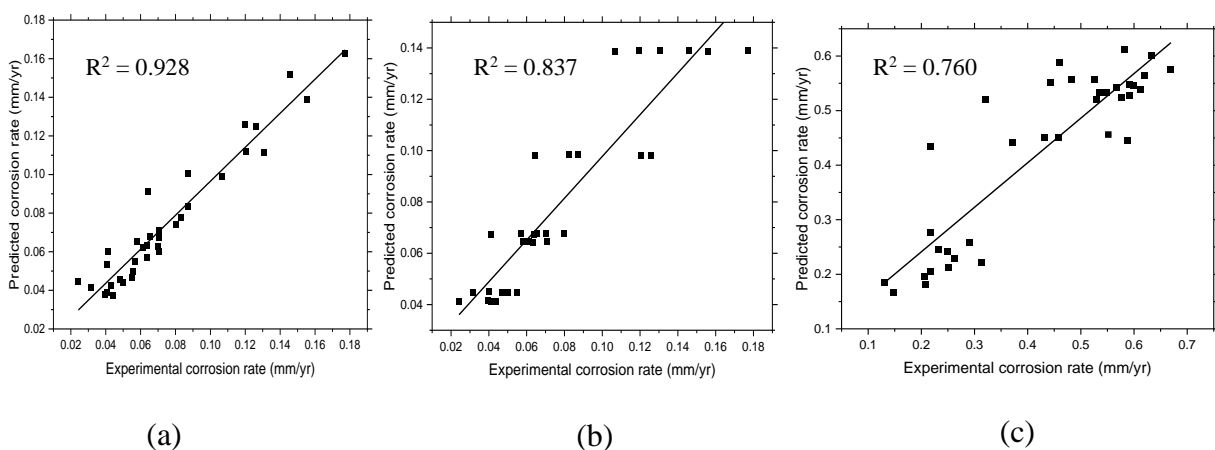


Figure 7.7 : A comparison of the predicted and experimentally determined CUI rates estimated using hyperbolic tangent activation function (a) 4 input parameters (DI, T, TS and SP), (b) 3 input parameters (DI, T, TS), (c) 2 input parameters (DI and T).

7.2.2) Effect of the network architecture on the prediction accuracy of CUI rate

In this section, the effect of a single and double hidden layers of the network architecture on the prediction accuracy of CUI rate is reported. A single and dual hidden layers were designed and introduced to the model to observe and compare the prediction abilities of both activation functions for CUI data. A single hidden layer means that both the training process and the underlying calculations behind the predictions including allocation of weights and bias to the input variables and adjustment of these values to minimize the mean square error take place within one architectural unit of the network.

On the other hand, a double hidden layer implies that the training and prediction process are carried out within two different architectural units. In this case, the information from one unit serves as the input to the next unit. In addition, the accuracy of single and dual hidden layers is likely to depend on the nature of the data as well as the data size. Most corrosion rate predictions using ANN use a single hidden layer in their model. However, it is not known whether there will be any difference in the prediction accuracy if the network architecture is changed from a single layer to a double layered architecture. Therefore, this result is intended to provide some information on the suitability of double hidden layers for CUI rate predictions, which will serve as a guide in designing predictive models for CUI. The result of this investigation is shown in Figure 7.8.

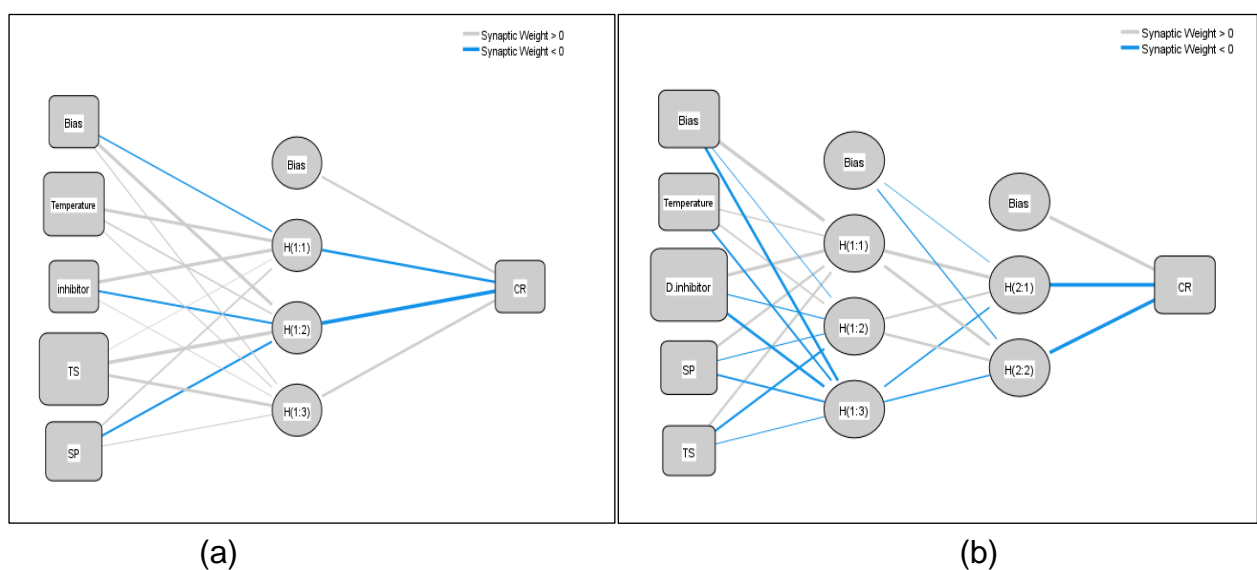


Figure 7.8 : Network architecture used in this study (a) single hidden layer and (b) double hidden layers

The prediction accuracy of single and double hidden layers in the literature has been unclear [18]. For instance, the researchers at Quest International University, Perak, Malaysia, have observed that a single layered architecture has a high accuracy of prediction of CUI rate [8], while Cai *et al.* [5] had observed that the neural network with a single hidden layer used to predict the corrosion rate of about 740 data sets was not suitable for predicting long term corrosion rate. However, both authors did not investigate the effect of using double hidden layers in their network; hence, it is not known what the accuracy would be as the comparison between both network designs for CUI has not been reported in the literature. Nevertheless, it is suspected that the number of hidden layers might have some effect on the accuracy as well as the duration of computation and may likely depend on the quantity of data sets to be analysed. Therefore, the results showing the accuracy of predictions using single and double hidden layers for both sigmoid and hyperbolic tangent activation functions are shown in Figure 7.9 and 7.10 respectively.

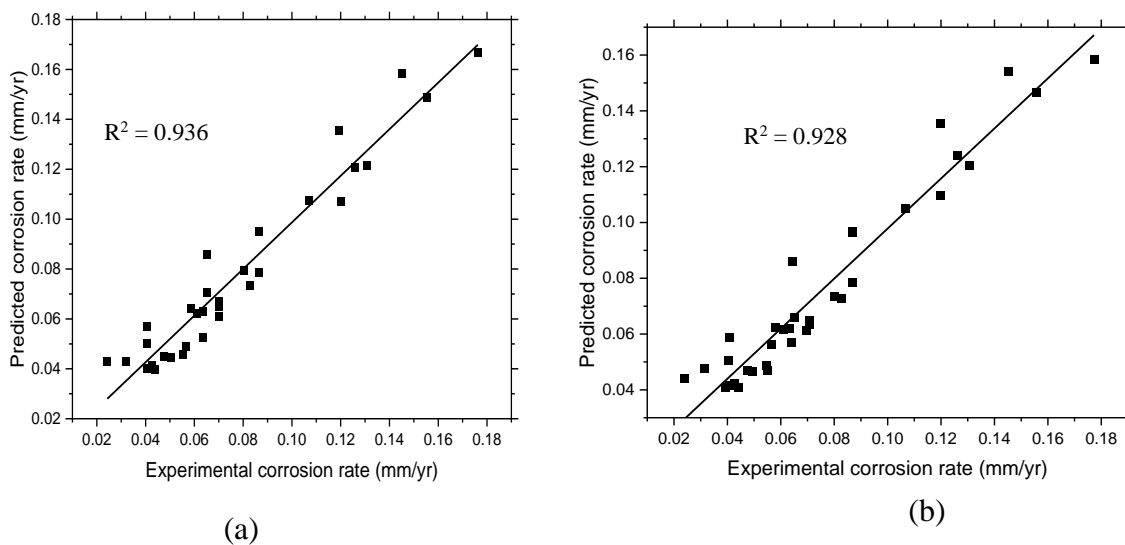
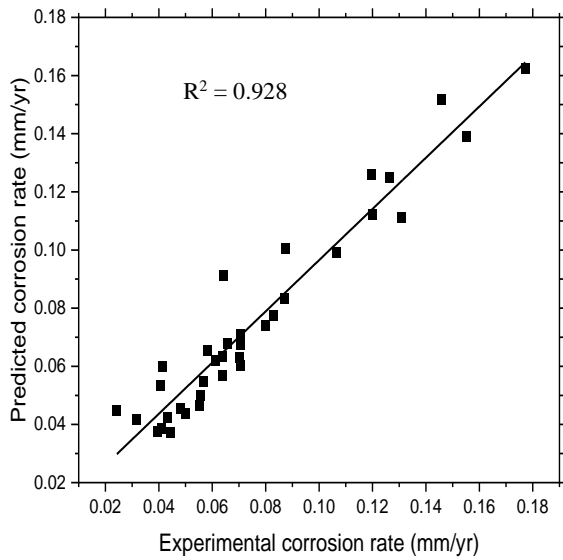
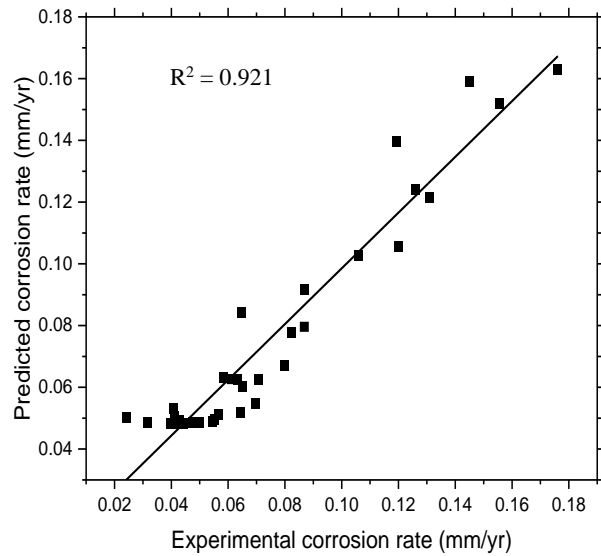


Figure 7.9 : Comparison of the prediction accuracy of (a) a single hidden layer and (b) a double hidden layer for a logistic sigmoid activation function.



(a)



(b)

Figure 7.10 : Comparison of the prediction accuracy of (a) a single hidden layer (b) a double hidden layer for a hyperbolic tangent function.

Results shown in Figures 7.9 and 7.10 representing the prediction accuracies of single and double hidden layers using a logistic sigmoid and hyperbolic tangent functions respectively show comparable prediction accuracies. The difference is about 0.3 % for a logistic function and 0.7 % for a hyperbolic tangent function which are in favour of a single layered network though this is quite negligible. The total data sets used for these predictions was 36 which was observed to have no significant difference in the prediction accuracy with increase in the number of hidden layers. In addition, Halama *et al.* [19] also reported good accuracy with predictions consisting of 59 data sets when a single hidden layer with 12 neurons was used in the network design to predict the mass loss of carbon steel as shown in Figure 7.11. Moreover, Paul [20] reported that increasing the number of neurons in the single layer could enhance prediction accuracy yielding a minimum mean square error as shown in Figure 7.12.

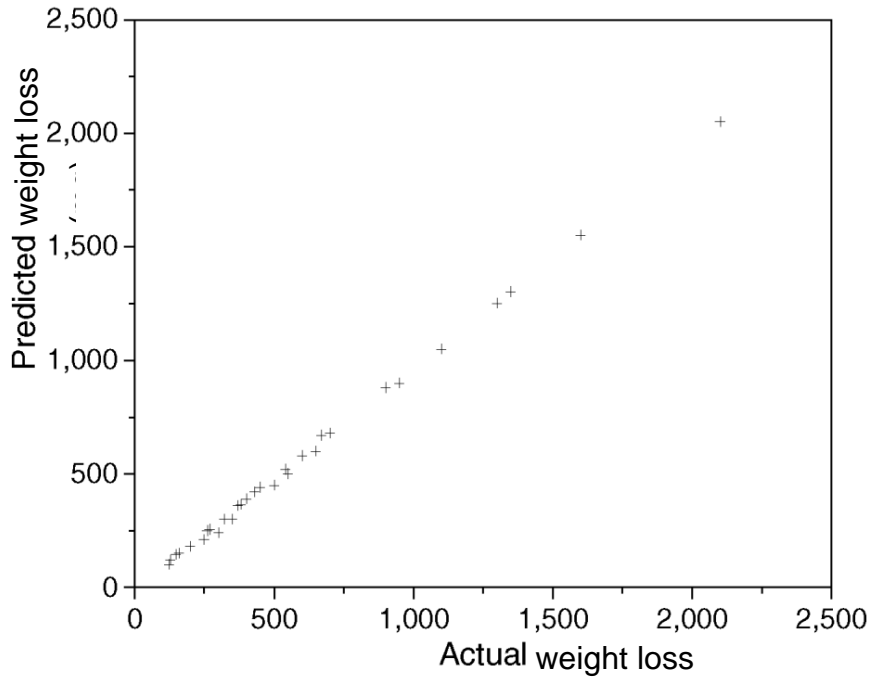


Figure 7.11 : Predicted weight loss (mg) versus actual weight loss (mg) of an atmospheric corrosion of carbon steel using 12 neurons in a single hidden layer [19].

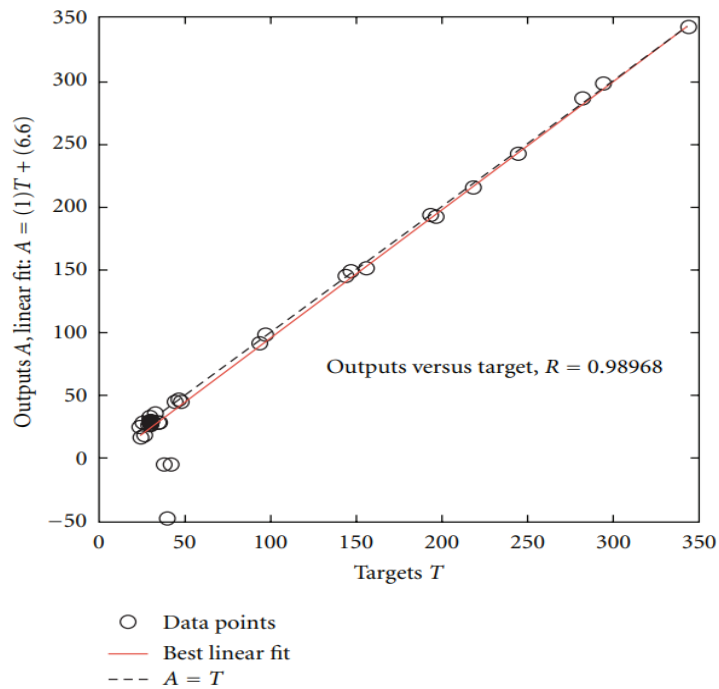


Figure 7.12 : Predicted weight loss (mg) versus target weight loss (mg) of mild steel in a marine environment [20].

However, it may not be advisable to generalize this result to a higher number of CUI data sets. This is because poor predictions have been reported for long term corrosion rate of steel (average correlation coefficient of 0.78 and average error of 0.39) carried out with about 740 data sets using just a single hidden layer in its network design [5]. Comparison of prediction accuracy of ANN with other machine languages for the prediction of corrosion rate of carbon steel using large number of data in just a single hidden layer showed the highest mean square error compared to other machine language programs [21]. This also agrees with the results of Almomani *et al.* [22] who observed an accuracy of 63.2 % when large experimental data was modelled using a single hidden layer architecture to predict the corrosion rate of carbon steel (Figure 7.13).

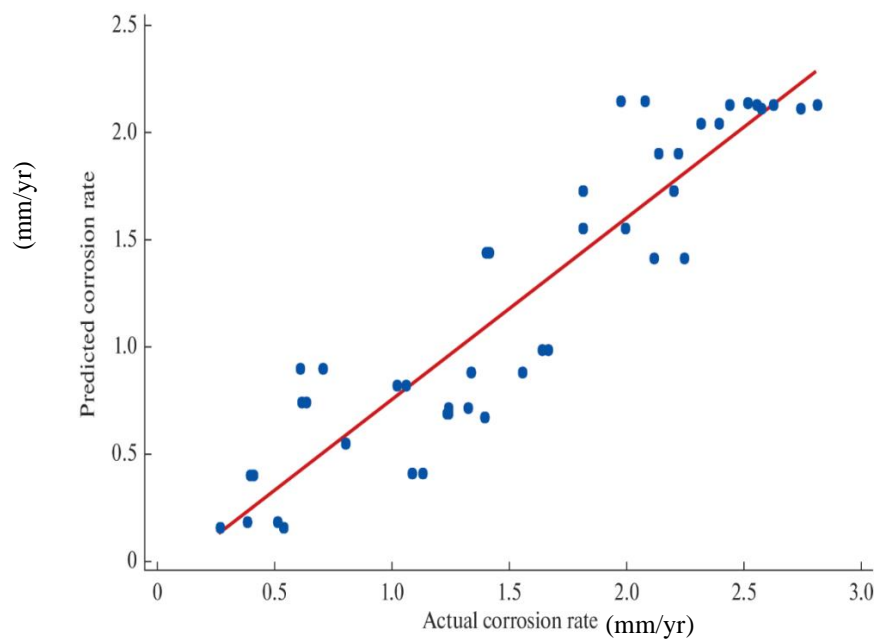


Figure 7.13 : Predicted and actual corrosion rates of carbon steel (mm/yr) using ANN [22].

Therefore, for data sets having at most the same size as what is used in this study, it would be preferable to use a single layered network rather than double hidden layers as it is more time efficient and shows similar accuracy of prediction. In addition, it is important to note that for both activation functions, the coefficient of determination is

not unity which suggests that it is not a perfect fit. This suggests that there is still need for improvement of accuracy of prediction which could be obtained by adding more input parameters that influences CUI.

7.3) Precision of the predicted CUI rate using ANN

In this section, the results showing the ability of ANN to make precise CUI rate predictions over repeated trials is presented for the first time. The corrosion rate predictions using artificial neural network in the literature are mostly based on a one-off prediction and the analysis of the predicted output is primarily focused on the accuracy of prediction [23], rather than consistency in making similar predictions over repeated trials. For a model to be reliable especially in a highly sensitive field such as corrosion studies, it is important that the model makes consistent repetitive predictions even though there might be slight difference in the predicted values, which is expected to be as minimized as possible. The slight difference is expected from the fact that the data sets used for training and actual prediction are sampled differently each time and might lead to slight difference in the outputs. In this study, the precision of ANN for CUI data was assessed over triplicate trials for both logistic and hyperbolic tangent functions, the results are shown in Figures 7.14 and 7.15 respectively.

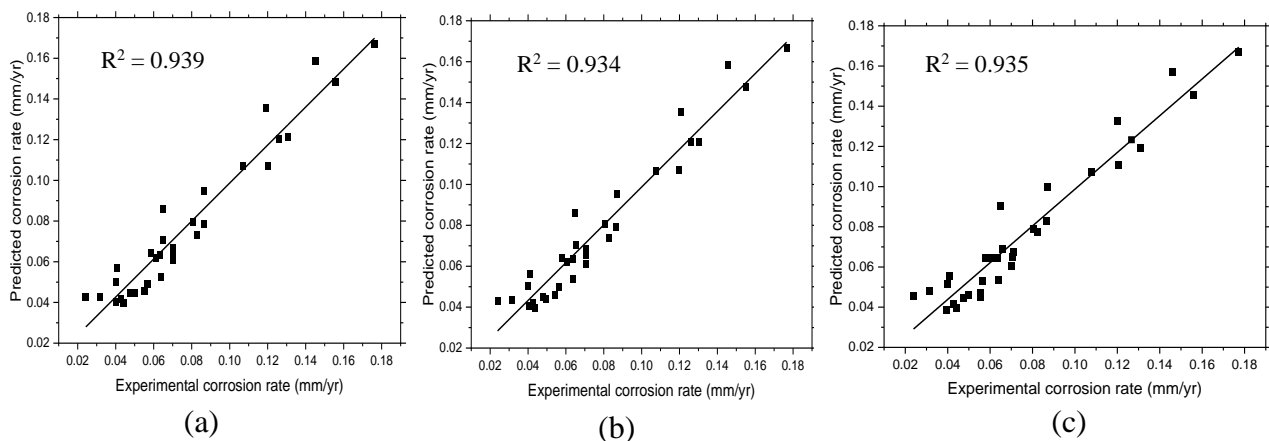


Figure 7.14 : Repeatability of the CUI rate prediction using logistic sigmoid activation function with one hidden layer.

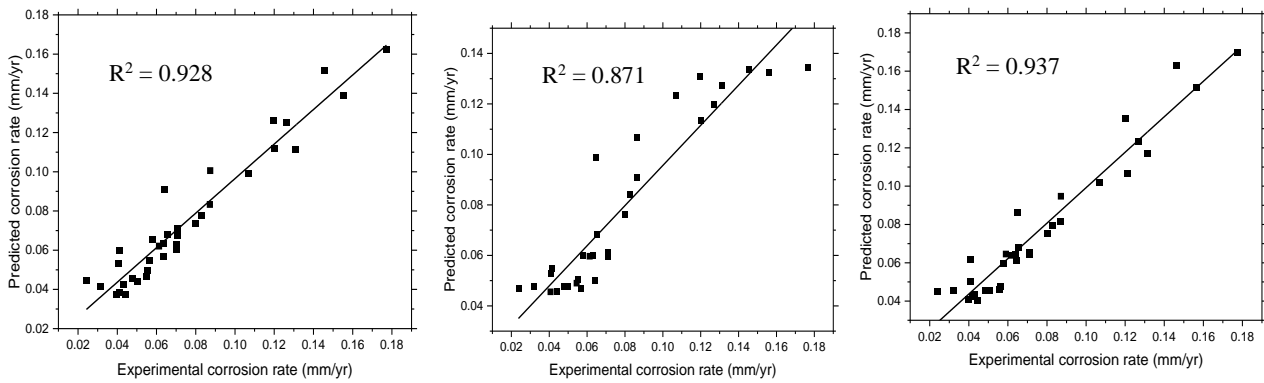


Figure 7.15 : Repeatability of the CUI rate prediction using a hyperbolic tangent activation function with one hidden layer.

Table 7.3 : Summary of studied parameters and the corresponding coefficient of determination

Parameters studied		Type of activation function	
		Sg(x)	Tanh(x)
Decreasing number of input parameters	4(DI, T, TS, SP)	0.939	0.928
	3(DI, T, TS)	0.839	0.857
	2(DI, T)	0.799	0.760
Number of hidden layers	Single	0.936	0.928
	Double	0.928	0.921
Repeatability	Trial 1	0.939	0.928
	Trial 2	0.934	0.871
	Trial 3	0.935	0.937

Sg(x): logistical sigmoid function, tanh(x): hyperbolic tangent function

The results of the triplicate predictions for both activation functions are quite consistent for both functions apart from the second repeated prediction using hyperbolic tangent activation function which seems more reduced compared to the rest of the outputs. The fact that the precision of prediction does not decrease sequentially according to the number of repetitions implies that the input data are randomly selected for training and test purposes. Nevertheless, the precision of logistic sigmoid activation function was better than hyperbolic tangent function. This could be attributed to the narrow range of logistic sigmoid function that is restricted to the probability range compared

to hyperbolic tangent function that has the tendency of predicting negative outputs which is not characteristic of corrosion data.

7.4) Conclusions

In this study, the ability of artificial neural network to predict the rate of corrosion of carbon steel under mineral wool insulation was assessed. This was based on the patterns observed between the studied input parameters which included the temperature of the pipe, quantity of electrolyte in the insulation, dosage of the inhibitor and positional arrangements of the metal samples. The studied data was first screened using principal component analysis tool of SPSS and the importance module of ANN to ensure that the input parameters have some relationship with the expected output. In both cases, the results indicated that dosage of the inhibitor and temperature had the strongest relationship, while the sample position had the lowest relationship. The correlation of quantity of electrolyte in the insulation with CUI rate was observed to be prominent when no inhibitor was used. However, in the presence of an inhibitor, the effect of quantity of electrolyte in the insulation with CUI rate had the lowest importance indicating the effectiveness of the inhibitor in mitigating CUI.

Some modelling parameters such as effect of number of input variables, single and double hidden layers as well as the choice of activation function which are known to affect the prediction accuracy of ANN in other applications and have never been studied using CUI data in the literature have been reported in this study. The results indicated an increase in the accuracy of prediction as the number of input parameters increased for both logistic and hyperbolic tangent activation functions. The prediction involving the four parameters had a better fit than the plot involving the two most significant parameters (temperature and dosage of inhibitor). This suggests that for CUI data, the accuracy of prediction is enhanced by including more variables responsible for corrosion of insulated metals rather than restricting the analysis to parameters with the highest importance only. This is because corrosion under insulation is a result of the cumulative effect of different variables rather than a single independent variable.

In addition, there was no significant difference between the predictions obtained from a single hidden layer and the output obtained from two hidden layers for the data size of 36 used in this study. It seems that the choice of number of hidden layers depend on the size of the input parameters. It has been reported in the literature that for large data size, it is advisable to use double hidden layers with multiple nodes instead of a single layer [24]. Therefore, it would be advisable to choose a single hidden layer for small number of data sets as this is more time efficient than double hidden layers.

The ability of artificial neural network to make precise CUI predictions over replicate trials was assessed for the first time. This is quite important in assessing the reliability of a model for corrosion rate predictions. In this study, there was only a slight improvement in the prediction accuracy obtained from logistic sigmoid activation function compared to the hyperbolic tangent function. This may be attributed to the fact that the logistic function is strictly restricted to outputs in the probability range and the CUI data used for the study was restricted to this range rather than the output range of the hyperbolic tangent function which includes negative numbers. However, a significant variation in precision was observed between the outputs of the logistic function and hyperbolic tangent function. For triplicate trials carried out to assess the repeatability of prediction, the output of logistic sigmoid function was more precise than the hyperbolic tangent function. This may likely be attributed to the narrow range of output of sigmoid function compared to the hyperbolic tangent function. However, this may not apply to other types of data as accuracy and precision of predicted output is influenced by the nature of input data, and the choice of the network parameters is important in obtaining the predicted output with a high accuracy and precision.

Therefore, this study indicates that the inclusion of more input parameters that have some relationship with the CUI rate in an ANN model built with a single hidden layer architecture for small data set less than or equal to the number used in this study (36) and a sigmoid activation function would yield a good and reproducible output that can be used to take proactive measures to prevent sudden failure of insulated metals in industry.

References

1. Mokhtar, A. A., Ismail, M. C., Zainordin, A. B., and Shahid, S. (2014). A framework for estimating piping reliability subject to corrosion under insulation. *MATEC web of conferences*, 13:1-5.
2. Caines, S., Khan, F. and Shirokoff, J. (2013). Analysis of pitting corrosion on steel under insulation in marine environments. *Journal of Loss Prevention in the Process Industries*, 26(6):1466-1483.
3. Erickson, T. H., Dash, L. C., Murali, J. J. and Ayers, R. (2010). Predicting the progression of wetness and corrosion under insulation damage in above ground pipelines. NACE publications, paper number 10373.
4. Pei, Z., Zhang, D., Zhi, Y., Yang, T., Jin, L., Fu, D., Cheng, X., Terry, H. A., Mol, J. M. C. and Li, X. (2020). Towards understanding and prediction of atmospheric corrosion of an Fe/Cu corrosion sensor via machine learning. *Corrosion Science*, 170(108697):1-9.
5. Cai, J., Cottis, R. A. and Lyon, S. B. (1999). Phenomenological modelling of atmospheric corrosion using an artificial neural network. *Corrosion Science*, 41:2001-2030.
6. El-Abassy, M., Senouci, A., Zayed, T., Mirahadi, F., Parvizsedghy, L. (2014). Artificial neural network models for predicting condition of offshore oil and gas pipelines. *Automation in Construction*, 45:50-65.
7. Cottis, R. A., Qing, L., Owen, G., Gartland, S. J., Helliwell, I. A. and Turega, M. (1999). Neural network methods for corrosion data reduction. *Materials and Design*, 20(4): 169-178.
8. Burhani, N. R. A., Muhammad, M. and Rosli, N. S. (2019). Combined experimental and field data sources in a prediction model for corrosion rate under insulation. *Sustainability*, 11(6853):1-13.
9. Chen, Z., Li, X., Wang, W., Li, Y., Shi, L. and Li, Y. (2023). Residual strength prediction of corroded pipelines using multilayer perceptron and modified feedforward neural network. *Reliability Engineering and System Safety*, 231:108980.

10. Thicke, P. H., Zhao, Z., Liu, P., Bao, F., Jin, Y. and Shi, P. (2020). An early stopping based artificial neural network model for atmospheric corrosion prediction of carbon steel. *Computers, Materials and Continua*, 65(3):2091-2109.
11. Wang, C., Li, W., Wang, Y., Yang, X., and Xu, S. (2020). Study of electrochemical corrosion on Q235A steel under stray current excitation using combined analysis by electrochemical impedance spectroscopy and artificial neural network. *Construction and Building Materials*, 247(118562):1-15.
12. Gandia, J. M., Monzon, P., Bataller, R., Campos, I., Lloris, J. M. and Soto, J. (2015). Principal component analysis applied to the study of carbon steel electrochemical corrosion. *The International Journal of Corrosion Processes and Corrosion Control*. 50(4):320-329.
13. Jolliffe, I. T. (2002). Principal component analysis, 2nd edition, Springer-Verlag, New York, pp. 1-477.
14. Ossai, C. I. (2019). A data-driven machine learning approach for corrosion risk assessment-A comparative study. *Big Data and Cognitive Computing*, 3(28):1-22.
15. Kaiser, H. F. (1991). Coefficient alpha for a principal component and the kaiser-guttman rule, *Psychological Reports*, 68:855-858.
16. Ferre, L. (1995). Selection of components in principal component analysis: A comparison of methods. *Computational Statistics and Data Analysis*, 19:669-682.
17. Ajiboye, A. R., Abdullah-Arshah, R., Qin, H. and Isah-Kebbe, H. (2015). Evaluating the effect of dataset size on predictive model using supervised learning technique. *International Journal of Software Engineering & Computer Sciences*, 1:75-84.
18. Khadom, A. A. and Mahdi, M. S. (2020). Mathematical regression and artificial neural network for prediction of corrosion inhibition process of steel in acidic media. *Journal of Bio- and Tribo-Corrosion*, 6(92):1-10.

19. Halama, M., Kreislova, K. and Leisbettens, J. V. (2011). Prediction of atmospheric corrosion of carbon steel using artificial neural network model in geographical regions. *Corrosion*, 67(6):1-6.
20. Paul, S. (2012). Modelling to study the effect of environmental parameters on corrosion of mild steel in seawater using neural network. *International Scholarly Research Network Metallurgy*, 2012:1-6.
21. Aghaaminiha, M., Mehrani, R., Colahan, M., Brown, B., Singer, M., Nestic, S., Vargas, S. M. and Sharma, S. (2021). Machine learning modelling of time-dependent corrosion rates of carbon steel in the presence of corrosion inhibitors. *Corrosion Science*, 193(109904):1-12.
22. Almomani, M. A., Momani, A. M., Abdelnabi, A. A. B., Al-Zqebah, R. S. and Al-Batah, M. S. (2022). Predicting the corrosion rate of medium carbon steel using artificial neural networks. *Protection of Metals and Physical Chemistry of Surfaces*, 58(2):414-421.
23. Kenny, E. D., Paredes, R. S.C., de Lacerda, L. A., Sica, Y. C., de Souza, G. P. and Lazaris, J. (2009). Artificial neural network corrosion modelling for metals in an equatorial climate. *Corrosion Science*, 51:2266–2278.
24. Li, Q., Wang, D., Zhao, M., Yang, M., Tang, J. and Zhou, K. (2021). Modelling the corrosion rate of carbon steel in carbonated mixtures of MDEA-based solutions using artificial neural network. *Process Safety and Environmental Protection*, 147:300-310.

CHAPTER 8: CONCLUSIONS AND FUTURE WORK

CHAPTER 8

CONCLUSIONS AND FUTURE WORK

8.1) Conclusions

The investigation of corrosion of carbon steel under mineral wool insulation included water absorption studies, effects of temperature, effectiveness of inhibitor in mitigating CUI, the distribution of electrolyte in the insulation, an assessment of the drying out times using galvanic current and impedance measurements as well as predictive modelling of the CUI rate using Artificial Neural Network. The water absorption studies were carried out to determine the time it will take for the insulation to be saturated with water as well as the variability associated with replicate measurements. Results indicated an increased absorption of water when the insulation was thermally treated at 250 °C compared to the untreated samples. This showed a continuous absorption over a 22-day period without saturation which agrees with the report of Williams and Evans (2010) who did not also observe any saturation after immersing the insulation in water for 60 days. The trials were quite variable as observed in the replicate trials which may likely be related to the properties of the insulation.

The effect of temperature on corrosion of carbon steel under insulation was assessed from 60 °C to 130 °C. Results indicated an increase in the corrosion rate with temperature up to 80 °C, further increase in temperature resulted in a decrease in the corrosion rate. The existence of a maximum point at 80 °C may be attributed to the competing effects of increased diffusion of oxygen which dominates at low temperature resulting in an increased corrosion rate with temperature and the decreasing solubility of oxygen and insulation dry out at higher temperatures resulting in a decreasing corrosion rate. The study revealed that carbon steel under insulation was still corroding at a lower rate at temperatures above 100 °C which might be as a result of the presence of water vapour within the insulation. A new commercial inhibitor (VpCl 619) consisting primarily of sodium molybdate was used to test the effectiveness in mitigating CUI. The results indicated good inhibition efficiency of 89 % when 5.2 g/m² dosage was used. The inhibition efficiency was observed to decrease when the dosage was decreased to 1.3 g/m². This suggests the need to maintain adequate

balance between the cost and effectiveness of protection when choosing an inhibitor for insulation.

In addition, it was found that the distribution of electrolyte in the insulation was not uniform. The bottom part of the insulation was observed to hold more test solution than the top parts resulting in more corrosion at the bottom compared to the top. This resulted in an increased corrosion rate at the bottom part of the rings. A new method to assess the insulation dry out using galvanic current measurements was investigated. The results indicated an initial increase in the galvanic current due to an increase in temperature up to the target temperature. Variable trends were observed when the temperature stabilized but decreases to 0 as the insulation dries out due to an increased solution resistance. This method was compared with the electrochemical impedance method where the results showed an initial decrease in impedance as the temperature increases to the target value due to an increased conductivity of the solution as the temperature increases. The impedance tends to stabilize as the temperature reaches the target value but starts increasing as the insulation also starts drying out which may be attributed to an increased solution resistance. Both methods showed a decrease in the drying times as the temperature is increased. However, the measurement of drying times by the impedance method was more reproducible compared to the galvanic current method which may be attributed to the sensitivity of the galvanic current method to slight changes in the degree of contact of the insulation with the metal rings for each trial.

The prediction of corrosion under insulation using Artificial Neural Network was carried out to assess the accuracy and precision of predictions which might indicate its suitability in predicting outcomes of CUI conditions. The effects of different modelling parameters such as number of hidden layers, choice of activation function and number of input parameters on the accuracy of prediction were assessed for the first time for CUI data. The results indicated that accuracy of prediction depends on the number of input parameters having some relationship with the predicted CUI rate. The four parameters included in the model had the highest accuracy compared to reduced number of input variables. Interestingly, it was observed that even the model involving variables having the highest importance on the CUI rate had a lower prediction accuracy compared to the model having the four input parameters. This suggests that

the more the input parameters having some relationship with the estimated output, the better the prediction accuracy. In addition, increasing the number of hidden layers seems not to have any effect on the CUI rate due to the small number of input data (36). However, a higher number of input data may likely show different results as including too many data in a single hidden layer will make the network clumsy which may affect the prediction accuracy.

8.2) Future works

The following are suggestions for future works that would expand the work further.

- ❖ Investigation of effect of different pH of electrolyte on CUI rate: The corrosion rate can also be affected by changes in pH of the test solution. Therefore, it would be important to assess the effectiveness of the inhibitor or monitoring the effect of temperature on the corrosion of insulated assets at a different pH to what is reported in this study.
- ❖ Investigation of the drying out of the insulation at a different frequency using electrochemical impedance measurements: This study assessed the drying out of the insulation at a frequency of 1kHz. It would be interesting to assess the response of the electrochemical impedance measurements at a higher frequency and a different scan rate.
- ❖ Inclusion of drying times and pH in the prediction model of ANN to assess the accuracy of prediction: In this study, the drying out of the mineral wool insulation was measured without measuring the corresponding corrosion rate. It would be interesting to measure the corrosion rate as the insulation dries out which could be used in the prediction model to assess the contribution of insulation dry out to the overall corrosion rate.
- ❖ Investigation of the penetration rate of water through mineral wool fibres using EIS or any other suitable technique: The penetration rate would provide more information on how fast the water or test solution was absorbed by the insulation. This could be useful in assessing the quality of the insulation as well as the risks or damage to the underlying equipment.

APPENDICES

Appendix A: Effects of temperature on CUI rate of carbon steel: This data includes the effect of temperature on the corrosion rate of each of the metal ring samples from 60 °C to 130 °C. Ring 1 represents the inlet ring where the silicone oil enters the rig, while ring 6 represents the outlet ring where the oil leaves the rig.

Table A.1: Corrosion rate of the six carbon steel rings at 60 °C

Ring Position	Corrosion rate (mm/yr)					
	Trial 1	Trial 2	Trial 3	Trial 4	Average	SD (1 σ)
R1	0.21	0.13	0.07	0.18	0.148	0.059
R2	0.15	0.23	0.32	0.14	0.209	0.085
R3	0.14	0.17	0.41	0.10	0.206	0.138
R4	0.28	0.20	0.27	0.26	0.252	0.034
R5	0.26	0.27	0.38	0.16	0.266	0.090
R6	0.21	0.24	0.27	0.22	0.233	0.026

Table A. 2: Corrosion rate of the six carbon steel rings at 70 °C

Ring Position	Corrosion rate (mm/yr)					
	Trial 1	Trial 2	Trial 3	Trial 4	Average	SD (1 σ)
R1	0.28	0.39	0.30	0.32	0.320	0.049
R2	0.41	0.76	0.64	0.51	0.579	0.149
R3	0.52	0.61	0.50	0.50	0.536	0.051
R4	0.51	0.74	0.64	0.56	0.613	0.097
R5	0.35	0.80	0.63	0.61	0.598	0.183
R6	0.32	0.50	0.50	0.47	0.445	0.084

Table A.3: Corrosion rate of the six carbon steel rings at 80 °C

Sample ID	Corrosion rate (mm/yr)					
	Trial 1	Trial 2	Trial 3	Trial 4	Average	SD (1 σ)
R1	0.46	0.37	0.62	0.67	0.528	0.137
R2	0.51	0.69	0.80	0.49	0.621	0.148
R3	0.76	0.81	0.60	0.50	0.670	0.142
R4	0.66	0.52	0.23	0.44	0.463	0.180
R5	0.93	0.58	0.58	0.44	0.635	0.210
R6	0.94	0.25	0.73	0.42	0.584	0.309

Table A. 4: Corrosion rate of the six carbon steel rings at 95 °C

Ring Position	Corrosion rate (mm/yr)					
	Trial 1	Trial 2	Trial 3	Trial 4	Average	SD (1 σ)
R1	0.43	0.46	0.68	0.54	0.531	0.108
R2	0.58	0.70	0.58	0.50	0.593	0.078
R3	0.47	0.56	0.51	0.66	0.550	0.084
R4	0.58	0.56	0.56	0.56	0.568	0.011
R5	0.68	0.48	0.59	0.61	0.593	0.081
R6	0.42	0.56	0.49	0.47	0.486	0.057

Table A.5: Corrosion rate of the six carbon steel rings at 110 °C

Ring Position	Corrosion rate (mm/yr)					
	Trial 1	Trial 2	Trial 3	Trial 4	Average	SD (1 σ)
R1	0.16	0.28	0.20	0.23	0.172	0.048
R2	0.07	0.47	0.50	0.44	0.372	0.200
R3	0.32	0.67	0.59	0.78	0.589	0.195
R4	0.10	0.69	0.53	0.50	0.459	0.255
R5	0.28	0.19	0.48	0.77	0.431	0.256
R6	0.47	0.42	0.76	0.56	0.553	0.150

Table A.6: Corrosion rate of the six carbon steel rings at 130 °C

Ring Position	Corrosion rate (mm/yr)					
	Trial 1	Trial 2	Trial 3	Trial 4	Average	SD (1 σ)
R1	0.07	0.16	0.13	0.16	0.13	0.042
R2	0.18	0.24	0.24	0.21	0.22	0.030
R3	0.33	0.34	0.31	0.27	0.31	0.027
R4	0.35	0.23	0.19	0.22	0.25	0.068
R5	0.38	0.25	0.22	0.31	0.29	0.070
R6	0.22	0.21	0.22	0.21	0.21	0.009

Appendix B: Effectiveness of VpCl 619 inhibitor at different temperatures: The data shown in Table B1 represents the measured corrosion rates in the presence of 5.2g/m² of the inhibitor. The inhibition efficiency was computed using the equation below:

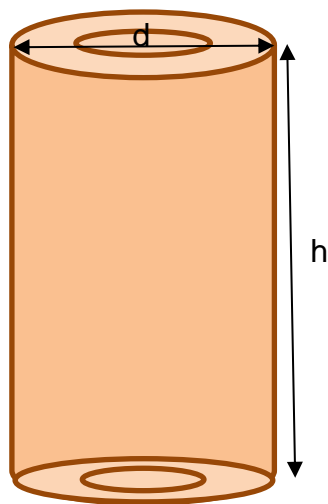
$$\text{Inhibition Efficiency (I.E.)}(\%) = \frac{CR_o - CR}{CR_o} \times 100$$

CR_o is the corrosion rate (mm/yr) without the use of inhibitor and CR is the corrosion rate (mm/yr) in the presence of the inhibitor.

Table B.1: Effectiveness of inhibitor at 80 °C

Corrosion rate (mm/yr) and inhibition efficiencies at different temperatures												
R. P	80 °C			95 °C			110 °C			130 °C		
	CR _o	CR	I.E (%)	CR _o	CR	IE (%)	CR _o	CR	I.E (%)	CR _o	CR	I.E (%)
1	0.52	0.08	84.8	0.53	0.07	86.7	0.21	0.04	81.3	0.13	0.02	81.6
2	0.62	0.06	89.4	0.59	0.07	88.1	0.37	0.05	85.1	0.21	0.04	80.2
3	0.67	0.07	89.5	0.55	0.06	89.4	0.58	0.05	90.7	0.31	0.04	86.9
4	0.46	0.04	91.1	0.56	0.06	88.8	0.45	0.04	89.6	0.24	0.04	83.5
5	0.63	0.06	89.9	0.59	0.06	89.7	0.43	0.05	88.3	0.29	0.04	86.3
6	0.58	0.05	90.2	0.48	0.07	85.5	0.55	0.03	94.2	0.21	0.04	79.5

Appendix C: Calculation of dosage of inhibitor: The dosage of the inhibitor was calculated as follows:



$$\text{Area of cylinder } (A) = 2\pi r(r + h), r = 0.5 \times d$$

$$\text{Density of inhibitor } (\rho) = \frac{\text{mass}(g)}{\text{volume } (l)}$$

$$\text{Volume of inhibitor required to cover the calculated area } A = \frac{1L \times A_{cal.}(m^2)}{A_{sp}(m^2)}$$

A_{cal.} Is the calculated area of the insulation, A_{sp} is the specified area in the product data sheet.

Appendix D: Effect of dosage of inhibitor on CUI of carbon steel: The results showing the effects of different dosages of the inhibitor ranging from 1.3 g/m², 3.6 g/m² and 5.2 g/m² are shown in Table D1 to D3 respectively.

Table D.1: Effectiveness of inhibitor at 1.3 g/m² at 80 °C

Ring Position	Corrosion rate (mm/yr)					
	Trial 1	Trial 2	Trial 3	Trial 4	Average	SD (1 σ)
R1	0.08	0.10	0.08	0.05	0.080	0.019
R2	0.05	0.09	0.06	0.05	0.065	0.018
R3	0.07	0.08	0.08	0.04	0.070	0.017
R4	0.04	0.05	0.06	0.02	0.041	0.015
R5	0.03	0.07	0.1	0.06	0.064	0.027
R6	0.04	0.09	0.05	0.04	0.057	0.026

Table D.2: Effectiveness of inhibitor at 2.6 g/m² at 80 °C

Ring Position	Corrosion rate (mm/yr)					
	Trial 1	Trial 2	Trial 3	Trial 4	Average	SD (1 σ)
R1	0.16	0.11	0.12	0.11	0.126	0.021
R2	0.14	0.11	0.13	0.10	0.120	0.016
R3	0.08	0.09	0.09	0.09	0.087	0.007
R4	0.08	0.05	0.07	0.06	0.064	0.010
R5	0.15	0.08	0.06	0.06	0.087	0.040
R6	0.08	0.07	0.10	0.08	0.083	0.016

Table D.3: Effectiveness of inhibitor at dosage of 5.2 g/ m² at 80 °C

Ring Position	Corrosion rate (mm/yr)					
	Trial 1	Trial 2	Trial 3	Trial 4	Average	SD (1 σ)
R1	0.17	0.18	0.18	0.17	0.177	0.004
R2	0.18	0.14	0.14	0.12	0.145	0.024
R3	0.18	0.14	0.13	0.17	0.155	0.026
R4	0.13	0.13	0.11	0.10	0.120	0.015
R5	0.13	0.13	0.13	0.13	0.131	0.002
R6	0.13	0.10	0.10	0.09	0.107	0.018

Appendix E: Measurement of Drying times using galvanic current and impedance measurements: The drying times of the insulation at different temperatures for both galvanic current and electrochemical impedance methods are presented in Tables E1 and E2 respectively.

Table E.1 comparison of drying times between galvanic current and impedance methods

	Temperature (°C)	Replicates	t ₀ (seconds) (0%) × 10 ³	t ₁ (seconds) (50%) × 10 ³	t ₂ (seconds) (90%) × 10 ³
Galvanic Current Method	70	Trial 1	25.014	27.160	28.154
		Trial 2	12.059	26.112	33.599
		Trial 3	8.039	16.098	22.095
	80	Trial 1	11.642	20.891	24.249
		Trial 2	12.313	21.035	24.168
		Trial 3	21.321	22.767	24.367
	90	Trial 1	11.686	15.915	17.918
		Trial 2	15.000	17.266	19.223
		Trial 3	13.588	14.384	14.985
	100	Trial 1	10.571	13.294	15.654
		Trial 2	7.598	9.577	17.241
		Trial 3	11.151	15.617	16.127
110	Trial 1	13.495	14.351	14.997	
	Trial 2	12.112	13.720	14.571	
	Trial 3	12.897	14.668	15.681	
Electrochemical Impedance Method	70	Trial 1	25.014	27.160	28.154
		Trial 2	16.059	26.112	33.599
		Trial 3	15.039	16.098	22.095
	80	Trial 1	11.642	20.891	24.249
		Trial 2	12.313	21.035	24.168
		Trial 3	21.321	22.767	24.367
	90	Trial 1	11.686	15.915	17.918
		Trial 2	15.000	17.266	19.223
		Trial 3	13.588	14.384	14.985
	100	Trial 1	10.571	13.294	15.654
		Trial 2	7.598	9.577	17.241
		Trial 3	11.151	15.617	16.127
110	Trial 1	13.495	14.351	14.997	
	Trial 2	12.112	13.720	14.571	
	Trial 3	12.897	14.668	15.681	

Appendix F: List of conference presentations

1. John B. Edet, Todd Green and Sudipta Roy (2018). Investigation of the water absorption profile of mineral wool insulation. A poster presentation at the

Research Day celebration at Chemical and Process Engineering, University of Strathclyde.

2. John B. Edet, Todd Green and Sudipta Roy (2019). Effect of temperature on corrosion of carbon steel under insulation. A poster presentation at Electrochem meeting (National conference) held at University of Strathclyde.
3. John B. Edet, Todd Green and Sudipta Roy (2020): Effect of temperature and vapour phase inhibitor on corrosion of carbon steel under insulation. A poster presentation at Butler meeting held virtually on twitter.
4. John B. Edet, Todd Green and Sudipta Roy (2021). Predictive modelling of corrosion of carbon steel under insulation using artificial neural network. An oral presentation at the Research Day celebration at Chemical and Process Engineering, University of Strathclyde.
5. John B. Edet, Todd Green and Sudipta Roy (2021). Design of test rig and effect of temperature on corrosion of carbon steel under insulation. An oral presentation at the Postgraduate research seminar, Department of Chemical and Process Engineering, University of Strathclyde.
6. John B. Edet, Todd Green and Sudipta Roy (2022). Investigation of corrosion of carbon steel under mineral wool insulation. A poster presentation at the European Corrosion Congress held in Berlin, Germany.